

ADVERTIMENT. La consulta d'aquesta tesi queda condicionada a l'acceptació de les següents condicions d'ús: La difusió d'aquesta tesi per mitjà del servei TDX (www.tesisenxarxa.net) ha estat autoritzada pels titulars dels drets de propietat intel·lectual únicament per a usos privats emmarcats en activitats d'investigació i docència. No s'autoritza la seva reproducció amb finalitats de lucre ni la seva difusió i posada a disposició des d'un lloc aliè al servei TDX. No s'autoritza la presentació del seu contingut en una finestra o marc aliè a TDX (framing). Aquesta reserva de drets afecta tant al resum de presentació de la tesi com als seus continguts. En la utilització o cita de parts de la tesi és obligat indicar el nom de la persona autora.

ADVERTENCIA. La consulta de esta tesis queda condicionada a la aceptación de las siguientes condiciones de uso: La difusión de esta tesis por medio del servicio TDR (www.tesisenred.net) ha sido autorizada por los titulares de los derechos de propiedad intelectual únicamente para usos privados enmarcados en actividades de investigación y docencia. No se autoriza su reproducción con finalidades de lucro ni su difusión y puesta a disposición desde un sitio ajeno al servicio TDR. No se autoriza la presentación de su contenido en una ventana o marco ajeno a TDR (framing). Esta reserva de derechos afecta tanto al resumen de presentación de la tesis como a sus contenidos. En la utilización o cita de partes de la tesis es obligado indicar el nombre de la persona autora.

WARNING. On having consulted this thesis you're accepting the following use conditions: Spreading this thesis by the TDX (www.tesisenxarxa.net) service has been authorized by the titular of the intellectual property rights only for private uses placed in investigation and teaching activities. Reproduction with lucrative aims is not authorized neither its spreading and availability from a site foreign to the TDX service. Introducing its content in a window or frame foreign to the TDX service is not authorized (framing). This rights affect to the presentation summary of the thesis as well as to its contents. In the using or citation of parts of the thesis it's obliged to indicate the name of the author

Scaling-up methodology, a systematical procedure for
qualifying NPP nodalizations. Application to the OECD/NEA
ROSA-2 and PKL-2 Counterpart test

PhD Thesis by:
V́ctor Mart́nez Quiroga
Director: Dr. Francesc Reventós Puigjaner
Institut de Tècniques Energètiques
UPC - Universitat Politècnica de Catalunya

A thesis submitted for the degree of
Philosophiæ Doctor (PhD)

October 21, 2014



To my family and you, my dear reader.

Acknowledgements

This Ph.D. Thesis would not be possible without the support of many people and institutions. It contains findings that were produced within the framework of the OECD/NEA ROSA, OECD/NEA ROSA-2 and OECD/NEA PKL-2 projects. I would like to express gratitude to the Management Board of each one of these projects for their consent to this publication. In addition, I would like to highlight the closeness, support, and advices of their heads, Dr. Hideo Nakamura and Mr. Klaus Umminger, that help me to focus conveniently the targets of this work. Likewise, I also want to thank to the Consejo de Seguridad Nuclear that has partially funded this research. In particular, I would like to recognize Fernando Pelayo, Julio Pérez and Miguel Sánchez-Perea, whose support and advices have done feasible this project.

Personal acknowledgments (in catalan and spanish)

Después de ocho años por fin concluyo una de las etapas más bonitas y duras de mi vida, y no me gustaría dejar escapar la oportunidad de agradecer y recordar a todas aquellas personas con las que he crecido personal y profesionalmente.

En primer lloc m'agradaria donar les gràcies al meu tutor, per haver estat un Professor en el sentit complert de la paraula. En un temps en que l'educació es valora només per les qualificacions i els temaris he tingut la sort d'haver pogut rebre una formació integral durant el meu doctorat. A dia d'avui puc dir que he après una matèria, però també un ofici i una forma d'entendre la feina i la vida; i això ha estat gràcies al "Professor" Francesc Reventós i Puigjaner.

Per altra part, m'agradaria donar les gràcies al meu company Jordi Freixa, persona que ha estat referència i mirall en el que reflexar-me durant tot el meu doctorat. Ell va ser el qui em va enganxar en tot aquest món de la termohidràulica, i el qui ha aconseguit revitalitzar la meva il·lusió per la recerca un cop ha estat de volta per Barcelona. Sense ell aquesta tesi no tindria principi ni final.

Tampoc em vull estar de donar-li les gràcies a la Marina. Per escoltar-me, per ajudar-me i per aconsellar-me. I sobretot per aguantar la meva poca memòria i la meva comunicació per senyals de fum (tu ja m'entens). Has estat la persona amb la qui he compartit més hores de feina durant aquests anys, una bona amiga i una confident. Espero que puguem continuar compartint feina molt de temps, per que no conec a ningú més constant i treballador que tu.

No em puc oblidar de la Cristina ni del Lluís. Aquests dos últims anys han estat força durs per a mi a nivell professional, i tots dos, de diferent manera, han estat un pilar sobre el que recolzar-me. Gràcies a tu Cristina, per emprendre l'aventura de crear una empresa amb mi. Espero que tot i les dificultats en que et trobes ara trobis forces per poder acabar el teu doctorat. T'ho mereixes. Gràcies a tu també Lluís, per donar-me feina i recolzament econòmic un cop se'm va acabar la beca de doctorat. Gràcies a això he pogut aprendre més en detall aspectes tècnics del codi i iniciar-me en un món excitant com és el de la fusió.

Durant aquests anys també he tingut la sort de compartir moments i amistat amb molts companys i amics. Gràcies Patricia, Elisabet, Olga, Elsa, Vitaly, Juan Pablo, Carles, Jacob, Santi, Eli, Max, Xavi, Sergio, José Felipe, Jacobo, ... De tots em quedo un record imborrable.

Por último, no puedo cerrar esta lista de agradecimientos sin recordarte a ti, la persona que siempre ha estado a mi lado cuando se tenía que estar. La única que sabe por todo lo que hemos

pasado juntos todos estos años. Mi fe, esa que pierdo tantas veces y que tú sueles rescatar cuando yo ya la doy por pérdida. Sin ti esta tesis no tendría sentido porque ni yo mismo lo tendría. Gracias Jeni.

Abstract

System codes along with necessary nodalizations are valuable tools for thermal hydraulic safety analysis. Qualifying both codes and nodalizations is an essential step prior to their use in any significant study involving code calculations. Since most existing experimental data come from tests performed on the small scale, any qualification process must therefore address scale considerations. Along these lines, the present thesis introduces a new scaling-up methodology that contributes to the qualification of Nuclear Power Plant (NPP) nodalizations by means of scale disquisitions.

The "UPC Scaling-up methodology" is a systematic procedure based on the extrapolation of Integral Test Facility (ITF) post-test simulations. There are three main pillars that support this procedure: judicious selection of experimental transients, full confidence in the quality of the ITF simulations, and simplicity in justifying discrepancies that appear between ITF and NPP counterpart transients.

The techniques that are presented include the so-called K_v scaled calculations as well as the use of two new approaches, "Hybrid nodalizations" and "Scaled-up nodalizations". These latter two methods have revealed themselves to be very helpful in producing the required qualification and in promoting further improvements in nodalization. "Scaled-up nodalizations" allow effects of the ITF scaling-down criterion to be checked. On the other hand, "Hybrid nodalizations" help the user to establish how design differences modify the results. In order to carry out these calculations, a Power-to-Volume-Scaling Tool (PVST) was developed. This software generates scaled-up input decks for RELAP5mod3 following the Power to Volume Scaling (PtoV) methodology. Within the presentation of this software, it is included a detailed description of the PtoV criterion together with the scaling distortions that are expected from its application to the RELAP5mod3 equations. PVST capabilities are also assessed on two post-test simulations that were carried out at the LSTF experimental facility within the framework of the OECD/NEA ROSA and ROSA-2 projects.

Finally, an assessment of the present methodology was carried out by making use of the OECD/NEA ROSA-2 and PKL-2 Counterpart Tests (an exhaustive description of both facilities and experiments is also included). One of the limitations of scaling methodologies is the impossibility to qualify their predictions because of a lack of counterpart experimental data at NPP level. Thus, the ROSA-2 PKL-2 Counterpart Test was of great value because it allows an identical transient to be compared between two facilities with relevant differences in both design and scale. The study of both LSTF and PKL counterpart tests has enabled us to define which phenomena could be well reproduced by the nodalizations and which phenomena could not, and also to establish the basis for future extrapolation to a NPP scaled calculation. On the other hand, the application of the UPC scaling-up methodology has demonstrated the fact that selected phenomena can be scaled-up and explained between counterpart simulations by carefully considering differences in both scale and design.

As future lines of research, in the short term it is planned to fully apply the present methodology to qualify NPP nodalizations for the correlation of core exit temperatures (CET) versus peak cladding temperatures (PCT). In the long term, it is also intended to fully integrate the "UPC scaling-up methodology" within scaling issue, and to focus the efforts on providing a definite answer to the scaling controversy on the extrapolation of code accuracy to NPP level.

Contents

| | |
|---|-------------|
| Acknowledgements | iii |
| Abstract | v |
| Contents | x |
| List of Tables | xi |
| List of Figures | xvi |
| Nomenclature | xvii |
| 1 Introduction | 1 |
| 1.1 Integral Test Facilities | 2 |
| 1.2 Best Estimate Codes | 5 |
| 1.2.1 RELAP5mod3 | 5 |
| 1.3 Scaling issue | 6 |
| 1.3.1 CSAU methodology | 6 |
| 1.3.1.1 CSAU approach for evaluating scaling effect | 7 |
| 1.3.2 H2TS methodology | 8 |
| 1.3.3 Ishii three level scaling approach | 9 |
| 1.3.4 Fractional Scaling Analysis | 10 |
| 1.3.5 Roadmap to scaling | 12 |
| 1.3.6 Uncertainty Method based on Accuracy Extrapolation | 12 |
| 1.4 NPP nodalization qualification and quality guarantee procedures | 15 |
| 1.4.1 Plant-scaled calculations | 16 |
| 2 ITFs | 19 |
| 2.1 LSTF | 19 |
| 2.1.1 Scaling principles | 20 |
| 2.1.2 Description of the facility | 21 |
| 2.1.2.1 Primary system | 21 |
| 2.1.2.1.1 Reactor Pressure Vessel | 21 |
| 2.1.2.1.2 Reactor coolant piping | 22 |
| 2.1.2.1.3 Reactor coolant pumps | 22 |
| 2.1.2.1.4 Pressurizer | 23 |
| 2.1.2.1.5 Steam generator primary side | 24 |
| 2.1.2.2 Secondary system | 24 |
| 2.1.2.3 Interfacing control systems | 24 |
| 2.1.2.3.1 Volume control system | 24 |
| 2.1.2.3.2 Emergency core cooling system | 24 |
| 2.1.2.3.3 Pressurizer spray system | 25 |

| | | |
|-----------|--|-----------|
| 2.1.2.3.4 | Pressurizer relief system | 25 |
| 2.1.2.3.5 | Main steam piping system | 25 |
| 2.1.2.3.6 | Feedwater system | 25 |
| 2.1.2.3.7 | Auxiliary feedwater system | 25 |
| 2.1.2.3.8 | Steam generator blowdown system | 25 |
| 2.1.2.4 | Instrumentation | 25 |
| 2.1.3 | Nodalization | 25 |
| 2.1.4 | Nodalization qualification | 30 |
| 2.1.4.1 | OECD/NEA ROSA Test 3.1 | 30 |
| 2.1.4.1.1 | High Power Natural Circulation Events | 30 |
| 2.1.4.1.2 | Test conditions and description of the transient | 30 |
| 2.1.4.1.3 | Post-test results | 32 |
| 2.1.4.1.4 | Liquid accumulation due to CCFL | 33 |
| 2.1.4.1.5 | Loop seal behavior | 33 |
| 2.1.4.1.6 | Conclusions | 33 |
| 2.1.4.2 | OECD/NEA ROSA Test 3.2 | 43 |
| 2.1.4.2.1 | High Power Natural Circulation Events | 43 |
| 2.1.4.2.2 | Test conditions and description of the transient | 43 |
| 2.1.4.2.3 | Post-test results | 45 |
| 2.1.4.2.4 | U-tubes oscillation during Natural Circulation | 46 |
| 2.1.4.2.5 | Sensitivity analysis: Impact of the environment heat losses | 46 |
| 2.1.4.2.6 | Conclusions | 47 |
| 2.2 | PKL | 56 |
| 2.2.1 | Scaling principles | 57 |
| 2.2.2 | Description of the facility | 58 |
| 2.2.2.1 | Primary system | 58 |
| 2.2.2.1.1 | Reactor Pressure Vessel | 58 |
| 2.2.2.1.2 | Reactor coolant piping | 60 |
| 2.2.2.1.3 | Reactor coolant pumps | 60 |
| 2.2.2.1.4 | Pressurizer | 60 |
| 2.2.2.1.5 | Steam generator primary side | 60 |
| 2.2.2.2 | Secondary system | 60 |
| 2.2.2.3 | Interfacing control systems | 61 |
| 2.2.2.3.1 | Volume control system | 61 |
| 2.2.2.3.2 | Emergency core cooling system | 61 |
| 2.2.2.3.3 | Residual heat removal system | 61 |
| 2.2.2.3.4 | Pressurizer spray system | 61 |
| 2.2.2.3.5 | Pressurizer relief system | 61 |
| 2.2.2.3.6 | Main steam piping system | 62 |
| 2.2.2.3.7 | Feedwater system | 62 |
| 2.2.2.3.8 | Auxiliary feedwater system | 62 |
| 2.2.2.3.9 | Steam generator blowdown system | 62 |
| 2.2.2.4 | Instrumentation | 62 |
| 2.2.3 | Nodalization | 62 |
| 2.2.4 | Nodalization qualification | 63 |
| 2.2.4.1 | OECD/NEA PKL-2 Test G3.1 | 64 |
| 3 | K_V scaled calculations | 75 |
| 3.1 | State of the art | 76 |
| 3.1.1 | UMAE methodology: Krsko K _V scaled calculation | 76 |
| 3.1.2 | Preliminary assessment of Scaled-up and Hybrid nodalizations | 76 |
| 3.1.3 | Asco NPP nodalization: K _V scaled calculation of the OECD/NEA ROSA-2 T3 | 77 |
| 3.1.4 | EPR NPP nodalization: K _V scaled calculation of the OECD/NEA ROSA T6.1 | 77 |

| | | |
|-----------|--|-----------|
| 3.1.5 | Scaling-up of BETHSY 9.1B Test results to Krsko NPP | 77 |
| 3.1.6 | Zion NPP nodalization: K_V scaled calculation of L2-5 test | 77 |
| 3.1.7 | Asco-2 NPP nodalization: K_V scaled calculation of LOBI BL-30 test | 78 |
| 3.1.8 | Asco-2 NPP nodalization: K_V scaled calculation of PKL F1.1 test | 78 |
| 3.1.9 | Mochovce NPP: BEPU analyses and K_V scaled calculation | 78 |
| 3.1.10 | WWER-100 NPP: Application of Bonuccelli methodology | 78 |
| 3.1.11 | LOFW: Evaluation of loss of feedwater in ITFs and NPPs | 78 |
| 3.1.12 | R. Bovalini: NPP scaled calculations of BWR SBLOCA scenario | 79 |
| 3.1.13 | "Scaling and counterpart test" | 79 |
| 3.1.14 | KNGR NPP: K_V scaled down calculations of a SBLOCA scenario | 79 |
| 3.1.15 | APR-1400 NPP: K_V scaled down calculation of a LBLOCA scenario | 79 |
| 3.1.16 | VVER 1000 simulators: Evaluation of counterpart test data | 79 |
| 3.1.17 | "Scaling Analysis in BEPU licensing of LWR" | 80 |
| 3.1.18 | "TH System codes in Nuclear Reactor Safety and Qualification Procedures" | 80 |
| 3.2 | K_V scaled calculation of OECD/NEA ROSA Test 3.1 | 80 |
| 3.2.1 | Asco-2 NPP nodalization | 80 |
| 3.2.1.1 | Conditioning phase | 81 |
| 3.2.1.2 | K_V factor | 83 |
| 3.2.1.3 | Break unit | 84 |
| 3.2.1.4 | Initial conditions | 84 |
| 3.2.2 | Results | 85 |
| 3.2.2.1 | Test phase | 85 |
| 3.2.2.2 | Local phenomena: liquid accumulation in UTs due to CCFL | 90 |
| 3.2.3 | Conclusions | 93 |
| 4 | PVST | 95 |
| 4.1 | Power to volume scaling methodology | 95 |
| 4.2 | ITF design: Application of the K_v factor | 96 |
| 4.2.1 | Vertical volumes | 97 |
| 4.2.2 | Multi-channel regions | 97 |
| 4.2.3 | Horizontal legs | 98 |
| 4.2.4 | Environment heat losses | 99 |
| 4.3 | RELAP5mod3 equations | 99 |
| 4.3.1 | Thermal hydraulic model | 99 |
| 4.3.1.1 | Field equations | 100 |
| 4.3.1.2 | Flow regime maps | 102 |
| 4.3.1.3 | Constitutive equations | 105 |
| 4.3.1.3.1 | Interphase friction | 105 |
| 4.3.1.3.2 | Wall friction | 105 |
| 4.3.1.3.3 | Interfacial heat and mass transfer processes | 107 |
| 4.3.1.3.4 | Virtual mass coefficient | 108 |
| 4.3.1.3.5 | Wall heat transfer models | 108 |
| 4.3.1.4 | Special processes | 108 |
| 4.3.1.4.1 | Choking flow | 108 |
| 4.3.1.4.2 | Counter current flow limitation | 111 |
| 4.3.1.4.3 | Water packing mitigation scheme | 112 |
| 4.3.1.4.4 | Thermal stratification model | 112 |
| 4.3.1.4.5 | Mixture level tracking model | 113 |
| 4.3.1.4.6 | Abrupt area change model | 113 |
| 4.3.1.4.7 | User specified form loss | 114 |
| 4.3.2 | Heat conduction model | 114 |
| 4.3.2.1 | Reflow model | 114 |
| 4.4 | RELAP5mod3: Power to volume Scaling distortions | 115 |

| | | |
|----------|---|------------|
| 4.4.1 | Vertical components | 115 |
| 4.4.2 | Multi-channel regions | 116 |
| 4.4.3 | Horizontal legs | 116 |
| 4.4.4 | Environment heat losses | 116 |
| 4.4.5 | Non condensable and boron transport equations | 117 |
| 4.5 | PVST | 117 |
| 4.6 | Assessment of PVST software | 119 |
| 4.6.1 | PtoV scaled-up nodalizations | 119 |
| 4.6.2 | Assessment of the environment heat losses effect | 123 |
| 4.6.3 | Assessment of the hydraulic diameters effect | 124 |
| 4.6.4 | Assessment of the Froude number effect | 126 |
| 5 | Scaling-up Methodology | 129 |
| 5.1 | NPP scenario validation matrix | 131 |
| 5.2 | Validation of ITFs tests and nodalizations | 131 |
| 5.3 | NPP scaled calculation | 133 |
| 5.4 | Scaling effect analyses | 135 |
| 5.4.1 | Scaled-up nodalizations | 135 |
| 5.5 | Design effect analyses | 137 |
| 5.6 | Expert judgment | 138 |
| 6 | Assessment of the UPC Scaling-up methodology | 141 |
| 6.1 | PKL-2 ROSA-2 Counterpart Test | 141 |
| 6.1.1 | ROSA-2 Test 3 Test conditions | 141 |
| 6.1.2 | PKL-2 G7.1 Test conditions | 142 |
| 6.1.3 | Experimental results | 142 |
| 6.2 | Results | 147 |
| 6.2.1 | PKL G7.1 Post-test analysis | 147 |
| 6.2.2 | LSTF Test 3 Post-test analysis | 149 |
| 6.3 | "Scaling effect analysis" and "Design effect analysis" evaluation | 157 |
| 6.3.1 | Scaling effect analysis | 157 |
| 6.3.2 | Design effect analysis | 163 |
| 6.3.2.1 | Core dryout delay | 163 |
| 6.3.2.2 | CETvsPCT correlation | 166 |
| 7 | Conclusions | 169 |
| 7.1 | Assessment of "UPC Scaling-up methodology" | 171 |
| 7.2 | Recommendations for future work | 172 |
| | Bibliography | 173 |

List of Tables

| | | |
|-----|---|-----|
| 2.1 | Differential pressures into the vessel | 27 |
| 2.2 | Test 3.1 Steady state conditions | 31 |
| 2.3 | Test 3.1 Main events | 32 |
| 2.4 | Test 3.2 Steady state conditions | 45 |
| 2.5 | Test 3.2 Main events | 46 |
| 2.6 | Test G3.1 Steady state conditions | 66 |
| 2.7 | Test G3.1 Main events | 66 |
| | | |
| 3.1 | Parameters not scaled with K_v factor | 84 |
| 3.2 | Initial conditions | 85 |
| 3.3 | Chronology of the main events in the test T3-1 | 86 |
| | | |
| 4.1 | Drift Flux Void Fraction Correlations for Vertical Bubbly-Slug Flow | 106 |
| 4.2 | Summary of Interfacial Areas and Heat Transfer Coefficients | 109 |
| 4.3 | Main events of OECD/NEA ROSA Test 3-1 | 120 |
| | | |
| 5.1 | NPP SBLOCA/IBLOCA validation matrix | 132 |
| | | |
| 6.1 | PKL and LSTF major features | 142 |
| 6.2 | Test conditions of Test 3 | 143 |
| 6.3 | Initial condition of PKL Test G7.1 | 148 |
| 6.4 | Main events of PKL G7.1 Test | 149 |
| 6.5 | Initial conditions of LSTF Test 3 | 152 |
| 6.6 | Test 3 main events | 154 |
| 6.7 | LSTF and PKL vessel differences | 166 |
| 6.8 | Core design differences | 166 |

List of Figures

| | | |
|------|--|----|
| 1.1 | CSAU methodology | 2 |
| 1.2 | Sketch of ITF facilities in comparison with Doel plant | 4 |
| 1.3 | CSAU generic procedure to evaluate code scaling-up capability | 7 |
| 1.4 | Flow diagram for the H2TS analysis | 8 |
| 1.5 | Flow chart Ishii three level scaling methodology | 10 |
| 1.6 | Three level synthesis | 11 |
| 1.7 | Roadmap to scaling | 13 |
| 1.8 | UMAE flow chart | 14 |
| 1.9 | Ascó qualification matrix | 16 |
| 1.10 | Primary pressure | 17 |
| 1.11 | U-tube collapsed liquid level | 18 |
| | | |
| 2.1 | The LSTF test facility | 20 |
| 2.2 | The LSTF test facility, loop arrangement and instrumentation | 22 |
| 2.3 | The LSTF test facility, view of the RPV | 23 |
| 2.4 | Distribution of measurement devices | 26 |
| 2.5 | LSTF normalized pressure vs. distance on broken loop | 27 |
| 2.6 | LSTF normalized pressure vs. distance on intact loop | 28 |
| 2.7 | LSTF nodalization: cartesian distribution | 28 |
| 2.8 | LSTF nodalization | 29 |
| 2.9 | Thermalhydraulic phenomena during SBLOCA without SCRAM (source JAEA) | 30 |
| 2.10 | LSTF system pressures | 34 |
| 2.11 | Break mass losses | 34 |
| 2.12 | Mass flow rate of primary system loops | 35 |
| 2.13 | Core collapsed level | 35 |
| 2.14 | SGs liquid level | 36 |
| 2.15 | Peak cladding temperature | 36 |
| 2.16 | Core Power | 37 |
| 2.17 | Core void fraction | 37 |
| 2.18 | Froude number on the broken loop hot leg | 38 |
| 2.19 | Flow regim number. Horizontal stratification associated to 12 value | 38 |
| 2.20 | Hot leg collapsed liquid level | 39 |
| 2.21 | Loop B liquid velocities | 39 |
| 2.22 | Loop B vapour velocities | 40 |
| 2.23 | Collapsed level of the Loop B UT | 40 |
| 2.24 | Collapsed level of the Loop B UT | 41 |
| 2.25 | Core collapsed level | 41 |
| 2.26 | Time integrated accumulator mass flow rate | 42 |
| 2.27 | Loop seal A collapsed level | 42 |
| 2.28 | Loop seal B collapsed level | 43 |
| 2.29 | Thermalhydraulic phenomena during LOFW without SCRAM | 44 |

| | | |
|------|--|----|
| 2.30 | LSTF core power | 47 |
| 2.31 | LSTF system pressures | 48 |
| 2.32 | Maximum and minimum cladding temperatures | 48 |
| 2.33 | SG riser collapsed liquid levels | 49 |
| 2.34 | Auxiliary feedwater | 49 |
| 2.35 | U-tubes upflow side differential pressure | 50 |
| 2.36 | Primary mass flow rate | 50 |
| 2.37 | PZR liquid level | 51 |
| 2.38 | Differential pressures in the SG inlet and hot leg of loop A | 51 |
| 2.39 | U-tube temperatures | 52 |
| 2.40 | U-tubes differential pressure during natural circulation phase | 52 |
| 2.41 | U-tubes differential pressure during reflux condensation phase | 53 |
| 2.42 | PRZ pressure during conditioning phase | 53 |
| 2.43 | Fluid temperature in the pressurizer | 54 |
| 2.44 | PZR collapsed liquid level | 54 |
| 2.45 | Time-integrated discharge flow through PORV | 55 |
| 2.46 | Maximum clad surface temperature | 55 |
| 2.47 | The PKL test facility | 56 |
| 2.48 | The PKL test facility, loop arrangement | 58 |
| 2.49 | The PKL test facility, view of the RPV | 59 |
| 2.50 | Distribution of measurement devices | 63 |
| 2.51 | PKL nodalization: radial distribution | 64 |
| 2.52 | PKL nodalization | 65 |
| 2.53 | Pressurizer pressure | 67 |
| 2.54 | SGs pressures | 68 |
| 2.55 | SGs riser collapsed level | 68 |
| 2.56 | Pressurizer collapse level | 69 |
| 2.57 | Cold leg temperatures | 69 |
| 2.58 | Hot leg temperatures | 70 |
| 2.59 | Main steam line discharge flow rate | 70 |
| 2.60 | SGs outlet temperature | 71 |
| 2.61 | SGs difference temperature | 71 |
| 2.62 | HPIS flow rate | 72 |
| 2.63 | Loops 1-4, flow rate wide range | 72 |
| 2.64 | Loops 1-4, flow rate narrow range | 73 |
| 2.65 | Loop 3 RCP ΔT | 73 |
| 2.66 | Loop 4 RCP ΔT | 74 |
| | | |
| 3.1 | Asco-2, Pressurized Water Reactor | 81 |
| 3.2 | Asco, nodalization | 82 |
| 3.3 | Conditioning phase | 83 |
| 3.4 | Pressurizer collapsed liquid level | 83 |
| 3.5 | Break junction sensitivity analysis | 84 |
| 3.6 | Primary and secondary pressures | 86 |
| 3.7 | Break mass flow rate | 87 |
| 3.8 | Cold legs mass flow rate | 87 |
| 3.9 | Secondary system mass inventory | 88 |
| 3.10 | Safety valves mass flow rate | 88 |
| 3.11 | Core collapsed liquid level | 89 |
| 3.12 | Primary system mass inventory | 89 |
| 3.13 | Maximum peak cladding temperature | 90 |
| 3.14 | Froude number | 91 |
| 3.15 | Velocities at the U-tubes inlet of the broken loop | 91 |

LIST OF FIGURES

| | | |
|------|---|-----|
| 3.16 | U-tube liquid accumulation in the broken loop | 92 |
| 3.17 | Primary-to-secondary heat transfer | 92 |
| 3.18 | System pressures | 93 |
| | | |
| 4.1 | Vertical volumes in reactor vessel | 97 |
| 4.2 | Dukler-Taitel flow regime map | 98 |
| 4.3 | Vertical flow regime map | 102 |
| 4.4 | Horizontal volumes flow regime map | 103 |
| 4.5 | High mixing volume flow regime map | 104 |
| 4.6 | ECC mixer volume flow regime map | 104 |
| 4.7 | RELAP5 Wall Heat Transfer Flow Chart | 110 |
| 4.8 | $\sqrt{H_g}$ vs. $\sqrt{H_f}$ for a Typical CCFL Correlation Vertical volumes flow regime map | 112 |
| 4.9 | Mesh point layout | 114 |
| 4.10 | Volume and Surface Elements Around a Mesh Point (i, j) | 115 |
| 4.11 | PVST general questions | 118 |
| 4.12 | PVST particular scaling questions | 119 |
| 4.13 | Secondary pressure | 121 |
| 4.14 | Safety valve mass flow rate | 121 |
| 4.15 | Core power | 122 |
| 4.16 | Core level | 122 |
| 4.17 | Total mass discharged across the break | 123 |
| 4.18 | Liquid temperatures in the riser of the SG | 123 |
| 4.19 | Environment heat losses | 124 |
| 4.20 | Primary-to-secondary heat transfer during conditioning phase | 125 |
| 4.21 | Energy transferred from primary to secondary during the transient | 125 |
| 4.22 | Internal energy of the liquid in the SG DC | 126 |
| 4.23 | Collapsed liquid level in the riser of the SG | 126 |
| | | |
| 5.1 | UPC Scaling-up methodology | 130 |
| 5.2 | PKL CETvsPCT curve | 133 |
| 5.3 | PKL CETvsPCT curve | 134 |
| 5.4 | U-tube collapsed liquid level | 134 |
| 5.5 | System pressures | 136 |
| 5.6 | Break mass flow rate | 136 |
| 5.7 | Core exit temperature | 137 |
| 5.8 | Core exit temperature | 138 |
| 5.9 | Core exit temperature | 139 |
| 5.10 | Core exit temperature | 139 |
| | | |
| 6.1 | LSTF system pressures | 144 |
| 6.2 | PKL system pressure | 145 |
| 6.3 | core collapsed liquid level | 145 |
| 6.4 | CETvsPCT curve | 146 |
| 6.5 | Peak cladding temperature | 146 |
| 6.6 | UPC PKL Pseudo 3D nodalization core channels | 147 |
| 6.7 | PKL G7.1 primary pressure | 148 |
| 6.8 | PKL G7.1 secondary pressure | 149 |
| 6.9 | PKL G7.1 Mass flow comparison | 150 |
| 6.10 | PKL G7.1 core exit temperature | 150 |
| 6.11 | PKL G7.1 PCTvsCET | 151 |
| 6.12 | Test 3 break mass flow rate | 151 |
| 6.13 | Test 3 system pressures | 152 |
| 6.14 | Test 3 core collapsed liquid level | 153 |

| | |
|--|-----|
| 6.15 Test 3 core exit temperature | 153 |
| 6.16 PCTvsCET curve during High pressure transient phase | 155 |
| 6.17 PCTvsCET curve during Low pressure transient phase | 155 |
| 6.18 UPC LSTF Pseudo 3D nodalization: core channels | 156 |
| 6.19 Test 3 system pressures | 156 |
| 6.20 System pressures | 158 |
| 6.21 Mass discharged through the break | 158 |
| 6.22 HL liquid level | 159 |
| 6.23 Break mass flow rate | 160 |
| 6.24 HL liquid level | 160 |
| 6.25 Break mass flow rate | 161 |
| 6.26 System pressures | 161 |
| 6.27 Core exit temperature | 162 |
| 6.28 Peak cladding temperature | 162 |
| 6.29 Core exit temperatures | 163 |
| 6.30 HL liquid level | 164 |
| 6.31 Core exit temperature | 164 |
| 6.32 Core exit temperature | 165 |
| 6.33 HL liquid level | 165 |
| 6.34 Core exit temperature | 166 |
| 6.35 HL liquid level | 167 |
| 6.36 PCTvsCET curve | 168 |
| 6.37 Core exit temperature | 168 |

Nomenclature

Acronyms

| | |
|--------|---|
| ACC | Accumulator |
| AFW | Auxiliary FeedWater |
| AM | Accident Management |
| ANAV | Associació Nuclear Ascó Vandellós |
| APEX | Advanced Plant EXperiment |
| ASM | Analytical Simulation Model |
| ATWS | Anticipated Transient Without Scram |
| BDBA | Beyond Design Basis Accidents |
| BE | Best Estimate |
| BEPU | Best Estimate Plus Uncertainties |
| BIC | Boundary and Initial Conditions |
| BWR | Boiling Water Reactor |
| CANDU | Canadian Deuterium-Uranium Reactor |
| CCFL | Counter Current Flow Limitation |
| CET | Core Exit Temperature |
| CFR | Code of Federal Regulations |
| CL | Cold Leg |
| COMBO | COntinuous Measurement of BOron concentration |
| CSAU | Code, Scaling, Applicability and Uncertainty |
| CSN | Consejo de Seguridad Nuclear |
| CSNI | Committee on the Safety of Nuclear Installations |
| DBA | Design Basis Accidents |
| DC | DownComer |
| ECCS | Emergency Core Cooling Systems |
| EOP | Emergency Operating Procedure |
| FA | Fuel Assembly |
| FCM | Fractional Change Metric |
| FFTBM | Fast Fourier Transform Based Method |
| FRC | Fractional Rate of Change |
| FSA | Fractional Scaling Analysis |
| H2TS | Hierarchichal Two-Tiered Scaling |
| HL | Hot Leg |
| HPSI | High Pressure Safety Injeccion |
| HS | Heat Structure |
| IAEA | International Atomic Energy Agency |
| IBLOCA | Intermediate Break LOCA |
| INEL | Idaho National Engineering Laboratory |
| INTE | Institut de Tècniques Energètiques (Institute of Energy Technologies) |
| IPA | Integral PArameters |

| | |
|--------|---|
| ITF | Integral Test Facility |
| JRC | Joint Research Centre |
| KWU | Kraftwerk Union |
| LBLOCA | Large Break LOCA |
| LOBI | LWR Off-normal Behaviour Investigation |
| LOCA | Lss of Coolant Accident |
| LOFW | Loss of Feed Water |
| LP | Lower Plenum |
| LPSI | Low Pressure Safety Injeccion |
| LS | Loop Seal |
| LSTF | Large Scale Test Facility |
| LWR | Light Water Reactor |
| MFW | Main FeedWater |
| MS | Main Steam |
| MSIV | Main Steam Isolation Valve |
| NDP | Non Dimensional Parameters |
| NEA | Nuclear Energy Agency |
| NPP | Nuclear Power Plant |
| OECD | Organization for Economic Cooperation and De- velopment |
| PCT | Peak Cladding Temperature |
| PIRT | Phenomena Identification and Ranking Table |
| PKL | Primärkreislauf (Primary System) |
| PSA | Probabilistic Safety Analysis |
| PtoV | Power to Volume |
| PUMA | Purdue University Multi-Dimensional Integral Test Assembly |
| PVST | Power to Volume Scaling Tool |
| PWR | Pressurized Water Reactors |
| PZR | Pressurizer |
| RCP | Reactor Coolant Pumps |
| RCS | Reactor Coolant System |
| RELAP | Reactor Excursion Leak Analysis Program |
| RHR | Residual Heat Removal |
| ROSA | Rig Of Safety Assessment |
| RPV | Reactor Pressure Vessel |
| RTA | Relevant Thermalhydraulic Aspects |
| RV | Relief Valve |
| SBLOCA | Small Break LOCA |
| SCRAM | Safety Control Rod Axe Man |
| SET | Separated Effects Tests |
| SG | Steam Generator |
| SIP | Safety Injection Pumps |
| SOT | Start Of Transient |
| STF | Separated effects Test Facilities |
| STRESA | Storage of Thermal REactor Safety Analysis Data |
| SVP | Single Valued Parameters |
| TH | Thermal-Hydraulics |
| TLS | Three Level-Synthesis |
| TSE | Time Sequence Events |
| UMAE | Uncertainty Methodology based on Accuracy Ex- trapolation |
| UNIPI | UNIversità di PIsa |

| | |
|-------|---|
| UP | Upper Plenum |
| UPC | Universitat Politècnica de Catalunya |
| UPTF | Upper Plenum Test Facility |
| USNRC | United States Nuclear Regulatory Commission |
| VVER | Water-Cooled Water-Moderated Power Reactor |
| WWER | Water-Cooled Water-Moderated Power Reactor |

Latin Letters

| | | |
|-----------|--|------------|
| A | area | m^2 |
| A_c | cross sectional area | m^2 |
| C_M | coefficient of virtual mass | |
| C_p | specific heat at constant pressure | J/kgK |
| D | pipe diameter | m |
| $DISS$ | energy dissipation function | W/m^3 |
| Fr | Froude number | - |
| FIF | liquid interphase drag coefficients | s^{-1} |
| FIG | vapour interphase drag coefficients | s^{-1} |
| FWF | liquid wall drag coefficients | s^{-1} |
| FWG | vapour wall drag coefficients | s^{-1} |
| G | mass flux | kg/m^2s |
| g | gravitational constant | m/s^2 |
| H | height | m |
| h | specific enthalpy | J/kg |
| h_c | heat transfer coefficient | W/m^2Kkg |
| $HLOSSF$ | form or frictional liquid losses | m/s |
| $HLOSSG$ | form or frictional vapour losses | m/s |
| j | superficial velocity | m/s |
| K | Friction factor | - |
| k | thermal conductivity | W/mK |
| k_b | Boltzman constant | J^0/K |
| K_v | power to volume scaling factor | - |
| l | length | m |
| Nu | Nusselt number | - |
| P | pressure | Pa |
| p | wetted perimeter | m |
| Q | volumetric heat addition rate | W/m^3 |
| q | heat flux | W/m^2 |
| Re | Reynolds number | - |
| t | time | s |
| U | specific internal energy | J/kg |
| \bar{V} | specific volume | m^3/kg |
| V | volume | m^3 |
| v | velocity | m/s |
| $VISF$ | numerical viscosity term in momentum equations | m^2/s^2 |
| $VISG$ | numerical viscosity term in momentum equations | m^2/s^2 |
| W | mass flow rate | kg/s |
| x | spatial coordinate | m |
| z | elevation change coordinate | m |
| zl | liquid level elevation change coordinate | m |

Greek Letters

| | | |
|---------------|---|-----------|
| α | void fraction | - |
| β | coefficient of isobaric thermal expansion | K^{-1} |
| δ | heat structure radial length | m |
| η | critical pressure ratio | - |
| ε | surface roughness | m |
| Γ | volumetric mass exchange rate | kg/m^3s |
| γ | heat capacity ratio | - |
| κ | coefficient of isothermal compressibility | Pa^{-1} |
| μ | viscosity | kg/ms |
| ν | fluid kinematic viscosity | m^2/s |
| ϕ | power | W |
| $\bar{\rho}$ | volumetric heat capacity | J/m^3K |
| ρ | density | kg/m^3 |
| σ | surface tension | J/m^2 |
| τ | wall shear stress | N |
| ξ | perimeter | m |

Superscripts

| | |
|----------|--|
| ' | thermal boundary layer/saturation property |
| + | dimensionless parameter |
| · | donored quantity |
| ~ | intermediate time variable |
| <i>B</i> | bottom |
| <i>L</i> | left |
| <i>R</i> | right |
| <i>S</i> | saturation |
| <i>s</i> | surface-gradient weight |
| <i>v</i> | volume-gradient weight |
| <i>T</i> | top |

Subscripts

| | |
|-------------|--|
| 0 | reference value |
| <i>b</i> | boron |
| <i>bub</i> | bubble |
| <i>c</i> | critical |
| <i>chan</i> | channel |
| <i>d</i> | droplet |
| <i>drp</i> | droplet |
| <i>f</i> | liquid |
| <i>g</i> | gas |
| <i>I</i> | interface |
| <i>i</i> | interface |
| <i>ITF</i> | Integral Test Facility |
| <i>j</i> | junction index |
| <i>K</i> | cell index |
| <i>L</i> | cell index |
| <i>l</i> | liquid, left boundary |
| <i>m</i> | mixture property, heat conduction mesh index |

Nomenclature

| | |
|---------------|--|
| <i>n</i> | noncondensables component, time step index |
| <i>p</i> | phase |
| <i>R</i> | Reference Plant |
| <i>r</i> | right |
| <i>s</i> | steam, saturation |
| <i>scaled</i> | parameter of an scaled input deck |
| <i>v</i> | vapour |
| <i>w</i> | wall |

1. Introduction

In September 1988 the U.S.NRC approved a revision of the ECCS rule (10 CFR part 50 [1]) by which BEPU calculations could be used for licensing. Likewise, CSAU Methodology, Figure 1.1, was presented by NRC [2] in order to establish the requirements for quantifying code uncertainties in specific scenarios and NPPs. The CSAU guidelines provided a very valuable roadmap for developing specific uncertainty methodologies ([3], [4] and [5]) and it showed the relevance of scaling issues when using system codes for ECCS licensing.

One of the CSAU methodology requirements (see step 9 in Figure 1.1) was to determine code accuracy. If the scenario involves an ECCS' actuation it is unavoidable to design scaled down facilities for the validation of system codes. And it is just at this point where the so-called "scaling controversy" starts. Experience has shown that there is no consensus for matching code validation on the scale of test facilities with code validation for a specific commercial NPP and a specific scenario. Objections are mainly based on two features:

- The design of a test facility "cannot completely satisfy all the scaling requirements. Thus scaling distortions are unavoidable (...)" [6]
- Intrinsic limitations of thermallyhydraulic codes. Namely, the simulation of two-phase flow regime transitions and the impossibility of qualifying their closure equations under transient and non-developed flow conditions [7].

Along these lines, several scaling analysis philosophies have been developed (H2TS [8] and [9] together with the Ishii three-level scaling approach [6]). Such developments have been applied in the design of new test facilities (APEX [10] and PUMA [6]) in order to identify and evaluate scaling distortion on experimental data. Furthermore, there is still a lack of a global response on the subject of scaling code capabilities to extend the experience acquired through experiments to the use of BEPU calculations for the licensing of NPPs. Part of the scientific community considers the use of system codes inappropriate and proposes quantitative methodologies for NPP design and safety analysis (FSA methodology, [11], [12], [13]). Alternatively, D'Auria et al. [14], developed the UMAE methodology for determining the uncertainty and similarity associated to the simulation of the ITF experiments in different nodalizations, and introduced a "roadmap to scaling" [7] in order to follow up and progress on the guidelines that were set up in the CSAU methodology.

Even though the main code scaling techniques presented in this thesis could be perfectly integrated within the "roadmap to scaling" concept presented in Reference [7] and UMAE methodology presented in Reference [14], it is not within the scope of the present methodology to further study the scaling of the capabilities of the system codes. Otherwise, Best Estimate Codes are widely applied within the nuclear industry for operational support and safety assessment. "UPC Scaling-up Methodology", explained in Chapter 5, aims to be a guideline for validating and improving NPP nodalizations with the knowledge obtained from the modeling of ITF Tests. The aim is to provide a tool for qualifying nodalizations.

In the following sections a more detailed overview of the scaling issue is provided along with the different methodologies and points of view that exist within the research community. A brief introduction of Integral Test Facilities, system codes and qualification procedures is also included. All these notions need to be understood for the proper comprehension of the different concepts that will be introduced later on.

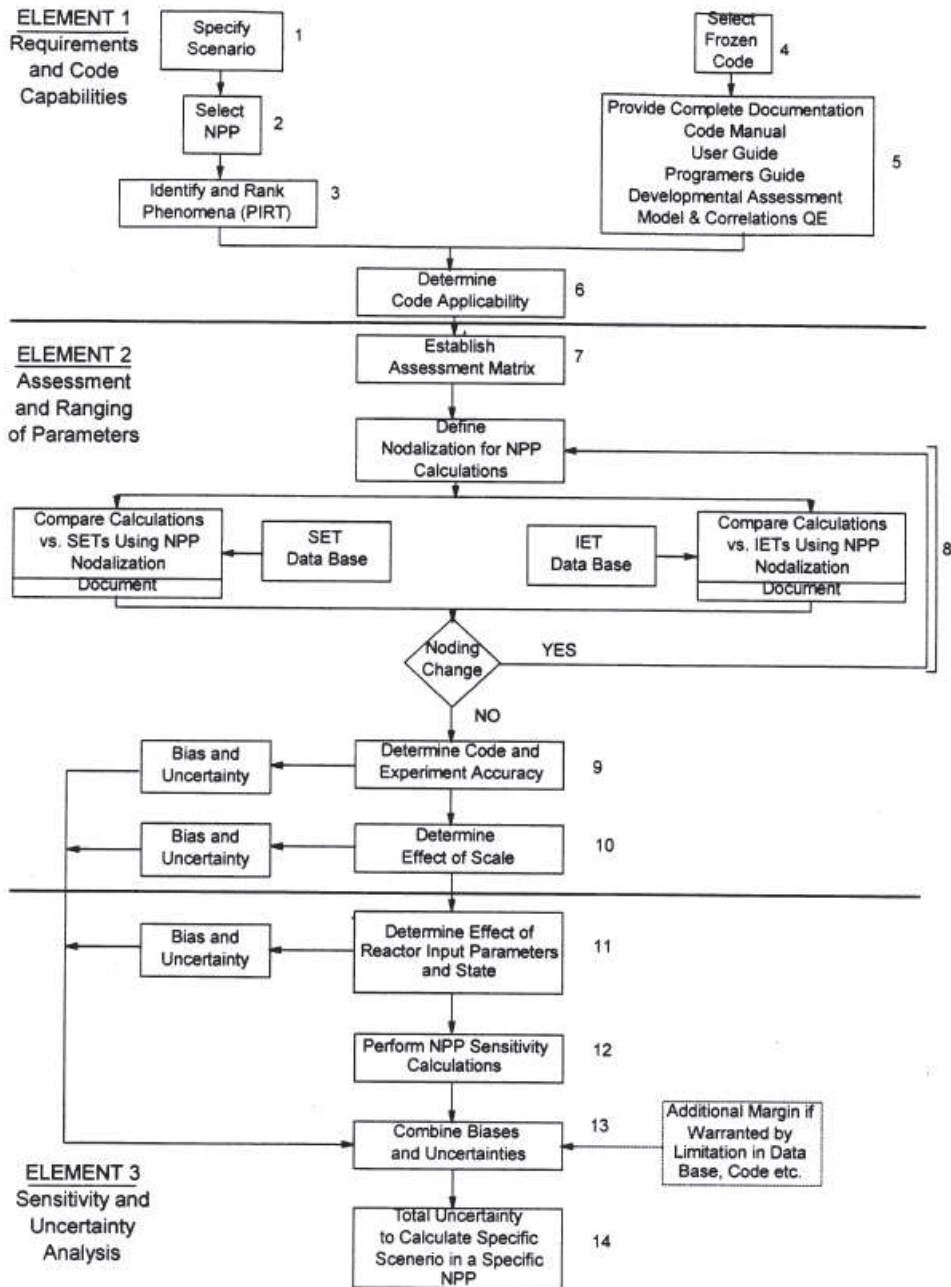


Figure 1.1: CSAU methodology

1.1 Integral Test Facilities

Integral test facilities (ITF) are experimental facilities that reproduce the overall behavior as well as the system components interactions of a NPP. They were born as a response to the nuclear industry needs of analyzing NPP accident scenario under safe and cost assumable conditions. Hence, the target of the ITF design is to achieve a compromise between reality and economical solvency, and it

is only feasible by reducing the geometrical dimensions.

The different scaling criteria that are used for designing ITFs were summarized by Navahandi [15] in three different approaches:

- *linear scaling*: it is a technique whereby linear dimensions of the test facility are directly reduced by a fixed scale factor, relative to the reference NPP. The main advantage of the linear approach is that timing of events are directly reduced by the same factor. On the contrary, accelerations need to be scaled by the inverse of the time factor, and rated controlled phenomena (such as flashing heat and mass transfer, or flow regime transitions) are also distorted in time relative to the reference NPP. Additionally, linear reduction implies very small geometric characteristics, what it is really inconvenient for NPP scaled-down facilities (and all those systems where heat and mass transfers are important) as heating surfaces must be reduced to small diameters. For all these reasons, linear scaling has been historically unattractive for scaling NPPs, and very few but not one can be highlighted.
- *time preserving -or power to volume scaling-*: this method is based on preserving power and flow distributions as well as time. It requires the ratio of the power in the ITF divided by the NPP power be equal to the ratio of the ITF volume divided by the NPP volume. Volume of each one of the components of the facility is scaled-down by reducing the area with this ratio and keeping its relative elevation. With an idealized power to volume scaling, time scale, fluid mass, energy distributions, velocities, accelerations and lengths are preserved. Power to volume scaling has been historically the most common methodology applied in the design of PWR ITFs. Further information about it can be found in Section 4.1.
- *Idealized time preserving*: it is a resemble of the time preserving scaling. Designer has more flexibility for modifying the geometries of those components for which local TH phenomena have a significant weight in the overall behavior of the system. Anyhow, geometrical readjustments must be always done without distorting the time scale. A good example of these kind of ITFs would be those that were designed specifically for simulating SBLOCA. For this transient, the preservation of flow regime transitions in the horizontal legs is essential, hence a readjustment of the lengths and the diameters of the cold and hot legs must be performed in order to preserve the Froude number and the power to volume scaling factor. Further information about this distortion can be found in Section 4.1.
- Finally, it is worth mentioning that new ITFs, like PUMA, ATLAS, or IIST, have been designed following the Ishii three level scaling approach that will be explained in more detail in Subsection 1.3.3.

Historically, the origin of the ITFs is dated at early 1960s, when USNRC requested to build an experimental reactor for verifying the capabilities of the ECCS to keep cooled the core under LOCA conditions. Initially, Semiscale (1965), a small, cheap and electrically heated facility, was built in order to confirm the attempt to construct a larger ITF. Results of the tests performed during 1970 and early 1971 (deficiencies in the ECCS effectiveness as a result of ECCS bypass at the inlet of the vessel) corroborate the need of building bigger facilities up for matching results. Hence, LOFT (1976), an actual nuclear facility was concluded, starting an exhaustive program based on LOCAs and ECCS effectiveness analyses. First ITFs programs were concentrated on that issues. On the contrary, after TMI-2 accident (1980s), efforts of the research community focussed on SBLOCA phenomena, and several electrically heated test facilities were constructed during the next 20 years. Some of the ITFs based on a PWR design (see Figure 1.2) were:

- *LOBI*: based on German PWR four loop design by two un-equal loops
- *SPES*: based on US three loops PWR by three equal loops
- *BETHSY*: based on French four loops PWR by two equal loops
- *LSTF*: based on Westinghouse four loops PWR by two equal loops

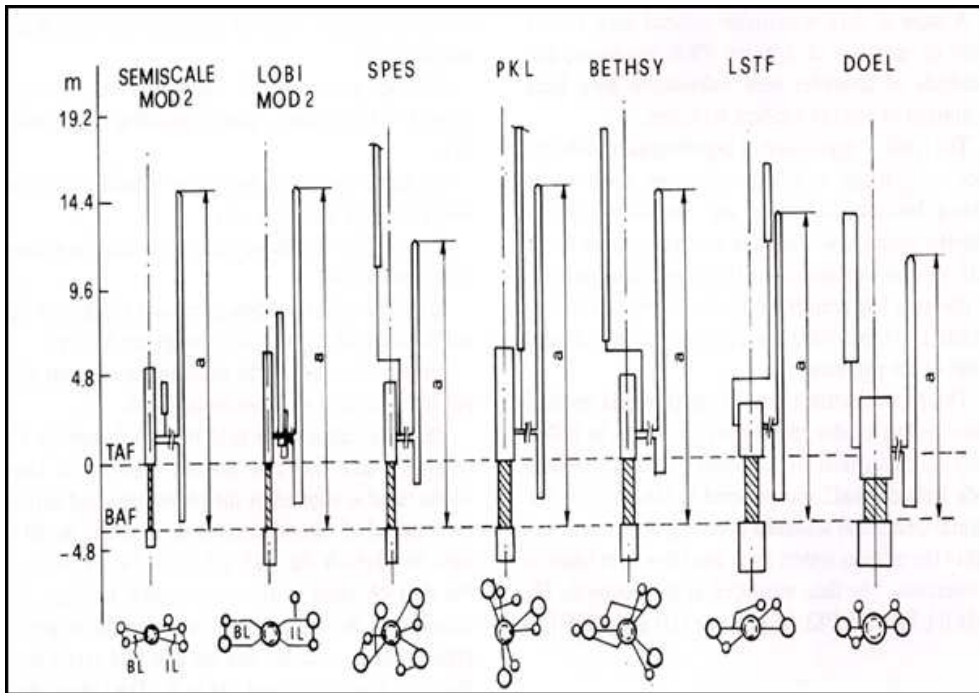


Figure 1.2: Sketch of ITF facilities in comparison with Doel plant

- *PSB*: based on Russian four loops VVER-1000 by four equal loops and horizontal SG tubes
- *PKL*: based on German PWR four loop design by four equal loops

Other ITFs worth to mention are those based on BWR design (MIST, UMCP, FIST, FIX-II, PIPER-ONE, ROSA-III, TITA, PUMA,...), VVER ITFs (as PACTEL from Finland, and PMK for Hungary), and those designed following the Ishii scaling approach (as ATLAS from South Korea, IIST from Taiwan, or PUMA from USA). Currently, it has been reported around 2000 thousand tests from dozens of ITFs the cost of which has been estimated around the Billion-Dollars (value of the year 2000 -further information in Reference [7]).

Even though the initial application of the ITFs test programs was the safety assessment, the key target of ITFs is the development and the qualification of BE codes. In that sense, the efforts of the research community have been focussed in two aspects, to facilitate the access to the huge database of ITF tests, and to generate counterpart transients in order to extend the analysis of the code accuracy to different scales.

About the data base access, relevant projects have been conducted by international institutions during the last 30 years. In this field, it is unavoidable to remark the work performed by the OECD/NEA with the CSNI Code Validation Matrix [16]. This report put in order the most relevant ITF transients performed during the 1980s (including the International Standard Problems -ISPs-), classifying them depending on the kind of LWR and scenario, and describing in detail the most relevant TH phenomena that took place and the quality of their recorded data. Another example in this area would be the STRESA database that has been carried out by the JRC, [17]. STRESA (Storage of Thermal REactor Safety Analysis Data) stores all the experimental data from LOBI in the JRC Petten site, providing a friendly-user environment to the analyst for downloading the information.

Finally, it is also worth to mention the relevance of the ITF counterpart tests. These kind of transients are characterized by reproducing equivalent events and TH processes. Similarity is achieved by matching the boundary and the initial conditions of different ITFs in basis to the scaling factors. Counterpart test are of great value given that allows checking the accuracy of the BE codes at

different scale for the same phenomena. Several counterpart tests have been performed in the last 30 years, being the most significant the SBLOCA tests carried out at LOBI, SPES, BETHSY, LSTF and PSB within 7 selected transients, [18]. Recently, a close collaboration between OECD/NEA ROSA-2 and OECD/NEA PKL-2 projects has generated a counterpart test between LSTF and PKL facilities. This transient is extensively analyzed in this thesis (see Chapter 6) and the basis for demonstrating the potentials and the capabilities of the qualification methodology that will be described in the following chapters.

1.2 Best Estimate Codes

During last 40 years, nuclear industry and research community have focused their main efforts on assessing the overall response of the NPPs during accident conditions. As a result of these efforts, several complex system codes have been developed with proven capabilities for simulating the main TH processes that occur during transient conditions of LWRs. In the early stage of the development, system codes were primarily applied to support the design of safety systems. Since 1978, with the publication of the 10CFR 50.46 rule [19], system codes started to be applied as a support to licensing with the creation of conservative versions. These programs were defined following the conservative model assumptions and boundary and initial conditions that the appendix K of the 10CFR 50.46 rule required for assuring conservative results in the critical safety parameters. In parallel, specially after, TMI-2 accident, several realistic or so-called "best-estimate" codes started to be developed. The main objective of these codes was to replace the "evaluation models", which used many conservative assumptions, by the best-estimate approach for more realistic predictions of PWR or BWR accidental transients that allow the reduction of safety margins. Best-estimate system codes are currently used for the following:

- Safety analysis of accident scenarios
- Quantification of the conservative analyses margin
- Licensing purposes if the code is used together with a methodology to evaluate uncertainties
- Probabilistic safety analysis -PSA-
- Development and verification of accident management procedures
- Reactors design
- Analysis of operational events

BE codes are normally based on a nonhomogeneous and nonequilibrium model, which simulates a two-phase fluid system plus transport of non-condensables and non volatile solute (boron). Balance equations (mass, momentum and energy) are simplified considering 1D fluid (in some cases, like TRACE, the code can include specific components with 3D solution capability) and decoupled phases (independent equations). Hence, closure equations and flow regime maps are required for estimating interphase mass and heat exchange as well as friction effects and wall heat exchanges. These equations, that are solved independently in specific correlations, are developed and tested taking advantage of the SETs. Code developers must assure that closure equations are validated for the full range of NPPs and facilities scales, and it is in this point where the scaling issue becomes essential.

Examples of BE codes are RELAP, TRAC, TRACE, CATHARE, ATHLET, MARS, ...

1.2.1 RELAP5mod3

The RELAP5mod3 is a light water reactor transient analysis code developed by the Idaho National Engineering Laboratory (INEL) for the U.S. Nuclear Regulatory Commission. It is framed within best estimates codes (like CATHARE, TRAC, ATHLET...), which try to reproduce realistically the physical phenomena in thermalhydraulics systems without considering conservative assumptions. This kind of codes started to become relevant after Three Mile Island (1979), time in which industry

and national regulatory bodies considered necessary to develop complex software that analyzes a wider variety of postulated accident conditions minimizing the amount of physical assumptions on the part of the user.

The main applications of RELAP5mod3 are rulemaking, licensing audit calculations, evaluation of accident mitigation strategies, evaluation of operator guidelines, experiment planning and analysis, and as a basis for a nuclear plant analyzer. Specific applications of this capability have included simulations of transients in LWR systems, such as loss of coolant, anticipated transients without scram (ATWS), and operational transients (loss of feedwater, loss of offsite power, station blackout, turbine trip...). On the other hand, RELAP5mod3 is a highly generic code, thus it can be used for simulating a wide variety of thermohydraulics transients in both nuclear and non-nuclear systems, involving mixtures of steam, water, noncondensable, and solute.

The code is designed to simulate any component of a LWR system, as well as nuclear power generation, heat transfer processes between the fluid and metal structures, and the whole plant control system and boundary conditions. Flow paths are modeled using finite control volumes connected by non-dimensional junctions and valves. Specific LWR components as pumps, jetmixers, separators or turbines have been also included. Wall-to-fluid heat transfer processes are modeled using flexible heat structure components, which allow to model and link any kind of LWR metal structure (pipe and vessel walls, vessel internals, grids, heat exchangers, fuel rods,...) with hydrodynamics nodes. Nuclear power generation is simulated using an internal point kinetics subroutine. About the control, a wide list of variables (integrals, derivatives, function, lag,...) and trips are available for defining realistically the logical of a power plant control system. Finally, time and control variable dependent volumes and junctions are included in order to be able to impose plant boundary conditions like environment pressures and temperatures, and/or safety systems injection rates.

About RELAP5mod3 physics, several approximations and assumptions are performed in the system equations in order to simulate conveniently the thermohydraulics of the fluid, the heat conduction inside the metal structures, and the transport of non-condensables and non volatile solute (boron) for the particular LWR systems. A detailed description of the RELAP5 equations can be found in Section 4.3.

1.3 Scaling issue

1.3.1 CSAU methodology

Code Scaling, Applicability and Uncertainty method is an extensive work made by the USNRC aimed at providing a suitable framework with which performs precise uncertainty and accuracy analyses of best-estimate codes. This methodology was presented as a response to the revision of the 10 CRF part 50 ECCS rule, for which the evaluation of the acceptance criteria could be done using realistic codes on condition that "uncertainties in the analysis method and inputs must be identified and assessed so that uncertainty in the calculated results can be estimated" and that "there is a high level of probability that the criteria would not be exceeded" [1]. The methodology is divided in three blocks of analysis (see Figure 1.1):

- *Requirements and Code Capabilities*: NPP, scenario and 'frozen' code must be selected and relevant phenomena must be identified and ranked.
- *Assessment and Ranging of Parameters*: NPP nodalization must be defined and code accuracy and scale distortion must be identified and quantified with the aid of an assessment matrix.
- *Sensitivity and Uncertainty Analysis*: total uncertainty over the acceptance criteria must be computed by performing sensitivity NPP calculations with the uncertainty biases reported in the previous step.

CSAU introduced a clear roadmap for completing suitable uncertainty analysis. On the contrary, no detailed information was supplied for computing the biases and the uncertainty of the code and the

scale, as well as specific techniques for making as the sensitivity computations as the estimation of the total uncertainty. As a response to this weakness, USNRC sponsored specific applications (SBLOCA uncertainty analysis using RELAP5 [20]). Furthermore, 6 papers were published in a special issue of Nuclear Engineering and Design [21], which provided a full description of the method. Below it is described the particular approach that N. Zuber, G.E. Wilson and et al. proposed in that issue for quantifying the effect of the scale in NPP scaled-up calculations.

1.3.1.1 CSAU approach for evaluating scaling effect

A rational flow diagram (see Figure 1.3) was presented in order to fulfill two aspects:

- To evaluate the capability of BE codes to scale-up processes from reduced scale test facilities to full scale nuclear power plants
- To quantify the effects of scale distortion and/or a limited data base, on code uncertainty to calculate a safety parameter of interest (for example peak clad temperature)

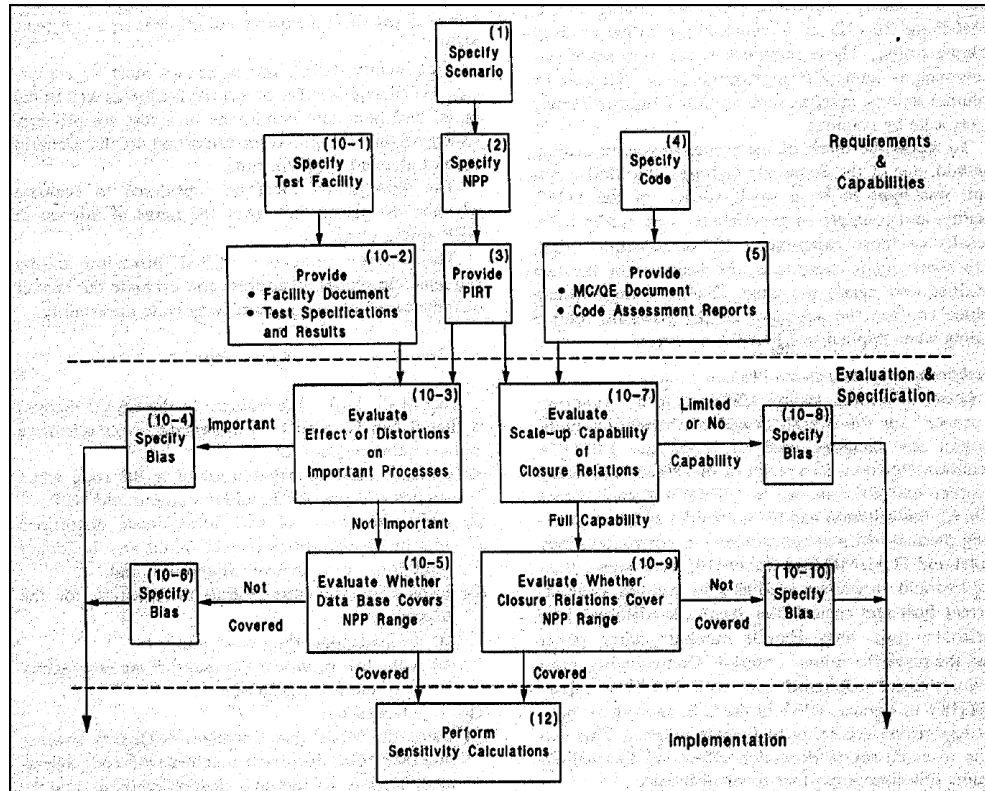


Figure 1.3: CSAU generic procedure to evaluate code scaling-up capability

The approach is divided in two blocks:

- *Requirements and capabilities (equivalent to the first step of the CSAU methodology):* NPP scenario must be selected identifying and ranking relevant TH processes. Once main processes are selected, information from the chosen test facilities (design reports and test experimental data bases) and chosen 'frozen code' (input manuals and models and correlations assessment reports) must be collected, assessed and arranged for a later evaluation.
- *Evaluation and specification:* two parallel assessments must be done at this level, one related to the data base uncertainty, and the other related to the scaling-up capabilities of the system

code. For the data base uncertainty, it is evaluated how the experimental results of the tests change in the scaling-up process. Two biases must be computed, one related with the degree of distortion that appears in the relevant phenomena, and the other one with the deviation that results must have for those ranges of the NPP that experimental test facility does not cover. Once experimental data has been assessed, code uncertainty must be determined. Two biases must be also computed, one related with the scaling-up capabilities of the closure relationships, that is how the scaling-down criterion of the ITF design affects the closure equations of the BE code. And the other one related with the capabilities of the BE equations to cover the whole range of NPP conditions.

Finally, once scale biases have been computed, analyst is ready for performing sensitivity and BEPU calculations.

1.3.2 H2TS methodology

Hierarchical-two-tiered scaling (H2TS) is a "comprehensive, systematic yet practical, auditable and traceable methodology" for evaluating the applicability of the experimental data from scaled-down facilities to nuclear power plant conditions, and hence, implicitly, the capability of the system codes and their special models (because they are qualified just at facility level) to scale-up TH data to full scale plant conditions. It is based on the premise that each TH process that occur in a system can be characterized by three parameters, volumetric concentrations, transfer areas, and time scales; and that all of them can be included just in the time scale parameter dependencies; hence, that is possible to determine TH process relevance with just one parameter. H2TS is divided in two levels of analysis (stages 3 and 4 of Figure 1.4), the "top-down system scaling analysis", and the "bottom-up process scaling analysis".

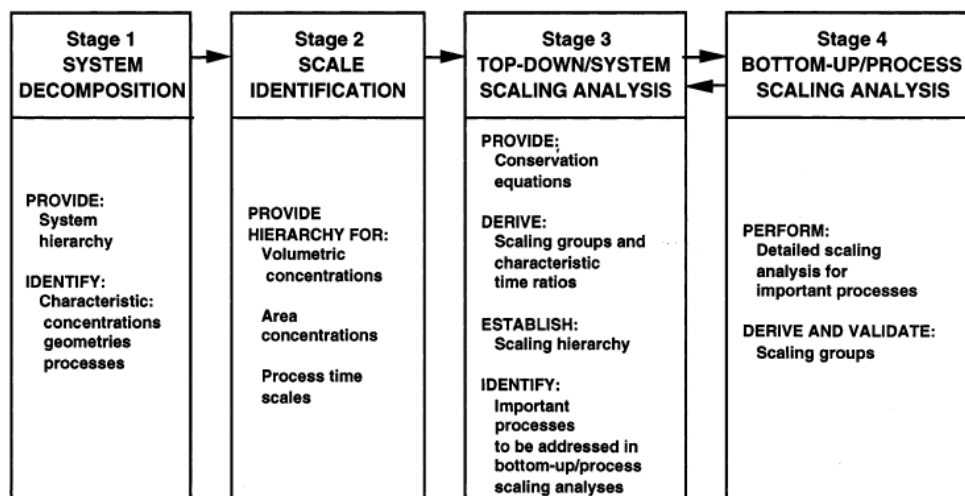


Figure 1.4: Flow diagram for the H2TS analysis

The top-down system scaling analysis gives an idea of the efficiency of the facility. At this level, the model to be analyzed (e.g. specific transient of a particular test facility) is hierarchically split in subsystems, modules, constituents,... until achieving relevant local processes that characterized the model (e.g. UTs condensation process for an SBLOCA transient). During this hierarchization process, volumetric weight factors are associated to each subsystem, module, constituent,... as well as time scales and transfer areas parameters, in order to give sense of the relevance of each one of them in the overall behavior of the model. Ratio between the time scale parameter of the processes and the time scale parameter of their subsystem, module, constituent,... gives their degree of relevance

in the overall behavior (Π , nondimensional characteristic time ratio). Deviation between the Π of the model (facility) and of the prototype (NPP) gives an idea of the level of scaling distortion for that process. Once the model has been split up in local processes and scaling deviations have been computed, analyst can judge the efficiency of the model, and hence, of the experimental data.

The bottom-up process scaling analysis provides the sufficiency of the experimental. At this level, dominant local processes identified in the top-down analysis are ranked and analyzed by a "step-by-step integral scaling" procedure. Scaling distortion of each one is recalculated along this systematic procedure also considering transition/transfer/parallel mechanisms between them. In this procedure, distortions of each process are computed one by one in series, from the most critical to the less one, finally obtaining a complete set of scaling criteria, transition criteria and time constants.

H2TS allows estimating the accuracy of the experimental data gained in scaled-down test facilities. On the contrary, H2TS does not provide a bias for analyzing safety margins of relevant TH parameters at prototype level (NPP). Therefore, when the uncertainty for the dominant mechanism in the key transfer process from prototype to model is large, separate test(s), focusing on that particular phenomena, is indicated for a precise evaluation of the distortion. Otherwise, experimental data is qualified.

1.3.3 Ishii three level scaling approach

Three level scaling approach (see Figure 1.5) is a systematic methodology for designing ITFs as well as for analyzing their generated experimental data relative to prototype conditions. The bases of the methodology are the conservation principles and the constitutive laws. It is divided in three levels of analysis, integral system scaling, control volume scaling and local phenomena scaling. The first two levels correspond to the top-down scaling and the third level represents the bottom-up scaling.

"Integral system scaling" level gives a dynamic scaling of the system components. Balance equations of each component are transcribed following the single-phase and the drift-flux two phase formulations, obtaining after their normalization under transient conditions 8 non-dimensional numbers that must be preserved. These are the Zuber, the Sub-cooling, the Froude, the Drift flux, the Friction, the Orifice, the Time and the Thermal Inertia numbers.

"Control volume and boundary flow scaling" evaluates the boundary flow conditions in the interconnections of each component. For those connections, it is considered essential to preserve the mass and the energy balances for a proper conservation of the balance equations in each one of the components. Additional scaling conditions are obtained for those connections with sinks/sources of mass and/or energy, like break connections and ECCS connections.

These two levels of scaling analyses yield the bulk of the information necessary to develop the scientific design of a test facility. However, they are not enough to guarantee the development of a well-scaled design. This is because in two-phase flow, relevant local phenomena depends on micro-scale ranges and cannot be fully represented by a simple one-dimensional drift-flux model. Hence,

"local phenomena scaling" is required. At this level, scaling analyses are focused on the various local phenomena, constitutive laws, and their impact on the overall scaling strategy. Depending on the special features of the prototype (NPP) to be scaled-down, additional scaling conditions will be added to those obtained from the levels one and two of the Ishii approach.

It must be also noted that Ishii three level scaling approach allows reducing the length/heights of the components in order to preserve the friction effects between the model and the prototype. In the case that lengths are reduced by a K_L , time scales are also reduced by a $\sqrt{K_L}$. Otherwise, if lengths are not reduced, Ishii scaling approach becomes close to the power-to-volume scaling methodology (see Reference [7]; further information about PtoV scaling method can be found in Section 4.1). For that case, the scaling numbers of the "integral system" and "control volume" scaling levels become equal to those of the PtoV approach, gaining a counterpart criterion.

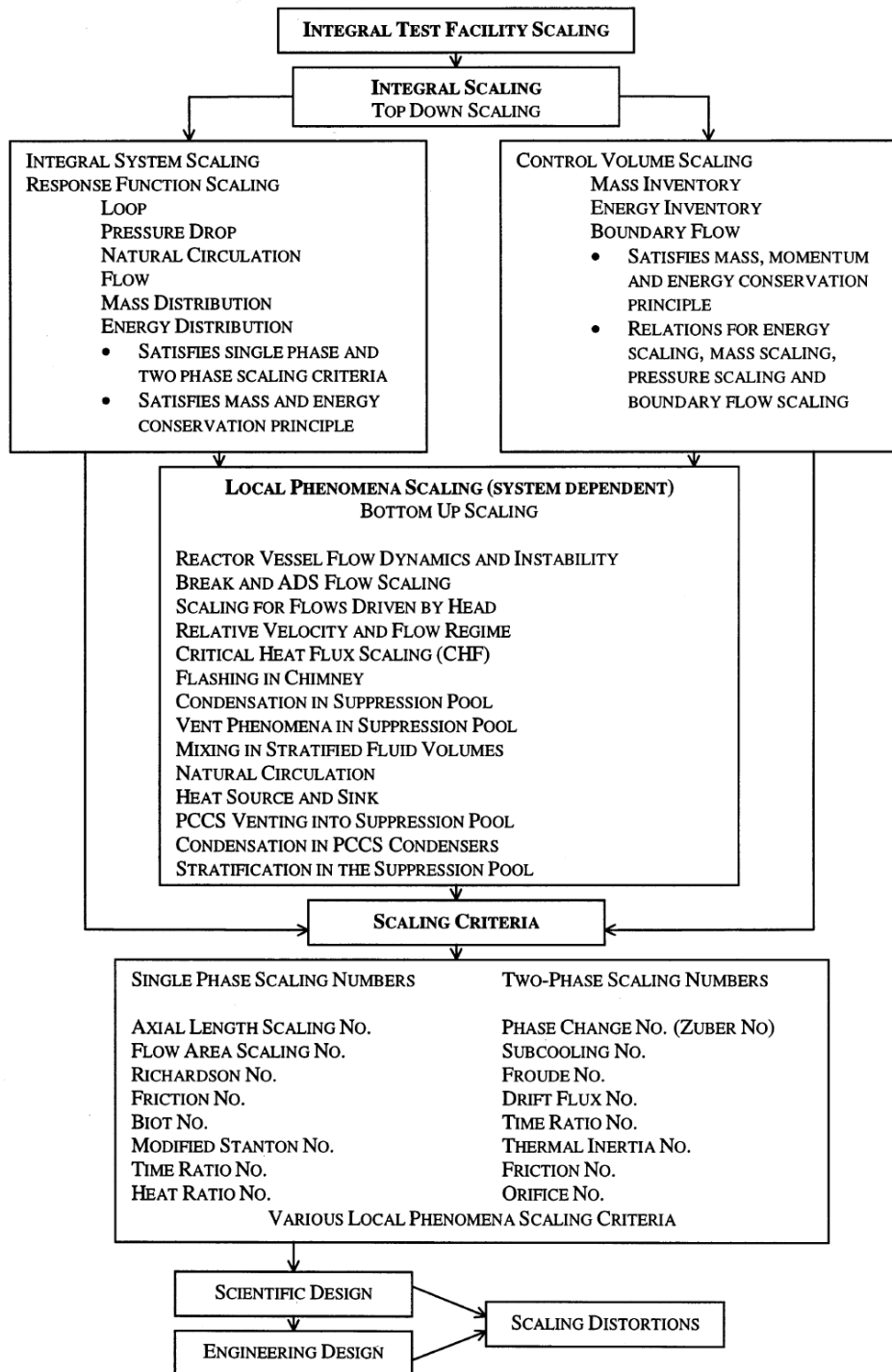


Figure 1.5: Flow chart Ishii three level scaling methodology

1.3.4 Fractional Scaling Analysis

FSA is a quantitative methodology based on the H2TS approach that has been developed to facilitate two aspects:

- scaling-up of time-dependent evolution processes involving an aggregate of interacting modules and processes (such as a NPP).
- the integration and organization of the information and data of interest to NPP design and safety analyses.

Two are the blocks in which relies the FSA, the fractional scaling and the hierarchy. Fractional scaling analysis identifies dominant processes, ranks them quantitatively according to their importance, and provides thereby an objective basis for establishing phenomena identification and ranking tables (PIRT) as well as a basis for conducting uncertainty analyses. At this level, two concepts are essential:

- *Fractional rate of change -FRC-*: parameter associated to system components that shows the degree of variation of an state variable because of the action of an agent of change (e.g. how it changes the pressure (state variable) in primary system (component) as a result of the break mass losses (agent)). This parameter is equivalent to specific frequencies of H2TS approach.
- *Fractional change metric -FCM-*: parameter that quantifies the effect that an agent of change has on the state variable. It is computed by multiplying the FRC of the agent by the time in which it is desired to estimate the evolution of the state variable. Consequently, processes having the same effect metric will be similar because their state variables have been changed by the same fractional amount. This parameter is equivalent to Π of the H2TS approach.

Furthermore, Hierarchical approach is required for analyzing the whole behavior of a system (i.e. NPP). FSA suggest an assessment at three hierarchical levels (three-level synthesis, TLS of Figure 1.6), process level, component level and system level:

| Level of Interest | Synthesis | Result |
|-------------------|--|---|
| Given Process | Of parameters via scaling | <u>Effect Metric Ω</u> Shows the effects of the process as the fraction of change |
| Given Component | Of processes via Effect Metrics Ω | <u>Process Hierarchy</u> Ranks the effect of each process |
| Given System | Of components via matrix assessment | <u>System Matrix</u> Shows the effects of <ul style="list-style-type: none"> • Component interactions • Changes made in components • Trade-offs |

Figure 1.6: Three level synthesis

- *Process level*: The synthesis of parameters governing a particular process is achieved via the effect of FCM. For scaling similarity, FCMs of the different processes should be equal for both the prototype (NPP) and the model (Facility).
- *Component level*: Processes that affect a component are ranked by magnitude (hierarchy process). For experiments, it establishes scaling priorities and, therefore, the design requirements. In addition, if distortions in geometry and/or time cannot be avoided in a given design, the process hierarchy will quantify their effects.
- *System level*: At this level, the synthesis is performed on system components via a System Matrix, which combines the components as rows with their processes (and related FCMs numbers) as columns. The System Matrix represents the scaled coefficients in the system of governing

differential equations for the whole model (facility). Therefore, the system matrix shows the effects of the components' interactions, how postulated changes in the components' design affect the model and what the trade-offs are as a consequence of optimizing it.

Two applications of FSA methodology on LOFT and BETHSY LOCA transients, [12] and [13], were performed in order to demonstrate the potentials of this approach for quantifying scaling distortions as well as for qualifying experimental data. No biases predictions for NPP experimental data extrapolation were reported in that papers.

1.3.5 Roadmap to scaling

On the basis of the wide, rich and robust database of scaling related research and system codes development and qualification studies, Professors F. D'Auria and G. M. Galassi establishes a roadmap to scaling in which BE codes are put as the "pivot" for assessing their scaling capabilities for BEPU calculations and therefore, for licensing. They argue, taking advantage of the extensive background of UNIPI ("scaling puzzle"), and of a clarifying "scaling pyramid" scheme, that accuracy independent of the scale has been sufficiently demonstrated with the dozens of qualified calculations that exist for the dozens of counterpart tests that have been performed at different scales; with the hundreds of qualified calculations of SETs performed at thousands of STFs; with the multiple qualified calculations at NPP scale for operational recorded transients and reported accident transients (TMI-2 NPP); and with the proven scale independence of conduction, heat transfer coefficients and sub-channel mixing equations of BE codes.

Hence, a roadmap to scaling was presented in order to provide a traceable way for putting in order all this background and to establish the basis for demonstrating the validity of BE codes for licensing at NPP level. The roadmap, shown in Figure 1.7, is divided in four consecutive levels.

In the former, scaling parameters must be achieved. It requires selecting the NPP and the scenario to be analyzed, determining the scaling strategy for doing the scaling analysis, and establishing which parameters must be analyzed (hierarchical strategies like the suggested in the H2TS approach can be useful obtaining the relevant T/H parameters). At this level, authors suggest PtoV scaling methodology (further information about PtoV can be found in Section 4.1) and rod surface temperature as the key targets.

In a second level, experimental data must be selected and scaling capabilities of the codes must be demonstrated at closure equations level. Authors strongly recommend the use of counterpart test for which it has been demonstrated their small uncertainty in the measurements (CSNI Validation Matrices of References [16] and [22]).

In the third level, similarity between the experimental data must be assured as well as that the code accuracy is independent of the scaling. For that, qualitative and quantitative criteria (like FFTBM) must be applied as for qualifying ITF nodalizations as for demonstrating that accuracy does not depend on the facility and on the scale. Several studies performed by UNIPI confirm both requirements (see Reference [23] and [24]).

Finally, in the fourth level, NPP nodalization capabilities must be proven in two steps. Formerly, NPP nodalization must be qualified taking advantage of the K_V scaled calculations (more detailed description can be found in Chapter 3), and lastly, reference NPP calculated scenario (following its particular boundary and initial conditions and EOPs must be compared in order to confirm its analogies with reported transients.

1.3.6 Uncertainty Method based on Accuracy Extrapolation

UMAE (see Figure 1.8) is a prototype method developed by the UNIPI for extrapolating the code accuracy of ITFs selected counterpart calculations in uncertainty boundaries for NPP related scenario simulations. This methodology requires the qualitative and quantitative qualification of the ITFs experimental data as well as the NPP and ITFs nodalizations.

For the experimental data of the selected counterpart transients, relevant TH phenomena (RTA) characterized by significant (SVP), non-dimensional (NDP), and integral (IPA) parameters, as well

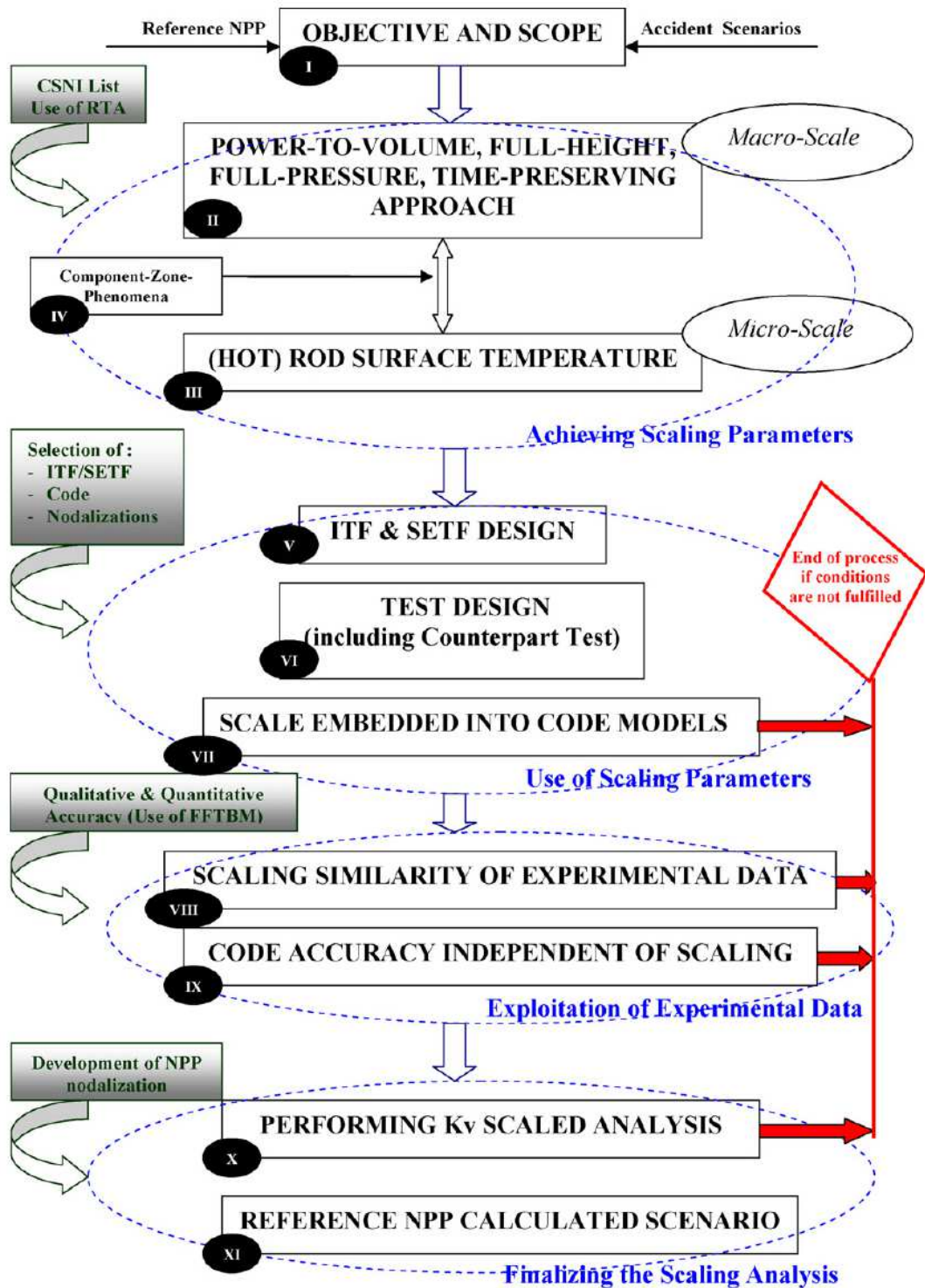


Figure 1.7: Roadmap to scaling

as significant time sequences of transient events (TSE) must be identified and compared. If qualitative and quantitative similarity between the parameters of the counterpart transients is proven,

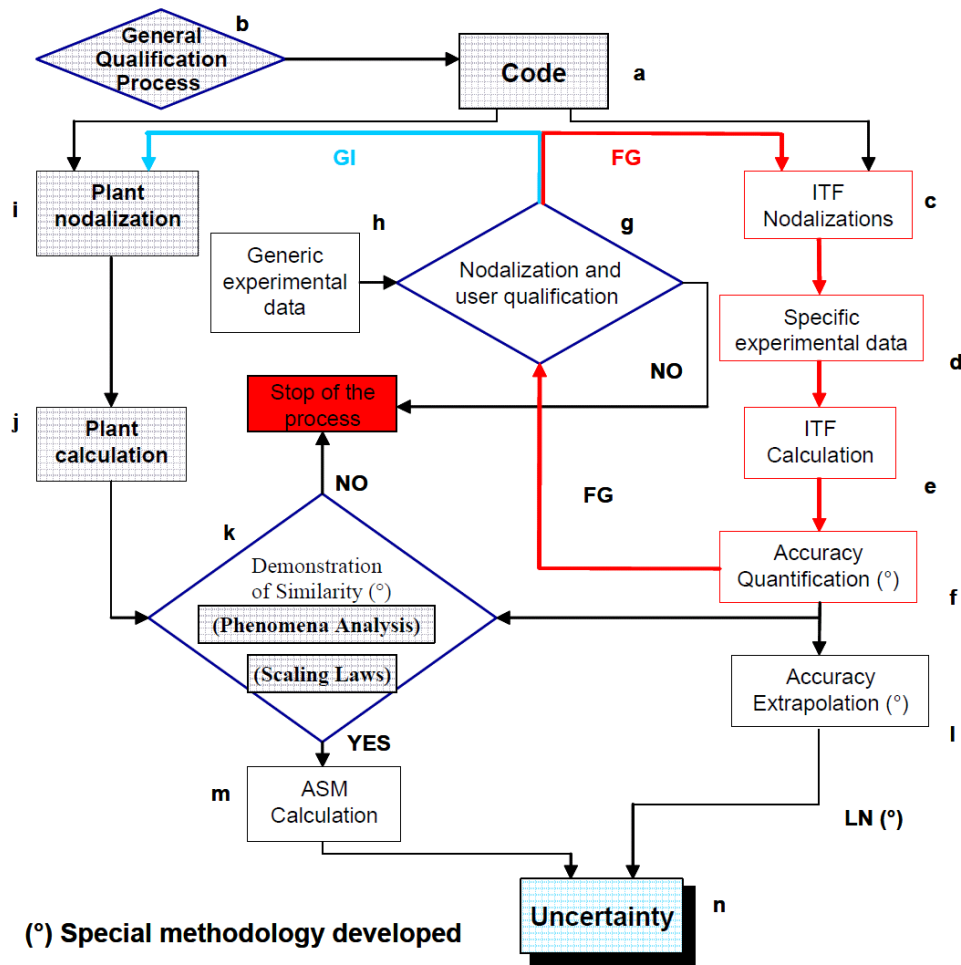


Figure 1.8: UMAEE flow chart

experimental databases will be qualified.

ITFs nodalizations must be checked once quality and analogy of counterpart tests have been assured. ITFs nodalizations must be qualified following the Bonucelli methodology that it is described in Section 1.4. On the other hand, NPP nodalization must be also qualified following the same methodology.

Once nodalizations have been qualified and code accuracy at ITF level has been computed, NPP nodalization must be also validated for the particular boundary and initial conditions of the counterpart tests. A K_V scaled calculation (a detailed description can be found in Chapter 3) must be done and similarity must be checked comparing the RTA, SVP, NDP, IPA and TSE parameters with the equivalent of the ITF transients. If sameness is demonstrated, NPP nodalization will be qualified for the selected scenario (ASM) and NPP "realistic conditions" calculations will be able to be done and ITFs calculations accuracy will be able to be extrapolated in uncertainty boundaries using the statistics described in Reference [25].

1.4 NPP nodalization qualification and quality guarantee procedures

Computational analysis and NPP nodalizations are both a widely used and well-developed application in nuclear engineering not limited to licensing. Most of the tasks, related to the support to Plant operation and control, are extensively discussed in two different IAEA safety reports ([26] and [27]). Some of them can be summarized as in the detailed description of [28] as:

- TH analysis of PSA sequences, mainly those of Level 1.
- Analysis of actual transients.
- NPP start-up test analysis.
- EOP validation analysis.
- Transient analysis for training support.
- Design modifications.
- Improvement of plant availability.

Results presented by the UPC in References [28], [29], [30], [31] and [32] show the usage and effective application of NPP nodalizations in the support to plant operation and control. In that sense, the quality assurance procedures play a key role in the continuous improvement of an NPP nodalization. Examples of NPP nodalization qualification methods are:

UPC Qualification Process of ANAV NPP models [33] [31]

UPC developed a specific methodology based on two levels of qualification: basic and advanced. In the basic level [33], NPP nodalization must be qualified taking as a reference three aspects: NPP Description reports, actual data of the plant operation (including expected and unexpected events) and DBA experiments performed in ITFs (by means of K_v scaled calculations (see Chapter 3). At this level, the application of the Code User Manual Guidelines is an imperative. As regards the advanced level [31], it includes qualification matrices (see Figure 1.9) that allow checking the robustness of nodalizations for different configurations and plant transients. These matrices relate several components of the plant with different real transients at different plant configurations. Therefore the consistency between experimental data and component results confirms the independent accuracy of the components modeling as well as the quality of the whole nodalization.

Bonuccelli qualification methodology [34]

Several papers have been published describing the qualification of ITF nodalizations [35] as well as VVER-1000 nodalizations [36]. This methodology is based on two levels of qualification (V&V validation and verification): steady-state and on-transient levels. In the first one, nodalization must be qualified for an steady-state level, following a: the guidelines of the Code User Manual, b: comparing the input data with the design reference values, and c: checking the results of the steady-state calculations (absolute values and time derivative time trends) with the available operational data. In a second step, so-called transient level, nodalization was qualified with a quantitative (using FFTBM) and qualitative comparison between several calculations of operational transients and their available NPP data.

Giralda methodology [37]

Developed by Iberdrola and recognized by the CSN, Giralda is a quality guarantee methodology used for both core and fuel licensing, and design. It has been used on Cofrentes NPP nodalizations based on CASME and SIMULATE codes. This methodology follows the guarantee guidelines of

1.4. NPP nodalization qualification and quality guarantee procedures

| | | * transient 1 * | * transient 2 * | * transient 3 * | * transient 4 * | * transient 5 * | * transient 6 * | * transient 7 * |
|---------------------------------------|-------------------------------------|--------------------------------|----------------------------------|---------------------------------|---------------------------------|--------------------------------|--------------------------------|---------------------------------|
| | | Reactor trip due to low flow | Reactor trip due to low SG level | Lead rejection from 100% to 50% | Lead rejection from 100% to 50% | Lead swing from 75% to 65% | Lead swing from 65% to 75% | Lead rejection from 100% to 50% |
| Pressurizer's safety system | valves | - | - | - | - | - | - | - |
| | control | - | - | - | - | - | - | - |
| Pressurizer's relief system | valves | - | - | - | - | - | - | - |
| | control | - | - | - | - | - | - | - |
| Pressurizer spray | valves | Spray valve's position/Primary | Spray valve's position/Primary | Spray valve's position/Primary | Primary pressure | Spray valve's position/Primary | Spray valve's position/Primary | Primary pressure |
| | control | pression | pression | pression | | pression | pression | |
| Pressurizer's heater | valves | Primary pressure | Primary pressure | Primary pressure | Primary pressure | Primary pressure | Primary pressure | Primary pressure |
| | control | | | | | | | |
| Main feedwater | main valves | - | - | Main feedwater's flow | Main feedwater's flow | Main feedwater's flow | Main feedwater's flow | Main feedwater's flow |
| | main valves control | | | | | | | |
| | bypass valves | - | - | - | - | - | - | - |
| | bypass valves control | | | | | | | |
| Auxiliary feedwater | turbopump control | - | - | Turbine driven pump speed | Turbine driven pump speed | Turbine driven pump speed | Turbine driven pump speed | Turbine driven pump speed |
| | turbine driven pump's valve control | Auxiliary feedwater's flow | Auxiliary feedwater's flow | - | - | - | - | - |
| | pump valves control | Auxiliary feedwater's flow | Auxiliary feedwater's flow | - | - | - | - | - |
| | | | | | | | | |
| High pressure injection system | control | - | - | - | - | - | - | - |
| Low pressure injection system | control | - | - | - | - | - | - | - |
| Steam dump | control | Average temperature | Average temperature | Average temperature | Average temperature | Average temperature | Average temperature | Average temperature |
| Turbine | | - | - | Turbine's valve position | - | Turbine's valve position | Turbine's valve position | - |
| Control rod system | control | - | - | - | - | - | - | Control rod insertion |

Figure 1.9: Ascó qualification matrix

the "Reference Safety Reports", the specific procedures associated to the particular tipology of the calculations, and the quality guarantee program estipulated by Cofrentes NPP. For the upgrading of the 'frozen codes' , it is required to perform benchmarks that must be evaluated by the regulatory body.

1.4.1 Plant-scaled calculations

As regards scaling, plant-scaled calculations (so-called K_v scaled analyses following Reference [7]) are strongly involved in the qualification process of nodalizations. They consist on adjusting the transient conditions of an NPP nodalization to the test conditions of an ITF experiment. It allows the behavior of NPP and ITF nodalizations to be compared under the same conditions in order to check the capabilities of an NPP nodalization and to improve it if required. Several K_v scaled calculations have been done during recent years ([38], [39], [40], [41], [36] and [42]). Related to the results of Reference [38], Figures 1.10 and 1.11 compare a PWR NPP nodalization with an LSTF post-test calculation in which CCFL and U-tube liquid accumulation took place. The nodalization of the U-tubes in the NPP nodalization was improved by following the conclusions of the LSTF post-test analysis. Results for the plant-scaled calculation showed that a similar system depressurization in both nodalizations (Figure 1.10) led to liquid accumulation taking place in a qualitatively similar way (Figure 1.11). This would be a clear example of how ITF modeling can improve NPP nodalizations.

More detailed information about K_V scaled calculations and the state-of-the art in that matter can be found in Chapter 3.

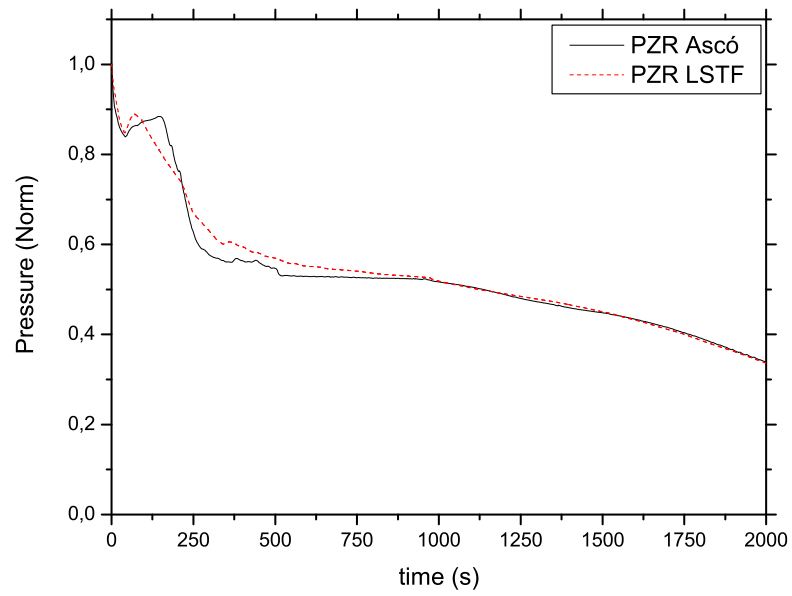


Figure 1.10: Primary pressure

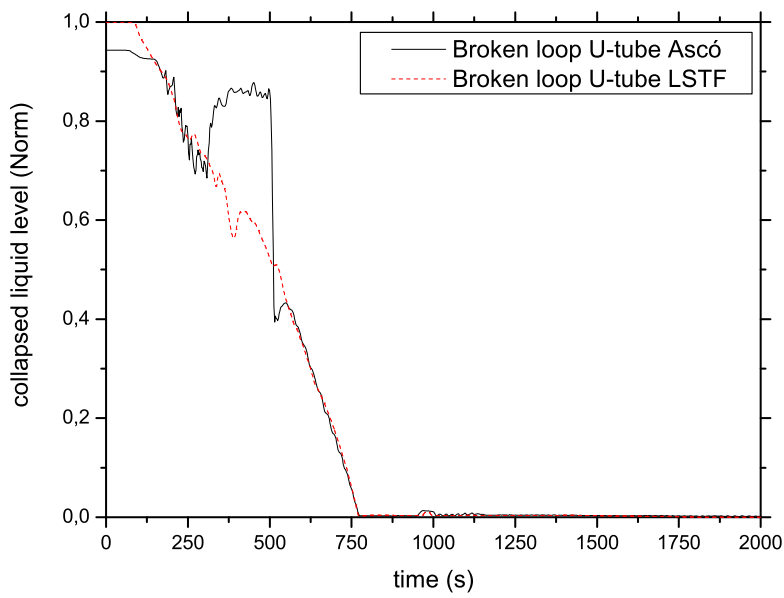


Figure 1.11: U-tube collapsed liquid level

2. ITFs

This chapter provides a detailed description of PKL and LSTF, the Integral Test Facilities that have been studied in the framework of the present Ph.D. thesis. The information of both plants is divided in the following items:

- "*Scaling principles*", a particular review of the scaling-down criteria followed in the design of the ITFs and their components.
- "*Description of the facility*", a general overview of the different components, control systems and instrumentation of the facilities.
- "*Nodalization*", a detailed description of the inputs that have been developed as well as the different improvements that have been added to the initial decks.
- "*Nodalization qualification*", a list of the different post-test analysis that have been performed during the Ph.D. thesis and that are not directly related with the OECD/NEA ROSA-2 PKL-2 Counterpart tests. These calculations have been essential for improving and qualifying the "base" ITFs nodalizations of PKL and LSTF, which is one of the basic steps of the "UPC scaling-up methodology" (further information can be found in Chapter 5).

2.1 LSTF

Since May of 1985, ROSA LSTF test facility, located in Tokai-Mura (Japan), has been used for extensive experimental and analytical investigations that study the integral behavior of pressurized water reactors under accident conditions. The LSTF facility replicates the entire primary system and most of the secondary system (except for the turbine and power generating systems) of the Tsuruga unit 2 NPP, a 4 loop Westinghouse-type design of 1100 MWe [43]. The scheme of LSTF is shown in Figure 2.1 [43].

The test facility models the entire primary system, most parts of the secondary side and all important engineered safety and auxiliary systems. Initially, LSTF was designed in the ROSA-IV program for studying the effectiveness of PWR ECCS during SBLOCAs and operational/abnormal transient. Nevertheless, thanks to their particular features (full pressure, wide and precise instrumentation, and the smallest scaling factor of the known ITFs), LSTF has been employed from 90s until today (in ROSA-V program, OECD/NEA ROSA project, OECD/NEA ROSA-2 project) for studying the relevant thermal hydraulic phenomena as well as the effectiveness of AM actions in case of beyond design basis accidents (BDBA). Gained experimental database has been also applied for the development and the validation of the BE codes. Among others, the study of the following transients and phenomena has been particularly interesting:

- Steam Generator Tube Rupture transients
- Anticipated transients without scram
- Effectiveness of Passive Safety features of PWRs and BWRs
- PV Upper-head and Bottom break LOCAs

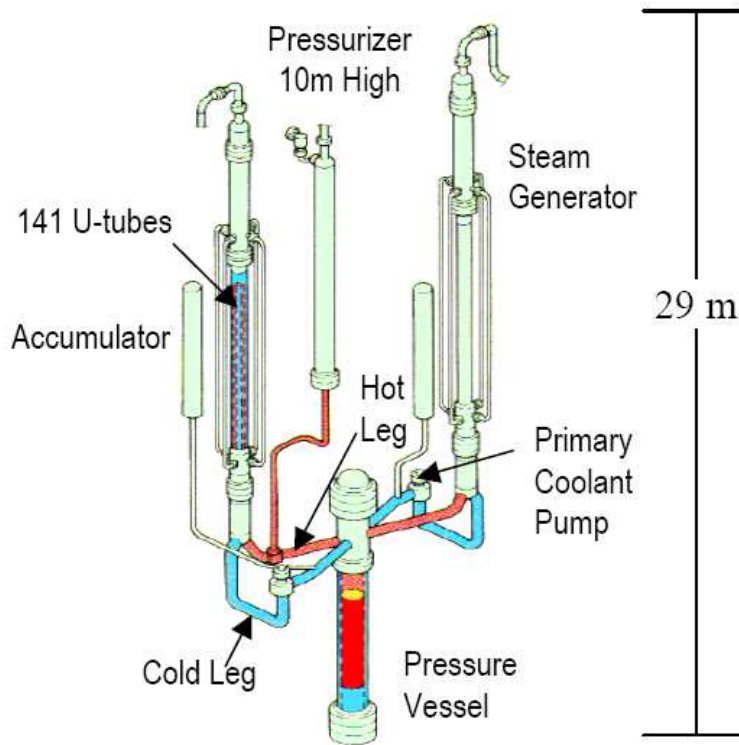


Figure 2.1: The LSTF test facility (source: JAEA [43])

- IBLOCAs
- Temperature Stratification during ECCS coolant injection
- Water hammer
- Natural Circulation with superheated steam
- CCFL at core outlet and U-tubes inlet
- Pressurized thermal shock
- High power natural circulation
- Effects of non-condensables gases in heat transfer across SG U-tubes
- Thermal stratification
- Correlation between CETs and PCTs for the assessment of cooldown AM actions

Finally, it is worth to mention that LSTF is also adapted for simulating well a next generation type PWR such as AP600 reactor.

2.1.1 Scaling principles

As said before, the LSTF facility models the nuclear steam supply system of a 1100 MW nuclear power plant on a scale of 1:48. Detailed design was based to the largest possible extent on the specific data of Tsuruga nuclear power plant, unit 2 [43].

The main aspects of the scaling principles, based on the Power to volume methodology, are:

- Full-scale hydrostatic head (elevations are preserved with a factor 1:1).

- Power, volume and cross sections are scaled down by a factor of 1:48.
- Pipe radius are scaled down by a factor of 6,9.
- The fuel rods are simulated by means of 1008 electrical heat rods with different relative powers to simulate the different rates of burned fuel. Dimensions and ratio of number of fuel rods to number of the guide thimbles are designed to be the same as the 17x17 fuel assembly of the reference PWR. The electrical fuel assemblies and the three different relative powers are disposed in a Cartesian distribution very likely as in a real plant. The maximum power of the facility is limited to 10 MW, which represents the 14% of the scaled down maximum power of a NPP.
- There are two symmetrical loops with an scale of 1 to 24 that is equivalent to 2 loops of the reference plant.
- The number of U-tubes in the steam generator is also scaled down; the whole bundle is substituted here by a total of 141 tubes per SG arranged in 9 different elevations. The total section keeps the scaling factor 1:24 as in the loops.
- Full scale frictional pressure loss designed to be equal to that in the reference PWR for scaled flow rates.
- Flow area in hot and cold horizontal legs is scaled to conserve the ratio of the length to the square root of pipe diameter (L/\sqrt{D} of the reference PWR).

In cases of conflicting requirements, simulation of the phenomena was given preference over consistent simulation of the geometry. For instance, in order to account for important phenomena in the hot legs such as flow separation and counter current flow limitation, the geometry of the horizontal legs is based on conservation of the Froude number as it was described by Taitel and Duckler [44]. Further details about Power to volume methodology can be found in Section 4.1.

The maximum power that facility can achieve is equivalent (taking into account the 1:48 scale factor) to the 14% of the maximum power of a NPP. Therefore, the facility is meant to simulate transients where the reactor has been scrammed. Normally, for transients without scram in which the periods with power greater than 14 % are significant, power decay is delayed for a while in order to add the same energy to the passive heat structures as in the actual NPP transient.

2.1.2 Description of the facility

2.1.2.1 Primary system

The primary system of the LSTF test facility is composed of the reactor pressure vessel (RPV), the two loops and the pressurizer. Each loop can be subdivided into the hot leg, the U-tube bundle, the loop seal, the RCP and the cold leg. The arrangement of the loops is shown in Figure 2.2.

2.1.2.1.1 Reactor Pressure Vessel

The RPV accomodates the core assemblies representing full length 17x17 fuel bundles [43]. It models the upper head plenum, the upper plenum, the reactor core, and the lower plenum. Its wall thickness has a pressure rating of 17.26 MPa. Figure 2.3 show the geometry of the RPV.

The upper head plenum distributes the water to the loops and to the upper plenum. The upper head bypass is modelled by eight symmetrical spray nozzles that join the upper head with the upper part of the downcomer. Therefore, the fluid temperature in the upper head is approximately equal to that in the downcomer at the steady operating conditions. The nozzle diameter can be changed according to the experiment objectives.

The top plate separates the upper head plenum from the upper plenum. Eight control guide tubes connect the highest part of the vessel to the outlet of the core. Coolant from the core is distributed in the upper plenum to the two hot legs.

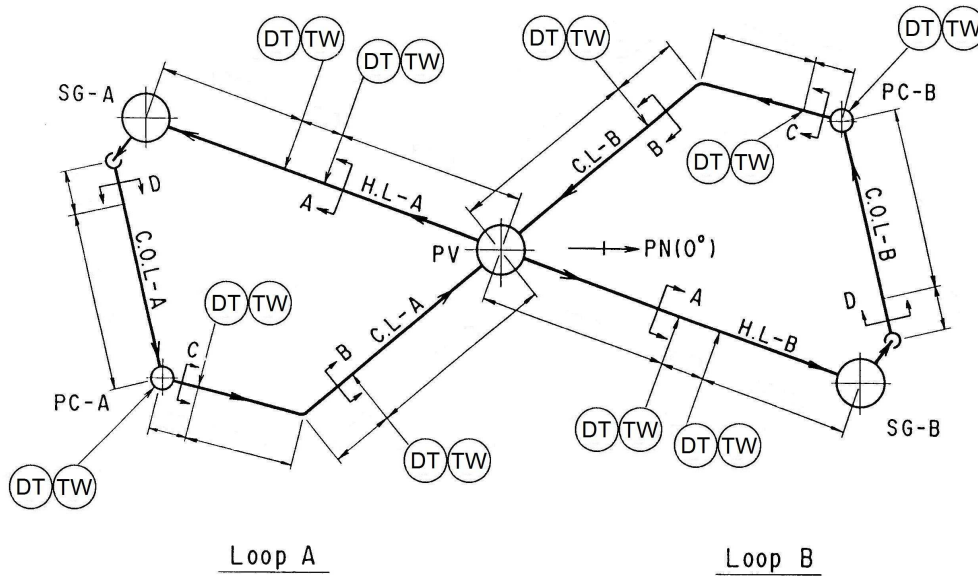


Figure 2.2: The LSTF test facility, loop arrangement and instrumentation (source: JAEA [43])

About the test bundle, it is composed by 1008 electrically heated rods including 24 instrumented heater rods and 96 non-heating rods which simulate control rod thimbles in the reference PWR. They are positioned in 16 square 7x7 bundles and in 8 semi-crescent shaped bundles. Three different power regions (high, mean and low) are present in the core with a chopped-cosine distribution of nine axial divisions. Additionally, core spacers are distributed at nine elevations and core grid is located at the core inlet.

The lower plenum gathers the coolant coming from the downcomer annulus. The extension of the 1008 fuel rods crosses the lower plenum but its influence over the transverse flow resistance is only slightly different compared with that of the modelled reactor [43].

Finally, the RPV downcomer is modelled as an annulus like a real PWR. Downcomer-to-hot-leg bypass is physically characterized by piping to reproduce the leakage between both components. Valves are also included in order to adjust the mass flow rate to the experiment objectives.

2.1.2.1.2 Reactor coolant piping

The reactor coolant piping is composed by the hot legs, loop seals and cold legs. The diameters and the lengths of the hot legs and the cold legs are adjusted to the L/\sqrt{D} of the reference PWR for preserving the Froude Number and the flow regime transitions. Possible break locations are placed in hot legs and cold legs of Loop B. All hot legs have nozzles that permit the entrance of the ECC systems. The surge line is connected to the hot leg of loop A.

The loop seals connect the steam generators to the reactor coolant pumps and have a U form as shown in Figure 2.1. Cold legs connect the RCPs with the downcomer annulus region.

2.1.2.1.3 Reactor coolant pumps

The reactor coolant pumps are canned-type centrifugal pumps with the configuration of the impeller, casing, inlet and outlet regions similar to those of the reactor coolant pump of the reference PWR. Pump speed is electrically controlled, and can be programmed to simulate any desired coast-down curve. Therefore, no flywheel is attached to the RCP rotor. Reverse rotation is not permitted, which is also the case for a real PWR.

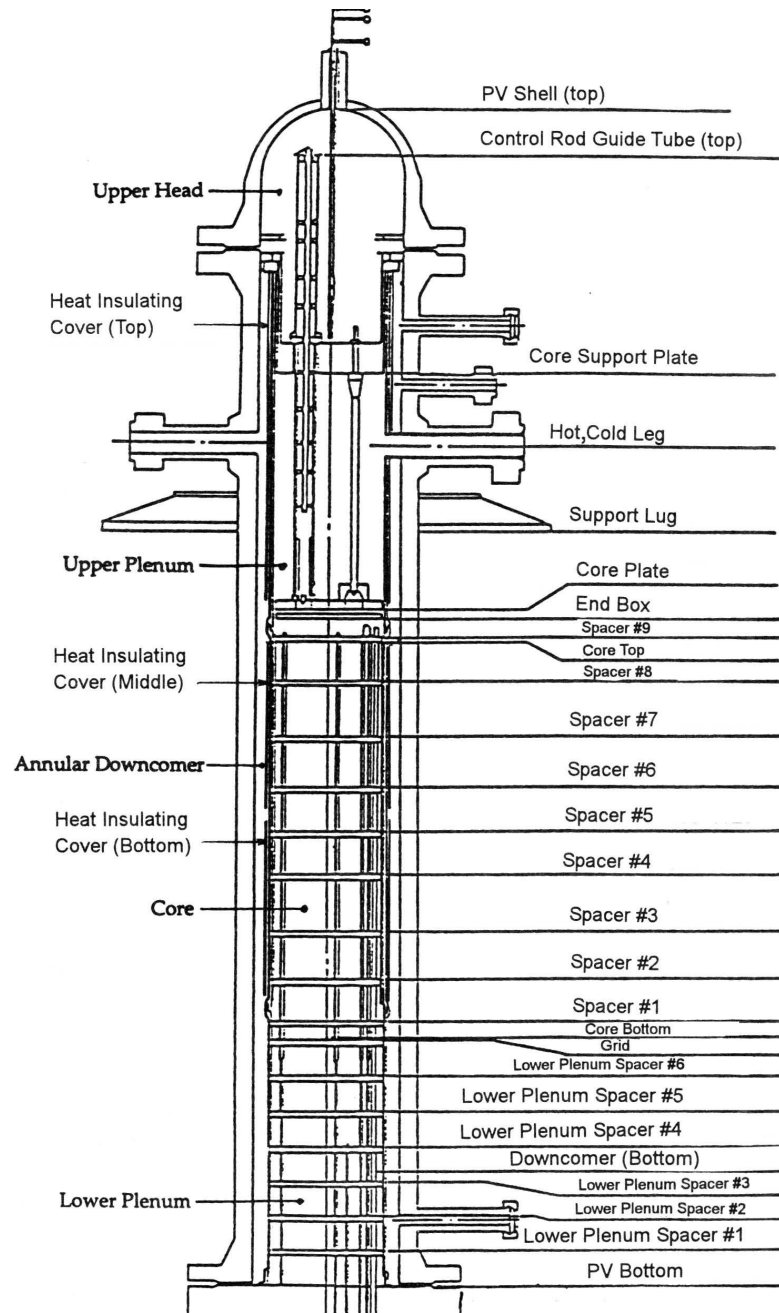


Figure 2.3: The LSTF test facility, view of the RPV (source: JAEA [43])

2.1.2.1.4 Pressurizer

The LSTF pressurizer is a full-height cylindrical vessel constructed from three steel cylinders and a heater flange. While the volume and area is scaled down from a commercial reactor, the elevation is kept equal. Because of the different proportions between elevation and diameter the LSTF pressurizer has more heat losses than in a NPP. This is compensated with Grayloc fasteners, trace heaters and thermal insulation. The pressurizer is connected to the hot leg of loop A by the surge line and to the cold leg of the loop A by the spray line. Nozzles are also provided to connect the pressurizer to the

lines where are located the safety/relief valves.

2.1.2.1.5 *Steam generator primary side*

The U-tubes are modelled as 141 U-tube shaped pipes in a square array with a pitch of 32.5 mm. The number of U-tubes has been scaled down by a factor of 48. The tubes are distributed in 9 different groups that have different elevations. The elevation difference between the lowest and the highest U-tube is 1.6 meters. These lengths are roughly in proportion to the different tube lengths in the reactor.

2.1.2.2 **Secondary system**

The secondary system is comprised of two SG-secondary sides with main steam line for each SG, the steam condensation system with the jet condenser and two cooling units, and the main and auxiliary feedwater systems. For the feedwater systems three pumps are used. The secondary coolant system was designed to simulate the secondary side of the reference PWR except for the turbine and power generating systems. Specifically, the LSTF secondary system is capable of simulating:

- Asymmetric thermal-hydraulic responses in two identical SGs
- Feed and bleed operation in secondary system
- Turbine bypass flow
- Pipe ruptures at the steam line, feedwater line and U-tubes.

2.1.2.3 **Interfacing control systems**

Most of the control system used in a common PWR are modelled in the LSTF test facility for both, the primary and the secondary system. The modelled systems cover a broad functionality; from normal operating systems to emergency systems. Hereafter a brief explanation of these systems is disclosed.

2.1.2.3.1 *Volume control system*

When the system is in operation, the letdown flow can be extracted from the gathering of the RCP the bottom of the pressure vessel. The charging is connected to the inlet of the RCPs. This system compensates for changes in volume of the coolant and supplies water adjusting the pressurizer liquid level.

2.1.2.3.2 *Emergency core cooling system*

The emergency core cooling system of the LSTF test facility is compound by the high pressure safety injection system (HPSI), the low pressure safety injection system (LPSI) and the accumulators. These ECCSs were designed to simulate those of the reference PWR. The operating envelope of each safety injection system can be adjusted to simulate an enhanced or degraded condition.

ECCS can be routed to several locations (hot legs, cold legs, UP, LP,...) allowing to study the effect of the injection location. ECCS injection nozzles in the cold legs are inclined 45 degrees (as in the reference PWR). All ECCS injection ports have an inner sleeve to minimize thermal shock when cold water is injected.

HPIS has two pumps, a high-pressure injection pump and a charging pump. On the contrary, LPIS is controlled by a centrifugal pump. Two accumulators simulate the accumulator injection system. Volumes are 1.5 times larger than the scaled volume of two of the four accumulators in the reference PWR. Each accumulator contains a heater and independent nitrogen charging system, hence the pressure and the temperature of each accumulator can be independently controlled.

2.1.2.3.3 Pressurizer spray system

The pressurizer spray system is used in three different ways: operational spraying, auxiliary spraying from the volume control system and auxiliary spraying from the extra borating system.

2.1.2.3.4 Pressurizer relief system

In a nuclear power plant the pipe discharges into the pressurizer relief tank whereas it is aligned with a separator tank in the LSTF test facility.

2.1.2.3.5 Main steam piping system

In the LSTF test facility the main steam (MS) piping system contains the MS relief isolation valve, the MS relief safety valves, turbine bypass valves and flow limiters and is thus capable of fulfilling all normal operational actions needed in a NPP. The cooldown in a PWR after a LOCA is performed by means of the MS relief valves.

2.1.2.3.6 Feedwater system

The feedwater piping system serves to supply water to the steam generators in power operation and during unit startup and shutdown. This system is controlled according to the SG level.

2.1.2.3.7 Auxiliary feedwater system

The auxiliary feedwater system is an emergency safety system used to guarantee the necessary SG water level and supply the SG with the required feed. The LSTF auxiliary feedwater system is capable of performing all operational actions that a commercial NPP would require. The controlling variable used for the auxiliary feedwater control valves is the measured SG level, as in the modelled reactor.

2.1.2.3.8 Steam generator blowdown system

The steam generator blowdown system in the LSTF test facility serves simply to interconnect two SG on the waterside in the event of loss of feedwater supply to one.

2.1.2.4 Instrumentation

LSTF test facility has about 1760 measurement points that permit an exhaustive analysis of the tests. There are measurement devices for cladding, wall and fluid temperature, differential temperatures, absolute and differential pressure, one and two phase mass flow, liquid levels, momentum flux, density and concentration of non-condensable gases. An example of the distribution of the measurements is shown in Figures 2.2 and 2.4.

Finally, it is worth to mention that the break discharge experimental data have to be computed from other values. One can calculate the break massflow by differentiating the level variation of the two separator vessels (where the discharged water goes) and subtracting the mass released through the separator relief line. Hence, the break massflow is expected to be just an estimation of the experimental value as other effects like fluid density and vaporization might interact.

2.1.3 Nodalization

A RELAP5mod3.3 nodalization of the LSTF test facility (see Figure 2.8) has been developed during the first part of this Ph.D. Thesis. It is based on a previous RELAP5mod3.2 nodalization that was supplied by JAEA. Main features of the developed nodalization are:

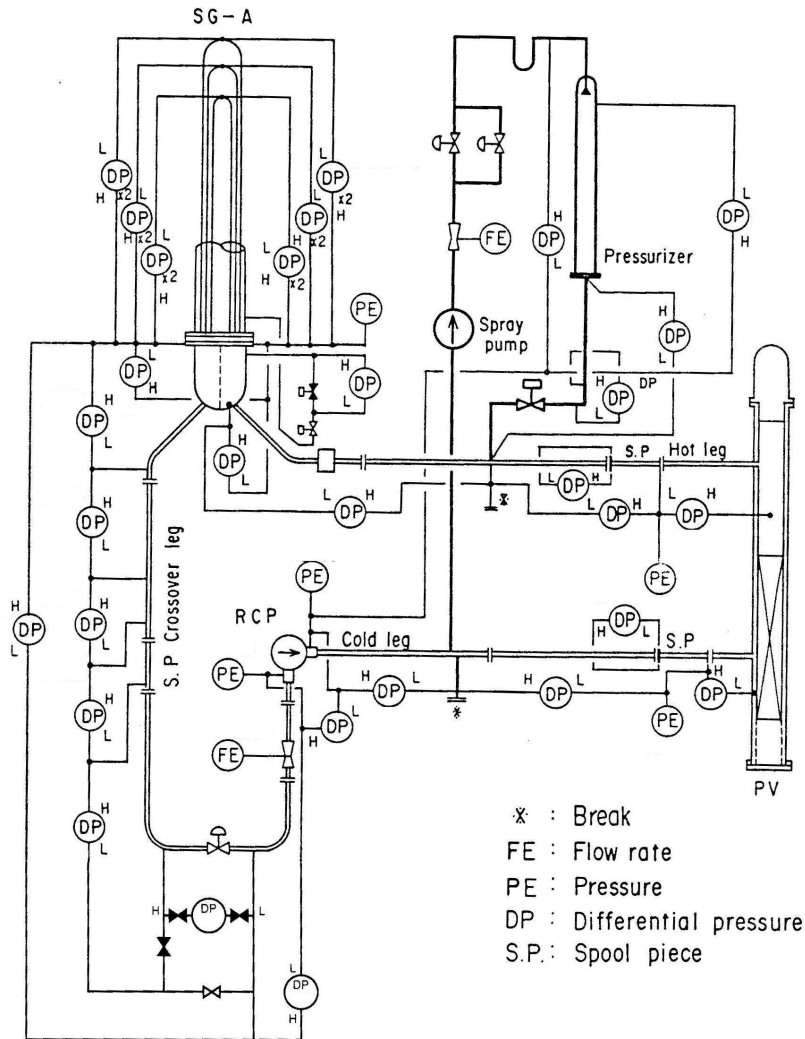


Figure 2.4: Distribution of measurement devices in the loop A (source: JAEA [43])

- 747 volumes
- 1287 junctions
- 1107 heat structures
- 9602 mesh points
- 129 trips
- 322 control variables

Several improvements have been added to the supplied nodalization:

- For the OECD/NEA ROSA Test 3.1 ("SBLOCA ATWS" transient) differential pressures around the loops (Figures 2.5 and 2.6) and also into the vessel (table 2.1) were adjusted to improve the steady-state conditions. Table two shows the deviation in kPa between predicted and experimental data. As RELAP5 code computes pressure in the middle of the volumes, differential pressures were corrected to level the heights.

| Vessel | Elevations [m] | Differential pressures [kPa] | Differential pressures -correcting elevations- [kPa] |
|----------------------|-------------------|---------------------------------|--|
| Upperhead | -2.19 | -9.58 | -1.0 |
| Upperplenum | -2.13 | -0.63 | -0.3 |
| Core | -3.64 | -1.39 | 0.54 |
| Lower plenum -total- | -1.42 | -3.96 | 0.6 |
| Downcomer | -8.8 | 1.53 | 0.0 |
| Total | -8.21 | 28.63 | 0.4 |

Table 2.1: Differential pressures into the vessel

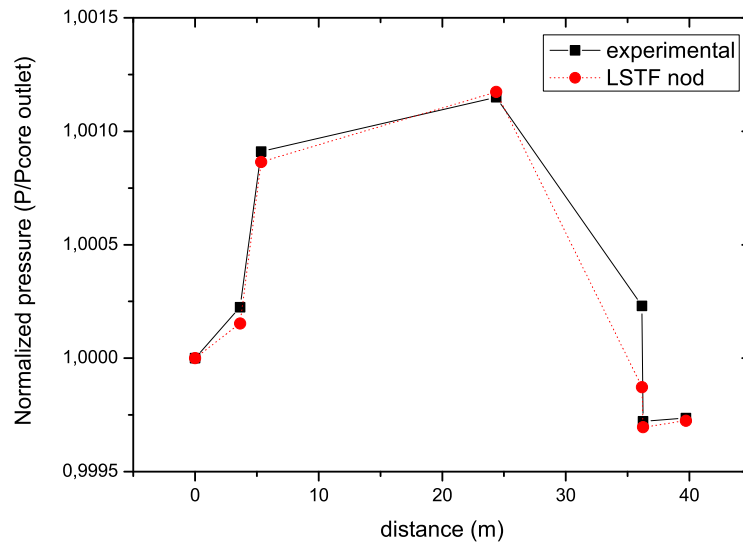


Figure 2.5: LSTF normalized pressure vs. distance on broken loop

- For the OECD/NEA ROSA Test 3.2 ("LOFW ATWS" transient), five U-tube models were designed (see Figure 2.8) to reproduce the nine LSTF U-tube types: one simulating the shortest one (this length was kept in order to reproduce the moment in which natural circulation is completely lost), and the others averaging of pair wise the rest of the lengths. Steam generators were also modified in the secondary side, increasing the number of volumes of the riser for improving the ΔT s along the UTs, and reproducing both annulus in the top and the bottom of the downcomer. Furthermore, surgeline was re-nodalized, keeping lengths and heights as well as pressure drops, location and orientation of its inlet nozzle in the hot leg, and reproducing the multiple orifices in the inlet of the pressurizer. Finally, the line between the pressurizer and the storage tank was changed taking into account geometries referred in [43] for the discharge lines nodalization.
- Finally, for the the OECD/NEA ROSA-2 Test 3 ("SBLOCA" Counterpart test), RPV nodalization criterion was completely modified. Downcomer annulus was split in two parallel components and transversal lengths, paths and RELAP5 momentum equations were activated in order

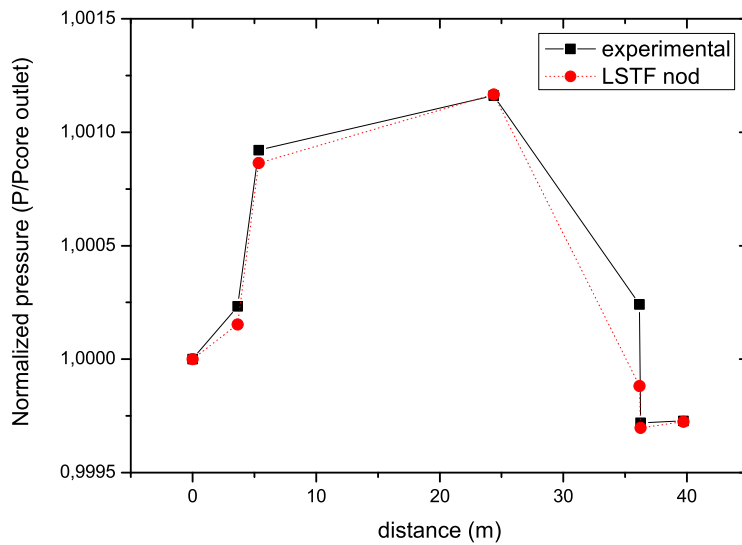


Figure 2.6: LSTF normalized pressure vs. distance on intact loop

to reproduce possible ECCS bypass. Core region was divided in 13 channels of 18 axial levels transversally distributed in the cartesian array that is reported in the facility description report [43] (see Figure 2.7). FAs transversal lengths and RELAP5 transversal momentum equations were also activated in order to take into account the possible ΔP s during saturated conditions and the real superheated flow path of the vapour during the core dryout. Finally, the upper plenum was modified simulating it with two channels, one hot channel, connected to the outlet of the hottest core channel, and another one simulating the rest of the plenum. Transversal momentum equations were activated too in order to consider ΔP s in the vessel that could affect flow path to the hottest channel during the refilling of this particular test conditions (HPIS is connected to the upper part of the UP).

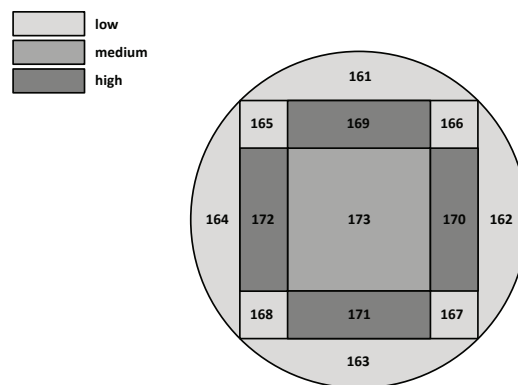


Figure 2.7: LSTF nodalization: cartesian distribution

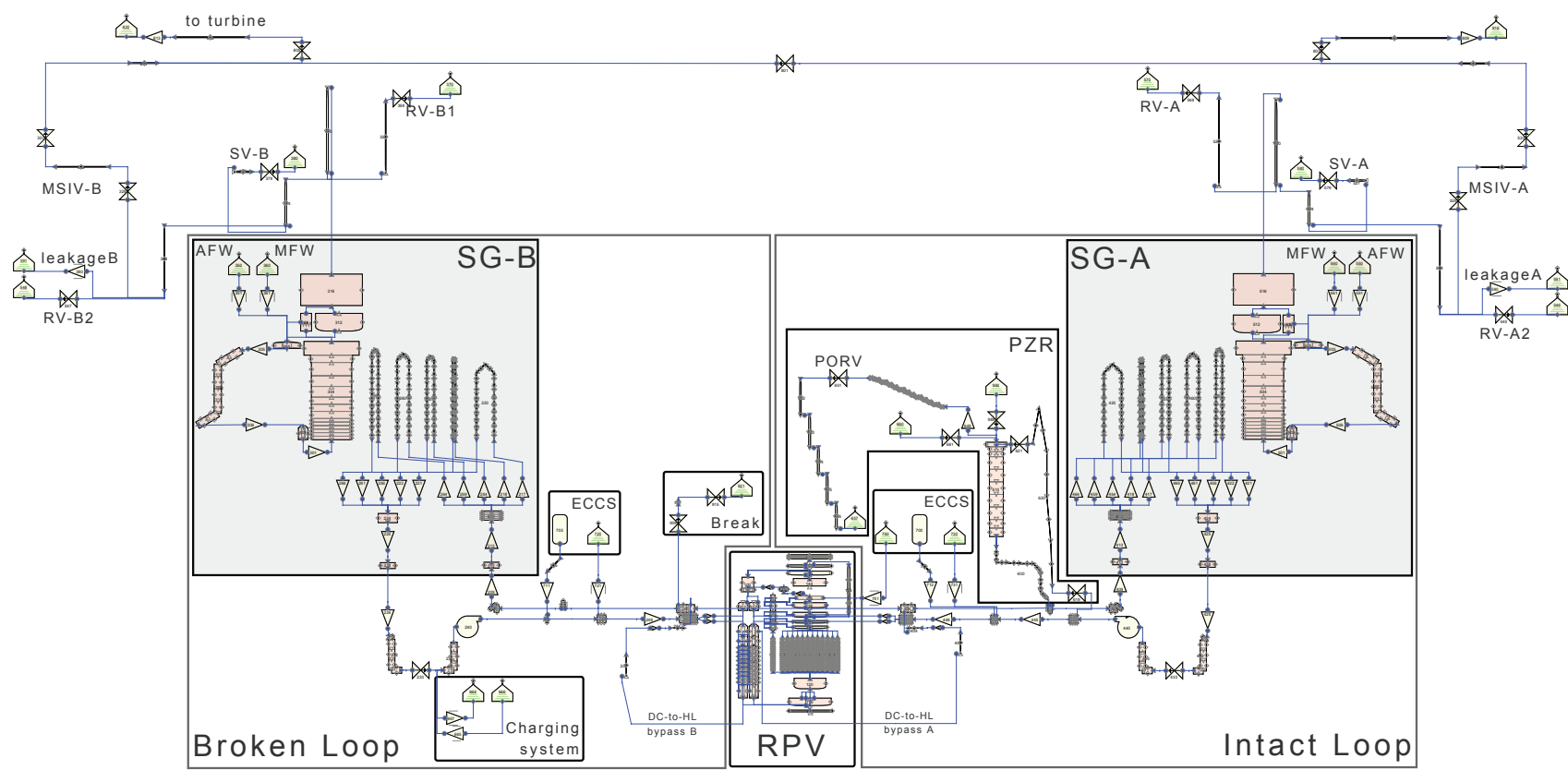


Figure 2.8: LSTF nodalization
29

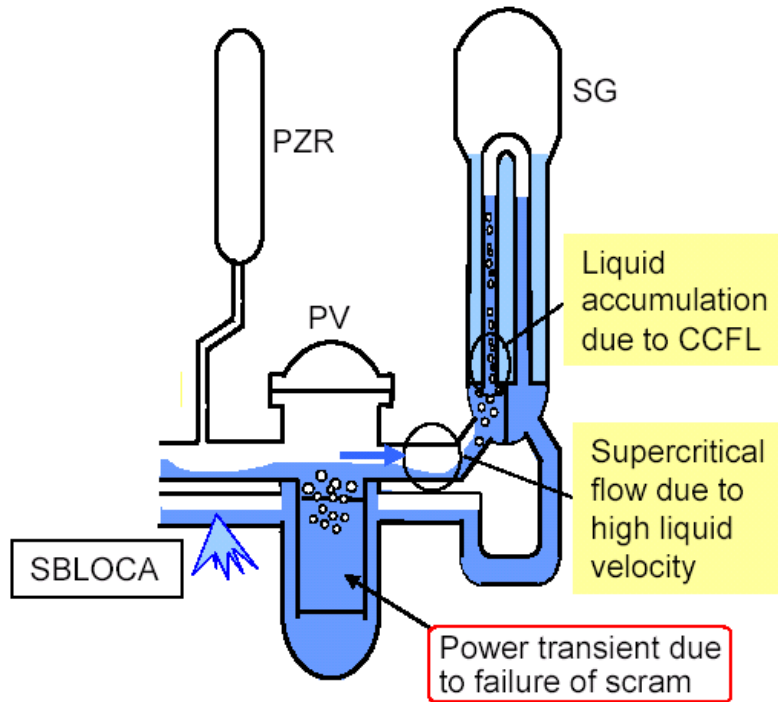


Figure 2.9: Thermohydraulic phenomena during SBLOCA without SCRAM (source JAEA)

2.1.4 Nodalization qualification

UPC LSTF nodalization capabilities have been tested during the participation of the UPC in the OECD/NEA ROSA and ROSA-2 projects. The input deck was continuously improved during the simulation post-test 3.1, 3.2 and the Counterpart test 3, as well as with the participation in the blind IBLOCA tests 1 and 2. All improvements were included in the previous post test calculations so a unique robust nodalization was able to represent all tests at a similar accuracy. Detailed below are the results of the test 3.1 and 3.2 that were published in References [45] and [46].

2.1.4.1 OECD/NEA ROSA Test 3.1

2.1.4.1.1 High Power Natural Circulation Events

High-power events are transients with failure of scram in which core power decrease is due to negative reactivity feedback. Depending on the transient characteristics, this situation can lead to a relatively high core power during a long time.

Natural circulation occurs in transients with gradual loss of mass inventory (SBLOCA or LOFW -losses across the pressurizer relief valve due to overpressure on the primary system-). While there is high core power and water in the loops, vapor and liquid with high velocity exit from the vessel to the hot legs inducing supercritical flow during natural circulation. This phenomenon affects the coolant distribution due to counter-current flow limitation (CCFL) during condensing reflux at the inlet of the steam generators and U-tubes which causes liquid accumulation in them (see Figure 2.9).

Break flow rate and liquid carry-over into the pressurizer are affected by this phenomenon too.

2.1.4.1.2 Test conditions and description of the transient

Test 3-1 simulates a SBLOCA (break size of 1%) with scram failure and loss-of-offsite-power (HPI and LPI are unavailable). Due to the high-core power, supercritical natural circulation exists in the

hot legs until the loops become empty. CCFL at the inlet of the steam generators and U-tubes during the two-phase natural circulation are objective of study in this test.

The hardware configuration of LSTF is described in References [43] and [47]. Some important points are the following:

- Break assembly: small break in the cold leg without pressurizer (1 % of the scaled cross-sectional area of the reference PWR cold leg).
- ECCs: HPI and LPI are unavailable simulating loss of off-site power.
- Core power curve: pre-determined from a previous volumetrically scaled analysis performed with SKETCH-INS/TRAC-PF, which reproduces the transient in a commercial PWR.
- LSTF core protection system: Core power is modified according to the maximum fuel rod surface temperature

Initial steady-state conditions were fixed according to the reference PWR conditions. Because of the LSTF initial core power (14 % of the scaled PWR nominal core power) core flow rate was set to 14 % of the scaled nominal flow rate to obtain the same PWR temperatures, and secondary pressure was raised to limit the primary-to-secondary heat transfer rate to 10 MW. Table 2.2 shows the steady state values of the simulation normalized by the real experimental values.

| Parameter | UPC RELAP5 nodalization |
|-------------------------------------|-------------------------|
| Core Power [kW] | 0.990 |
| Hot leg temperature [K] | 1.0 / 0.9997 |
| Cold leg temperature [K] | 1.001 / 1.0 |
| Mass flow rate [kg/s] | 1.04 / 1.021 |
| Primary pressure [Pa] | 1.001 / 1.001 |
| Pressurizer level [m] | 1.003 |
| Secondary pressure [Pa] | 0.971 |
| Secondary side liquid level [m] | 0.998 / 0.998 |
| Main feed water temperature [K] | 1.003 / 0.998 |
| Auxiliary feedwater temperature [K] | 1.001 / 0.999 |
| Accumulators pressure [Pa] | 1.0 |
| Accumulators temperature [K] | 1.0 / 1.0 |
| Steam flow rate [kg/s] | 1.002 / 1.029 |

Table 2.2: Test 3.1 Steady state conditions

The transient is started opening the break at $t = 0$ s. After 20 seconds the scram signal is generated causing the closure of the MSIV and the stop valve (turbine trip); pressurizer heater is off, main feed water is closed and auxiliary feed water is started. Three seconds later, coast-down of the primary coolant pumps is initiated. Until 300 seconds while there is high core power, secondary pressure rises over the specified set-point causing the continuous opening of the SG relief valves and generating two-phase natural circulation in the primary loops. Between 300 and 1,600 seconds of the transient, the primary system is coupled with the isolated secondary system, which is depressurized with the cool auxiliary feed water that condenses vapor of the steam generators.

About 1,100 seconds, core liquid level starts to decrease rising the average temperature of the system. Then, the LSTF core protection system actuates decreasing the core power until the maximum fuel rod surface temperature is achieved. As a result of the low power, the primary pressure

falls down below the secondary. About 2,100 seconds after the start of the transient, the accumulator injection system initiates causing a loop seal clearing in the loop without pressurizer 100 seconds later. At 5,547 seconds the break is closed and the transient finished.

The main events are described in table 2.3.

2.1.4.1.3 Post-test results

Table 2.3 shows the chronology of the main events occurred in Test 3-1, comparing the experimental values with the calculated ones.

| Main Events | Experimental [s] | Calculated |
|--|------------------|---------------|
| Start of the test | 0.0 | 0.0 |
| SCRAM signal: · Turbine trip and closure MSIV · PZR heater off · End of MFW and begin of AFW | 20.0 | 20.0 |
| Start of RCPs coastdown | 23.0 | 23.0 |
| RCPs stop | 272.0 | 272.0 |
| End of continuous opening of SG RVs, End of two phase natural circulation, break flow from single-phase liquid to two-phase flow | About 300.0 | About 300-400 |
| Core liquid level starts to decrease (core uncovery) | About 1100.0 | About 1100.0 |
| Core power decrease by LSTF core protection system | 1630.0 | 1707.0 |
| Max. fuel rod surface temperature | 1825.0 | 1875.0 |
| Primary pressure lower than SG secondary pressure | About 1900.0 | 1875.0 |
| Initiation of accumulator injection system | About 2100.0 | 2180.0 |
| Loop seal clearing only in loop without PZR | About 2200.0 | 2898.0 |
| End of the transient | 5547.0 | 5547.0 |

Table 2.3: Test 3.1 Main events

As shown in Figure 2.10 primary and secondary pressure have good agreement with the experimental data until 2,100 s, when the initiation of the accumulator injection system causes some discrepancies on primary pressure and break mass flow (see Figure 2.11). In the UPC-INTE model, accumulators refill cold legs increasing the mass flow across the break.

Figures 2.12 and 2.13 show how the UPC-INTE model reproduces natural circulation and emptying of the core.

The UPC-INTE model performs a good secondary cooldown. It reproduces continuous opening of the relief valves during natural circulation (see secondary pressure in Figure 2.10) and adjusts correctly the steam generators collapsed liquid level (see Figure 2.14).

Figure 2.15 shows rod surface temperature has a quite good agreement with experimental data until the initiation of accumulators because of a correct LSTF core protection system implementation (see Figure 2.16).

Finally, it is observed that with a pre-determined core power curve (Figure 2.16) RELAP code predicts the increase in core void fraction (Figure 2.17) that induces the negative reactivity feedback

which is the main factor of core power drop).

2.1.4.1.4 Liquid accumulation due to CCFL

Supercritical flow during two-phase flow Natural Circulation induces liquid accumulation in the U-tubes during reflux condensation because of counter current flow limitation in the inlet U-tube and in the bottom of the inlet plenum (see Figure 2.9). Partial core drop is observed as a result of this accumulation.

RELAP5mod3.3 reproduces supercritical flow (Froude number > 1) during the two-phase flow natural circulation (see Figure 2.18) and simulates related phenomena like horizontal stratification in the hot leg (Figure 2.19) and a partial drop of its level during supercritical flow (Figure 2.20 shows an asymmetrical drop of the UPC-INTE model collapsed liquid level during a 100-200 seconds interval which seems to be related to the Froude number values of Figure 2.18).

RELAP5/mod3.3 simulates a small negative liquid velocity (Figure 2.21) and a positive gas velocity (Figure 2.22) at the U-tube inlet during one-phase gas flow with high vapour velocity (from 400 seconds to 800 seconds approximately). These velocities justify counter current limitation at the U-tubes inlet and a possible liquid accumulation in them.

As shown in Figures 2.23 and 2.24, although asymmetrical effect is not reproduced, the UPC-INTE model simulates the U-tube liquid accumulation phenomenon and its related partial core level drop (see Figure 2.25).

2.1.4.1.5 Loop seal behavior

The UPC-INTE model shows discrepancies in primary pressure and break mass flow rate after the initiation of the accumulator injection system. In the simulation there is an important delay between the accumulators entrance (2180 seconds -see Figure 2.26-) and the loop seal clearing in the broken loop (2898 seconds -see Figure 2.28; black-green lines show the level between the SG outlet and the loop seal bottom, and red-blue lines show the level between the loop seal bottom and the pump inlet-).

As shown in Figure 2.26, there are important discrepancies in the accumulator injection. This could be one of the factors why water distribution around the loops is different between the UPC-INTE model and the experimental data (see in Figures 2.27 and 2.28 the opposite loop seal behavior after the initiation of accumulators system).

2.1.4.1.6 Conclusions

A developed model of the LSTF Test Facility has been adjusted and has proved to be a suitable tool to simulate the behavior of this facility.

The post-test calculation for Test 3-1 has been performed. Model predictions were in quite good agreement with the available experimental data. Several conclusions have been obtained from the study of local phenomena (U-tube liquid accumulation due to CCFL and loop seal behavior) and preliminary calculations:

- RELAP5/mod3.3 reproduces supercritical flow and liquid accumulation in the U-tubes during High-Power Natural Circulation.
- There is an important delay in the loop seal clearing as a result of a different accumulator injection and an incorrect water distribution around the primary system after their actuation.

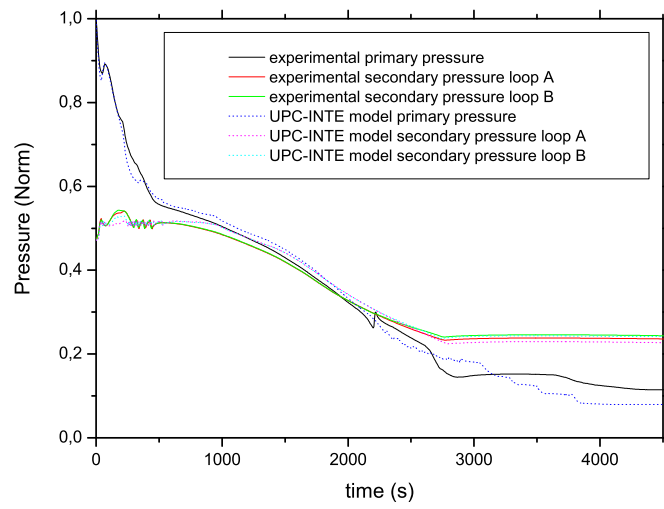


Figure 2.10: LSTF system pressures

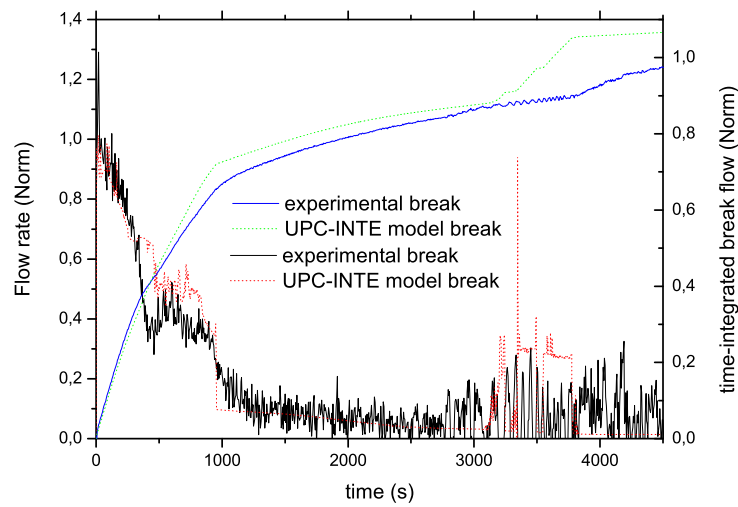


Figure 2.11: Break mass losses

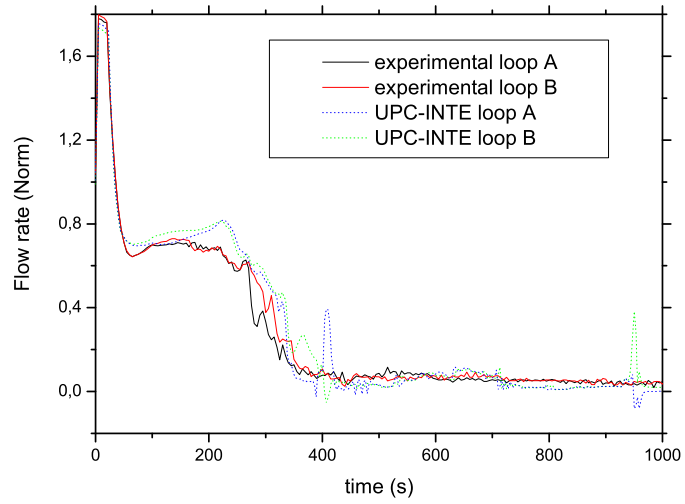


Figure 2.12: Mass flow rate of primary system loops

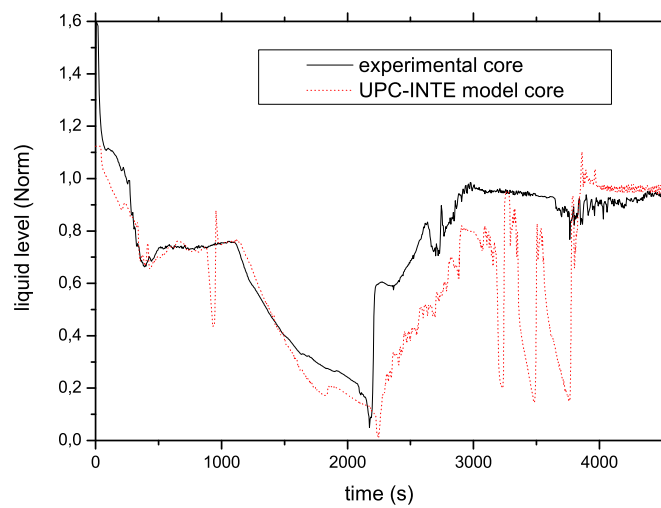


Figure 2.13: Core collapsed level

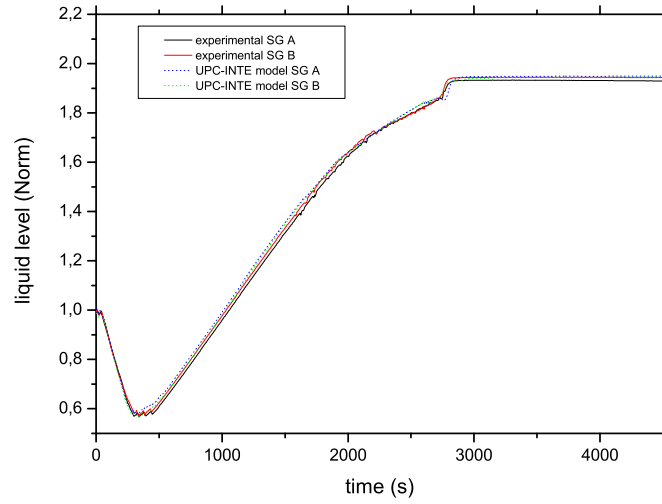


Figure 2.14: SGs liquid level

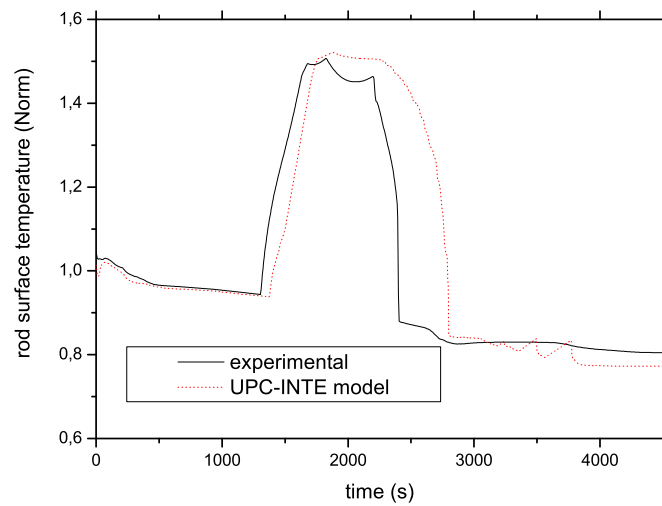


Figure 2.15: Peak cladding temperature

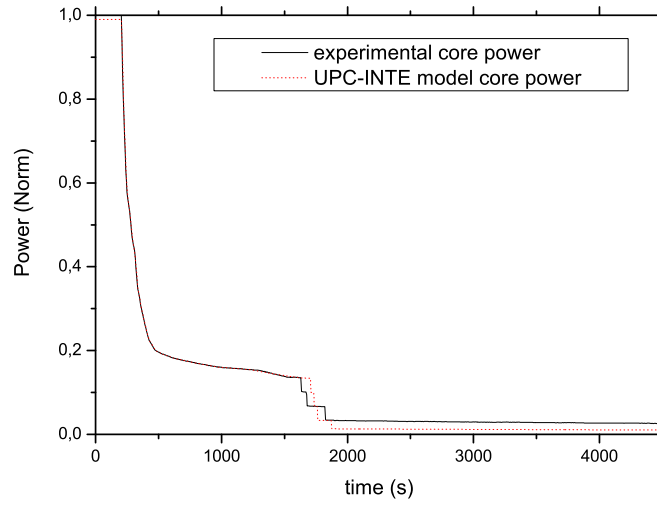


Figure 2.16: Core Power

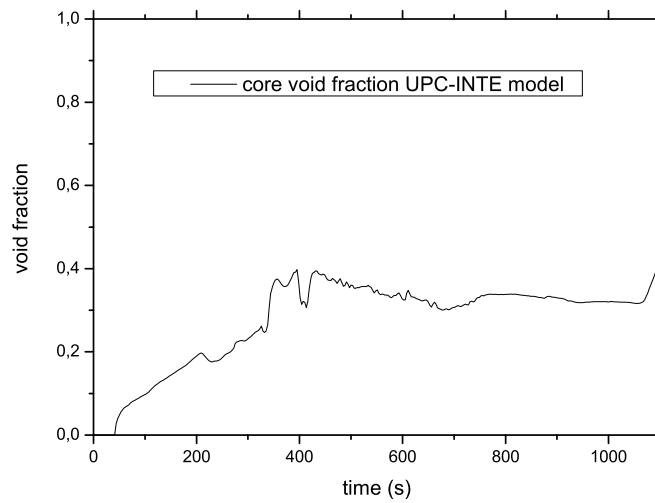


Figure 2.17: Core void fraction

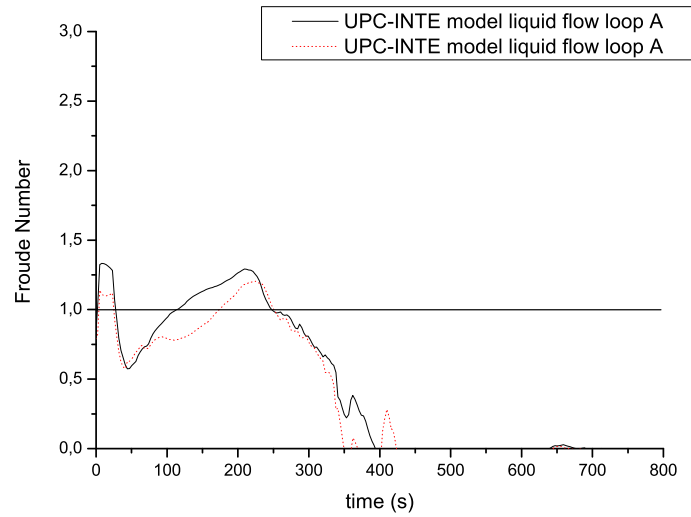


Figure 2.18: Froude number on the broken loop hot leg

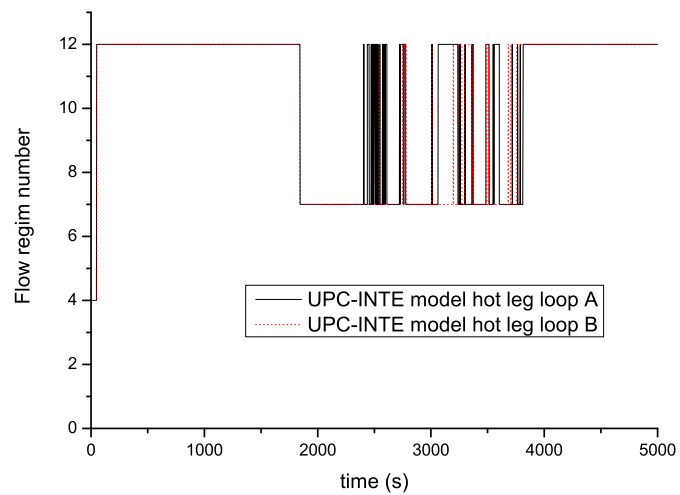


Figure 2.19: Flow regim number. Horizontal stratification associated to 12 value

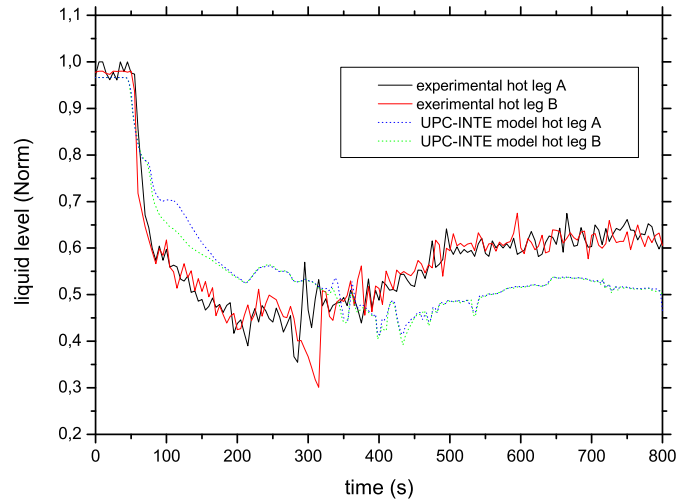


Figure 2.20: Hot leg collapsed liquid level

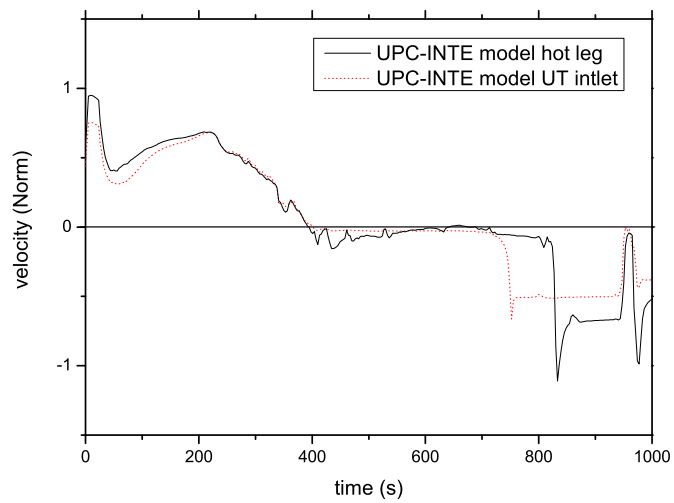


Figure 2.21: Loop B liquid velocities

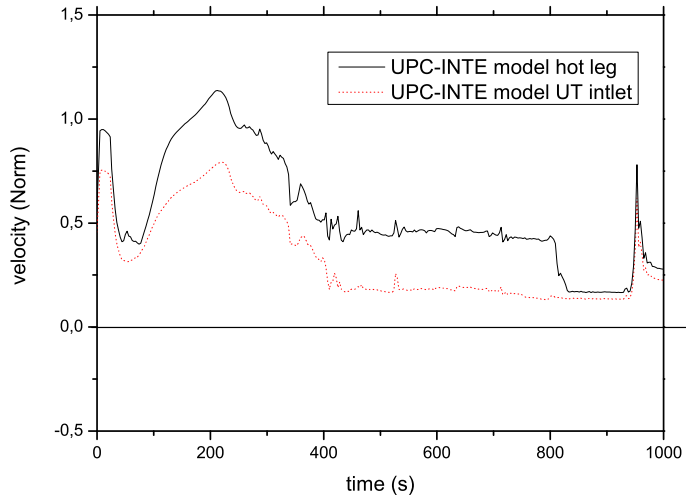


Figure 2.22: Loop B vapour velocities

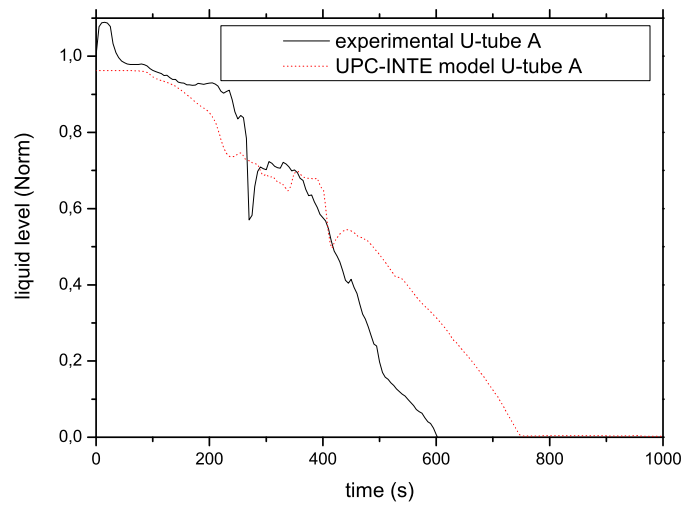


Figure 2.23: Collapsed level of the Loop B UT

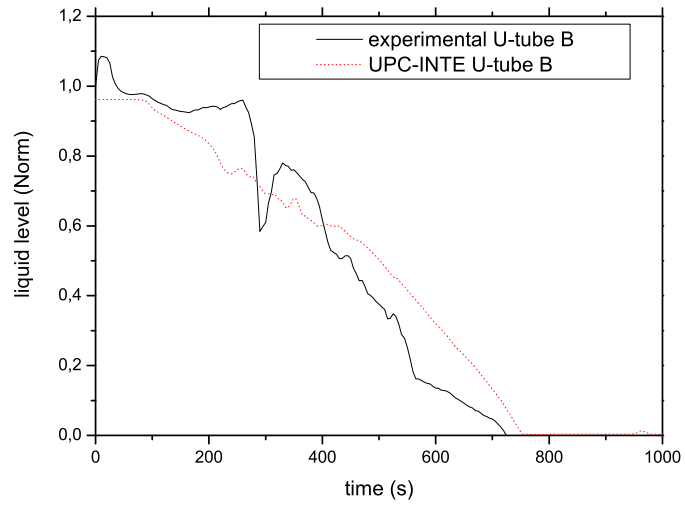


Figure 2.24: Collapsed level of the Loop B UT

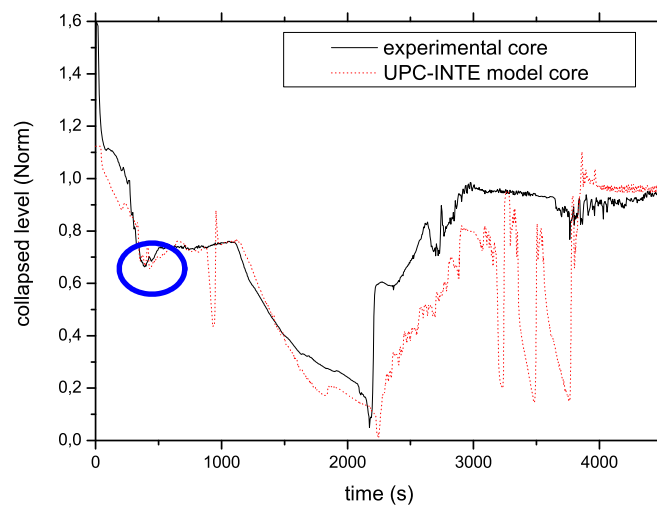


Figure 2.25: Core collapsed level

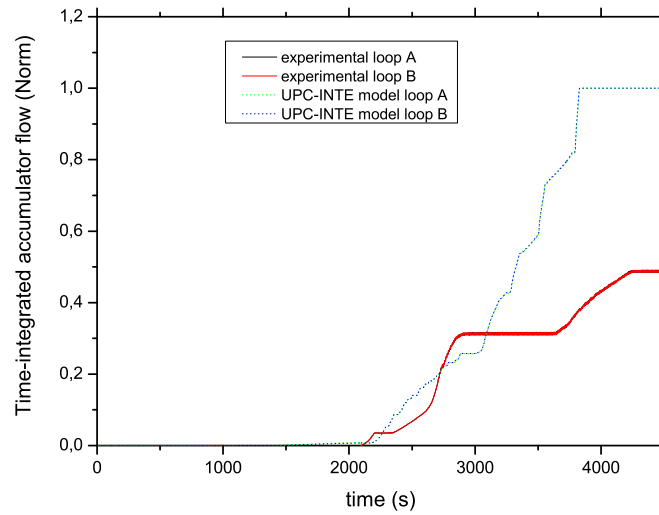


Figure 2.26: Time integrated accumulator mass flow rate

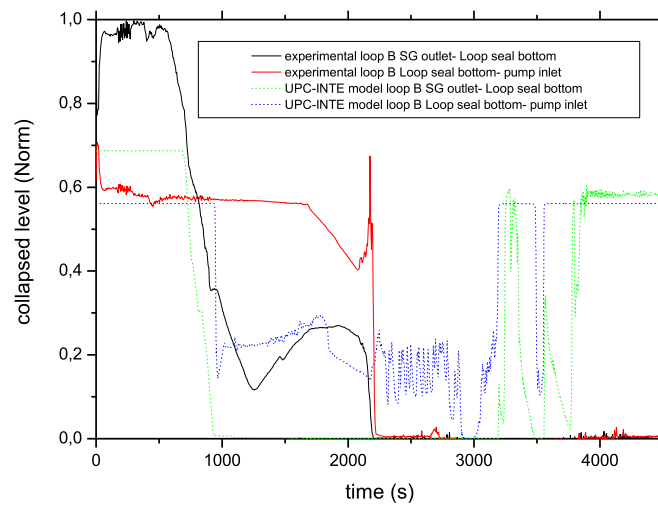


Figure 2.27: Loop seal A collapsed level

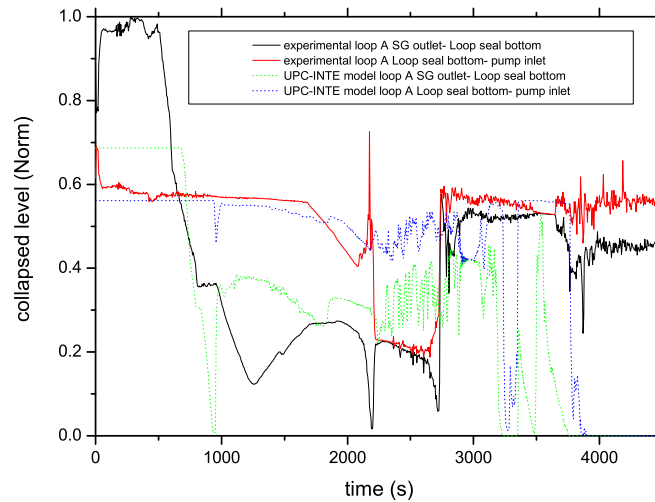


Figure 2.28: Loop seal B collapsed level

2.1.4.2 OECD/NEA ROSA Test 3.2

2.1.4.2.1 High Power Natural Circulation Events

High-power events are transients with failure of scram in which core power decrease is due to negative reactivity feedback. Depending on the transient characteristics, this situation can lead to a relatively high core power during a long time.

Natural circulation occurs in transients with gradual loss of mass inventory (SBLOCA or LOFW -losses across the pressurizer relief valve due to overpressure on the primary system-). While there is high core power and water in the loops, vapor and liquid with high velocity exit from the vessel inducing supercritical flow during natural circulation. This phenomenon can modify significantly the coolant distribution affecting the core cooling. Particularly, for a LOFW-ATWS, the high pressure drop in the pressurizer PORV pulls in the supercritical flow in the hot leg at the surge line inlet nozzle, causing a counter-current flow limitation (CCFL) in the bottom of the pressurizer. It avoids that coolant returns to vessel for cooling the core (see Figure 2.29).

2.1.4.2.2 Test conditions and description of the transient

Test 3-2 simulates a LOFW transient without scram under the assumption of a total failure of the HPIS system and an actuation of the AFW. Liquid accumulation in the U-tubes during the natural circulation and coolant carryover from the hot leg into the pressurizer are objective of study in this test.

The hardware configuration of LSTF is described in References [43] and [47]. Some important points are the following:

- ECCs: HPI and LPI unavailable simulating loss of off-site power.
- AFW: initiated when SG collapsed liquid level is less than its 3%.
- Core power curve: pre-determined from a previous volumetrically scaled analysis performed with RELAP5 code using one-point-kinetics model, which reproduces the transient in a commercial PWR. (see Reference [48] and [49] for more detailed information). As LSTF core power

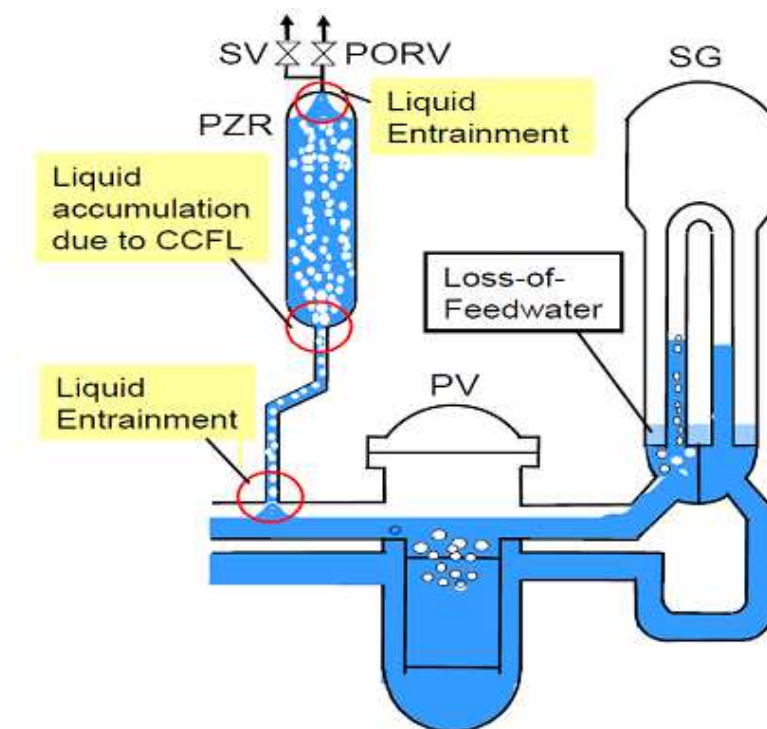


Figure 2.29: Thermalhydraulic phenomena during LOFW without SCRAM

is limited to the 14 % of the scaled reference plant nominal power, the portion higher than 10 MW is cut-off (see first 200 s of Figure 2.30).

- LSTF core protection system: Core power is modified according to the maximum fuel rod surface temperature.
- PZR heaters: shut off with the scram signal (proportional heater) and when the PZR level becomes lower than its 20 % (backup heater).

Initial steady-state conditions were fixed according to the reference PWR conditions. Because of the LSTF initial core power (14 % of the scaled PWR nominal core power), core flow rate was set to 14 % of the scaled nominal flow rate to obtain the same PWR temperatures, and secondary pressure was raised to limit the primary-to-secondary heat transfer rate to 10 MW. Table 2.4 shows the steady state values of the simulation normalized by the real experimental values.

The transient starts at $t=0$ seconds with the loss of main feedwater in the secondary system. After 50 seconds the scram signal is generated causing the closure of the MSIV and the stop valve (turbine trip); pressurizer proportional heater is switched off and coastdown of the primary coolant pumps is initiated. Primary and secondary pressure raise to the set point of the PORV and steam generators (SG) relief valves initiating a continuous cycle opening at 330 seconds. Thirty seconds before approximately, pumps stop and natural circulation is started, changing from single to two phase flow about the 1,150 seconds. During this period, SG collapsed liquid level decreases below its 3 % switching on the AFW and achieving a semi-equilibrium energy balance in the test facility until the core dry out (core power and SG levels keep more or less constant until 26,000 seconds during PZR PORV and SG RV valves continuous opening).

Until 12,000 seconds, natural circulation increases gradually, time in which mass flow rate drops as a result of the whole core boiling and a large voiding in the SG U-tubes. Then, liquid levels of the U-tubes start to oscillate asymmetrically affecting the primary mass flow rate, the primary-to-

| Parameter | UPC RELAP5 nodalization |
|-------------------------------------|-------------------------|
| Core Power [kW] | 1.01 |
| Hot leg temperature [K] | 1.003 / 1.003 |
| Cold leg temperature [K] | 1.001 / 1.001 |
| Mass flow rate [kg/s] | 0.98 / 0.965 |
| Primary pressure [Pa] | 1.001 |
| Pressurizer level [m] | 0.999 |
| Secondary pressure [Pa] | 0.998 |
| Secondary side liquid level [m] | 1.000 / 0.9998 |
| Main feed water temperature [K] | 1.0 / 1.0 |
| Auxiliary feedwater temperature [K] | 1.0 / 1.0 |
| Accumulators pressure [Pa] | 1.0 |
| Accumulators temperature [K] | 1.0 / 1.0 |
| Steam flow rate [kg/s] | 1.034 / 1.035 |

Table 2.4: Test 3.2 Steady state conditions

secondary heat transfer and the discharge across the PORV valve. About 15,800 seconds, pressurizer becomes empty of liquid. Natural circulation keeps until 24,000 seconds approximately, time in which SG inlet liquid levels drops and reflux condensation begins.

About 25,700 seconds, significant increase occurs in the fuel rod surface temperature due to core dry out, initiating the LSTF core protection system about 26,000 seconds. It causes core quenching and the primary system depressurization. At 32,000 seconds approximately, SG are refilled, AFW is closed and pressures of both systems become constant, so transient is finished.

The main events are described in table 2.5.

2.1.4.2.3 Post-test results

Table 2.5 shows the chronology of the main events occurred in Test 3-2, comparing the experimental values with the calculated ones:

As shown in Figure 2.31, primary and secondary pressure in the UPC-INTE LSTF model have good agreement with the experimental data until maximum fuel clad temperature is reached at 26,220 seconds (see Figure 2.32), simulating correctly primary-to-secondary cooldown and SG collapsed liquid levels (see Figure 2.33) during the actuation of the AFW (see Figure 2.34).

Figure 2.32 shows UPC-INTE LSTF model reproduces quite well the whole core boiling and so, the beginning of U-tube liquid levels oscillation (see Figure 2.35).

However, although simulation reproduces primary mass flow rate drop related with the whole core boiling (see Figure 2.36), it exists a relative delay between UPC-INTE LSTF model and experimental data that affects the mass flow rate into the pressurizer and its partial refilling (see Figure 2.37). Its phenomenon holds up the emptying of the pressurizer, but even in this case, all these events are qualitatively well reproduced in the simulation.

Finally, the UPC-INTE LSTF model shows a quite good agreement simulating the partial emptying of the SG inlet and hot leg, and the initiation of reflux condensation (see Figure 2.38).

| Main Events | Experimental [s] | Calculated |
|--|------------------|---------------|
| Loss of feedwater | 0.0 | 0.0 |
| SCRAM signal: · Turbine trip and closure MSIV · PZR heater off · Closure of MSIVs | 50.0 | 50.0 |
| RCPs stop | 300.0 | 300.0 |
| Initiation of AFW | 1030.0 | 1080.0 |
| Natural circulation from single phase to two phase | 1150.0 | 1100.0 |
| Significant level oscillation begins in U-tubes (whole core boiling) | About 12000.0 | About 12500.0 |
| Initiation of reflux and condensation phase | 23500.0 | 23030.0 |
| Core power decrease by LSTF core protection system | 25700.0 | 26090.0 |
| Maximum fuel rod surface temperature | 26220 | 26320 |
| Termination of auxiliary feedwater | 32100.0 | 32100.0 |

Table 2.5: Test 3.2 Main events

2.1.4.2.4 U-tubes oscillation during Natural Circulation

Significant liquid level oscillations start in the U-tubes when the whole core reaches the saturation temperature. Although UPC-INTE LSTF model reproduces this phenomenon, it is worth mentioning their amplitudes decrease faster than in the experimental data (Figure 2.35). Figure 2.39 compares U-tubes liquid temperatures with the saturation temperature in the core exit and in the SG riser. Comparison shows that in the simulation, U-tubes liquid temperatures oscillate less in this range, generating lower condensation in the steam generator. This fact justifies liquid level amplitudes in the U-tubes decrease faster in the UPC-INTE LSTF model.

Figures 2.40 and 2.41 show the frequency of the U-tubes liquid oscillations during natural circulation and reflux condensation respectively. Comparison with the experimental data and primary and secondary pressures shows UPC-INTE LSTF model reproduces oscillations of liquid in the U-tubes during the natural circulation. Coupling between PORV valve continuous opening and U-tubes liquid level oscillations becomes evident when reflux and condensation is achieved (see Figure 2.41).

2.1.4.2.5 Sensitivity analysis: Impact of the environment heat losses

Preliminary simulations taking into account experimental procedures and boundary conditions of LSTF/ROSA Test 3-2 showed an unexpected increase of the pressurizer primary pressure during the conditioning phase (see Figure 2.42). Liquid temperatures reached saturation quickly suggesting an overheating in the pressurizer (see Figure 2.43). Moreover, calculation of the system energy balance showed an important disagreement in the environment heat losses between the experimental data and the simulation during the conditioning phase of the transient.

Sensitivity analysis was performed over preliminary simulations to analyze and fix the environment heat losses. A set of simulations were modelled increasing gradually heat losses, especially in the pressurizer. Results showed environment heat transfer affects significantly the pressurizer collapsed liquid level (see Figure 2.44) and the PORV discharge mass flow rate (see Figure 2.45), delaying the dryout of the core (see Figure 2.46) and so, the depressurization of the primary system as a result of

the initiation of the LSTF core protection system. The UPC-INTE LSTF model was taken as a base case.

2.1.4.2.6 Conclusions

UPC-INTE LSTF model developed for LSTF Test 3-1 [45] has been adjusted to the LSTF Test 3-2 proving its suitability to simulate the behavior of this facility.

Model predictions for Test 3-2 were in quite good agreement with the available experimental data. Several conclusions have been obtained from the study of local phenomena and sensitivity analysis. First, that RELAP5/mod3.3 reproduces U-tubes liquid level oscillations during High-Power Natural Circulation. Although condensation in U-tubes, which affects to the amplitude of the oscillations, is slightly under predicted by the code, the main events of the transient don't change significantly. On the other hand, sensitivity analysis shows the significance of the environment heat losses simulation. For long transients with a relatively high-core power, an incorrect implementation of the environment heat transfer causes discrepancies in the core power heat removal. Particularly, for Test 3-2, they modify wrongly the mass discharge through the PORV.

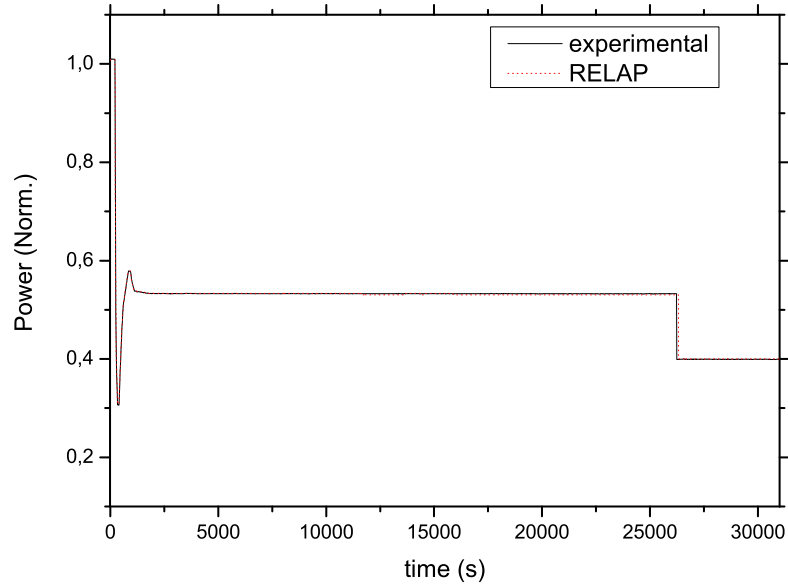


Figure 2.30: LSTF core power

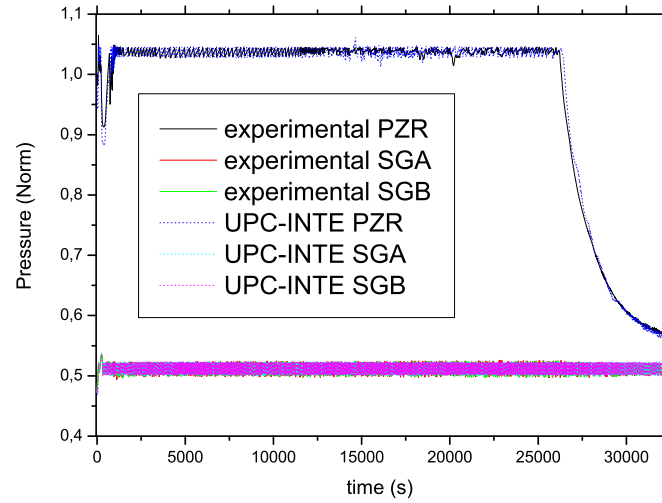


Figure 2.31: LSTF system pressures

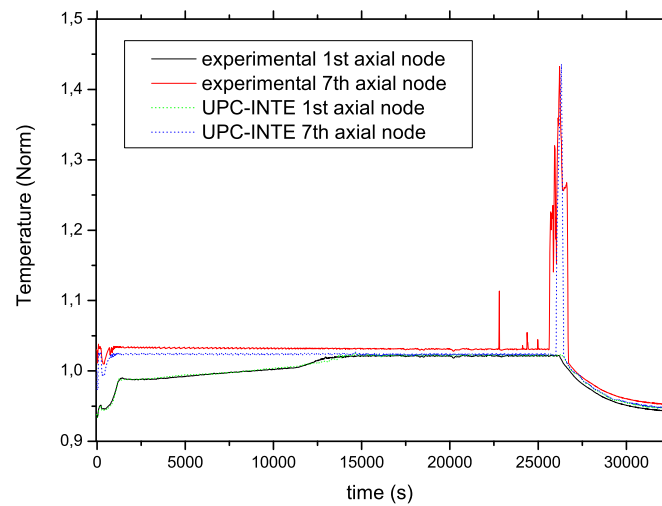


Figure 2.32: Maximum and minimum cladding temperatures

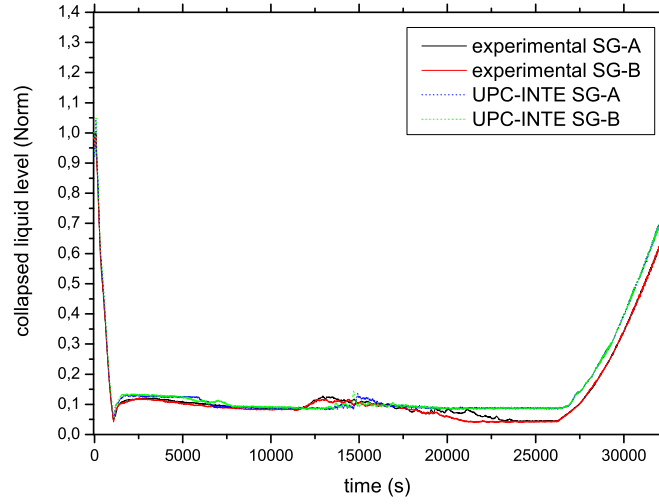


Figure 2.33: SG riser collapsed liquid levels

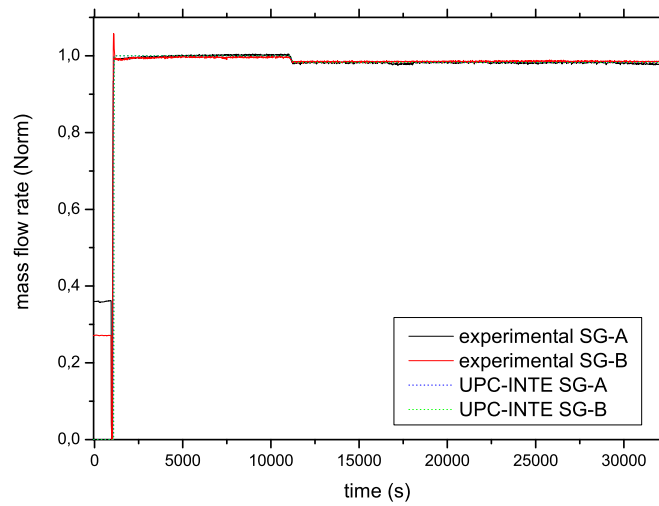


Figure 2.34: Auxiliary feedwater

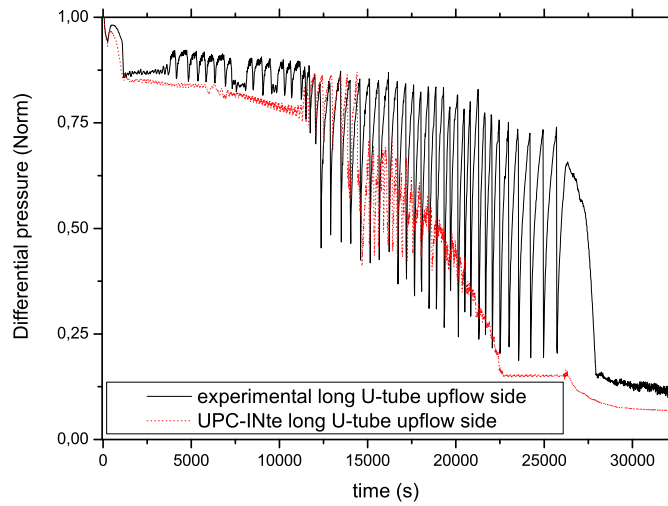


Figure 2.35: U-tubes upflow side differential pressure

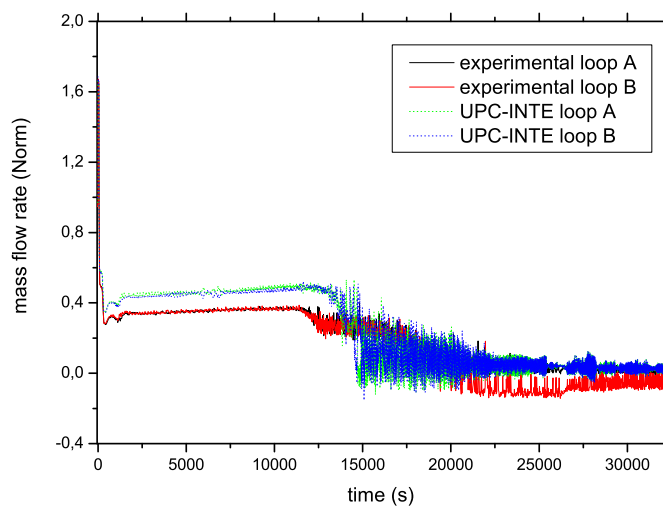


Figure 2.36: Primary mass flow rate

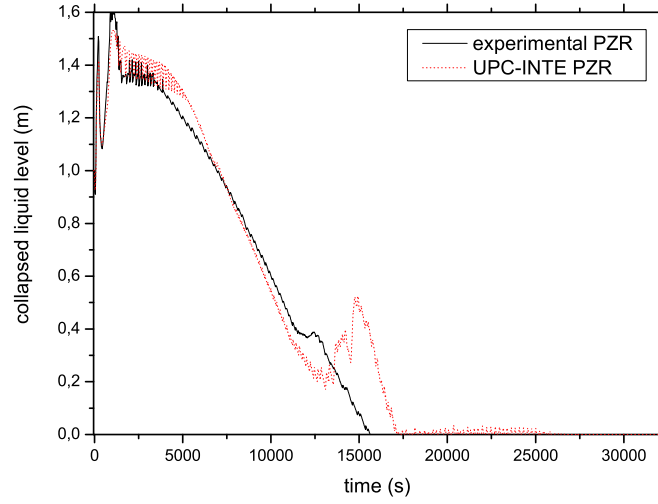


Figure 2.37: PZR liquid level

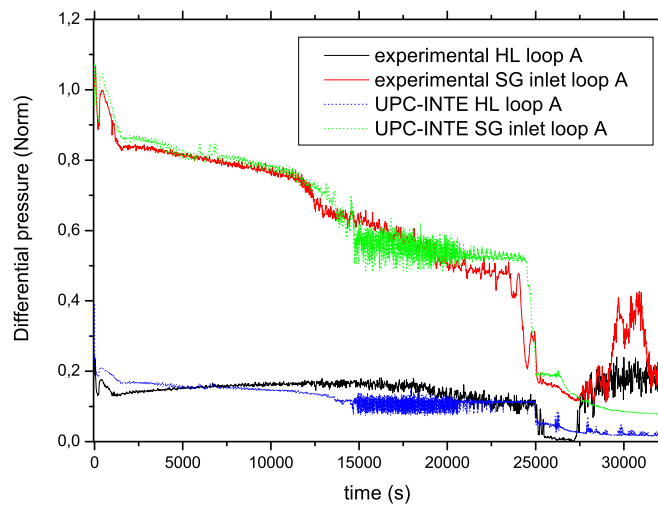


Figure 2.38: Differential pressures in the SG inlet and hot leg of loop A

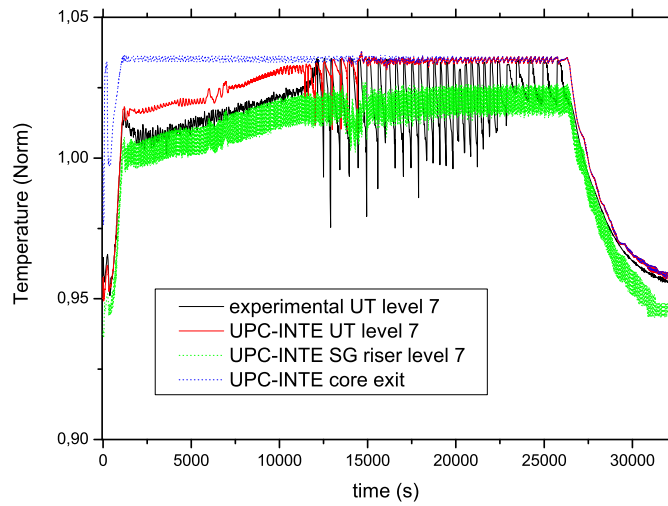


Figure 2.39: U-tube temperatures

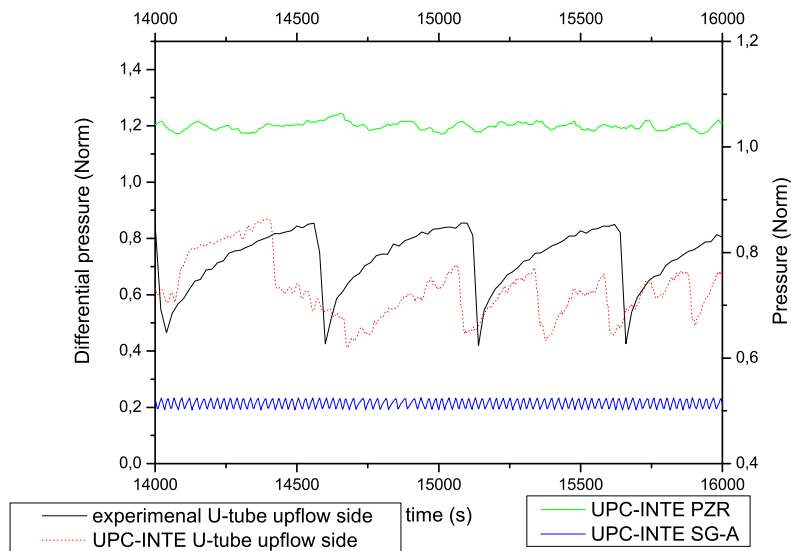


Figure 2.40: U-tubes differential pressure during natural circulation phase

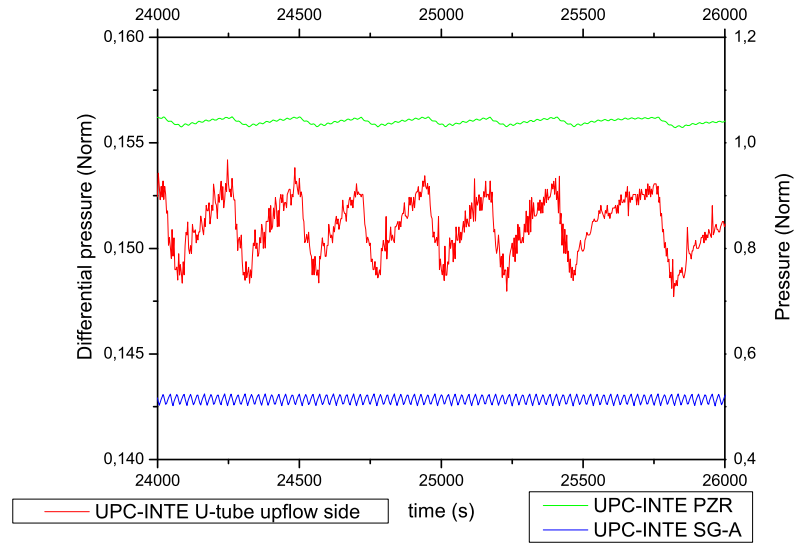


Figure 2.41: U-tubes differential pressure during reflux condensation phase

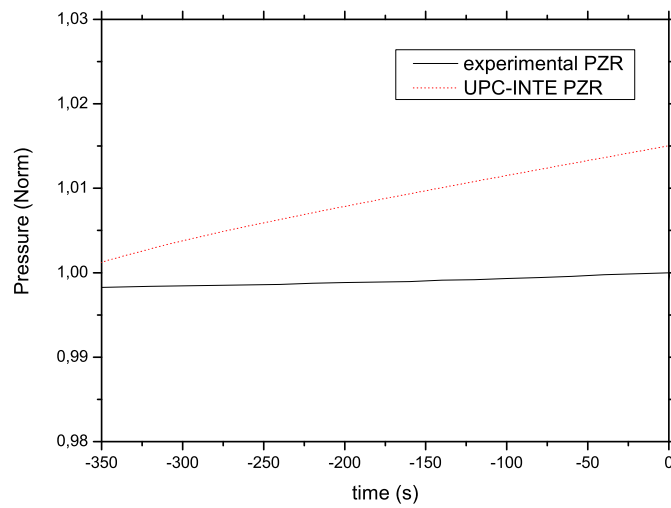


Figure 2.42: PRZ pressure during conditioning phase

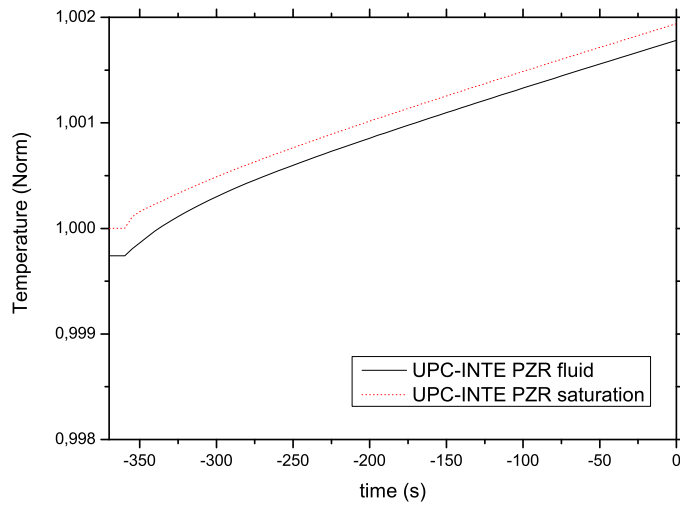


Figure 2.43: Fluid temperature in the pressurizer

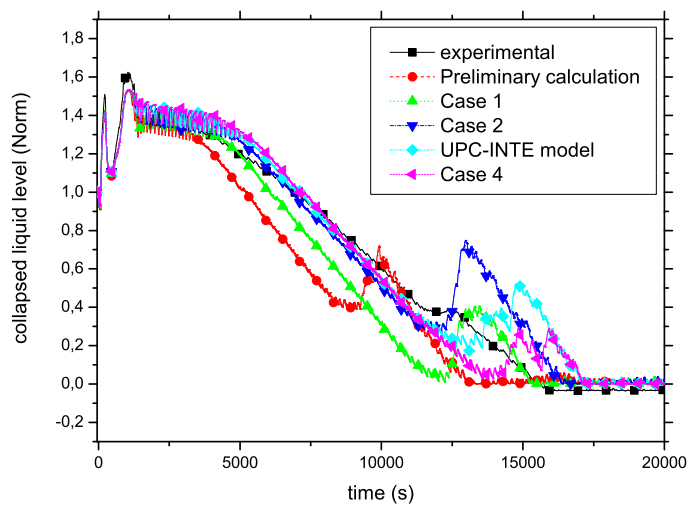


Figure 2.44: PZR collapsed liquid level

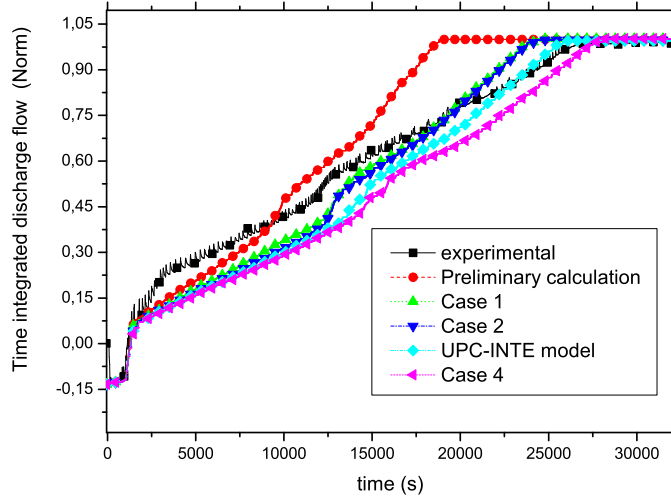


Figure 2.45: Time-integrated discharge flow through PORV

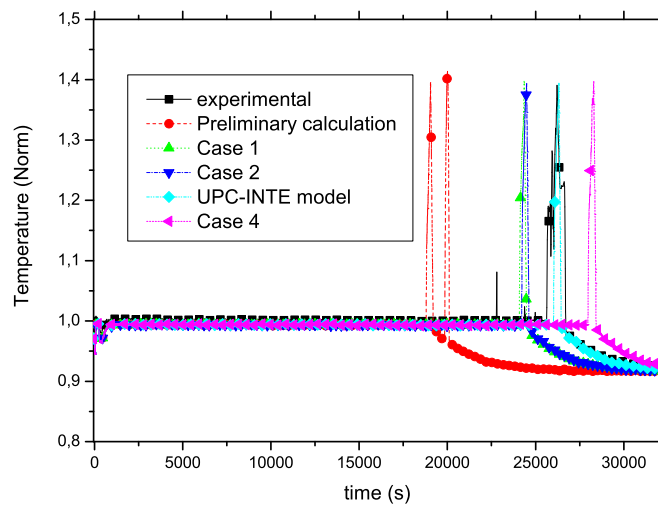


Figure 2.46: Maximum clad surface temperature

2.2 PKL

For nearly 40 years, Framatome ANP's large-scale facility PKL, located in Erlangen (Germany), has been used for extensive experimental investigations to study the integral behavior of pressurized water reactors under accident conditions. The PKL facility replicates the entire primary system and most of the secondary system (except for the turbine and condenser) of a 1300-MW PWR plant of a Siemens design, with elevations scaled 1:1 and axial diameters by a factor of 12 [50]. The scheme of the PKL test facility is shown in Figure 2.47 [51].

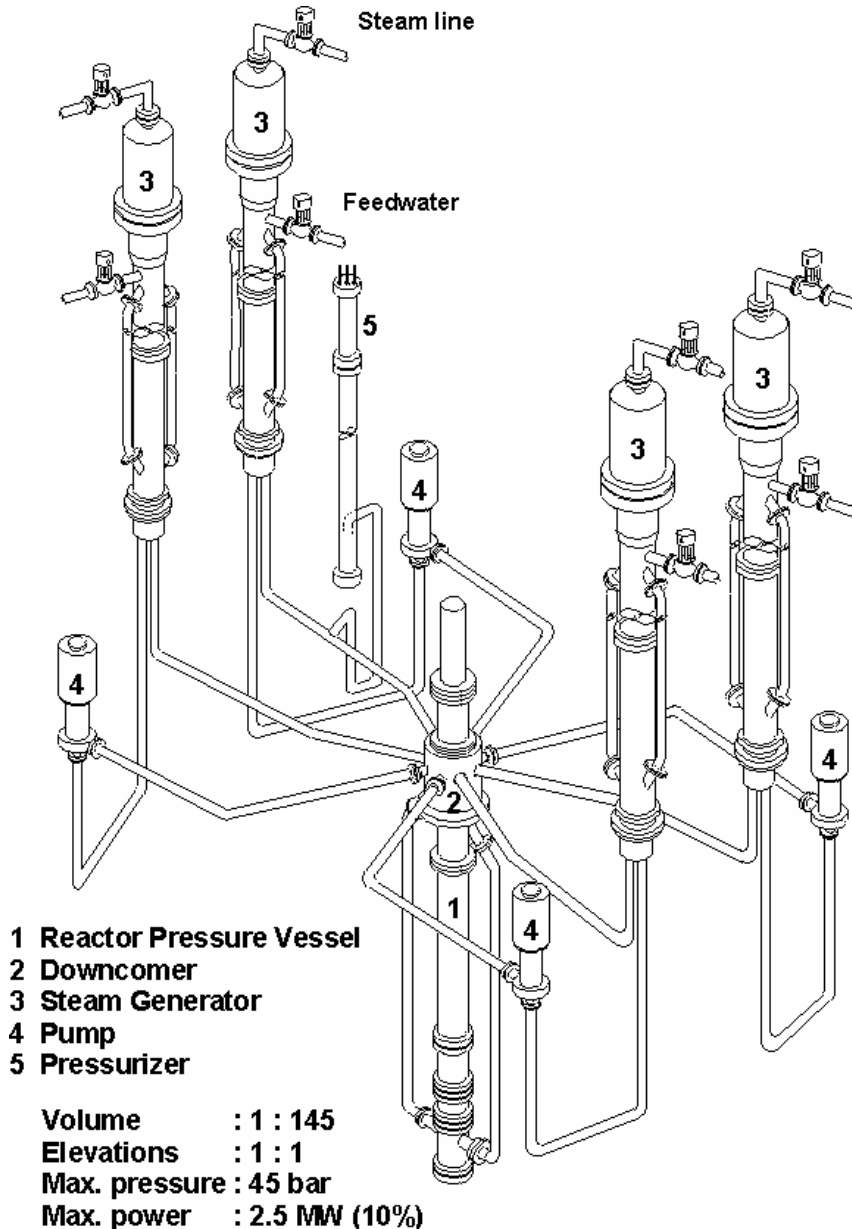


Figure 2.47: The PKL test facility (source: Framatome ANP)

The test facility models the entire primary system, most parts of the secondary side and all important engineered safety and auxiliary systems. In order to investigate the influence of non-

symmetric boundary conditions (e.g. only 2 out of 4 SIPs are in operation) on the system behavior, PKL is equipped with four primary loops which are symmetrically arranged around the RPV as in a real PWR. Each loop contains a RCP and a fully scaled SG with prototypical tubing.

The prime objective behind all tests performed is to study thermal-hydraulic processes in PWRs, not only in terms of the integral behavior of the entire system but also with respect to the behavior of individual components or subsystems [50]. The experiments conducted cover a broad spectrum of topics, ranging from tests performed to study large and small LOCAs when the facility was first built, to simulations of accident transients.

The PKL test facility in cooperation effort with OECD (Organization for Economic Cooperation and Development) has been used on the study of boron dilution transients during the last twenty years. The study was part of the SETH project that was afterwards continued by the OECD/PKL project. Several tests have been carried out with regard to SBLOCA and loss of RHR. Among others, the study of the following phenomena has been particularly interesting:

- Reflux-condensation conditions
- Natural circulation establishment
- SG capacity to remove residual heat under shutdown conditions
- Formation and transport of boron diluted slugs

2.2.1 Scaling principles

As said before, the PKL facility models the nuclear steam supply system of a 1300 MW nuclear power plant on a scale of 1:145. Detailed design was based to the largest possible extent on the specific data of Philippsburg nuclear power plant, unit 2 [50].

The main aspects of the scaling principles, based on the Power to volume methodology, are:

- Full-scale hydrostatic head
- Power, volume and cross sections are scaled down by a factor of 1:145
- Pipe radius are scaled down by a factor of 12
- The fuel rods are simulated by means of 314 electrical heat rods with different power to simulate the different rates of burned fuel. The electrical rods are disposed as three different regions very likely as in a real plant. The maximum power of the facility is limited to 2.5 MW which represents the 10% of the scaled down maximum power of a NPP
- The number of U-tubes in the steam generator is also scaled down; the whole bundle is substituted here by a total of 28 tubes arranged in 7 different elevations. The total section keeps the scaling factor of 1 to 145.
- Simulation of all four loops
- Full scale frictional pressure loss for single phase flow
- The downcomer is modelled as an annulus in the upper part while for the lower part it is split in two symmetrical pipes. Although this part is clearly different from a real plant, it preserves the frictional pressure losses and does not unacceptably distort the volume/surface. However, it has to be taken into account when mixing in the downcomer and other phenomena are studied.

In cases of conflicting requirements, simulation of the phenomena was given preference over consistent simulation of the geometry. For instance, in order to account for important phenomena in the hot legs such as flow separation and counter current flow limitation, the geometry of the hot legs is based on conservation of the Froude number and was finally designed on the basis of experiments at the full scale UPTF [50]. Further details about Power to volume methodology can be found in Section 4.1.

One of the goals of the PKL test facility is that, unlike other facilities, here all 4 loops are simulated separately. In other facilities like LOBI the four or three loops are simulated by means of

two different loops, one for the broken loop and another one that simulates the others. This feature takes relevance for transients with asymmetrical behavior.

The maximum power the facility can achieve is equivalent (taking into account the 1:145 scale factor) to the 10% of the maximum power of a NPP. Therefore, the facility is meant to simulate transients where the reactor has been scrammed. Besides, the primary pressure of the facility is limited to 45 bar and the secondary pressure to 56 bar. This means that the first part of a SBLOCA, which would start with a primary pressure of around 160 bar, cannot be simulated or has to be simulated differently. All in all, the range of pressure allows simulation over a wide temperature range (250°C to 50°C) that is particularly applicable to the cooldown procedures investigated.

2.2.2 Description of the facility

2.2.2.1 Primary system

The primary system of the PKL test facility is composed of the reactor pressure vessel (RPV), the four loops and the pressurizer. Each loop can be subdivided into the hot leg, the U-tube bundle, the loop seal, the RCP and the cold leg. The arrangement of the loops is shown in Figure 2.48.

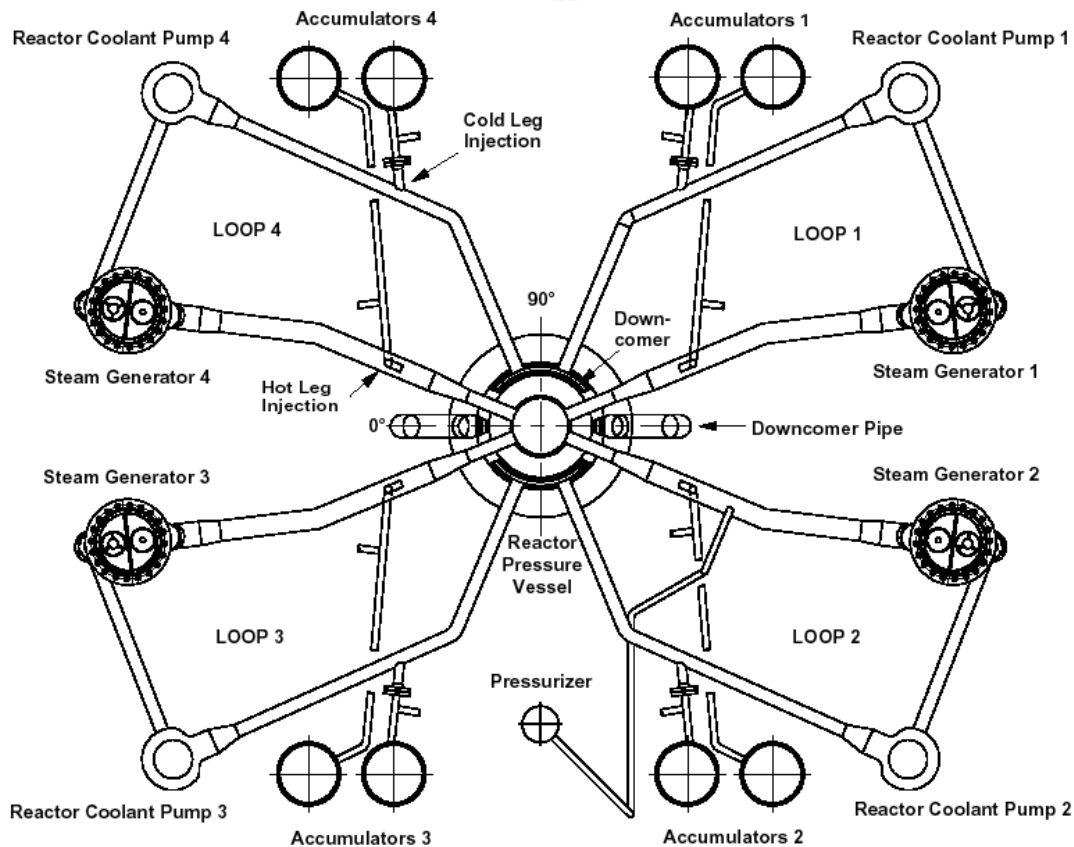


Figure 2.48: The PKL test facility, loop arrangement (source: Framatome ANP [52])

2.2.2.1.1 Reactor Pressure Vessel

The RPV is made of chromium nickel steel, it is a cylinder of various diameters along its height (348/422/392mm) and has a wall thickness of 12 and 16 mm [50]. It models the upper head plenum,

the upper plenum, the reactor core, the reflector gap and the lower plenum. Figure 2.49 show the geometry of the RPV.

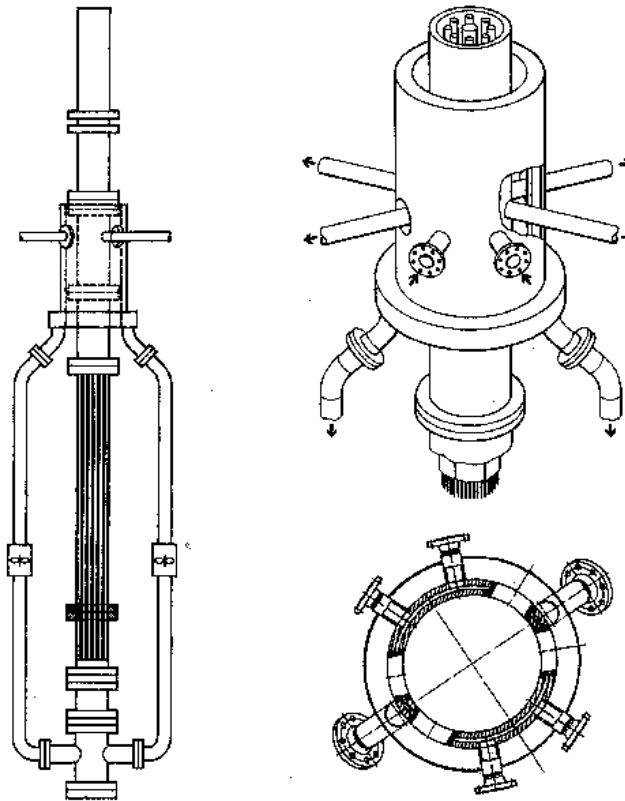


Figure 2.49: The PKL test facility, view of the RPV (source: Framatome ANP)

The upper head plenum distributes the water to the loops and to the upper plenum. A relevant aspect of the upper head plenum is a baffle ring, which is an annular gap in the lower part that prevents direct injection of water from the downcomer into a steam void which might be present. The water backs up in this annular gap and then runs over the ring, which acts as an obstruction and distributes the water uniformly around its circumference into the upper head plenum.

The upper head bypass is modelled by four symmetrical pipes that join the upper head with the upper part of the downcomer. One of the purposes of the bypass is to enable detection of asymmetric flow phenomena in the RCS. A throttling valve is placed on the middle of each bypass to model the appropriate loss of the total mass flow. The orifice throat has a length of 5mm and its section is able to have two different diameters; 3.9mm or 6.8mm.

The top plate separates the upper head plenum from the upper plenum. It is a plate with nine orifices that serves to contrast the pressure loss. The upper plenum is the region between the upper head and the core. Coolant from the core is distributed here to the four hot legs.

About the test bundle, it is composed by 314 electrically heated rods. There are also 26 control rod guide thimbles. The fuel rods are arranged in three concentric zones so all of them can be heated independently at different power rates. These regions are surrounded by a wrapper so a gap is formed between the test bundle and the core wall. The flow crossing the reflector gap represents the coolant that does not touch the fuel rods. The overall flow resistance in the reflector gap is designed in such a way that, when all RCPs are in operation, 1% of the total primary side mass flow passes the reflector gap as in the reference reactor.

The lower plenum gathers the coolant coming from the two downcomer nozzles. The extension of the 314 fuel rods crosses the lower plenum but its influence over the transverse flow resistance is

only slightly different compared with that of the modelled reactor [50].

Finally, the RPV downcomer is modelled as an annulus in the upper part to gather the coolant of the four cold legs and continues as two stand pipes connected to the lower plenum. Although the geometry is quite different from the one in the reference reactor, the hydraulic diameter is equal and the frictional pressure losses are preserved.

2.2.2.1.2 Reactor coolant piping

The reactor coolant piping is composed by the hot legs, loop seals and cold legs.

Originally the diameter of the hot legs was 80.08 mm. However, studies performed in the full scale UPTF test facility indicated that the diameter of the hot legs should be larger for an accurate modeling of two phase flow phenomena. Since it was not possible to change the diameter of the hot leg junction with the RPV, the hot leg diameter was progressively increased from the RPV nozzle as shown in Figure 2.48. Possible break locations are placed in hot legs of loops one and two. All hot legs have a scoop that permits the entrance of the ECC systems. The surge line is connected to the hot leg of loop 2.

The loop seals connect the steam generators to the reactor coolant pumps and have a U form as shown in Figure 2.47. The inside diameter of the loop seal is 80.8 mm.

The cold legs connect the RCPs with the downcomer annulus region. The diameter of the cold legs is again 80.8 mm. Possible break locations are found in loops 1 and 2. Unlike in the hot legs, here the entrance of the ECC systems is modelled by a nozzle connected to the cold leg with an inclination of 60 degrees.

2.2.2.1.3 Reactor coolant pumps

The reactor coolant pumps in the PKL test facility are vertical single-stage centrifugal pumps. They are driven by variable-speed motors provided with anti-reverse rotation devices. The variable-speed motors allow scaled mass flows and also starting and coast-down time histories to be simulated. The loss coefficient of the shut-down reactor coolant pump can be set by means of a butterfly valve upstream of the pump.

The pumps are shut down in all PKL tests that are simulated in this dissertation.

2.2.2.1.4 Pressurizer

The PKL pressurizer is an esbelt cylinder with an inner diameter of 220 mm and a total height of 13.525 m. While the volume and area is scaled down from a commercial reactor, the elevation is kept equal. Because of the different proportions between elevation and diameter the PKL pressurizer has more heat losses than in a NPP. This is compensated with two different heater systems.

The pressurizer is connected to the hot leg of loop 2 by the surge line. The surge line connection and the routing of the line are modelled to scale. The surge line is extended downwards into the PZR by a 90° elbow connected to a straight pipe. The surge line is around 11 m long.

2.2.2.1.5 Steam generator primary side

The U-tubes are modelled as 28 U-tube shaped pipes with an outside diameter of 22 mm and a wall thickness of 1.2 mm. The number of U-tubes has been scaled down by a factor of 145. The tubes are distributed in seven different groups that have different elevations. The elevation difference between the lowest and the highest U-tube is 2 meters. These lengths are roughly in proportion to the different tube lengths in the reactor.

2.2.2.2 Secondary system

The secondary system is formed basically by the secondary side of the steam generator. The U-tube bundle is surrounded by a cylinder of a diameter of about 400 mm that forms the riser of the SG.

The diameter over the riser increases to 700 mm to form the steam plenum, in this region the main steam line begins. In the steam plenum there is a funnel that gathers the condensed water and drives it to the downcomer.

The downcomer of the SG is modelled as an annulus in the upper part and then it splits in two symmetrical pipes to the lower part of the SG where the two pipes are joined again forming an annular downcomer.

2.2.2.3 Interfacing control systems

Most of the control system used in a common PWR are modelled in the PKL test facility for both, the primary and the secondary system. The modelled systems cover a broad functionality; from normal operating systems to emergency systems. Hereafter a brief explanation of these systems is disclosed.

2.2.2.3.1 Volume control system

When the system is in operation, the letdown flow is extracted from the RCP of loop 3 and the charging is connected to all four cold legs. This system compensates for changes in volume of the coolant and supplies water to the pressurizer spray system that can be extra borated to modify the primary system boron concentration.

2.2.2.3.2 Emergency core cooling system

The emergency core cooling system of the PKL test facility is compound by the high pressure safety injection system (HPSI), the low pressure safety injection system (LPSI) and the accumulators. While The HPSI can inject water when the pressure is lower than 45, the LPSI starts to inject when the pressure falls under 10 bar. There is one injection pump for each system (HPSI and LPSI) that is able to simulate the 1,2,3 or 4 injection pumps that are used in a PWR. Both the high and the low pressure safety injection systems can be connected to all four cold and hot legs. There are 8 accumulators in the PKL test facility, one for each cold and hot leg. The accumulators are designed for an operating pressure of 50 bar (nitrogen blanket pressure) and start to inject automatically when the RCS pressure falls below 26 bar.

2.2.2.3.3 Residual heat removal system

Usually, the RHR system of real plant is the same as the ECC. In the PKL test facility the RHR and the ECC are independent systems. The residual heat removal system performs two main actions in the PKL test facility: decay heat removal during shutdown and cooldown and post-LOCA residual heat removal from the core. The system lines are connected with the ECC lines before entering the RCS.

2.2.2.3.4 Pressurizer spray system

The pressurizer spray system is used in three different ways: operational spraying, auxiliary spraying from the volume control system and auxiliary spraying from the extra borating system.

2.2.2.3.5 Pressurizer relief system

In a nuclear power plant the pipe discharges into the pressurizer relief tank whereas it is aligned with a separator tank in the PKL test facility.

2.2.2.3.6 Main steam piping system

In the PKL test facility the main steam (MS) piping system contains the MS relief isolation valve, the MS relief control valve, The MS isolation valve and warm-up control valve and is thus capable of fulfilling all normal operational actions needed in a NPP. The only limitation is the system pressure that cannot exceed 60 bar. The cooldown in a PWR after a LOCA is performed by means of the MS relief valves.

2.2.2.3.7 Feedwater system

The feedwater piping system serves to supply water to the steam generators in power operation and during unit startup and shutdown. This system is controlled according to the SG level.

2.2.2.3.8 Auxiliary feedwater system

The auxiliary feedwater system is a emergency safety system used to guarantee the necessary SG water level and supply the SG with the required feed. The PKL auxiliary feedwater system is capable of performing all operational actions that a commercial NPP would require. The controlling variable used for the auxiliary feedwater control valves is the measured SG level, as in the modelled reactor.

2.2.2.3.9 Steam generator blowdown system

The steam generator blowdown system in the PKL test facility serves simply to interconnect two SG on the waterside in the event of loss of feedwater supply to one.

2.2.2.4 Instrumentation

PKL test facility has about 1500 measurement points that permit an exhaustive analysis of the tests. There are measurement devices for cladding, wall and fluid temperature, absolute and differential pressure, one and two phase mass flow, density and boron concentration. An example of the distribution of the measurements is shown in Figure 2.50.

Sixty of the measurement devices are identical to those that are used in a commercial plant to simulate what an operator would control in case of accident.

Finally, it is worth to mention that the break discharge experimental data have to be computed from other values. One can calculate the break massflow by differentiating the level variation of the two separator vessels (where the discharged water goes) and subtracting the mass released through the separator relief line. Hence, the break massflow is expected to be just an estimation of the experimental value as other effects like fluid density and vaporization might interact.

2.2.3 Nodalization

A nodalization of the PKL test facility (see Figure 2.52) has been used in this Ph.D. Thesis in order to simulate the PKL Counterpart Test G7-1. It is based on a previous RELAP5mod3.3 UPC-INTE nodalization that was created and developed by Jordi Freixa for his Ph.D. Thesis (Reference [53]). Main features of the nodalization were:

- 438 volumes
- 468 junctions
- 331 heat structures
- 1356 mesh points

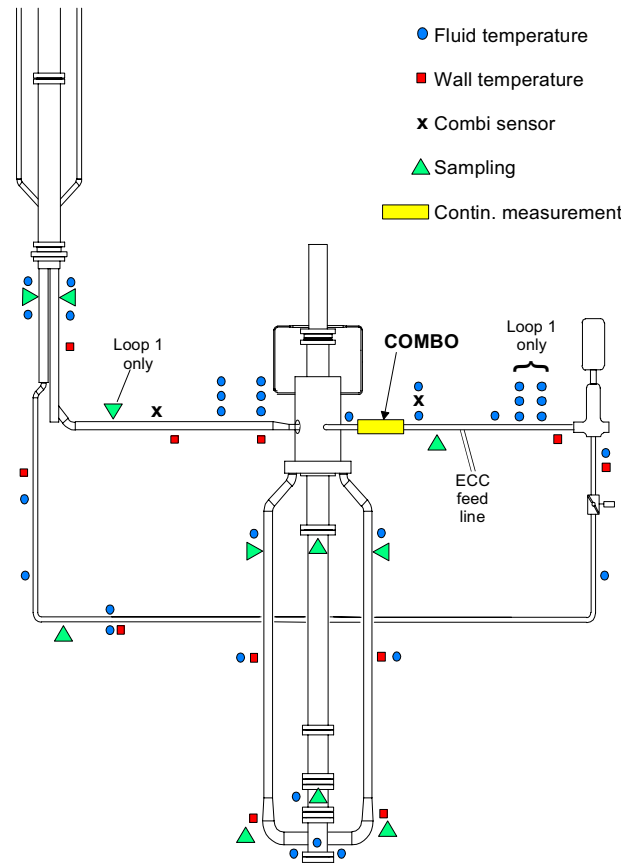


Figure 2.50: Distribution of measurement devices (source: Framatome ANP)

Several improvements have been added to the base nodalization for the simulation of the OECD/NEA PKL-2 G3.1 and G7.1 tests. For the experiment G3.1 ("Main steam line break" transient) steam lines of the secondary side were improved in order to simulate properly the secondary flow paths upstream the break. Additionally, SGs and PZR heaters were re-nodalized more realistically with a view to improve the ratio between the primary and the secondary environment heat losses. Furthermore, finer meshing was implemented in the core and the upperplenum for the post-test G7.1. Core pipe was divided in three radial channels (see Figure 2.51) of 14 axial levels, and the bottom volumes of the upperplenum were increased from one to three. Besides cross-flows and transversal momentum equations were activated in the core. The purpose of these changes was to reproduce with the code the correlation between the CET and the PCT that was reported in the experiment. All the improvements that were added during this thesis can be seen with grey and dot lines of the Figure 2.52.

2.2.4 Nodalization qualification

Base nodalization of the PKL facility was qualitatively qualified during the Ph. D Thesis of Jordi Freixa ([53], [54] and [40]). Nodalization capabilities were tested for the OECD/SETH and OECD/PKL boron dilution transients. The input deck was continuously improved during the simulation of five tests (E1.1, E2.2, E2.3, F1.1 and F1.2) and various problems were faced at each transient. All improvements were included in the previous post test calculations so a unique robust nodalization was able to represent all tests at a similar accuracy. The final results showed a close agreement between the simulations and the experimental data, demonstrating the quality and the confidence of the

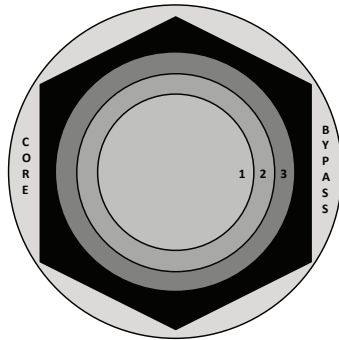


Figure 2.51: PKL nodalization: radial distribution

UPC PKL nodalization for reproducing boron dilution events (mainly in the loops region), natural circulation and SBLOCA scenario.

Related to qualification of the particular improvements that has been upgraded in this Ph.D. Thesis (see Section 2.2.3), two post-tests were performed linked to the participation of the UPC in the OECD/PKL-2 project. Results of the G3.1 test are described below. For the PKL Counterpart test, a detailed description of the post-test simulation can be found in its particular Section 6.2.1.

2.2.4.1 OECD/NEA PKL-2 Test G3.1

UPC participated in the second phase (post-test analyses) of the *Analytical exercise on OECD-NEA PKL-2 Project Test 3.1: Main Steam Line Break Transient in PKL-III Facility*, [55]. This test is a fast cooldown transient, namely a main steam line break. The design of the experiment involved two phases: the first based on the 0.1A break in the main steam line as initiating event, and the second consisting in the emergency core cooling system injections by means of the high pressure injection system connected with the cold legs 1 and 4. During the Phase I, focus was given to pressurized thermal shock and re-criticality aspects. On the other hand, the second phase of the test addressed the effects of the injections in cold legs on the single phase natural circulation in the loops, when the pressurized safety valve was operated.

Particular boundary conditions of the transient were:

- RCS completely filled with water and fully in operation
- Core power constant at 260 kW, equivalent to 0.8 % of decay power
- 0.1A break inside containment in the main steam line of SG 1 (fill level equal to 9.2 m)
- The unaffected SGs 2 - 4 are isolated from the break (MS isolation valves are closed) and filled with water ($h = 12.2$ m)
- Pressurizer in hot conditions, approximately at 250 °C (PRZ heater in operation until the SOT)
- All SGs are isolated from feed water system
- Reactor coolant pumps are shut off at start of test, i.e. occurrence of break (coast down)

In the following text, a qualitative description of the code results based on the calculated time trends is presented. In general, UPC simulation shows a quite good agreement as for the steady state conditions (see table 2.6) as for the main events (see Table 2.7). Starting with Figure 2.53, results are in well agreement with experimental data until the total clearing of the broken SG. (700 seconds approximately, see Figure 2.53) Note that the calculated pressure decreases slightly slower than the experimental data. Nevertheless, HPI system and PZR safety valve are working properly. Figure 2.54 show the pressure in secondary side of the SGs. The broken loop empties slightly faster than

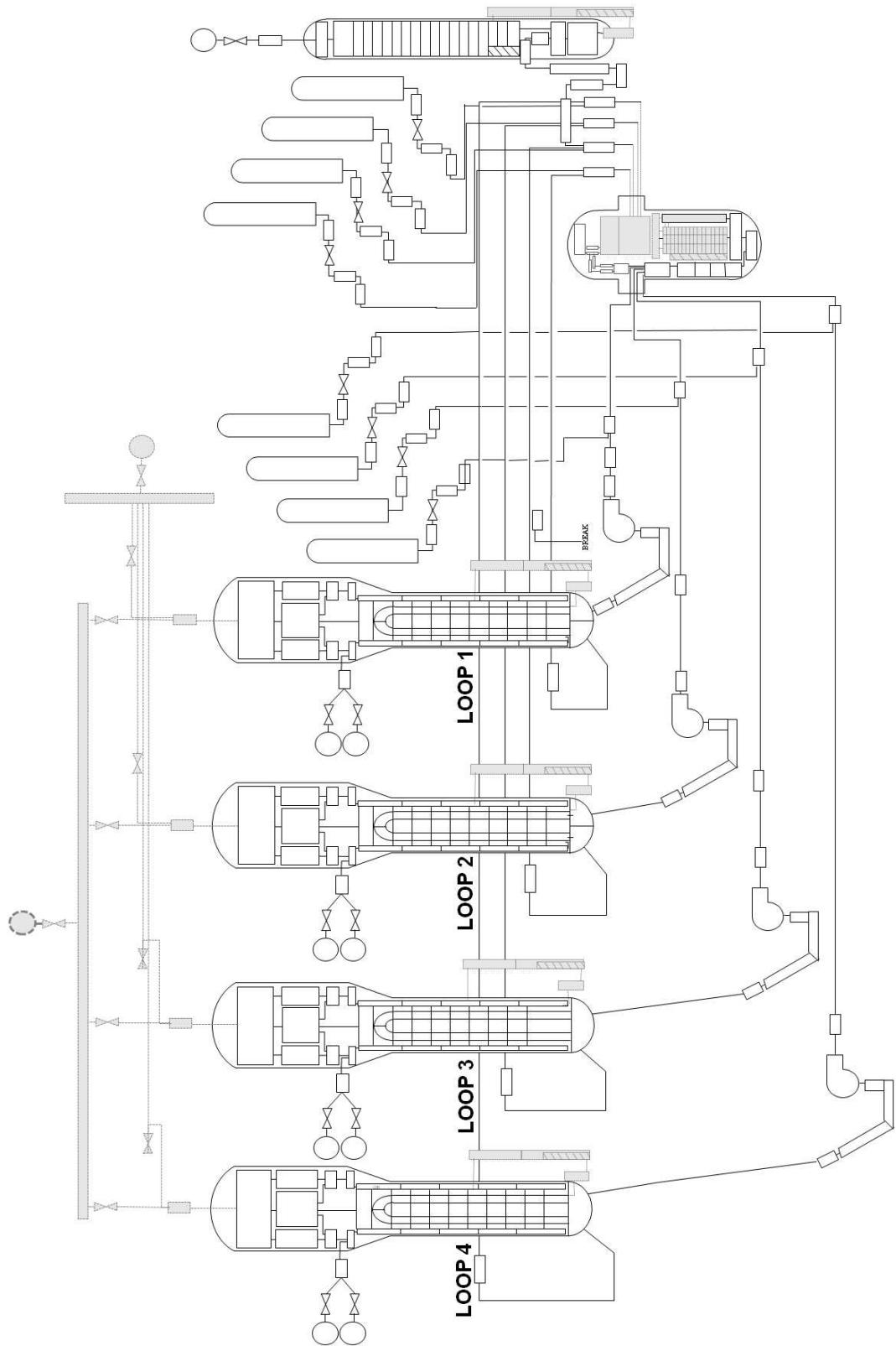


Figure 2.52: PKL nodalization

experimental data, while intact loops have a simultaneous depressurization to experimental, probably as a consequence of a good concordance of heat losses and primary to secondary heat transfer because of natural circulation in the intact loops.

| Parameter | Experimental | Calculated |
|---------------------------------|-------------------------------|-------------------------------|
| Core Power [kW] | 206.8 | 259.9 |
| Hot leg temperature [K] | 516.6 / 517.7 / 516.9 / 516.7 | 517.0 / 517.1 / 517.1 / 517.1 |
| Cold leg temperature [K] | 516.6 / 515.5 / 515.6 / 515.6 | 516.5 / 516.4 / 516.5 / 516.6 |
| Mass flow rate [kg/s] | 33.9 / 33.7 / 33.8 / 33.7 | 33.7 / 33.6 / 33.6 / 33.6 |
| Primary pressure [Pa] | 4.14e+6 | 4.14e+6 |
| Secondary pressure [Pa] | 3.45 / 3.45 / 3.47 / 3.45 | 3.49 / 3.49 / 3.49 / 3.50 |
| Secondary side liquid level [m] | 9.2 / 12.3 / 12.2 / 12.2 | 9.01 / 12.2 / 12.2 / 12.3 |
| Main feed water temperature [K] | 478.7 / 508.6 / 509.3 / 513.7 | 327.5 / 487.5 / 507.5 / 513.0 |
| SGs riser temperature [K] | 514.6 / 514.8 / 514.9 / 514.2 | 515.7 / 515.9 / 515.9 / 515.9 |
| SGs downcomer temperature [K] | 467.2 / 508.5 / 510.9 / 513.9 | 479.6 / 515.6 / 514.7 / 515.4 |
| Core inlet temperature [K] | 515.6 / 515.5 / 515.6 / 515.5 | 516.5 / 516.4 / 516.5 / 516.6 |
| Core outlet temperature [K] | 516.6 / 517.7 / 516.9 / 516.7 | 517.0 / 517.1 / 517.1 / 517.1 |
| RCPs in operation [rad/s] | 263.9 / 261.3 / 266.2 / 262.8 | 277.5 / 276.7 / 276.7 / 276.7 |
| Loops mass flow [kg/s] | 33.9 / 33.8 / 33.8 / 33.8 | 33.7 / 33.6 / 33.6 / 33.6 |
| SGs difference temperature [K] | 0.68 / 0.42 / 0.15 / 0.17 | 0.42 / 0.33 / 0.37 / 0.35 |

Table 2.6: Test G3.1 Steady state conditions

| Main Events | Experimental [s] | Calculated |
|--|------------------|------------|
| Start of the test | 0.0 | 0.0 |
| Blockage of RCPs; butterfly valve closed to simulate blocked RCP | 210.0 | 210.0 |
| Minimum temperature at RPV-inlet of loop 1 is reached | 600.0 | 900.0 |
| Complete evaporation of affected SG1 | 1000.0 | 1050.0 |
| HPIS switched on (cold leg) in loop 1 and 4 | 1030.0 | 1280.0 |
| Opening of the PZR-SV at P = 42 bar | 1420.0 | 1704.0 |
| PZR-SV closed | 1470.0 | 1760.0 |
| PZR completely filled with water | 1820.0 | 1980.0 |
| PZR-SV opens agains at P = 47 bar | 1840.0 | 2026.0 |
| HPIS flow rate reduced | 2150.0 | 2150.0 |
| End of the transient | 4410.0 | 4500.0 |

Table 2.7: Test G3.1 Main events

Good agreement in SGs levels and PRZ levels can be observed in Figures 2.55 and 2.56. It is noticeable to remark the level rise in intact loops due the liquid stack in "dome" during the steady state calculation. This is a consequence of riser regulated liquid level. A stable biphasic regime in riser makes liquid reaches separator level, bypassing water to steam dome.

Cold and hot leg temperatures for each loop are shown in Figure 2.57 and 2.58 respectively. A good agreement is in general noticeable for both Figures. Lower cold leg temperatures are reached in loop number one with some delay compared to experimental data, this can be a consequence of lower depressurization in primary side. Time trends for hot leg temperature are very similar to experimental data. Nevertheless in phase two of the experiment the calculated hot leg temperatures remains slightly higher this can be a consequence of the thermal heat losses modelization. It is also interesting to remark that previous calculations show differences in steady state fluid temperatures and butterfly valve blockage affect the ΔT in first 400 seconds of the transient.

Figure 2.59 shows the main steam line discharge flow rate. A discharge coefficient of 0.75 was used to adjust the full clearing of the broken steam generator with experimental time trends.

Figure 2.60 shows the SGs outlet temperatures, as the other Figures a good agreement with experimental data can be observed. Figure 2.61 shows the SGs difference temperatures. It is noticeable in both Figures, the abrupt decrease of the temperatures once the affected SG is empty. The heat transfer in the modeled SG decreases abruptly than the experimental data. Slightly lower temperatures in SGs outlet on second phase of the transient suggest lower primary to secondary heat transfer and the observed discrepancy between secondary pressures.

Figure 2.62 shows adjustments made for HPI flow rate.

Figures 2.63 and 2.64 show the mass flow rate along the loops for wide and low range. It is noticeable in Figure 2.64, only for loops 1 and 4, than there is a good agreement to experimental data once the RCPs are blocked. The abrupt change of the mass flow for loop 1, around 700 seconds after the break is a consequence of the faster SG1 clearing.

Finally Figures 2.65 and 2.66 show a comparison between the temperatures before and after the loops 2 and 3 RCP. These Figures are attached to show the effect of the reactor coolant pump cooling system. Since we could not reach the same negative ΔT , this could be one of the reasons of the discrepancies between calculated and experimental data.

In addition, post-test simulation was quantitatively qualified in the analytical benchmark following the FFTBM. Results for the overall transient obtained a good accuracy qualification (0.27 for the amplitude and 11.0 for the frequency).

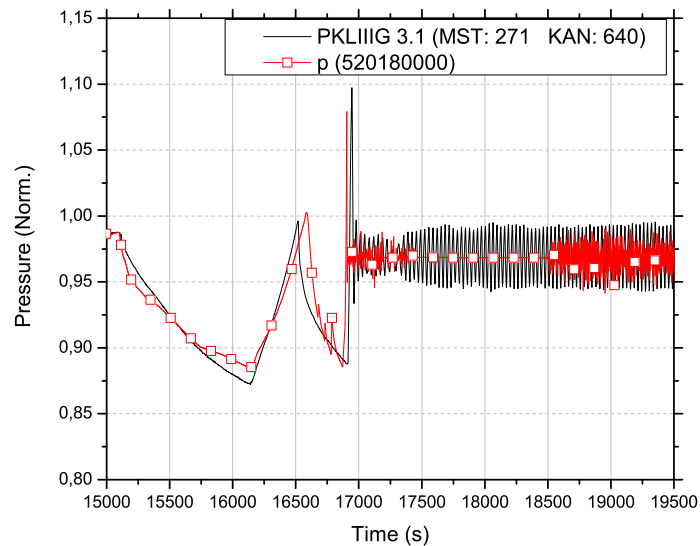


Figure 2.53: Pressurizer pressure

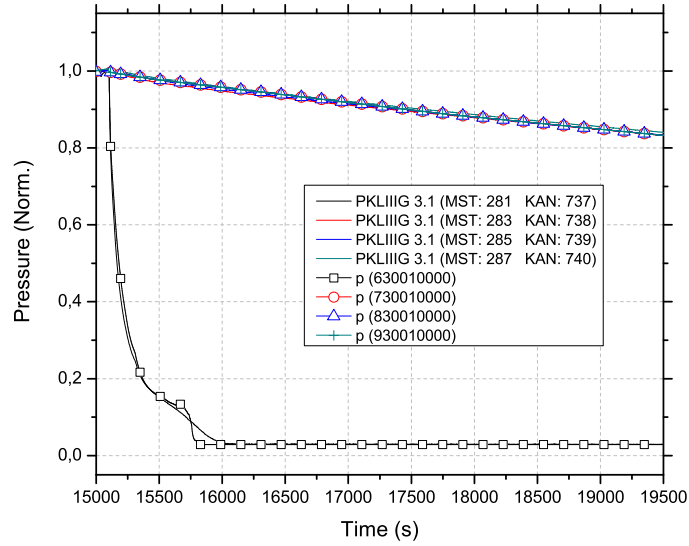


Figure 2.54: SGs pressures

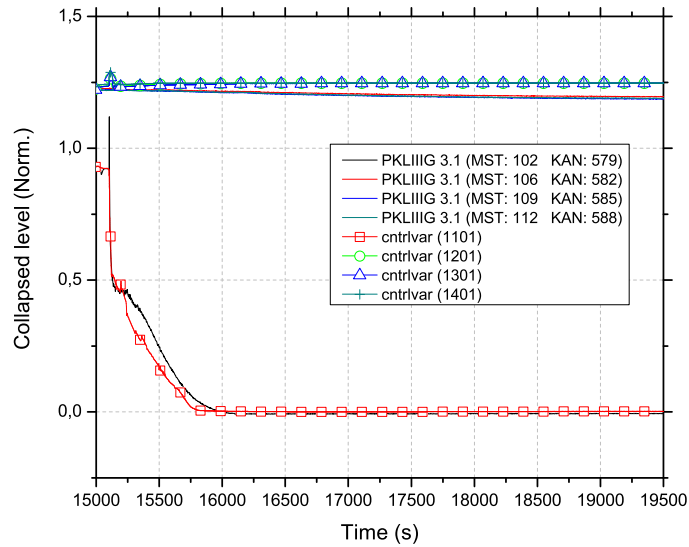


Figure 2.55: SGs riser collapsed level

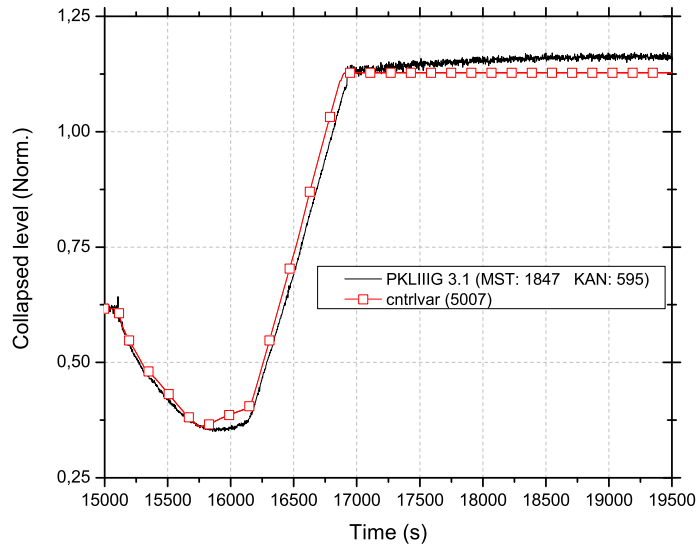


Figure 2.56: Pressurizer collapse level

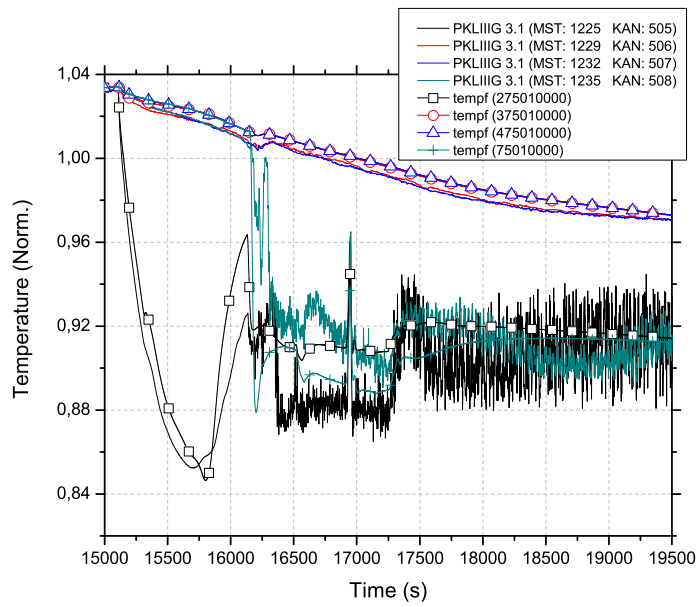


Figure 2.57: Cold leg temperatures

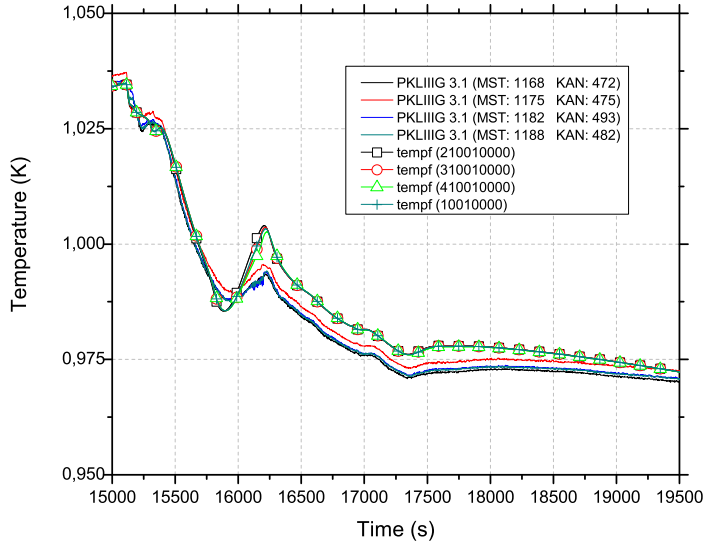


Figure 2.58: Hot leg temperatures

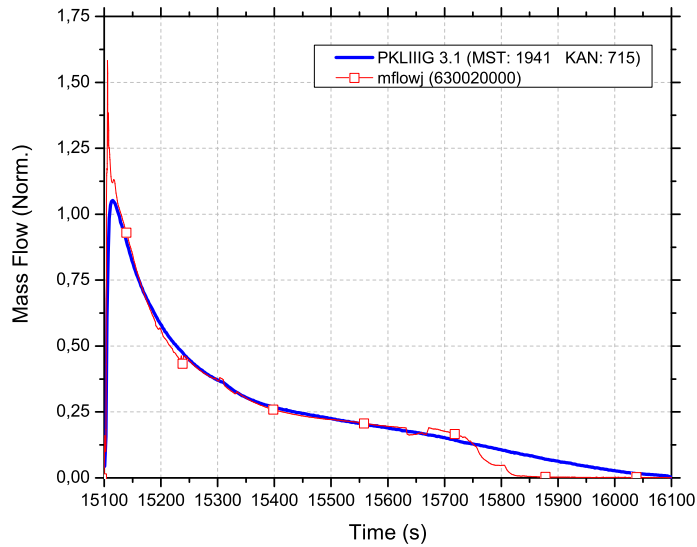


Figure 2.59: Main steam line discharge flow rate

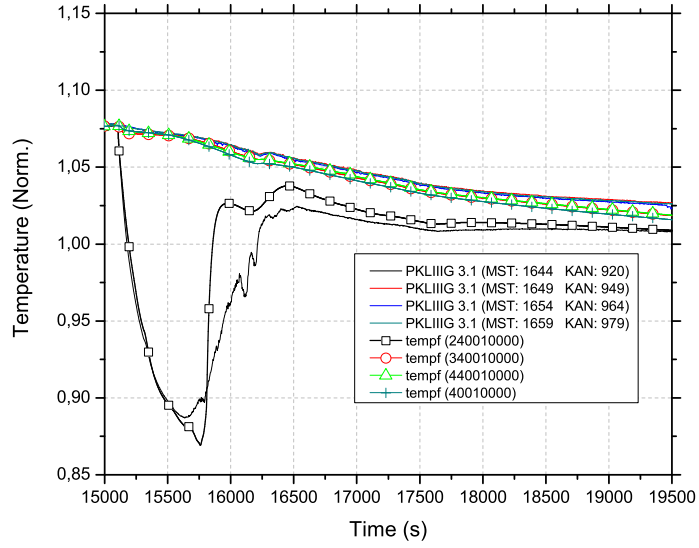


Figure 2.60: SGs outlet temperature

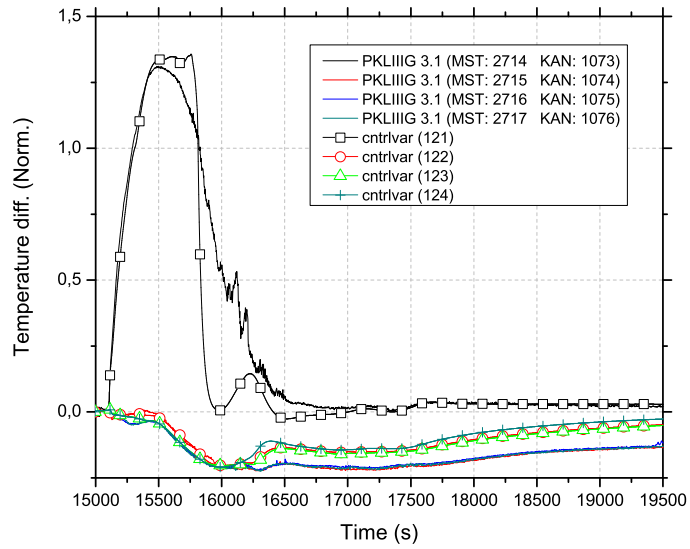


Figure 2.61: SGs difference temperature

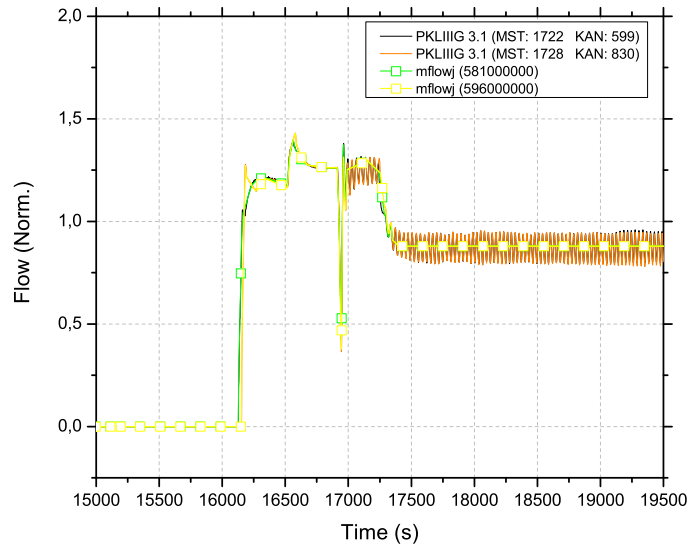


Figure 2.62: HPIS flow rate

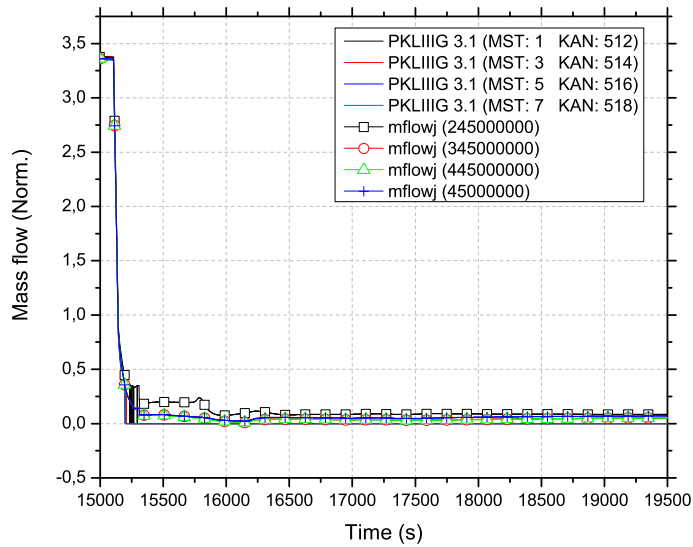


Figure 2.63: Loops 1-4, flow rate wide range

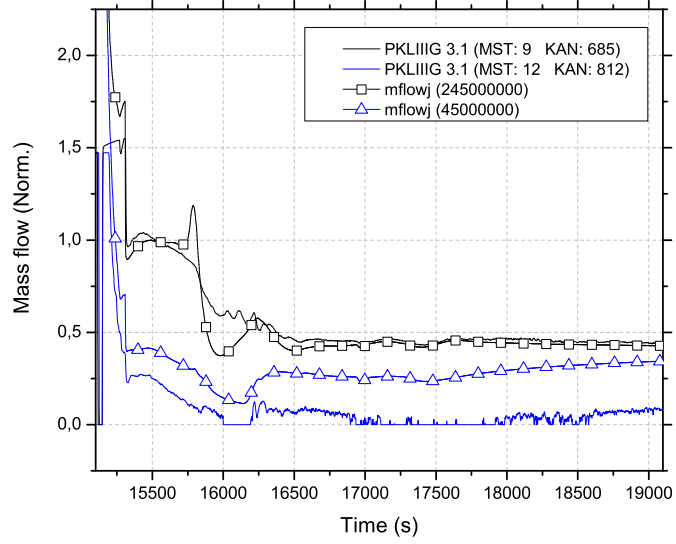


Figure 2.64: Loops 1-4, flow rate narrow range

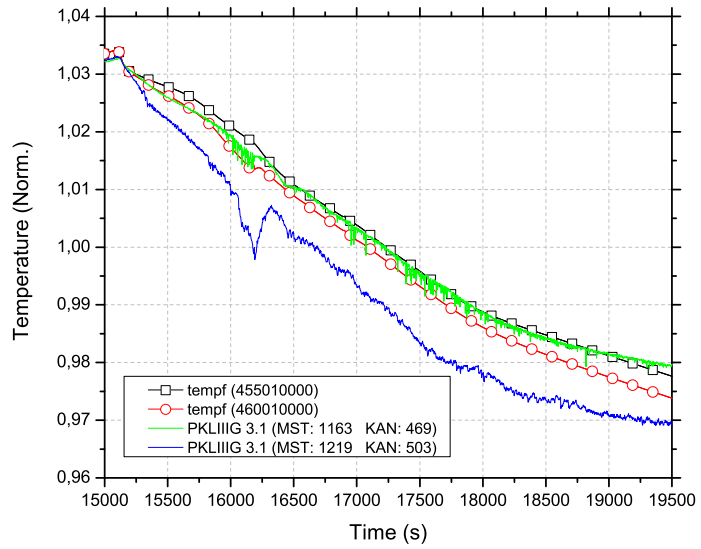
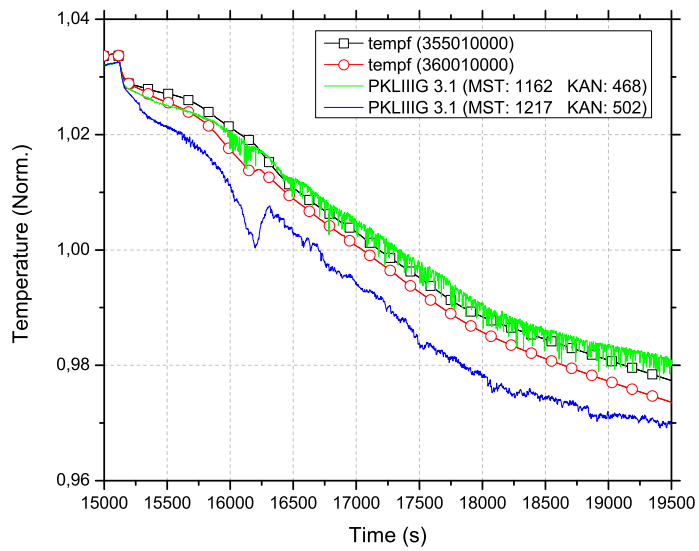


Figure 2.65: Loop 3 RCP ΔT

Figure 2.66: Loop 4 RCP ΔT

3. K_v scaled calculations

In the framework of the NPP nodalization qualification and quality guarantee procedures, K_v scaled calculations are of great value because they allow testing capabilities of NPP nodalizations and plant response under accident conditions. A K_v scaled calculation is a system code simulation in which defined ITF test conditions are scaled-up to an NPP nodalization in order to reproduce the same scenario. It allows the behavior of the NPP and ITF nodalizations to be compared under the same conditions and hence, to check the validity of the NPP nodalization and to improve it when needed.

In a plant scaled calculation, experimental conditions and safety actions are adapted without modifying the NPP nodalization. Special care is taken in order to prevent overdetermined systems. The most significant parameters are:

- Steady-state conditions
- Break size
- Break unit and containment
- Core power decay curve (if it is experimentally imposed)
- Pump coastdown curves (if they are experimentally imposed)
- Scram set point
- Isolation set points
- ECCS's set points
- ECCS injection curves (pressure versus mass flow curves)
- Blow down set points
- Specifications of the blow down valves (area, opening and closing ratios)
- Feed water controllers.
- PZR heater controllers (If this is the case)

The scaling-up adjustment is performed by following the scaling criterion and using scaling factors recalculated for the specific NPP nodalization. These are usually different from those used in the ITF design (related to the ITF reference plant). As explained in ref. [6] and [37], three scaling criteria can be adopted for designing scaled-down systems:

- Time reducing or linear scaling
- Time preserving or volume scaling
- Idealized time preserving

A greater number of ITF tests have been performed in facilities that have been designed using the Power to Volume scaling criterion, which encompasses time preserving scaling. Hence, the following scaling-up techniques will be related with the Power to Volume scaling. A further explanation about this criterion can be found in Section 4.1.

One of the important points of this activity is the calculation of the NPP scaling factor (K_v factor) which was commonly computed as the ratio between the primary liquid volume of the NPP and the ITF. This criterion should be revised given that several NPP components (PZR, SG plenums, pumps, ...) can differ significantly in volume with those of the ITF reference plant and is due to dissimilar design. The author of the present thesis suggests checking which components and parameters have a local scaling factor close to the reference ITF volumetric factor in the ITF system description report. Subsequently the analyst should calculate the scaling factor as an average of the same local factors applied to the chosen NPP. Normally core power, core volume and total number of U-tubes (for PWR) are a good reference.

As regards the "UPC scaling-up methodology" that is presented in this thesis, K_v scaled (so-called plant scaled) calculation is a unique calculation with two aims:

- To check the applicability of the ITF test in the NPP nodalization for phenomena that has been validated in post-test analyses.
- Being a reference for justifying as an expert judgment those discrepancies that appear in comparison with the results of the post-test analysis. Therefore, scaled-up and hybrid nodalizations explained in Sections 5.4.1 and 5.5 will be essential.

And it is in this second point where the "UPC scaling-up methodology" introduces a revision. As it will be seen in the state of the art of the K_v scaled calculations, previous applications qualified and justified discrepancies that appeared between the NPP and ITF simulations with the backup of qualitative techniques (i.e. "on transient" qualification of Bonuccelli's methodology) and the background of the analyst. As a plus, the present methodology allows identifying discrepancy sources with a systematic procedure, supporting judgment of the analyst and reducing its arbitrariness. More detailed information about this technique can be found in Chapter 5.

The following Sections will go through the state of the art of the K_v scaled calculations, and an example with a particular application to the Asco-2 NPP nodalization. The state of the art contains relevant references of performed K_v scaled calculations as well as methodologies that integrate this technique and reports that mention it. Similar scaled calculations that are called with other names are also included. On the other hand, the particular application to the Asco-2 NPP nodalization is based in the OECD/NEA ROSA Test 3-1 that has been described in Section 2.1.4.1.

3.1 State of the art

3.1.1 UMAE methodology: Krsko K_v scaled calculation

A full application of UMAE methodology is done by professor D'Auria [14] over the SBLOCA Counterpart test that was performed in BETHSY, LOBI, LSTF and SPES facilities. The extrapolation of the post-test simulations accuracies (with RELAP5mod2) is applied to the PWR Krsko NPP nodalization. A K_v scaled calculation is completed as a step of the UMAE methodology for qualifying the Krsko nodalization in an "on transient level" of the Bonuccelli methodology. It is mentioned that the uncertainty related with the nodalization qualification of the K_v scaled calculation is included in the errors bands of the final Krsko SBLOCA simulation, but it is not described how to compute it and which is its relative weight versus the reported and referenced error bands.

3.1.2 Preliminary assessment of Scaled-up and Hybrid nodalizations

A preliminary assessment of the "Scaled-up" and "Hybrid nodalizations" was carried out by Santiago Lucas in his master thesis [56]. Two K_v scaled calculations of LOBI BL-30 and B-44 were performed over the Asco-2 NPP input deck. Results of the K_v scaled calculations shown a good agreement for reproducing the TH phenomena of the experiment. Some discrepancies were reported for the BL-30 transient, related with the primary system depressurization, HPIS injection, and mass inventory after core dryout occurrence. Additionally, for the BL-44 test, it was also noticed discrepancies in system

pressures, ECCS response and timing of core uncoveries after secondary system isolation signal. In both cases, it was demonstrated that discrepancies between ITF and K_v scaled calculations could be justified by the different environmental heat losses of both facilities. Hence, it was demonstrated the potentials of "Scaled-up calculations" and intermediate simulations for qualifying and improving NPP nodalizations.

3.1.3 Asco NPP nodalization: K_v scaled calculation of the OECD/NEA ROSA-2 test 3

A K_v scaled calculation of the OECD/NEA ROSA-2 Test 3 is applied to an Asco NPP nodalization by Jordi Freixa [57]. This transient is characterized for analyzing the effectiveness of the CET AM signal in the detection and mitigation of core heat up. Scalability between Asco and LSTF was analyzed in order to select the best K_v factor for the specific scenario. Results showed a very similar response between the LSTF nodalizations and the Asco NPP nodalization. Only a few scaling issues were detected (e. g. significant differences between the K_v factor associated to the loops and the equivalent of the RPV) without being justified with sensitivity analyses. It was also concluded the relevance of 3D modeling for reproducing properly the CET response. Finally, a simulation of the actual NPP scenario conditions was done pointing out the necessity of further studies in this field as well as the importance of nodalization quality assurance.

3.1.4 EPR NPP nodalization: K_v scaled calculation of the OECD/NEA ROSA test 6.1

A K_v scaled calculation of the OECD/NEA ROSA Test 6.1 is applied to an EPR NPP nodalization by Jordi Freixa [41]. This test reproduces a SBLOCA at the UH of the RPV. Two different K_v factors are applied to the BICs of the primary and secondary systems because of the differences in the geometries of the EPR and Westinghouse SGs. TRACE calculations show very similar results in comparison with experimental data. The only significant discrepancy is observed in the faster depressurization associated to the core uncover. Possible distortion sources are listed and analyzed with sensitivity analyses of local scaling factors (break, passive HS, ...) and independent calculations. Discrepancies are partially justified by the different hardware configuration of the RPVs.

3.1.5 Scaling-up of BETHSY 9.1B Test results to Krsko NPP

An exhaustive work [42] [58] [59] [60] was conducted by Professor Petelin with RELAP5 in order to analyze the effects of the scaling-up in ITFs results. A preliminary K_v scaled calculation of BETHSY 9.1B SBLOCA test (ISP-27) was performed over a Krsko NPP nodalization showing significant discrepancies in relevant TH phenomena as peak cladding temperatures and system depressurization. Intermediate scaled-up nodalizations with the size of Krsko NPP were generated in order to analyze the effects of the scale: the first one preserving the Froude number, the second splitting the loops from two to three, and third one preserving the tensile stress of the structures materials. This last nodalization showed a close agreement with the BETHSY 9.1B test results, justifying the impact of the walls and passive structures in the behavior of an SBLOCA. No conclusions were reported about the discrepancies of the K_v scaled calculation with the BETHSY test.

3.1.6 Zion NPP nodalization: K_v scaled calculation of L2-5 test

In the framework of the A. Petrucci Ph.D. thesis [61] it was included a RELAP5 K_v scaled calculation of the LOFT L2-5 LBLOCA Test. Boundary and Initial conditions of the test were scaled-up to ZION NPP nodalization with the ratio between the primary side coolant volumes of the NPP and the facility. Results demonstrate the capabilities of Zion nodalization to reproduce main phenomena of the experiment. No new phenomena are brought in the K_v scaled calculation and discrepancies are as a result of the differences in the hardware configuration. With the K_v scaled calculation,

the nodalization was "on transient" qualified following the Bonuccelli methodology. The discrepancy sources are listed in the document but not justified.

3.1.7 Asco-2 NPP nodalization: K_v scaled calculation of LOBI BL-30 test

A K_v scaled calculation of LOBI BL-30 experiment is applied to Asco-2 NPP nodalization by Patricia Pla [39]. Results show good agreement with experimental data with some discrepancies in the accumulator behavior. Possible distortion sources are listed but not justified. To complete and compare the results, for the same NPP nodalization two other calculations are included: a non scaled reference calculation of a 5% SB-LOCA in the cold leg with all the typical NPP safety systems connected, and a SB-LOCA calculation with only the break area scaled and all the typical NPP safety systems connected. Both calculations led to a safe shutdown.

3.1.8 Asco-2 NPP nodalization: K_v scaled calculation of PKL F1.1 test

Boron dilution events during SBLOCA are tested by Jordi Freixa [40] with RELAP5mod3.3 at NPP level. The selected plant and test are Asco-2 and PKL F1.1 test. K_v factor is calculated with the ratio of the total volume of the loops. BIC are scaled-up from PKL test, and pressures of Asco NPP are reduced to 45 bars in order to start the transients at identical pressures. The K_v scaled calculation yields similar results as the ones obtained in the PKL nodalization and experimental data. It was necessary to renodalize the loops with finer meshing in order to avoid some numerical diffusion and to simulate properly the slug formation and evolution. Several base and sensitivity cases with actual Asco EOPs actions are also simulated. The most important features of the test are similar in the simulations.

3.1.9 Mochovce NPP: BEPU analyses and K_v scaled calculation of PMK-2 PH4-SLB test

A BEPU analysis using CIAU methodology is applied by Marian Kristof [62] in a K_v scaled calculation of the PH4-SLB test. The selected NPP is the VVER-440/213 Mochovce plant and the selected scenario is a surge line break accident. All major phenomena of the experiment are successfully simulated. Some differences in the timing are reported as a result of discrepancies in the depressurization rate during ECCS injection. Authors justify the discrepancies with the differences in the design of some components (safety injection pumps) and BIC. No sensitivity analyses are performed for justifying those discrepancies.

3.1.10 WWER-100 NPP: Application of Bonuccelli methodology

This paper, written by G. Aprile [36], shows the application of the Bonuccelli methodology for qualifying a WWER-1000 Plant Nodalization (for Kozlodoy-5 NPP). Two steps are applied. In the first, nodalization is qualified for an steady-state level, following a: the guidelines of the Code User Manual, b: comparing the input data with the design reference values, and c: checking the results of the steady-state calculations (absolute values and time derivative time trends) with the available operational data. In a second step, so-called transient level, nodalization was qualified with a quantitative (using FFTB) and qualitative comparison between several calculations of operational transients and their available NPP data. Finally, VVER nodalization was also qualified by comparing an SBLOCA transient in a Western Type PWR (Krsko NPP) with a K_v scaled calculation.

3.1.11 LOFW: Evaluation of loss of feedwater in ITFs and NPPs

The paper completed by Professor D'Auria [63] deals with the evaluation of the capabilities of RELAP5mod3 in simulating TH phenomena associated to LOFW scenario and related AM procedures. Two pos-test analyses are performed for the LOBI BT-17 and SPES-1 SP-FW-02 tests being compared with previously qualified RELAP5mod2 calculations. Related with the scaled calculations, a

counterpart transient is also simulated in a NPP nodalization predicting the Nuclear Plant response under the same plant scenario.

3.1.12 R. Bovalini: NPP scaled calculations of BWR SBLOCA scenario

This paper (Bovalini, [64]) summarizes the main results obtained by UNIPI with RELAP5mod2 simulations of the SBLOCA counterpart experiments carried out in BWR ITFs. Test facilities are PIPER-ONE, FIST and ROSA-III, and tests are respectively PO-SB-07, 984 and 6SB2C. The transient simulates a small break in the recirculation line of a BWR-6 with the high-pressure injection systems unavailable. Two scaled-up counterpart tests are done for a typical BWR NPP nodalization. From the simulation of the ITFs test code accuracy is assessed and extrapolated to the NPP simulations.

3.1.13 "Scaling and counterpart test"

Several Counterpart Test calculations (of PIPER-I, FIST, ROSA-III, SPES, SEMISCALE, LOBI, PKL, BETHSY and LSTF facilities) and K_v scaled calculations (Caorso BWR NPP, Doel and Krsko PWR NPPs) were performed by Professor D'Auria and et. al. [65] for different test scenarios (BWR SBLOCA, PWR NC, SBLOCA and LOFW) in order to compare results at different scales and to attempt to scale-up as the phenomena measured in small scale facilities as the accuracy of the codes. Analyses of experimental data confirmed that direct scaling extrapolation from ITFs to NPPs is unrealistic and the need to use system codes for performing the scaling analyses.

3.1.14 KNGR NPP: K_v scaled down calculations of a SBLOCA scenario

This paper (J. Song, [66]) compares the results given by three different RELAP5mod3 nodalizations under counterpart SBLOCA conditions. The input decks are a whole model of the Korean next generation reactor (KNGR), and two scaled-down nodalizations representing two kinds of KNGR experimental test facilities, one following the power-to-volume scaling criterion, and the other reducing the heights and therefore, the timing. Results show close agreement between the three inputs, validating the applied scaling-down criteria.

3.1.15 APR-1400 NPP: K_v scaled down calculation of a LBLOCA scenario

Similarity between APR-1400 and a scaled-down model with reduced-height is evaluated for a LBLOCA by H. Park [67]. The selected code is MARS. APR-1400 NPP nodalization is scaled-down following the scaling criterion used in ATLAS ITF design. Boundary and initial conditions are also scaled as in a K_v scaled calculation, hence counterpart transients are compared. Results show very similar TH response (pressures, break mass flow rates, PCTs, void fractions distributions, ...) as in the NPP as in the scaled-down nodalization. The authors conclude that similarity is expected in a hypothetical ATLAS LBLOCA test.

3.1.16 VVER 1000 simulators: Evaluation of measured and calculated counterpart test data

The article written by Professor D'Auria [68] is focused on testing the "scaling strategy" followed in the design SBLOCA PSB-VVER counterpart test as well as the capabilities of RELAP5mod3 for simulating the phenomena of the same scenario at different scales. Comparison between experimental data of the different counterpart tests shows high similarity, reproducing the same TH phenomena with similar time trends. On the other hand, the results of the calculations obtained high accuracy following the FFTB quantitative qualification criterion. It demonstrates, together with the other qualified SBLOCA counterpart post-test simulations, the capabilities of RELAP5mod3 for reproducing the same TH phenomena at different scales.

3.1.17 ”Scaling Analysis in BEPU licensing of LWR”

This paper (D’Auria [69]) is based on the roadmap to scaling introduced by F. d’Auria and G. M. Galassi in the article [7]. Particularly, it summarizes the roadmap and characterizes it for using best-estimate codes for licensing within the frame of BEPU calculations, establishing a strategy for qualifying not only code, but also the code-user (that must be guaranteed) and the final NPP nodalizations. This application is strictly connected with the availability of suitable experimental data and facilities, as far as Counterpart test and similar tests that demonstrate the preservation of thermalhydraulic processes regardless of the scale. K_v scaled calculations are mentioned for qualifying NPP nodalizations in an ”on transient level” of the Bonuccelli methodology.

3.1.18 ”TH System codes in Nuclear Reactor Safety and Qualification Procedures”

This paper (A. Petruzzi, [70]) provides a detailed overview of the relevance of the qualification procedures as for validating the code as for qualifying the NPP nodalizations. About this point, it shows the potential problems and errors that can be found in the nodalization process and gives a general approach for qualifying NPP nodalizations with ITF experiments. It is mentioned the importance of the K_v scaled calculations but does not describe an specific procedure for qualifying these calculations (just comparison between calculation trends and application of FFTBM for quantitative qualification).

3.2 K_v scaled calculation of OECD/NEA ROSA Test 3.1

This Section is focused on the simulation (with RELAP5/mod 3.3) and the scaling-up of the ROSA LSTF Test 3-1 experiment (an Anticipated Transient Without Scram -ATWS- during 1 % cold leg small break LOCA) to the Spanish Asco-2 NPP nodalization using K_v scaled calculations technique. One of the aims of this work [38] was to check if the main phenomena in the test are actually reproduced in the plant calculation. The description of the facility as well as the experiment and the post-test calculation are provided in Sections 2.1 and 2.1.4.1.

3.2.1 Asco-2 NPP nodalization

Asco-2 NPP (Figure 3.1) is a Westinghouse design PWR with 1000 MWe. It has a 3-loop configuration with the pressurizer connected to the second loop. There are two HPSI and two LPSI pumps that inject to a common header connected to all loops. Accumulators are connected to each cold leg and have independent lines.

The Asco-2 NPP nodalization (Figure 3.2) has been validated during several years covering a large amount of transients [28] [32] [31] [39] [40] . During the last decades, it has proven its capability to face new problems. All primary and secondary systems are included; moreover, all control systems have been implemented as they are in the real plant. The code used is a version of RELAP5/mod3.3. All in all the model is composed by the following components:

- 549 hydrodynamic volumes
- 1454 control variables
- 219 variable trips
- 431 logical trips
- 241 tables
- 117 interactive variables

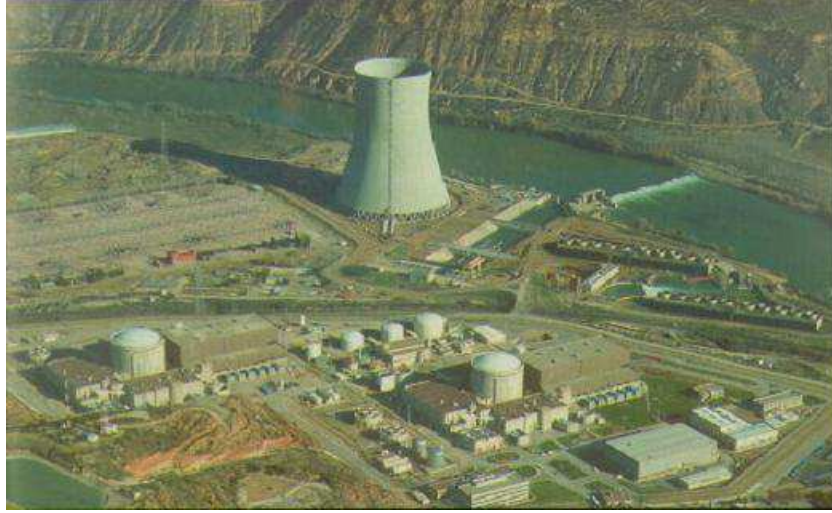


Figure 3.1: Asco-2, Pressurized Water Reactor

Two criteria were used in the scaling up of the BICs:

- Design of a conditioning phase to adjust the Asco NPP steady state parameters to the ROSA/LSTF Test 3-1 initial conditions (plant working at 14 % of its nominal power).
- Calculation of a K_v factor to adjust those parameters and/or geometries with large discrepancies once steady state conditions are established (main feedwater, nuclear power, break junction, accumulator volumes, ...).

3.2.1.1 Conditioning phase

The conditioning phase is divided into three intervals (see Figure 3.3):

- -2000 to -1800 seconds: Asco NPP model working at 100 % of its nominal power. A time-dependent-volume is used to fix the primary pressure and temperature conditions.
- -1800 to -1400 seconds: Nuclear power, primary mass flow rate, main feedwater and primary-to-secondary heat transfer are linearly decreased to 14 % of its nominal values. The time-dependent-volume is not used.
- -1400 to 0 seconds: Asco NPP model works at 14 % of its nominal values. Other parameters like the pressurizer level and the secondary steam generator level are fixed to LSTF initial conditions during this period (see Figure 3.4).

DIAGRAMA DE NODALIZACIÓN DE ASCO

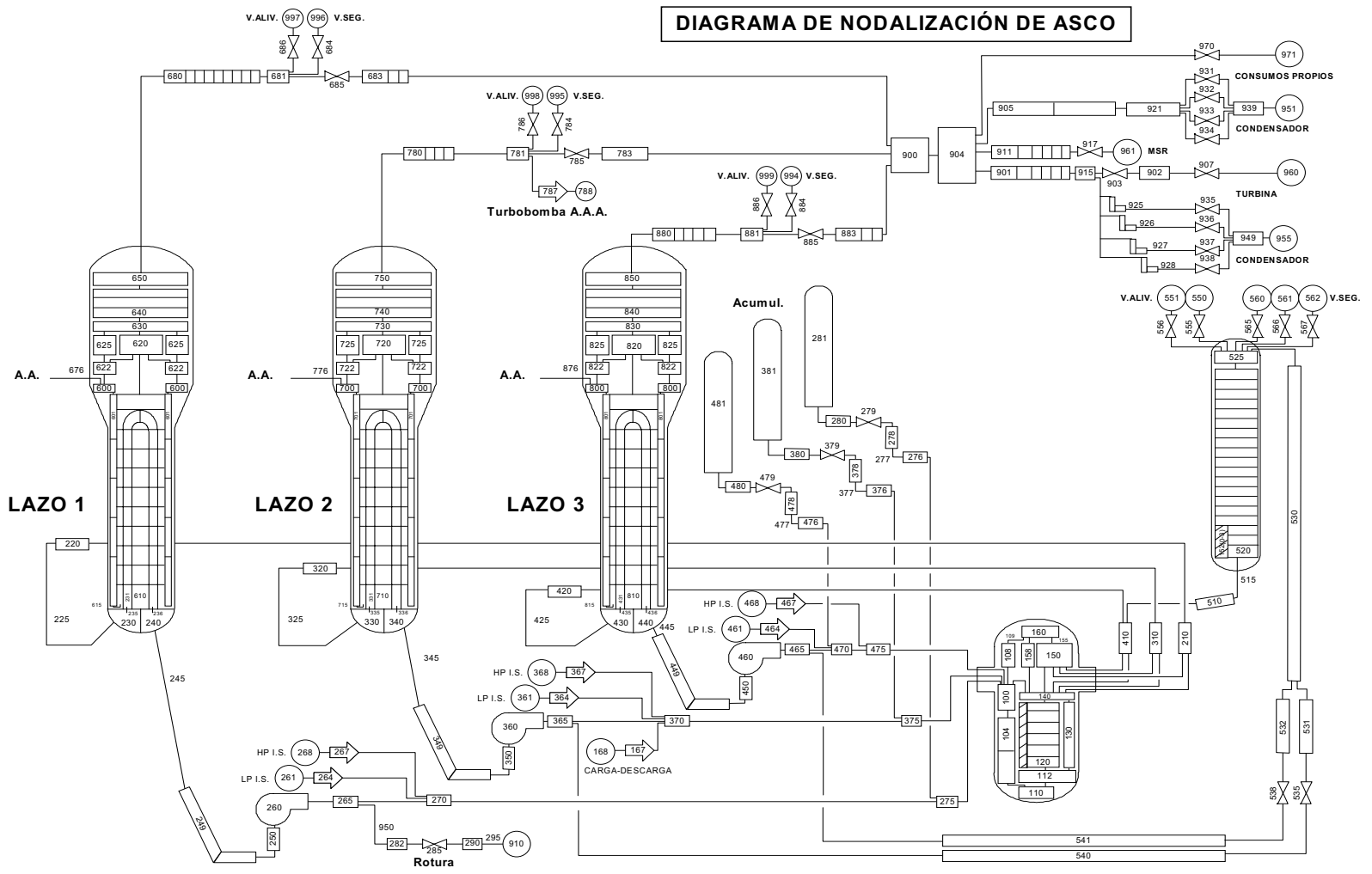


Figure 3.2: Asco-2, nodalization

3.2. *Kv scaled calculation of OECD/NEA ROSA Test 3.1*

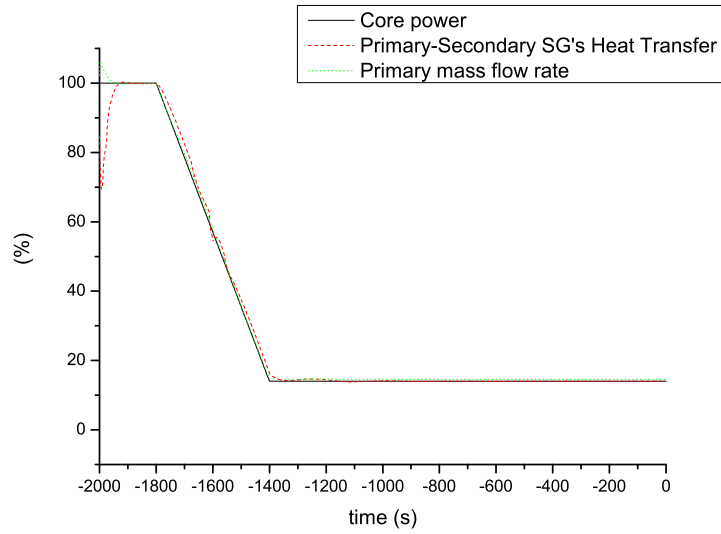


Figure 3.3: Conditioning phase

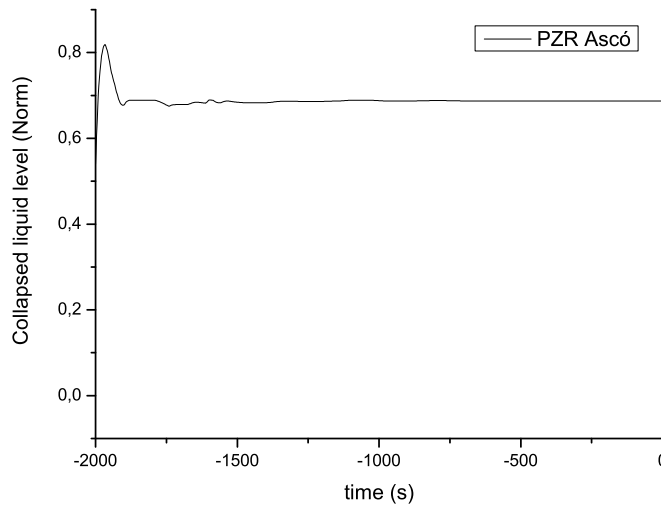


Figure 3.4: Pressurizer collapsed liquid level

3.2.1.2 K_v factor

LSTF test facility has a scaling factor of 48 but this value varies depending on the geometry or on the plant parameter analyzed. It happens because many aspects like flow regime or heat transfer are taking into account when a test facility is designed. LSTF scaled parameters with less discrepancies regarding "48 factor" were chosen to calculate a comparable average LSTF-Asco K_v factor obtaining a proposal value of 40.

Initial conditions (nuclear power, primary mass flow rate, main feedwater) and geometries (accumulator volumes) similar to its theoretical scaled value were not modified to respect its original

plant design (see table 3.1); parameters are normalized to the scaled up steady state values of LSTF simulation). Auxiliary feedwater was scaled taking into account the K_v factor.

| | Asco NPP RELAP simulation [Norm] |
|----------------------------|-------------------------------------|
| Nuclear power | 1.026 |
| Primary mass flow rate | 0.987 |
| Main feedwater flow rate | 1.029 |
| Steam flow rate | 1.025 |
| Accumulators volume | 0.975 |
| Accumulators liquid volume | 0.991 |

Table 3.1: Parameters not scaled with K_v factor

3.2.1.3 Break unit

The break unit was modeled using the sK_v factor and reproducing the LSTF pipes and junctions between the orifice assembly and the storage tank. Henry-Fauske coefficients used and validated for the LSTF Test 3-1 post-test were maintained. To set the orifice section the initial scaled value was modified adjusting the break mass flow rate of the Asco NPP model to the LSTF theoretical scaled plot (see Figure 3.5). The cross section was set to $2.57 \cdot 10^{-3} m^2$.

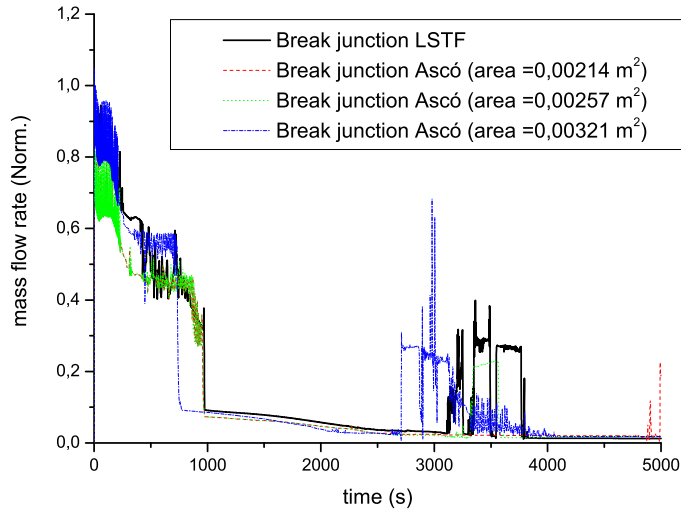


Figure 3.5: Break junction sensitivity analysis

3.2.1.4 Initial conditions

Table 3.2 compares initial conditions between the Asco-2 NPP scaled model and the LSTF Test 3-1 simulation. Values are normalized to the measured Test 3-1 steady state conditions.

Secondary side collapsed liquid level was modified to adjust the Asco NPP secondary mass with the LSTF scaled secondary mass. The aim of this change was to scale-up the amount of energy that can be stored in the coolant of the secondary system.

| | Asco NPP RELAP simulation (1/40) | LSTF RELAP simulation (loops w / wo PZR) |
|--------------------------------|--|--|
| Core power | 1.016 | 0.990 |
| Hot leg temperature | 1.0002 | 1.0 / 0.9997 |
| Cold leg temperature | 0.997 | 1.001 / 1.0 |
| Mass flow rate (x loop) | 1.026 / 1.024 | 1.04 / 1.021 |
| Downcomer-to-hot-leg bypass | - | 1.001 / 1.001 |
| Pressurizer pressure | 1.007 | 1.003 |
| Pressurizer liquid level | 0.971 | 0.971 |
| Secondary-side pressure | 0.998 | 0.998 / 0.998 |
| Secondary-side liquid level | 1.225 | 1.003 / 0.998 |
| Main feedwater temperature | 0.998 | 1.001 / 0.999 |
| Auxiliar feedwater temperature | 1.003 | 1.0 |
| Main feedwater flow rate | 1.036 | 1.008 / 1.031 |
| Accumulators pressure | 1.0 | 1.0 |
| Accumulators temperature | 1.0 | 1.0 / 1.0 |
| Steam flow rate | 1.029 | 1.002 / 1.029 |

Table 3.2: Initial conditions

3.2.2 Results

3.2.2.1 Test phase

Table 3.3 shows the chronology of the main events occurred in Test 3-1, comparing the experimental values with the UPC LSTF model and the Asco NPP Scaled model. The comparison between two models is described as follows

Primary and secondary pressure have good agreement with experimental data until 2,200 s, when the initiation of the accumulator injection system causes some discrepancies on the primary pressure and the break mass flow rate (see Figures 3.6 and 3.7). It is worth mentioning that there is an asymmetrical depressurization of the broken loop steam generator after primary pressure becomes lower than the SG secondary-side pressure. This phenomenon does not occur in the LSTF simulation (probably as a result of two symmetrical loops LSTF scaling). Asymmetrical termination of natural circulation is noticed in the Scaled Asco NPP simulation too (see Figure 3.8).

Figure 3.9 shows a similar secondary mass behavior with more losses in the Asco NPP Scaled model during natural circulation due to the safety valves opening which does not occur in UPC LSTF model (see Figure 3.10). Auxiliary feedwater is closed at 2,450 seconds to prevent water filling the SG separators (the volume factor of the SG is smaller than the K_v factor applied to the auxiliary feed water).

Figure 3.11 shows how the Asco NPP scaled simulation reproduces emptying of the core. Figures 3.12 and 3.13 show that the total primary system mass and the rod surface temperature have a quite good agreement with the LSTF simulation until the initiation of the accumulators injection.

| Event | Experimental | UPC LSTF nodalization | Asco NPP nodalization |
|--|-------------------|-----------------------|-----------------------|
| | [s] | [s] | [s] |
| Break | 0 | 0 | 0 |
| SCRAM signal: Turbine trip and closure MSIV PZR heater off End of MFW and begin of AFW | 20 | 20 | 20 |
| Start of RCPs coastdown | 23 | 23 | 23 |
| RCPs stop | 272 | 272 | 272 |
| End of continuous opening of SG RVs, End of two-phase natural circulation, break flow from single-phase liquid to two-phase flow | About 300 | 300-400 | 300-400 |
| Core liquid level starts to decrease (core uncover) | About 1100 | About 1100 | 1125 |
| Core power decrease by LSTF core p protection system | 1630 | 1707 | 1705 |
| Max. fuel rod surface temperature = 903 K | 1825 | 1890 | 2030 |
| Primary pressure lower than SG secondary pressure | About 1900 | 1875 | 2130 |
| Initiation of accumulator injection system | About 2100 | 2180 | 2240 |
| Loop seal clearing only in loop without PZR | About 2200 | 2898 | 3100 |
| End of the transient | 5547 | 5547 | 5547 |

Table 3.3: Chronology of the main events in the test T3-1

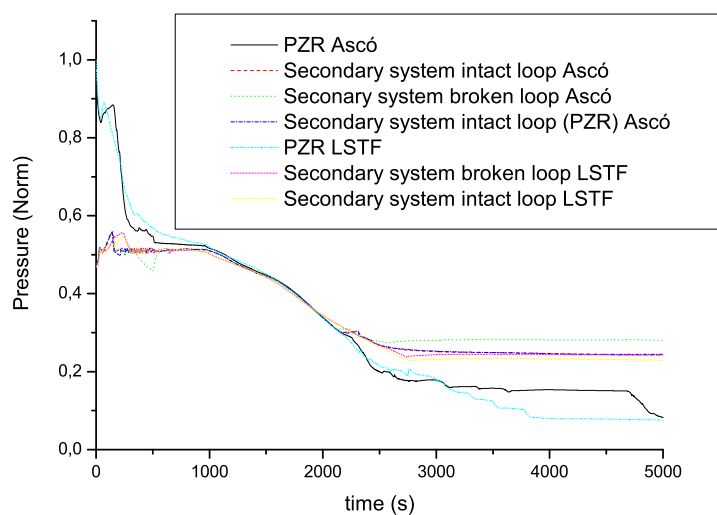


Figure 3.6: Primary and secondary pressures

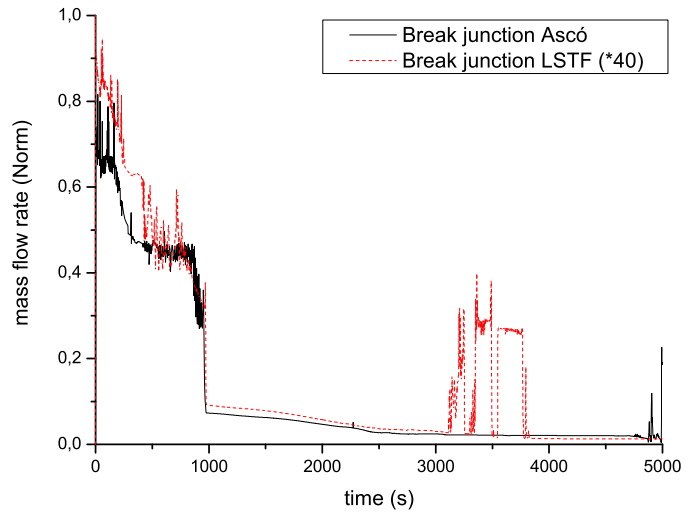


Figure 3.7: Break mass flow rate

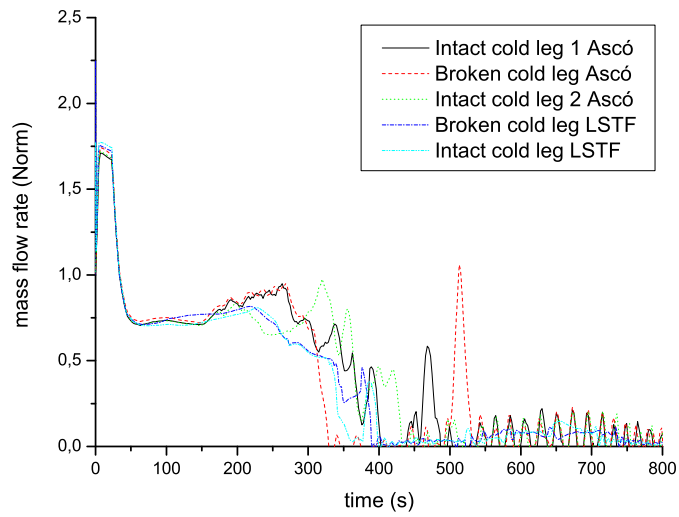


Figure 3.8: Cold legs mass flow rate

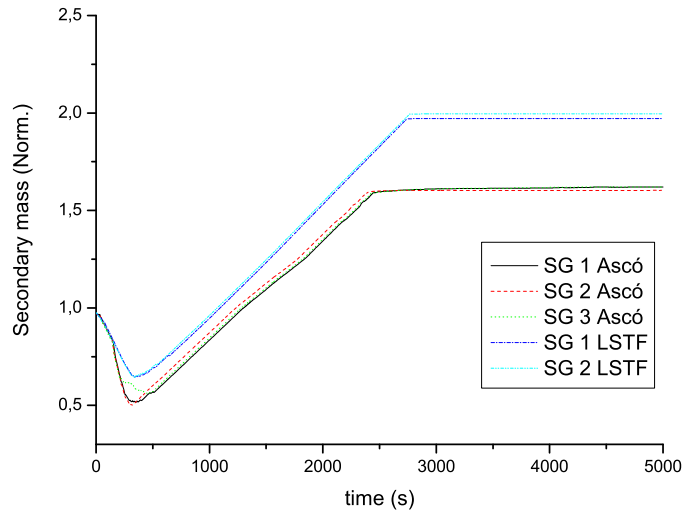


Figure 3.9: Secondary system mass inventory

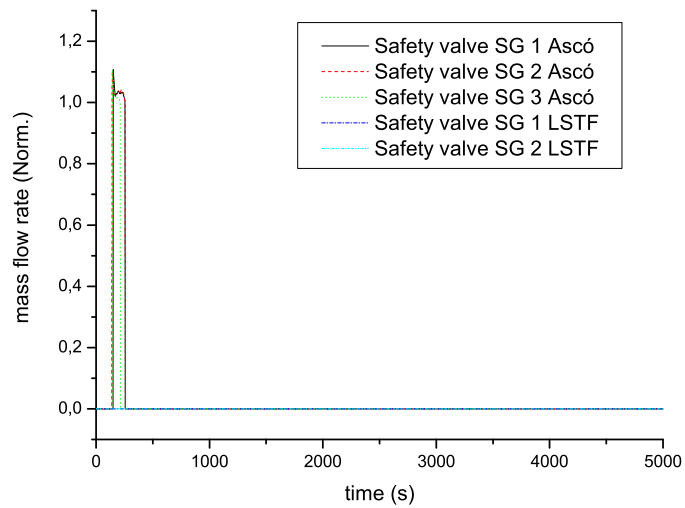


Figure 3.10: Safety valves mass flow rate

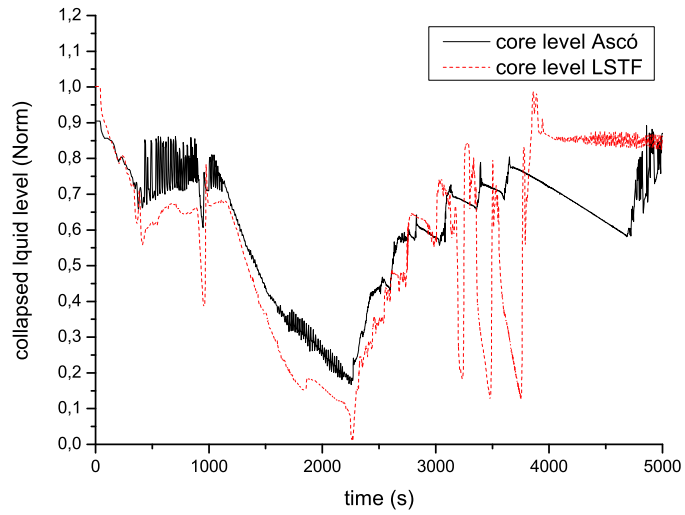


Figure 3.11: Core collapsed liquid level

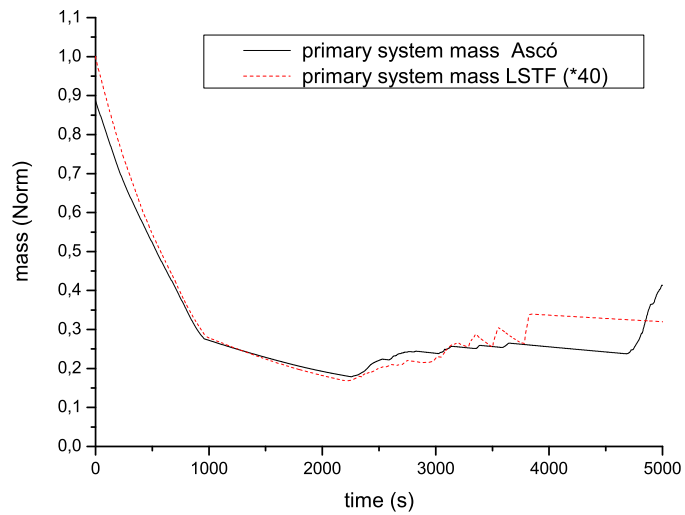


Figure 3.12: Primary system mass inventory

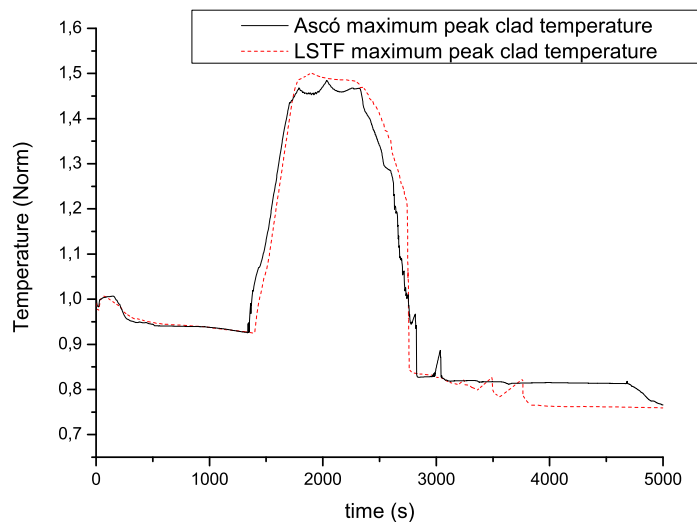


Figure 3.13: Maximum peak cladding temperature

3.2.2.2 Local phenomena: liquid accumulation in UTs due to CCFL

Supercritical flow during the two-phase flow Natural Circulation induces liquid accumulation at the U-tubes during reflux and condensation because of the counter current flow limitation in the U-tube inlet and in the bottom of the inlet plenum (see Figure 2.9).

RELAP5/mod3.3 reproduces the supercritical flow ($Froude > 1$) during the two-phase flow natural circulation (see the evolution of the Froude Number until 310 seconds in Figure 3.14). During the period of reflux and condensation (from 350 to 750 seconds, Figure 3.15), fluid velocity becomes nearly zero, while there is still gas circulation. This phenomenon justifies the need of modeling counter current flow limitation and the associated U-tube liquid accumulation. Figure 3.16 shows that this local phenomenon is quite well reproduced by RELAP5/mod3.3.

Liquid accumulation in the U-tubes affects directly to the primary-to-secondary heat transfer. During reflux and condensation, water remains stagnant at the U-tubes and heat transfer decays abruptly (see Figure 3.17). It causes a sharp depressurization in the broken loop steam generator and a partial increase in the primary pressure (Figure 3.18). This phenomenon does not occur in LSTF simulation, probably as a result of a smaller U-tube liquid accumulation (Figure 3.16) which does not affect to the primary-to-secondary heat transfer.

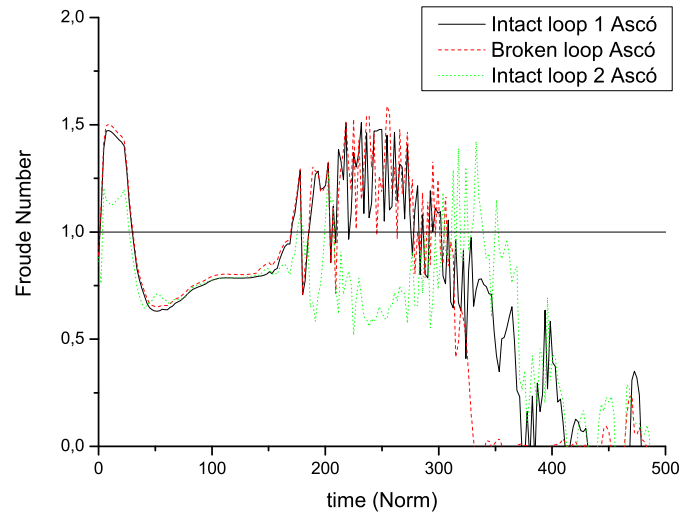


Figure 3.14: Froude number

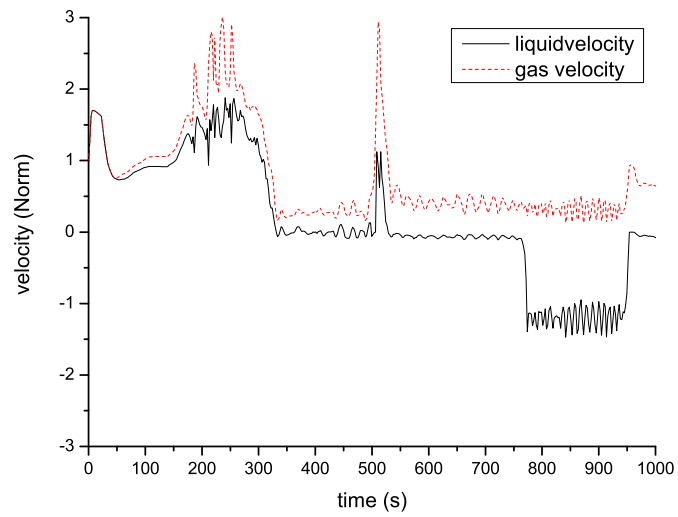


Figure 3.15: Velocities at the U-tubes inlet of the broken loop

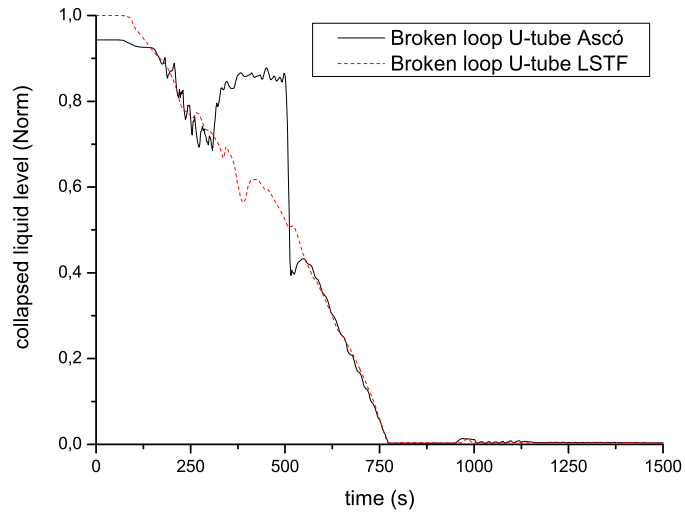


Figure 3.16: U-tube liquid accumulation in the broken loop

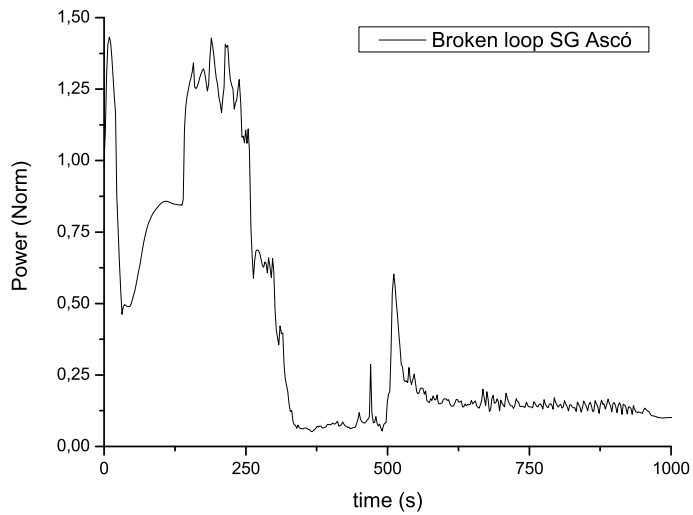


Figure 3.17: Primary-to-secondary heat transfer

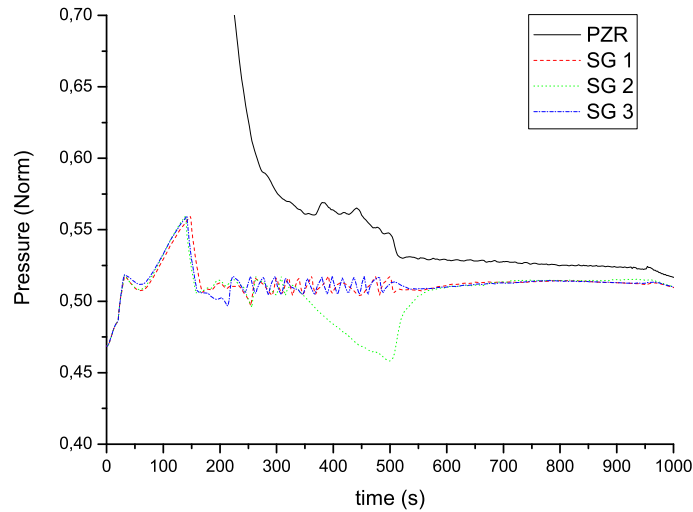


Figure 3.18: System pressures

3.2.3 Conclusions

A K_v scaled calculation of the ROSA/LSTF Test 3-1 experiment has been performed. Model predictions have been compared with a previous ROSA/LSTF Post-Test 3-1 calculation showing a quite good agreement between them and reproducing main TH phenomena. Several conclusions have been obtained from the study of local phenomena (U-tube liquid accumulation due to CCFL) and from several preliminary calculations:

- RELAP5/mod3.3 reproduces supercritical flow and liquid accumulation in the U-tubes during High-Power Natural Circulation.
- As there are some discrepancies between the LSTF/Reference PWR scaling factor and the volume factors of different LSTF parameters, it would be interesting to keep the original values of the plant if possible. Only in case of important differences with the scaled-up values, they should be changed using the K_v factor.
- Stagnant liquid at the U-tubes during reflux and condensation can affect the primary-to-secondary heat transfer, and consequently, both system pressures.
- Other differences between both simulations, like the asymmetrical depressurization of the broken loop steam generator after decoupling or asymmetrical termination of natural circulation, could be the result of having two symmetrical loops in LSTF.

The results of this study show the capabilities of Asco RELAP5/mod3.3 nodalization to deal with phenomena involved in natural circulation at high power like most of ATWS scenarios related to commercial NPPs analysis. On the other hand, some local qualitative discrepancies have been reported between the ITF simulation and the NPP K_v scaled calculation (water accumulated in the UTs during CCFL). In order to guarantee the quality NPP nodalization, further studies should be conducted in the future to justify if code, ITF scaling-down criterion, Asco NPP hardware design, or nodalization are generating this discrepancy.

4. PVST

The aim of this chapter is to introduce the Power to Volume Scaling Tool (PVST), a RELAP5mod3 add-on that allows generating scaled-up input decks following the Power to Volume Scaling methodology. The contents are divided in several sections:

- *"Power to Volume scaling methodology"* describes the equational basis of the K_v factor that is applied for designing scaled-down facilities following the PtoV scaling method.
- *"ITF designs: Application of the K_v factor"* shows the particular criteria applied in the design of the main components of an ITF, given that they vary depending on the relevance of the thermalhydraulic processes to be reproduced.
- *"RELAP5mod3 equations"* introduces all the equations involved in the code calculation as well as their dependencies.
- *"RELAP5mod3: Power to Volume scaling distortions"* compares the parameters affected by the scaling criterion with the dependencies of the RELAP5mod3 equations, in order to establish which are the scaling distortions that the code will introduce when PtoV scaling method is applied on a nodalization.
- *"PVST"* describes the software and the main features that have been included based on the background acquired from the previous sections.
- *"Assessment of PVST software"* shows the capabilities of the program under particular calculations. Main features are tested in order to check if the reported scaling distortions can be by caught easily by PVST.

4.1 Power to volume scaling methodology

Power to volume scaling is one of the most common methods used in the design of ITFs, especially the PWR experimental facilities built during the 80s and 90s. Scaling criteria are obtained by simplifying the balance equations of the system under certain assumptions and requirements. Taking into account that reactor flows are mainly dominated by large sources and sinks of power and momentum (core power, high depressurization rates, pumps, ...), interphase interactions are omitted, and mass, momentum and energy equations are analyzed for one directional single phase fluid (radial fluxes are also neglected). Thus, dimensionless equations used in the power to volume scaling approach are

$$\frac{\partial \rho^+}{\partial t^+} + \left[\frac{v_0 t_0}{l_0} \right] \frac{\partial \rho^+ v^+}{\partial x^+} = 0 \quad (4.1)$$

$$\rho^+ \frac{\partial v^+}{\partial t^+} + \left[\frac{v_0 t_0}{l_0} \right] \rho^+ v^+ \frac{\partial v^+}{\partial x^+} = - \left[\frac{P_0}{l_0} \frac{t_0}{\rho_0 v_0} \right] \frac{\partial P^+}{\partial x^+} - \left[\frac{\xi_0}{A_{c0}} K v_0 t_0 \right] \frac{\xi^+ \rho \kappa v^2}{A_c^+} - \left[\frac{g t_0}{v_0} \right] g^+ \rho^+ \quad (4.2)$$

$$\rho^+ \frac{\partial h^+}{\partial t^+} + \left[\frac{v_0 t_0}{l_0} \right] \rho^+ v^+ \frac{\partial h^+}{\partial x^+} = \left[\frac{\xi_0}{A_{c0}} \frac{q_0 t_0}{\rho_0 h_0} \right] \frac{\xi^+ q^+}{A_c^+} - \left[\frac{P_0}{\rho_0 h_0} \right] \frac{\partial P^+}{\partial t^+} - \left[\frac{v_0 t_0}{l_0} \frac{P_0}{\rho_0 h_0} \right] v^+ \frac{\partial P^+}{\partial x^+} \quad (4.3)$$

Where superscript + makes reference to normalized parameters and subscript zero to the normalizing values of the reference plant.

For obtaining the power to volume scaling parameters, it is considered that equations (4.1) to (4.3) must be equal for both the reference plant and the ITF, hence:

$$\begin{aligned}
 \left[\frac{vt}{l} \right]_R &= \left[\frac{vt}{l} \right]_{ITF} \\
 \left[\frac{P t}{\rho l v} \right]_R &= \left[\frac{P t}{\rho l v} \right]_{ITF} \\
 \left[\frac{\xi}{A_c} K v t \right]_R &= \left[\frac{\xi}{A_c} K v t \right]_{ITF} \\
 \left[\frac{g t}{v} \right]_m &= \left[\frac{g t}{v} \right]_{ITF} \\
 \left[\frac{\xi}{A_c} \frac{q t}{\rho h} \right]_R &= \left[\frac{\xi}{A_c} \frac{q t}{\rho h} \right]_{ITF} \\
 \left[\frac{P}{\rho h} \right]_R &= \left[\frac{P}{\rho h} \right]_{ITF}
 \end{aligned} \tag{4.4}$$

In order to preserve the equalities in Equation 4.4, the power-to-volume approach considers that the fluid properties and pressure are the same in both systems, and in addition the lengths of the system in the direction of the fluid are preserved, thus the following correspondences are valid:

$$\frac{P_R}{P_{ITF}} = \frac{\rho_R}{\rho_{ITF}} = \frac{h_R}{h_{ITF}} = \frac{l_R}{l_{ITF}} = \frac{t_R}{t_{ITF}} = 1 \tag{4.5}$$

With these assumptions, the following power-to-volume relations are obtained:

$$\frac{\phi_R}{\phi_{ITF}} = \frac{W_R}{W_{ITF}} = \frac{V_R}{V_{ITF}} = \frac{A_R}{A_{ITF}} = K_v \tag{4.6}$$

$$\left[\frac{\xi}{A_c} K \right]_R = \left[\frac{\xi}{A_c} K \right]_{ITF} \tag{4.7}$$

Further information about the calculation of the power to volume scaling factors can be found in Reference [71]. It is worth mentioning that condition (4.7) cannot be accomplished since perimeter (ξ) depends on the hydraulic diameter of the component to scale. Given that power to volume scaling conditions cannot be perfectly preserved between the facility and the reference plant, and some assumptions, like the omissions of the interphase interactions in the balance equations, are decisive for the proper reproduction of the thermohydraulic processes in specific components(e.g. heat exchange in the core and the SGs), a specific definition of the scaling factors is carried out depending on the components of the LWR.

4.2 ITF design: Application of the K_v factor

Integral Test Facilities are designed with the aim of analyzing the whole response of a commercial NPP under accidental conditions. Emergency Operational Procedures (EOPs), Accident Management and safety margins are the targets of their design, hence it becomes essential to reproduce thermohydraulic phenomena as close as possible to their reference plant. As shown in the previous section, several simplifications are applied in the power to volume scaling approach, thus specific transcription of the scaling factors is necessary depending on the component and the relevance of the thermohydraulic processes to reproduce. In the following subsections it is considered that the coolants of the ITF and the reference plant are identical and hence, fluid properties conditions of relationship (4.5) are accomplished.

4.2.1 Vertical volumes

Vertical volumes are scaled-down in order to preserve the inventory ratio, the balance equations under operational conditions (liquid single phase) and the pressures drops along the flow path. Thus, ITF and reference plant heights are the same in order to keep water columns, and volumes are scaled with the K_v factor just modifying the cross sectional area:

$$(\rho g H)_R = (\rho g H)_{ITF} \quad (4.8)$$

$$\frac{A_R}{A_{ITF}} = K_v \quad (4.9)$$

Components like vessel and SGs plenums are scaled-down following these relationships. On the other hand, the downcomer of the SGs and the reactor vessel can show relevant mixture conditions for accident scenario and require a particular expert judgment for the scaling-down. Subcooled water mixes with saturated coolant when AFW and ECCs are operative. If it occurs under shut-down conditions (low power), interphase frictions, mass and heat transfers cannot be neglected and they can affect to the correct reproduction of the reactor cooldown. Thus, in some ITFs designs, downcomers are scaled-down following (4.8) and (4.9), but also modifying the hydraulic diameter in order to minimize the impossibility to reach (4.7) and the impact of the single phase assumption in the power to volume scaling approach. In any case, despite the engineering approaches, it is impossible to remove completely the effect of the hydraulic diameter in the friction losses and the interphase interactions, thus scaling distortions cannot be completely avoided under these particular accident conditions. In the Figure 4.1 it is shown a comparison between the vessel design of a NPP and PKL. It can be noticed that downcomer has been modified from an annulus to two pipes so that the diameters are modified but the heights and scaled-down volumes are preserved. With this approach the hydraulic diameter is increased and becomes close to that of the downcomer in the reference plant

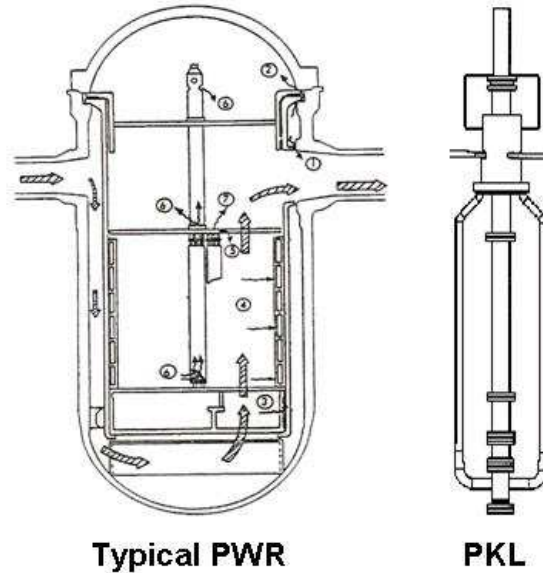


Figure 4.1: Vertical volumes in reactor vessel

4.2.2 Multi-channel regions

For multi-channel regions in where the relevant heat exchange processes of the facility take place, i.e. core region and SG riser, it is essential to scale identical flow regimes and heat transfers behavior

independently of the transient conditions. Thus, since the power to volume scaling approach neglects two-phase interactions, a multichannel criterion is applied in order to preserve identical geometries and flow paths. This consists of keeping the geometries of the NPP channels (heights, hydraulic diameters and pitch-to-rod diameter ratio) but reducing their number by the K_v factor for the ITF and thus preserving the volume scaling criterion:

$$\begin{aligned} V_R &= V_{chan} \cdot (num.chan_R) = K_v V_{chan} \cdot (num.chan_{ITF}) = K_v V_{ITF} \\ D_R &= D_{ITF} \\ H_R &= H_{ITF} \end{aligned} \tag{4.10}$$

With this criterion, as flow paths are identical, thermohydraulic processes are identical in each channel (without considering radial distribution feedback) and power to volume scaling factors are preserved for an overall application of the scaling approach.

4.2.3 Horizontal legs

Flow regime transitions in horizontal volumes (cold and hot legs) become essential during SBLOCA transients. Depending on their coolant mixture conditions, break discharging, core quenching, and primary-to-secondary heat transfer will be affected. Thus, for a proper scaling-down of horizontal legs, it is necessary to preserve flow regime transitions.

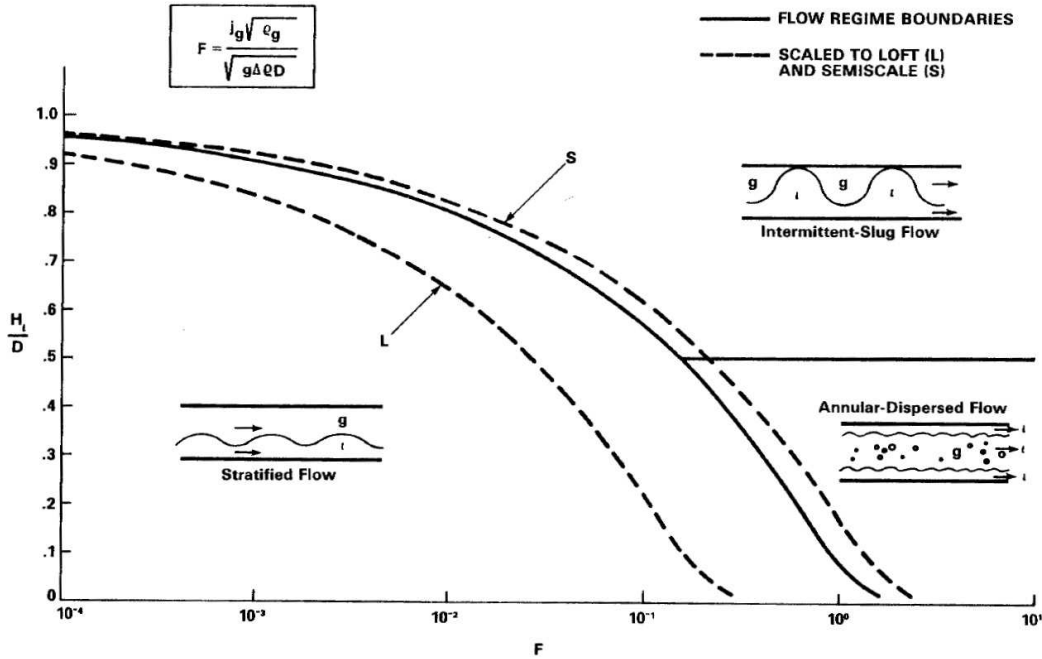


Figure 4.2: Dukler-Taitel flow regime map

Therefore, an additional power to volume scaling relationship is considered based on classical works performed by Taitel and Dukler [44] [72]. They observed, as it is shown in the diagram of the Figure 4.2, that flow regime transitions depends on the horizontal stratified level and the Froude number. Hence, for preserving Froude number as well as the power to volume scaling conditions for the volume and the mass flow rate

$$\begin{aligned} \left(\frac{v_g \sqrt{\rho_g}}{\sqrt{g \Delta \rho D}} \right)_R &= \left(\frac{v_g \sqrt{\rho_g}}{\sqrt{g \Delta \rho D}} \right)_{ITF} \\ W_R &= K_v W_{ITF} \\ V_R &= K_v V_{ITF} \end{aligned} \quad (4.11)$$

it must be accomplished that

$$\left(\frac{L}{\sqrt{D}} \right)_R = \left(\frac{L}{\sqrt{D}} \right)_{ITF} \quad (4.12)$$

On the other hand, as diameters and lengths are not preserved, (4.7) is not accomplished and scaling distortions can be expected at very low pressures because of the frictional effects.

4.2.4 Environment heat losses

Environment heat losses do not change with the same K_v factor as volumes and power (4.6). For vertical volumes, power transferred by conduction and convection processes changes as

$$\begin{aligned} \phi_{wR} &= -k_R A_R \frac{\partial T_R}{\partial x_R} = -k_{ITF} \pi D_R L_R \frac{\partial T_{ITF}}{\partial x_{ITF}} \\ &= -\sqrt{K_v} k_{ITF} A_{ITF} \frac{\partial T_{ITF}}{\partial x_{ITF}} = \sqrt{K_v} \phi_{wITF} \end{aligned} \quad (4.13)$$

$$\begin{aligned} \phi_{wR} &= -h_{cR} A_R (T_w - T_f) = -h_{cITF} \pi D_R L_R (T_w - T_f) \\ &= -\sqrt{K_v} h_{cITF} A_{ITF} (T_w - T_f) = \sqrt{K_v} \phi_{wITF} \end{aligned} \quad (4.14)$$

and for horizontal volumes,

$$\begin{aligned} \phi_{wR} &= -k_R A_R \frac{\partial T_R}{\partial x_R} = -k_{ITF} \pi (K_v)^{2/5} D_{ITF} (K_v)^{1/5} L_{ITF} \frac{\partial T_{ITF}}{\partial x_{ITF}} \\ &= -(K_v)^{3/5} k_{ITF} A_{ITF} \frac{\partial T_{ITF}}{\partial x_{ITF}} = (K_v)^{3/5} \phi_{wITF} \end{aligned} \quad (4.15)$$

$$\begin{aligned} \phi_{wR} &= -h_{cR} A_R (T_w - T_f) = -h_{cITF} \pi (K_v)^{2/5} D_{ITF} (K_v)^{1/5} L_{ITF} (T_w - T_f) \\ &= -(K_v)^{3/5} h_{cITF} A_{ITF} (T_w - T_f) = (K_v)^{3/5} \phi_{wITF} \end{aligned} \quad (4.16)$$

Hence, the impact of the environment heat losses is not preserved in the ITF and scaling distortions are expected. For reducing the environment heat losses, the walls of the ITF pipes are usually covered by thick rockwool insulators and heaters may be used in several parts of the facility to compensate for heat losses.

4.3 RELAP5mod3 equations

4.3.1 Thermal hydraulic model

The RELAP5mod3 thermohydraulic model is based on a nonhomogeneous and nonequilibrium model, which simulates a two-phase fluid system plus transport of non-condensables and non volatile solute (boron). For the fluid system, balance equations (mass, momentum and energy) are simplified: on the one hand, only one dimension is considered and vapour and liquid are decoupled, thus independent equations for both phases are obtained. On the other hand, since nuclear reactor flows are

dominated by large sources and sinks of momentum, its effects are considered secondary to mass and energy conservation for reactor safety analysis, and momentum equations are reduced to Bernoulli equations for steady, incompressible and frictionless flow. Finally, differential equations are discretized for the numerical solution applying time and space averaging. As a result of all these approximations, effects like turbulent fluctuations, axial diffusion and transversal gradients and fluxes, which affect decisively to interfacial and wall interaction processes, are neglected. Hence, it becomes necessary to introduce flow regime maps and constitutive equations to simulate the fluid behavior realistically. These constitutive models compute the effects independently in specific correlations. Their results, that vary depending on the kind of flow regime, are added to the final solution of the field equations by the terms like FWG, FWF, DISS, FI, Γ , C and Q.

Furthermore, extra correlations have been also added to RELAP5mod3 in order to simulate properly special processes that are not computed by the state equations (choked flow, momentum losses due to abrupt area changes, ...).

4.3.1.1 Field equations

The RELAP5mod3 thermohydraulic model solves eight field equations for eight primary dependent variables. The primary dependent variables are pressure (P), phasic specific internal energies (U_g , U_f), void fraction (α_g), phasic velocities (v_g , v_f), noncondensable quality (X_n), and boron density (ρ_b). The independent variables are time (t) and distance (x). Equations are, the sum and difference mass equation

$$\begin{aligned} & (\alpha_g \rho_g + \alpha_f \rho_f)_j^{n+1} - (\alpha_g \rho_g + \alpha_f \rho_f)_j^n + \left\{ \left[\dot{\alpha}_g^n \dot{\rho}_g^n (v_g)_{j+1/2}^{n+1} + \dot{\alpha}_f^n \dot{\rho}_f^n (v_f)_{j+1/2}^{n+1} \right] A_{j+1/2} \right. \\ & \left. - \left[\dot{\alpha}_g^n \dot{\rho}_g^n (v_g)_{j-1/2}^{n+1} + \dot{\alpha}_f^n \dot{\rho}_f^n (v_f)_{j-1/2}^{n+1} \right] A_{j-1/2} \right\} (\Delta t / V_j) = 0 \end{aligned} \quad (4.17)$$

$$\begin{aligned} & (\alpha_g \rho_g - \alpha_f \rho_f)_j^{n+1} - (\alpha_g \rho_g - \alpha_f \rho_f)_j^n + \left\{ \left[\dot{\alpha}_g^n \dot{\rho}_g^n (v_g)_{j+1/2}^{n+1} - \dot{\alpha}_f^n \dot{\rho}_f^n (v_f)_{j+1/2}^{n+1} \right] A_{j+1/2} \right. \\ & \left. - \left[\dot{\alpha}_g^n \dot{\rho}_g^n (v_g)_{j-1/2}^{n+1} - \dot{\alpha}_f^n \dot{\rho}_f^n (v_f)_{j-1/2}^{n+1} \right] A_{j-1/2} \right\} (\Delta t / V_j) = 2 (\Gamma_g)_j^{n+1} \Delta t \end{aligned} \quad (4.18)$$

the vapour and liquid energy equations,

$$\begin{aligned} & (\alpha_g \rho_g U_g)_j^{n+1} - (\alpha_g \rho_g U_g)_j^n + P_j^n \left(\alpha_g^{n+1} - \alpha_g^n \right) \\ & + \left[\left(\dot{\alpha}_g \dot{\rho}_g \dot{U}_g \right)_{j+1/2}^n + (\dot{\alpha}_g^n)_{j+1/2} P_j^n \right] (v_g)_{j+1/2}^{n+1} A_{j+1/2} (\Delta t / V_j) \\ & - \left[\left(\dot{\alpha}_g \dot{\rho}_g \dot{U}_g \right)_{j-1/2}^n + (\dot{\alpha}_g^n)_{j-1/2} P_j^n \right] (v_g)_{j-1/2}^{n+1} A_{j-1/2} (\Delta t / V_j) \\ & = \left\{ [-h_f^* / (h_g^* - h_f^*)]^n Q_{ig}^{n+1} - [h_g^* / (h_g^* - h_f^*)]^n Q_{ig}^{n+1} + Q_{wg}^n + DISS_g^n \right\} \Delta t \end{aligned} \quad (4.19)$$

$$\begin{aligned} & (\alpha_f \rho_f U_f)_j^{n+1} - (\alpha_f \rho_f U_f)_j^n + P_j^n \left(\alpha_f^{n+1} - \alpha_f^n \right) \\ & + \left[\left(\dot{\alpha}_f \dot{\rho}_f \dot{U}_f \right)_{j+1/2}^n + (\dot{\alpha}_f^n)_{j+1/2} P_j^n \right] (v_f)_{j+1/2}^{n+1} A_{j+1/2} (\Delta t / V_j) \\ & - \left[\left(\dot{\alpha}_f \dot{\rho}_f \dot{U}_f \right)_{j-1/2}^n + (\dot{\alpha}_f^n)_{j-1/2} P_j^n \right] (v_f)_{j-1/2}^{n+1} A_{j-1/2} (\Delta t / V_j) \\ & = \left\{ [-h_f^* / (h_g^* - h_f^*)]^n Q_{if}^{n+1} - [h_g^* / (h_g^* - h_f^*)]^n Q_{if}^{n+1} + Q_{wf}^n + DISS_f^n \right\} \Delta t \end{aligned} \quad (4.20)$$

and the sum and difference momentum equations.

$$\begin{aligned}
 & \left[(\alpha_g \rho_g)_{j+1/2}^n (v_g^{n+1} - v_g^n)_{j+1/2} + (\alpha_f \rho_f)_{j+1/2}^n (v_f^{n+1} - v_f^n)_{j+1/2} \right] \Delta x_{j+1/2} \\
 & + 1/2 (\alpha_g \rho_g)_{j+1/2}^n \left[(v_g^2)_{j+1}^n - (v_g^2)_j^n \right] \Delta t + 1/2 (\alpha_f \rho_f)_{j+1/2}^n \left[(v_f^2)_{j+1}^n - (v_f^2)_j^n \right] \Delta t \\
 & - 1/2 \left[(\alpha_g \rho_g)_{j+1/2}^n VISG_{j+1/2}^n + (\alpha_f \rho_f)_{j+1/2}^n VISF_{j+1/2}^n \right] \Delta t = - (P_{j+1} - P_j)^{n+1} \Delta t \\
 & + [\rho_{j+1/2}^n g - (\alpha_g \rho_g)_{j+1/2}^n (v_g)_{j+1/2}^{n+1} FWG_{j+1/2}^n - (\alpha_f \rho_f)_{j+1/2}^n (v_f)_{j+1/2}^{n+1} FWF_{j+1/2}^n \\
 & - (\Gamma_g)_{j+1/2}^n (v_g - v_f)_{j+1/2}^n] \Delta x_{j+1/2} \Delta t + \left[(\alpha_g \dot{\rho}_g)_{j+1/2}^n HLOSSG_{j+1/2}^n v_{g,j+1/2}^{n+1} \right. \\
 & \left. + (\alpha_f \dot{\rho}_f)_{j+1/2}^n HLOSSF_{j+1/2}^n v_{f,j+1/2}^{n+1} \right] \\
 & (1 + \frac{C_M \rho_m^2}{\rho_g \rho_f})_{j+1/2}^n [(v_g^{n+1} - v_g^n) - (v_f^{n+1} - v_f^n)]_{j+1/2} \Delta x_{j+1/2} \\
 & + \frac{1}{2} (\frac{\dot{\alpha}_g \dot{\rho}_g}{\alpha_g \rho_g})_{j+1/2}^n [(v_g^2)_{j+1}^n - (v_g^2)_j^n] \Delta t - \frac{1}{2} (\frac{\dot{\alpha}_g \dot{\rho}_g}{\alpha_g \rho_g})_{j+1/2}^n VISG_{j+1/2}^n \Delta t \\
 & + \frac{1}{2} (\frac{\dot{\alpha}_f \dot{\rho}_f}{\alpha_f \rho_f})_{j+1/2}^n [(v_f^2)_{j+1}^n - (v_f^2)_j^n] \Delta t - \frac{1}{2} (\frac{\dot{\alpha}_f \dot{\rho}_f}{\alpha_f \rho_f})_{j+1/2}^n VISF_{j+1/2}^n \Delta t \\
 & = - (\frac{\rho_f - \rho_g}{\rho_f \rho_g})_{j+1/2}^n (P_{j+1} - P_j)^{n+1} \Delta t \\
 & - \left\{ FWG_{j+1/2}^n (v_g)_{j+1/2}^{n+1} - FWF_{j+1/2}^n (v_f)_{j+1/2}^{n+1} - \left[\frac{\Gamma_g^n (\rho_m v_I^{n+1} - \alpha_f^n \rho_f^n v^{n+1} - \alpha_g^n \rho_g^n v^{n+1})}{(\alpha_g \rho_g \alpha_f \rho_f)^n} \right]_{j+1/2} \right\} \\
 & + (\rho_m FI)_{j+1/2}^n (v_g^{n+1} - v_f^{n+1})_{j+1/2} \Delta x_{j+1/2} \Delta t - \left[\frac{1}{2} (\frac{\dot{\alpha}_g \dot{\rho}_g}{\alpha_g \rho_g})_{j+1/2}^n HLOSSG_{j+1/2}^n v_{g,j+1/2}^{n+1} \right. \\
 & \left. - \frac{1}{2} (\frac{\dot{\alpha}_f \dot{\rho}_f}{\alpha_f \rho_f})_{j+1/2}^n HLOSSF_{j+1/2}^n v_{f,j+1/2}^{n+1} \right] \Delta t + (\frac{\rho_m}{\rho_g \rho_f})_{j+1/2}^n (\rho_f - \rho_g)_{j+1/2}^n g (H_{j+1}^n - H_j^n) \Delta t
 \end{aligned} \tag{4.22}$$

For considering non-condensables and boron transport, two extra field equations are included. For the numerical solution of the boron transport equations, there are two available options. The upwind difference scheme, that follows the equation

$$V_L (\rho_{b,L}^{n+1} - \rho_{b,L}^n) + (\dot{\rho}_{j+1}^n v_{j+1}^{n+1} A_{j+1} - \dot{\rho}_j^n v_j^{n+1} A_j) \Delta t = 0 \tag{4.23}$$

and the Godunov scheme, for which the numerical solution is

$$\rho_{b,L}^{n+1} = \rho_{b,L}^{n+1} + \frac{\Delta t}{V_L} A_j F_j^n - \frac{\Delta t}{V_L} A_{j+1} F_{j+1}^n \tag{4.24}$$

where

$$F_{j+1}^n = \frac{1}{2} [v_{f,j+1}^{n+1/2} (\rho_{b,j+1}^{n,L} + \rho_{b,j+1}^{n,R}) + |v_{f,j+1}^{n+1/2}| (\rho_{b,j+1}^{n,L} + \rho_{b,j+1}^{n,R})] \tag{4.25}$$

Finally, non condensable transport continuity equation is written as follows

$$\begin{aligned}
 & V_L \left[\rho_{g,L}^n X_{n,L}^n (\tilde{\alpha}_{g,L}^{n+1} - \alpha_{g,L}^n) + \alpha_{g,L}^n X_{n,L}^n (\tilde{\rho}_{g,L}^{n+1} - \rho_{g,L}^n) + \alpha_{g,L}^n \rho_{n,L}^n (\tilde{X}_{g,L}^{n+1} - X_{g,L}^n) \right] \\
 & + (\dot{\alpha}_{g,j+1}^n \dot{\rho}_{g,j+1}^n \dot{X}_{n,j+1}^n v_{g,j+1}^{n+1} A_{j+1} - \dot{\alpha}_{g,j}^n \dot{\rho}_{g,j}^n \dot{X}_{n,j}^n v_{g,j}^{n+1} A_j) \Delta t = 0
 \end{aligned} \tag{4.26}$$

These equations are associated to the semi-implicit scheme, which is the most common numerical scheme applied for simulating regular transients. RELAP5mod3 also offers the possibility to use a nearly implicit scheme (usually applied for semi-steady state conditions), where the same field equations are solved with modified quadratic terms of the velocity in the momentum equations (4.21) and (4.22) as follows:

$$(v^2)^{n+1} \approx (v^2)^n + \Delta (v^2)^{n,n+1} \approx (v^2)^n + 2v^n (v^{n+1} - v^n) \quad (4.27)$$

4.3.1.2 Flow regime maps

RELAP5mod3 have defined 4 flow regimes maps based on classical works performed by Taitel and Dukler [44] [72] and also by Ishii [73][74][75]. These are: one horizontal maps for flows in pipes (Figure 4.4) ; one vertical map for flows in pipes, annuli, and bundles (Figure 4.3); one high mixing map for flow in pumps (Figure 4.5); and the so called ECC mixer map for flows in horizontal pipes near ECC injection port (Figure 4.6). Their transitions depend on the fluid properties and conditions (velocities, densities, liquid fractions and surface tensions), gravity, pipe dimensions (diameter), and the water level for stratified flows (Θ).

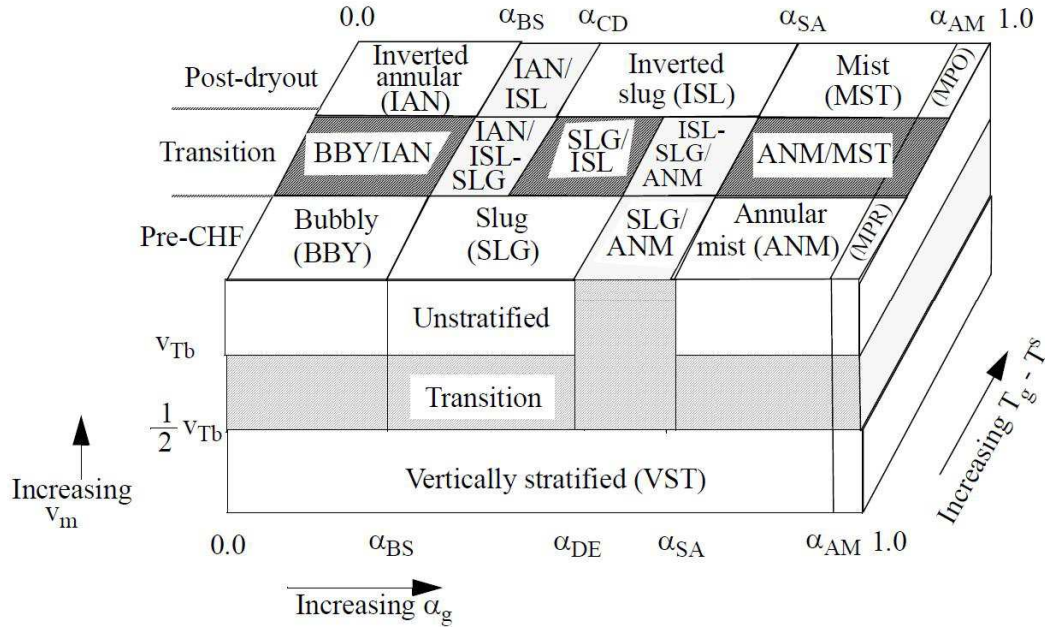


Figure 4.3: Vertical volumes flow regime map [76]

Specifically, transitions in the vertical flow regime map are governed by the parameters (v_{Tb}), α_{BS} , α_{CD} , α_{DE} , α_{SA} and α_{AM} (see Figure 4.3). Their dependencies are:

$$v_{Tb} = 0.35 \left[\frac{gD(\rho_f - \rho_g)}{\rho_f} \right] \quad (4.28)$$

$$\alpha_{BS} = \begin{cases} \alpha_L & G_m \leq 2000 \text{ kg/m}^2\text{s} \\ \alpha_L + 0.001 (0.5 - \alpha_L) (G_m - 2000) & 2000 < G_m \leq 3000 \text{ kg/m}^2\text{s} \\ 0.5 & G_m > 3000 \text{ kg/m}^2\text{s} \end{cases} \quad (4.29)$$

$$\alpha_{SA} = \min(\alpha_{crit}^f, \alpha_{crit}^e) \quad (4.30)$$

with

$$\alpha_{crit}^f = \begin{cases} \frac{1}{v_g} \left[\frac{gD(\rho_f - \rho_g)}{\rho_g} \right]^{1/2} & \text{for upflow} \\ 0.75 & \text{for downflow and countercurrent flow.} \end{cases} \quad (4.31)$$

and

$$\alpha_{crit}^e = \frac{3.2}{v_g} \left[\frac{g\sigma(\rho_f - \rho_g)}{\rho_g^2} \right]^{1/4} \quad (4.32)$$

$$\alpha_{DE} = \max(\alpha_{BS}, \alpha_{SA} - 0.05) \quad (4.33)$$

$$\alpha_{AM} = 0.9999 \quad (4.34)$$

$$\alpha_{CD} = \alpha_{BS} + 0.2 \quad (4.35)$$

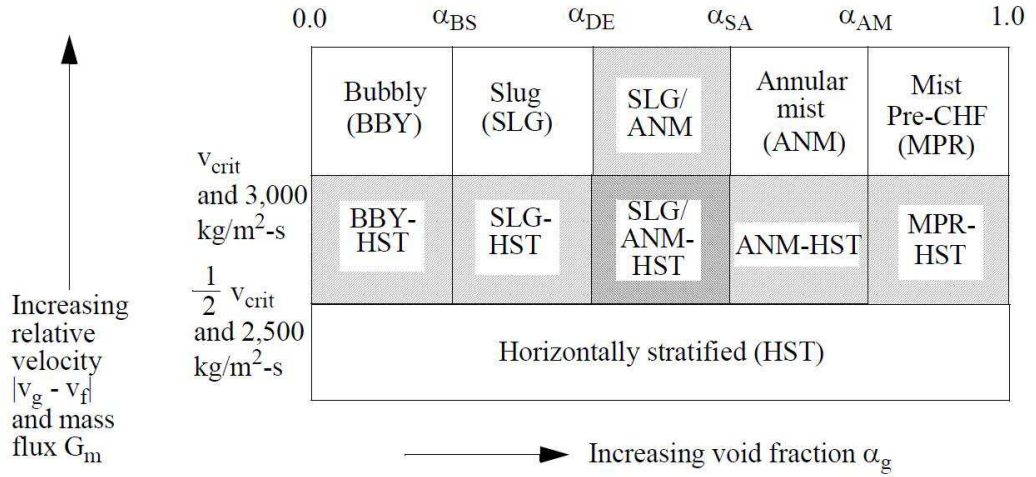


Figure 4.4: Horizontal volumes flow regime map [76]

For horizontal volumes, transitions are governed by the following parameters v_{crit} , α_{BS} , α_{DE} , α_{SA} , α_{AM} (Figure 4.4). The particular dependencies are:

$$\alpha_{BS} = \begin{cases} 0.25\alpha_L & G_m \leq 2000 \text{ kg/m}^2\text{s} \\ 0.25 + 0.00025(G_m - 2000) & 2000 < G_m \leq 3000 \text{ kg/m}^2\text{s} \\ 0.5 & G_m > 3000 \text{ kg/m}^2\text{s} \end{cases} \quad (4.36)$$

$$\alpha_{DE} = 0.8 \quad (4.37)$$

$$\alpha_{SA} = 0.75 \quad (4.38)$$

$$\alpha_{AM} = 0.9999 \quad (4.39)$$

$$v_{crit} = \frac{1}{2} \left[\frac{(\rho_f - \rho_g) g \alpha_g A}{\rho_g D \sin \Theta} \right]^{1/2} (1 - \cos \Theta) \quad (4.40)$$

where the angle Θ is related to the liquid level with respect to the bottom of the volume.

Finally, the High mixing volume flow regime map depends only on the vapour void fraction (see Figure 4.5), and transitions of the ECC mixer volume flow regime map are tabulated with the constant dimensionless gas velocities and liquid-to-vapour volumetric ratios stipulated in the diagram of Figure 4.6.

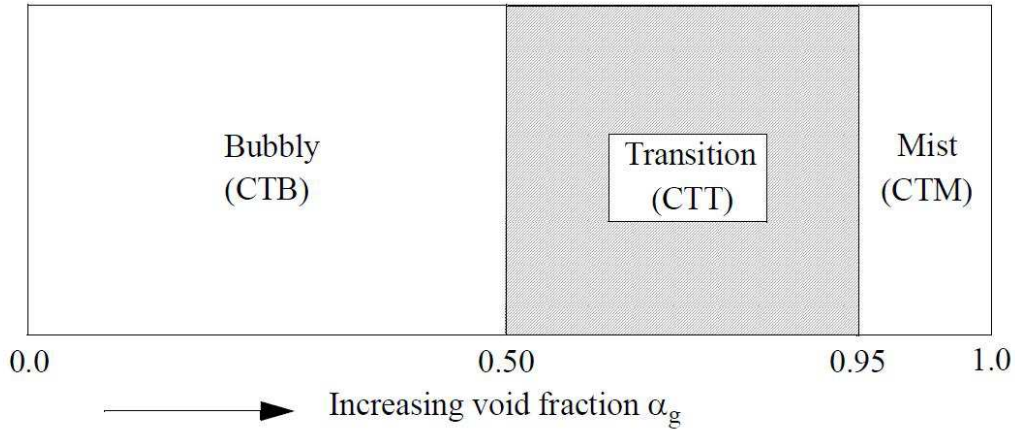


Figure 4.5: High mixing volume flow regime map [76]

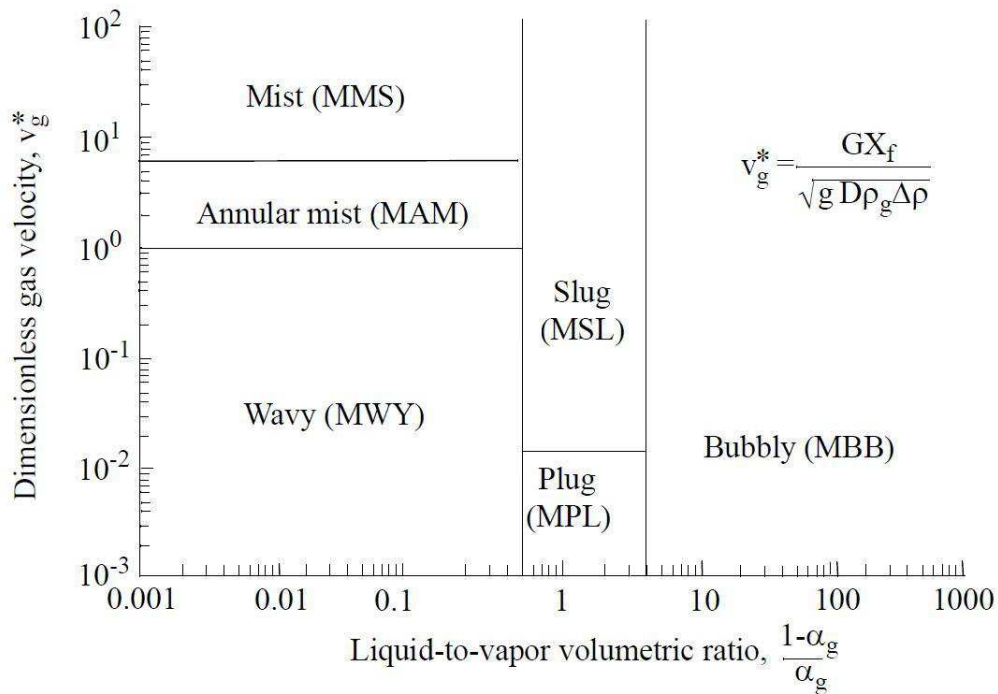


Figure 4.6: ECC mixer volume flow regime map [76]

Once flow regime maps are defined, constitutive equations allow the computation of those phenom-

ena that have been neglected in the balance equations by means of correlations based on experimental data. These are interphase friction, wall friction, virtual mass coefficient and interfacial heat and mass transfer.

4.3.1.3 Constitutive equations

4.3.1.3.1 Interphase friction

RELAP5mod3 uses two different models, the drift flux method, which is applied to bubbly and slug flows for the vertical pipes, and the drag coefficient method, which is applied to the rest of flow regimes and components. For both models, FI depends on the following relationship

$$\frac{\left(\frac{F_{ig}}{\alpha_g \rho_g} + \frac{F_{if}}{\alpha_f \rho_f}\right)}{\rho_m (v_g - v : f)} \quad (4.41)$$

where it is considered that

$$F_{ig} = F_{if} = F_i \quad (4.42)$$

Particularly, in the drift flux method F_i is equal to

$$F_i = C_i |C_1 v_g - C_0 v_f| (C_1 v_g - C_0 v_f) \quad (4.43)$$

with

$$C_i = \frac{\rho_g \rho_f^3 (\rho_f - \rho_g) g}{v_{gj}^2} \quad (4.44)$$

and

$$C_1 = \frac{1 - \rho_g C_0}{1 - \rho_g} \quad (4.45)$$

C_0 and v_{gj} , the drift distribution coefficient and the vapour drift velocity, are independent parameters computed by the drift flux correlations, that vary depending on the cell geometry (diameter) and the mass flux (see table 4.1). In addition, each correlation depends on the fluid properties and conditions (pressure, void fraction, densities, phase velocities, viscosities and surface tension), gravity, and cell dimensions (diameter).

On the other hand, in the drag coefficient method, F_i is equal to

$$F_i = \frac{1}{8} \rho_c |v_g - v_f| (v_g - v_f) C_D S_F a_{gf} \quad (4.46)$$

where C_D , S_F , and a_{gf} are the drag coefficient, the shape factor and the interfacial area per unit volume. The form of these coefficients vary depending on the flow regime, fluid properties and conditions (pressure, void fraction, densities, phase velocities, viscosities, surface tension and stratified liquid level), gravity, and cell geometry (diameter). For the sake of scaling considerations, it is worth mentioning for slug non vertical flow conditions, a_{gf} also depends on the cell length. Further information about the drift flux and drag coefficient correlations can be found in Section 3.3.6 of Reference [76].

4.3.1.3.2 Wall friction

In order to compute the wall friction forces, RELAP5mod3 uses the following relationships for the liquid and vapor phases:

$$FWF(\alpha_f \rho_f v_f) A = \tau_f p_f = \alpha_f \left(\frac{dP}{dx} \Big|_{2\phi} \right) \left(\frac{Z^2}{\alpha_g + \alpha_f Z^2} \right) A \quad (4.47)$$

| Flow rates | Rod bundles | Small pipes D ≤ 0.018m | Intermediate pipes 0.018m ≤ D ≤ 0.08m | Large pipes 0.08m ≤ D |
|---|---------------------|--|---|---|
| High upflow rates G ≥ 100 kg/m ² s | EPRI (2) (eprij) | EPRI (3) (eprij) | EPRI (9) (eprij) | Churn- turbulent bubbly flow (14) Transition (15) Kataoka-Ishii (16) (katokj) |
| Medium up- flow rates 50 kg/m ² s ; G ≤ 100 kg/m ² s | | Transition (5) | Transition (13) | |
| Low upflow, downflow, and countercurrent flow rates -50 kg/m ² s G ≤ 50 kg/m ² s | | Zuber-Findlay slug flow (4) (zfslgj) | Churn- turbulent bubbly flow (10) Transition (11) (Kataoka-Ishii (12) (katokj) | |
| Medium down- flow rates -100 kg/m ² s G ≤ -50 kg/m ² s | | Transtion (5) | Transition (13) | |
| High downflow rates G ≤ -100 kg/m ² s | | EPRI (3) (eprij) | EPRI(9) (eprij) | |

Table 4.1: Drift Flux Void Fraction Correlations for Vertical Bubbly-Slug Flow [76]

$$FWG(\alpha_g \rho_g v_g) A = \tau_g p_g = \alpha_g \left(\frac{dP}{dx} \Big|_{2\phi} \right) \left(\frac{Z^2}{\alpha_g + \alpha_f Z^2} \right) A \quad (4.48)$$

where

$$\frac{dP}{dx} \Big|_{2\phi} = \phi_f^2 \left(\frac{dP}{dx} \right)_f = \phi_g^2 \left(\frac{dP}{dx} \right)_g = \frac{1}{2D} \left\{ \lambda_f \rho_f (\alpha_f v_f)^2 + C \left[\lambda_f \rho_f (\rho_f v_f)^2 \lambda_g \rho_g (\alpha_g v_g)^2 \right]^{1/2} + \lambda_g \rho_g (\alpha_g v_g)^2 \right\} \quad (4.49)$$

$$Z^2 = \frac{\lambda_f (Re_f) \rho_f v_f^2 \frac{\alpha_{fw}}{\alpha_f}}{\lambda_g (Re_g) \rho_g v_g^2 \frac{\alpha_{gw}}{\alpha_g}} \quad (4.50)$$

α_{fw} and α_{gw} are respectively the liquid and vapour void fractions at the wall. Their values depend on the flow regime of the cell. On the other hand, λ is the Darcy-Weisbach friction factor, which varies depending on the turbulent or laminar condition of the fluid as,

$$\lambda \begin{cases} \lambda_L = \frac{64}{Re\Phi_S} & 0 \leq Re \leq 2200 \\ \lambda_{L,T} = \left(3.75 - \frac{8250}{Re}\right) (\lambda_{3000} - \lambda_{2200}) + \lambda_{2000} & 2200 < \lambda \leq 3000 \\ \frac{1}{\sqrt{\lambda_T}} = -2\log_{10} \left\{ \frac{\varepsilon}{3.7D} + \frac{2.51}{Re} \left[1.14 - 2\log_{10} \left(\frac{\varepsilon}{D} - \frac{21.25}{Re^{0.9}} \right) \right] \right\} & Re > 3000 \end{cases} \quad (4.51)$$

Where ε is the wall roughness and Φ_S is a user-input shape factor introduced for non-circular channels. Further information about the wall friction correlations can be found in Section 3.3.8 of Reference [76].

4.3.1.3.3 Interfacial heat and mass transfer processes

For the interfacial mass and heat transfer, two domains, the "bulk" and the "wall", are considered in order to represent the fluid near the heated wall and in the bulk. Thus, near the wall, interfacial mass exchange is computed when a condensation or an evaporation process occurs in two-phase mixture conditions as follows:

$$\Gamma_w = \frac{q_f A_w}{V \left[\max \left(h_g^s - h_f, 10^4 \frac{J}{kg} \right) \right]} Mul \quad (4.52)$$

where q_f is the wall heat flux, A_w the surface of the wall, V volume of the cell, and Mul is

$$Mul = \frac{\min(h_f, h_f^s) - h_{cr}}{(h_f^s - h_{cr})(1 + \varepsilon)} \quad (4.53)$$

with

$$\varepsilon = \frac{\rho_f \left[h_f^s - \min(h_f, h_f^s) \right]}{\rho_g h_{fg}} \quad (4.54)$$

Mul varies depending on the critical enthalpy parameter:

$$h_{cr} = \begin{cases} h_{f,sat} - \frac{StC_{pf}}{0.0065} & Pe > 70000 \\ h_{f,sat} - \frac{NuC_{pf}}{455} & Pe < 70000 \end{cases} \quad (4.55)$$

where

$$St = \frac{Nu}{Pe} \quad (4.56)$$

$$Nu = \frac{q_f D}{k_f} \quad (4.57)$$

$$Pe = \frac{G_t DC_{pf}}{k_f} \quad (4.58)$$

Once the mass transfer near the wall is determined, the total interfacial mass exchange can be computed as:

$$\Gamma_g = - \frac{H_{ig} (T^S - T_g) + H_{if} (T^S - T_f)}{h_g^* - h_f^*} + \Gamma_w \quad (4.59)$$

where the volumetric heat transfer coefficients depend on the heat transfer coefficient and the interfacial area.

$$H_{ip} = \frac{k_p}{L} Nu a_{gf} = h_{ip} a_{gf} \quad (4.60)$$

Table 4.2 shows the correlations associated to both parameters. The type of Correlation vary depending on the flow regime and the fluid conditions (superheated/subcooled liquid or gas).

The Correlations of the heat transfer coefficients mainly depend on the fluid properties (ν , k , σ , β), fluid conditions (densities, void fractions, temperatures, relative velocity), gravity and on the hydraulic diameter of the cell. Considering the scaling issue it is important to notice that for vertical stratified flows, interfacial area will change depending on the length of the cell. Further information about the interfacial heat transfer correlations and dependencies can be found in Chapter 4.8 of Reference [77].

4.3.1.3.4 Virtual mass coefficient

Virtual mass is an interface drag force related with the relative acceleration of the fluid phases as a result of the bubble generation. It affects the momentum equations (4.22) and its coefficient is determined based on the void fraction, following the equations

$$C_M = \begin{cases} \frac{1}{2} \frac{(1+2\alpha_g)}{(1-\alpha_g)} & 0 \leq \alpha_g < 1/2 \\ \frac{1}{2} \frac{(3-2\alpha_g)}{\alpha_g} & 1/2 \leq \alpha_g \leq 1 \end{cases} \quad (4.61)$$

4.3.1.3.5 Wall heat transfer models

Wall to fluid heat transfer is defined by

$$q = h_{c,g} (T_w - T_{ref,g}) + h_{c,f} (T_w - T_{ref,g}) \quad (4.62)$$

Reference temperatures can be the local gas or liquid temperature or the saturation temperature, depending on the heat transfer coefficient correlation being used.

Heat transfer coefficients are calculated from specific heat transfer correlations. These are determined by a logical diagram (see Figure 4.7) that establish 11 heat transfer modes depending on different fluid parameters (void fraction, fluid temperatures, wall temperature, non-condensable mass, quality, enthalpies, and equilibrium quality) and the type of hydraulic cell (defined in the the heat structure input cards).

Heat transfer correlations depend on the fluid properties (β , μ , C_p , k , σ , ν), fluid conditions (densities, α , fluid temperatures, static quality, saturation temperatures, relative velocities), temperature of the wall, channel geometry (that is defined specifically by the user in the heat structure input cards -i.e. parallel plates, vertical bundle, CANDU fuel bundle,...-), gravity, and hydraulic diameter. It is also noticeable, for scaling considerations, that for natural convection heat transfer coefficient also depends on the channel length. Further information about wall heat transfer coefficient correlations can be found in the Chapter 4.2 of Reference [77]

4.3.1.4 Special processes

4.3.1.4.1 Choking flow

Two models have been included in order to compute choked conditions when sound speeds are achieved in the junctions as a result of high pressure drops, the Ransom-Trapp and the Henry Fauske model.

The Ransom-Trapp model includes two numerical methods that are applied depending on the upstream flow conditions, the subcooled model and the two phase-one component model. Sub-cooled model considers that choked conditions occur when saturated conditions are achieved in the throat.

| Flow Type | a_{gf} | $h_{if,SHL}$ | $h_{if,SCL}$ | $h_{if,SHG}$ | $h_{if,SCG}$ |
|--|---|--|---|--|--------------------------------|
| Bubbly | $\frac{3.6\alpha_{bub}}{d_b}$ | Lee-Ryley Plesset-Zwick or 0 | Unal or 0 | $10^4 f(\Delta T_{sg})$ | $10^4 f(\Delta T_{sg})$ |
| Slug: | | | | | |
| Bubbles | $\frac{3.6\alpha_{gs}(1-\alpha_{TB})}{d_b}$ | Lee-Ryley Plesset-Zwick | Unal | $10^4 f(\Delta T_{sg})$ | $10^4 f(\Delta T_{sg})$ |
| Taylor bubbles | $\frac{4.5}{D}\alpha_{Tb}(2.0)$ | $3 \cdot 10^6 f(\Delta T_{sf})$ | Sieder-Tate | Lee-Ryley | $10^4 f(\Delta T_{sg})$ |
| Annular-mist: | | | | | |
| Drops | $\frac{3.6\alpha_{fd}(1-\alpha_{ff})}{d_d}$ | $\frac{k_f}{d_d}(\Delta T_{sf})$ | Brown $\cdot f(\Delta T_{sf})$ | Lee-Ryley | $10^4 f(\Delta T_{sg})$ |
| Liquid film | $\frac{4}{D}(1-\alpha_{ff})^{1/2}$ (2.5) | $3 \cdot 10^6$ | Theofanous | Dittus-Boelter | $10^4 f(\Delta T_{sg})$ |
| Inverted Annular: | | | | | |
| Bubbles | $\frac{3.6\alpha_{bub}(1-\alpha_B)}{d_b}$ | Lee-Ryley Plesset-Zwick | Unal | $10^4 f(\Delta T_{sg})$ | $10^4 f(\Delta T_{sg})$ |
| Vapour film | $\frac{4}{D}(1-\alpha_B)^{1/2}$ (2.5) | $3 \cdot 10^6$ | Dittus-Boelter | $\frac{k_g}{D}(\Delta T_{sg})$ | $\frac{k_g}{D}(\Delta T_{sg})$ |
| Inverted slug: | | | | | |
| Drops | $\frac{3.6\alpha_{drp}(1-\alpha_B)}{d_d}$ | $\frac{k_f}{D}(\Delta T_{sf})$ | Brown $\cdot f(\Delta T_{sf})$ | Lee-Ryley | Lee-Ryley |
| Taylor drops | $\frac{4.5}{D}\alpha_B(2.5)$ | $\frac{k_f}{D}(\Delta T_{sf})$ | Brown $\cdot f(\Delta T_{sf})$ | $\frac{k_g}{D}(\Delta T_{sg})$ | $\frac{k_g}{D}(\Delta T_{sg})$ |
| Dispersed (droplet,mist) | $\frac{3.6\alpha_{drp}}{d_d}$ | $\frac{k_f}{D}f(\Delta T_{sf})$ | Brown $\cdot f(\Delta T_{sf})$ | Lee-Ryley $\cdot f(\Delta T_{sf})$ or 0 | $10^4 f(\Delta T_{sg})$ |
| Horizontal stratified | $\frac{4\sin\theta}{\pi D}$ | Dittus-Boelter $\cdot f(\Delta T_{sf})$ | Dittus-Boelter | Dittus-Boelter $10^4 f(\Delta T_{sg})$ | $10^4 f(\Delta T_{sg})$ |
| Vertical stratified | $\frac{A_c}{V}$ | $h_{if,REG}$ | McAdams | McAdams | $h_{ig,REG}$ |
| Vertical stratified or level model with a jet junction | $\frac{A_c}{V}$ | $h_{if,REG}$ | Brown-Khoo-Sonin, Brown-Helmick-Sonin, Sonin-Shimko-Sun, Theofanous | $h_{ig,REG}$ | $h_{ig,REG}$ |

Table 4.2: Summary of Interfacial Areas and Heat Transfer Coefficients [77]

At this point, there is a sudden vaporization and sound speed is drastically reduced choking the velocities at the junction. For this model, which considers mechanical equilibrium ($v_g=v_f$), choked velocity is computed by the relationship:

$$v_{throat} = \frac{\dot{\rho}_j}{\rho_{throat}} \frac{A_j}{A_{throat}} v_j = \frac{\rho_K}{\rho_{throat}} \frac{A_j}{A_{throat}} v_j = \frac{JCAT}{ATHROT} v_j \quad (4.63)$$

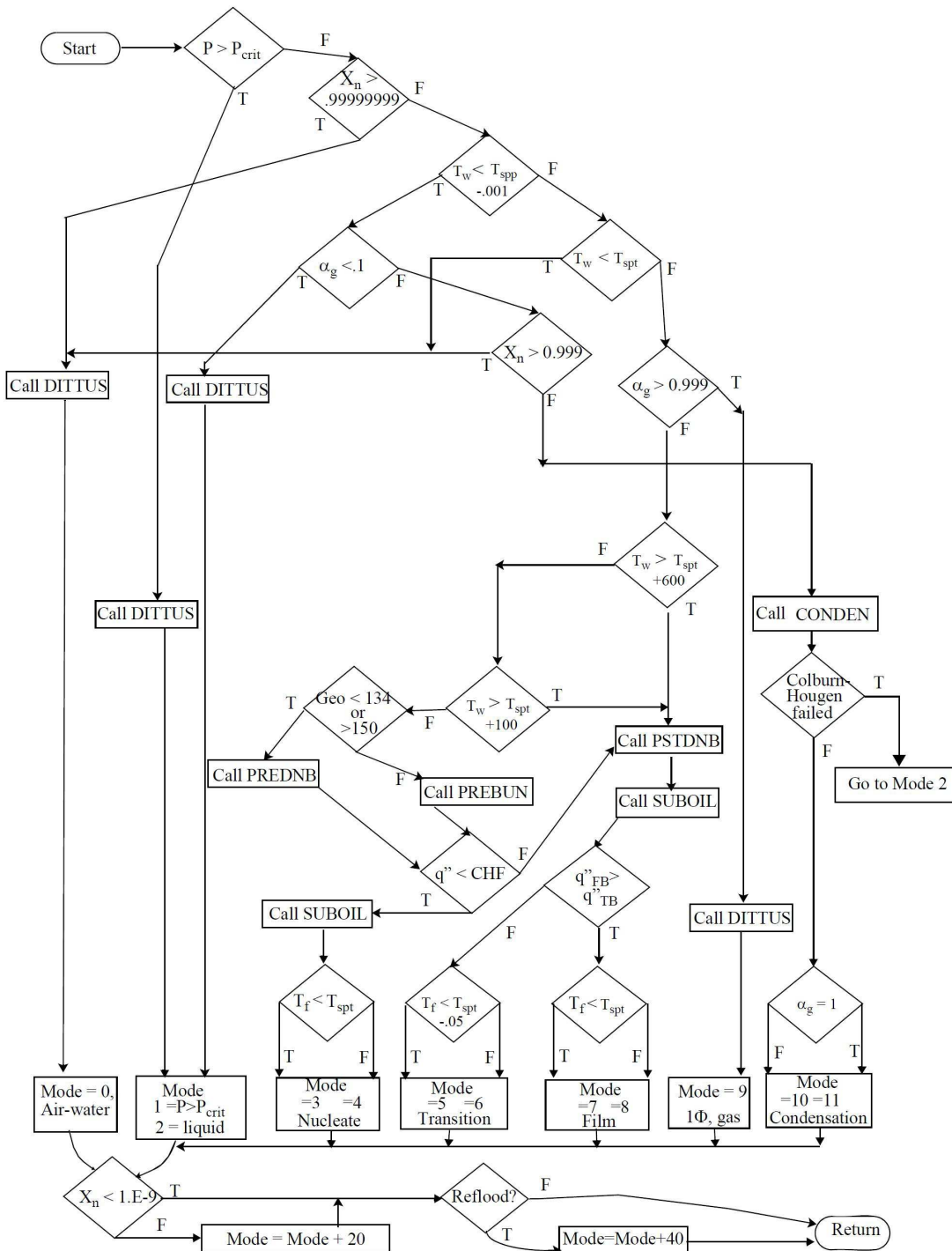


Figure 4.7: RELAP5 Wall Heat Transfer Flow Chart [77]

where ATHROT is the area ratio, and JCAT is

$$JCAT^n = \frac{\dot{\alpha}_{f,j}^n \dot{\rho}_{f,j}^n + \dot{\alpha}_{g,j}^n \dot{\rho}_{g,j}^n}{\rho_{throat}^n} \quad (4.64)$$

On the other hand, the two phase model recalculates the fluid conditions at the throat considering a nonhomogeneous fluid model with thermal equilibrium and without wall drag effects. With these assumptions, the relationships obtained for choked velocities are:

$$v_{f,j}^{n+1} = \tilde{v}_{f,j}^n + \frac{\partial \tilde{v}_{f,j}^{n+1}}{\partial P} (P_K^{n+1} - P_K^n) \quad (4.65)$$

$$v_{g,j}^{n+1} = \tilde{v}_{g,j}^n + \frac{\partial \tilde{v}_{g,j}^{n+1}}{\partial P} (P_K^{n+1} - P_K^n) \quad (4.66)$$

In both models, fluid conditions must be recalculated iteratively with the choked velocities by making use of different correlations that depend on the following parameters: fluid conditions in the upstream (pressure, fluid velocities, quality, void fractions, enthalpies), fluid properties (C_{pn} , σ , entropies, β , k_B , κ) gravity, and discharge coefficients.

The Henry-Fauske model is based in the assumption that choked conditions are achieved when mass flux is maximum respect to the throat pressure. It considers the fluid in mechanical equilibrium and without exchange of heat and mass through the junction. Thus the mass flux equation for the Henry-Fauske model is:

$$G_c^2 = \left\{ \frac{X_0 \bar{V}_v}{\eta/P} + (\bar{V}_v - \bar{V}_{l,0}) \left[\frac{(1 - X_0) N}{(s_{\dot{V},eq} - s_{l,eq})} \frac{ds_{l,eq}}{dP} - \frac{X_o C_{p,v} (1/\eta - 1/\gamma)}{P_t (s_{v,0} - s_{l,0})} \right] \right\}_t^{-1} \quad (4.67)$$

For which it is necessary to solve both mass flux and throat pressure iteratively. These depend on the fluid conditions in the upstream (Pressure, specific volumes, quality, void fractions, enthalpies), the fluid properties (C_{pn} , γ , σ , η , entropies, β , k_B , κ) and gravity.

Further information about the specific choking models correlations can be found in Chapters 7.2 and 7.3 of Reference [77].

4.3.1.4.2 Counter current flow limitation

RELAP5mod3 includes an special model for simulating liquid interception under countercurrent flow conditions. The CCFL model includes two user-input options, the Kutateladze and the Wallis correlations, that follow the relationship:

$$H_g^{1/2} + mH_f^{1/2} = c \quad (4.68)$$

where

$$H_g = j_g \left[\frac{\rho_g}{gw(\rho_f - \rho_g)} \right]^{1/2} \quad (4.69)$$

$$H_f = j_f \left[\frac{\rho_f}{gw(\rho_f - \rho_g)} \right]^{1/2} \quad (4.70)$$

$$w = D_j^{1-\beta} L^\beta \quad (4.71)$$

$$L = \left[\frac{\sigma}{g(\rho_f - \rho_g)} \right]^{1/2} \quad (4.72)$$

c , m , and β are parameters defined by the user in the input deck. The user may select the Wallis or the Kutateladze models with the β parameter (0 for Wallis, 1 for Kutateladze) or a mixture of both

models ($0 < B < 1$), and m and c define the interception limit. Thus, for a given fluid conditions, if liquid downflow velocity exceeds the limit characterized by equation (4.68) (inaccessible region of Figure 4.8), it will be recalculated following the equation:

$$m^2 c_{f,j}^n v_{f,j}^{n+1} \left[c (c_{g,j}^n)^{1/2} (v_{g,j}^n)^{-1/2} - c_{g,j}^n \right] v_{g,j}^{n+1} = c^2 - c (c_{g,j}^n)^{1/2} (v_{g,j}^n)^{1/2} \quad (4.73)$$

where c_f and c_g are

$$c_g = \frac{H_g}{v_g} \quad (4.74)$$

$$c_f = \frac{H_f}{v_f} \quad (4.75)$$

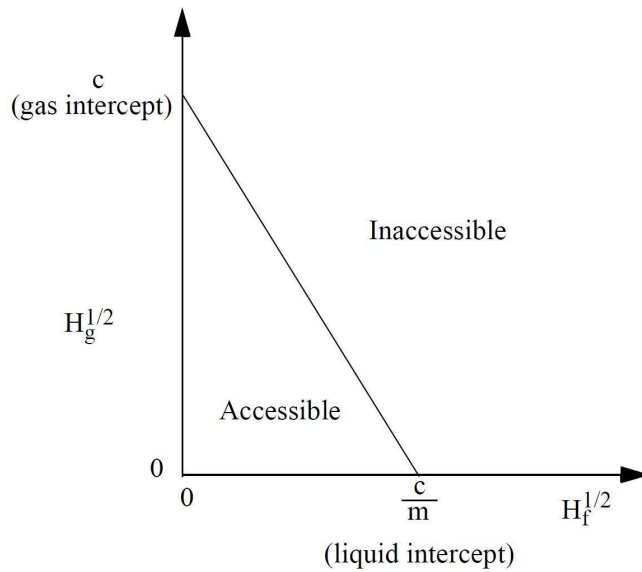


Figure 4.8: $\sqrt{H_g}$ vs. $\sqrt{H_f}$ for a Typical CCFL Correlation Vertical volumes flow regime map [77]

Further information about CCFL model can be found in Chapter 7.4 of Reference [77].

4.3.1.4.3 Water packing mitigation scheme

This model is introduced to mitigate unphysical large pressure spikes that may appear when Eulerian-type computer codes are used to analyze integral systems tests or reactor accidents. These fictitious pressure spikes are sometimes calculated when steam is disappearing from, and water is about to fill, a control volume. The detection of this phenomenon depends on the pressure, the void fraction in the filling volume, and the temperature of the liquid. For the water packing mitigation scheme no new parameters are introduced to the liquid momentum equations and only the coefficient that multiplies the pressure change in the filling volume is modified.

Further information about water packing model can be found in Chapter 3.4.6 of Reference [76].

4.3.1.4.4 Thermal stratification model

A thermal stratification model is included to improve the accuracy of solutions when warmer fluid appears above colder fluid in a vertical stack of cells. In this case, there is a sharp thermal front between the two fluids because of the density differences between them. Depending on the thermal

front location, its velocity and the internal energies of the contiguous cells, fluid conditions for the resolution of the cell field equations, and interphase heat transfer coefficients on the thermal front location will be modified. Thermal front locations are computed as

$$dzl_L = dz_L \left(\frac{U_{fL}^+ - U_{fL}}{U_{fL}^+ - U_{jL}} \right) \quad (4.76)$$

and the front velocity depends on

$$v_{front} = \frac{dzl_L^n - dzl_L^{n-1}}{\Delta t} \quad (4.77)$$

Finally, the new interphase heat transfer coefficients are rewritten as follows:

$$H_i^{neq f} = H_{if} \left(1 - \frac{dzl_L}{dzL} \right) \quad (4.78)$$

Further information about the thermal stratification model can be found in Chapter 3.4.9 of Reference [76].

4.3.1.4.5 Mixture level tracking model

A particular mixture level tracking has been included in order to compensate the inherent limitation of the finite-difference scheme used in RELAP5mod3 and in order to allow a coarser nodalization. Fluid conditions on the mixture level cell are modified for the resolution of the mass and energy balance equations. New averaged values vary depending on the proper new level location and its velocity (how it does move from volume to volume). Wall heat transfer coefficients are also modified if hydrodynamic volumes are linked with heat structures. The location of the mixture level and associated velocity depend on the fluid properties (surface tension), the fluid conditions (void fractions of contiguous cells, densities, velocities) the cell geometry (area ratio, hydraulic diameter, cell height) and gravity.

Finally, heat flux is corrected as follows:

$$q_{wg} = h_g (T_w - T_g) \left(1 - \frac{dzl_L}{dzL} \right) \quad (4.79)$$

$$q_{wf} = h_f (T_w - T_f) \left(\frac{dzl_L}{dzL} \right) \quad (4.80)$$

Further information about the mixture level tracking model can be found in Chapter 3.4.8 of Reference [76].

4.3.1.4.6 Abrupt area change model

The basic hydrodynamic model is formulated for slowly varying (continuous) flow area variations. Therefore, it was necessary to include analytical models for computing the form losses that exist on sudden area changes and orifices. For these junctions, quasi-steady continuity and momentum balances are employed, and numerical implementation is such that hydrodynamic losses are independent of upstream and downstream nodalization. Under these approximations, and considering the Borda-Carnot model, form losses will vary depending on fluid velocities, fluid densities, interphase friction, and void fractions, area ratios and length in the upstream and downstream volumes. Further information about the abrupt area change model can be found in Chapter 7.1 of Reference [77].

4.3.1.4.7 User specified form loss

Singular pressure drops can be introduced by the user in the input deck with the forward and backward loss coefficients (K). The terms included in the discretized equations are

$$HLOSSG_j^n = \frac{1}{2}K|v_{g,j}^n| \quad (4.81)$$

$$HLOSSF_j^n = \frac{1}{2}K|v_{f,j}^n| \quad (4.82)$$

4.3.2 Heat conduction model

Heat structures provided in RELAP5mod3 permit the calculation of the heat transferred across solid boundaries of hydrodynamic volumes. They are represented by one dimensional heat conduction equations in rectangular, cylindrical, or spherical geometries, which are discretized in the radial direction as it is shown in the layout of Figure 4.9.

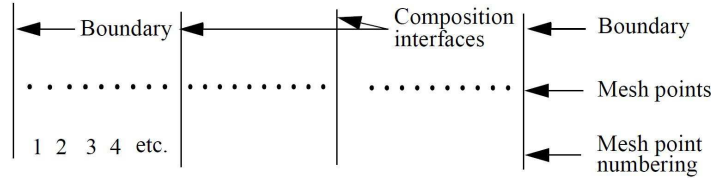


Figure 4.9: Mesh point layout [77]

The basic difference equation for computing the temperatures at the m-th mesh point is

$$\frac{(T_m^{n+1} - T_m) \bar{G}_m}{\Delta t} = (T_m - T_{m-1}) k_{lm} \delta_{lm}^s + (T_{m+1} - T_m) k_{rm} \delta_{rm}^s + P_f P(t) (Q_{lm} \delta_{lm}^v + Q_{rm} \delta_{rm}^v) \quad (4.83)$$

with

$$\bar{G}_m = \bar{\rho}_{lm} \delta_{lm}^v + \bar{\rho}_{rm} \delta_{rm}^v \quad (4.84)$$

P_f is the factor that relates the reactor power (or power from a table) to the heat generation rate for a particular heat structure; $P(t)$ is the time-varying function and may be reactor power, power from a table, or a control variable; and $Q(x)$ is the space-dependent function.

4.3.2.1 Reflood model

Two-dimensional heat conduction model has been included in order to simulate axial heat conduction during core rewetting processes. For this model, both rectangular and cylindrical coordinates can be used, with reference to a 2D node as in Figure below

The integration of the heat conduction equation over the elemental cell yields the following form of finite difference equation

$$\frac{(T_{i,j}^{n+1} - T_{i,j}) \bar{G}_{i,j}}{\Delta t} = a_{i,j}^L T_{i-1,j} + a_{i,j}^R T_{i+1,j} + a_{i,j}^T T_{i,j+1} + a_{i,j}^B T_{i,j-1} - (a_{i,j}^L + a_{i,j}^R + a_{i,j}^T + a_{i,j}^B) T_{i,j} + S_{i,j} \quad (4.85)$$

where heat conduction parameters are decoupled in axial ($a_{i,j}^T + a_{i,j}^B$) and radial ($(a_{i,j}^L + a_{i,j}^R)$) directions. Finally, the heat source term is defined as

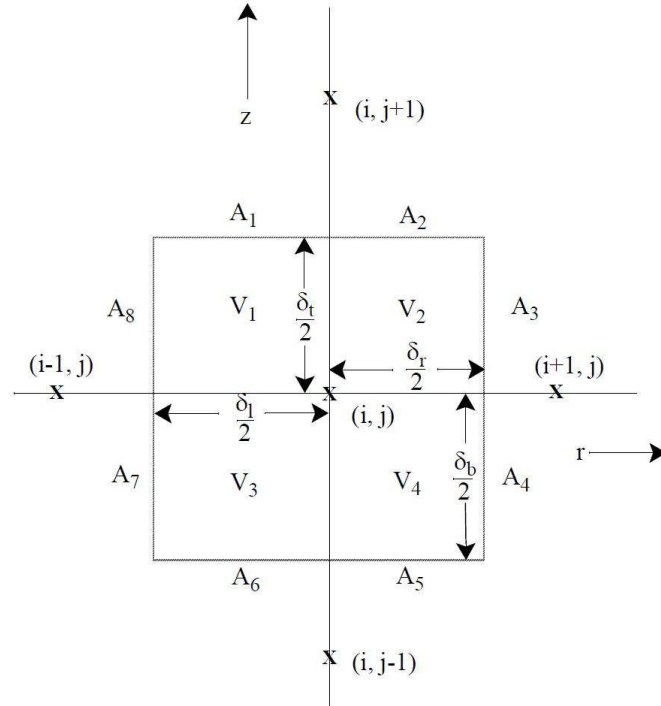


Figure 4.10: Volume and Surface Elements Around a Mesh Point (i, j) [77]

$$S_{i,f} = P_f P(t) (Q_l^T V_1 + Q_l^B V_3 + Q_r^T V_2 + Q_r^B V_4) \quad (4.86)$$

with $Q_l^T = Q_l^B$ and $Q_r^T = Q_r^B$ if the entire cell is within the same heat structure.

4.4 RELAP5mod3: Power to volume Scaling distortions

The comparison between ITF RELAP5mod3 calculations and K_v scaled-up calculations with an NPP RELAP5mod3 input deck will yield inevitably scaling distortions. As it is described in relationship (4.5), scaling factors are obtained by considering that pressures, fluid properties and time are preserved. Hence, if NPP input decks are scaled, fluid tables and initial conditions (P, U, α and ρ) will be kept equal. On the contrary, geometries and volumetric parameters of the components will be modified depending on the K_v factor (see equation (4.6)) and specific criteria that can be added as a result of the relevance that particular thermohydraulic processes can have over the global response of the plant simulation (see the ITF applications of the K_v factor described in Section 4.2). As a result of these considerations, some differences between both prototype and scaled nodalizations will exist in their particular solutions of the RELAP5 equations described in Section 4.3. Expected differences are listed in the following subsections depending on the type of component.

4.4.1 Vertical components

For vertical components, volume and area are scaled with the same K_v factor, thus, initial velocities and cell lengths (height) are equal in both nodalizations. Considering balance equations ((4.17) to (4.22)), identical expressions are obtained after replacing known parameters (initial values, geometries and time step), hence scaling distortions can only exist if terms of the closure equations and special

processes are different ($\Gamma_g, Q_{i,g}, Q_{i,f}, Q_{w,g}, Q_{w,f}$ DISS, FWF, FWG, FI, HLOSSG, HLOSSF, C_M). As it is shown in Sections 4.3.1.3.2, 4.3.1.3.3 and 4.3.1.3.5, interphase interactions, wall friction and wall heat exchange depend on the hydraulic diameter and the flow regime, which in turn depends on the hydraulic diameter as well. Therefore, scaling distortions can be expected for vertical components under mixture conditions as a result of differences in hydraulic diameter.

Other special processes like mixture level tracking model and thermal stratification model do not add scaling distortion given that elevations are preserved and equations (4.76), (4.77), (4.78), (4.79), (4.80) do not change after applying the scaling criteria.

4.4.2 Multi-channel regions

No scaling distortions are associated to multi-channel regions given that geometries, fluid properties and initial conditions are identical for both nodalizations (see scaling factor in section 4.1). Anyhow, if crossflows are defined between multi-channels (i.e. parallel channels in a PWR core nodalization), scaling distortions can be noticed under asymmetrical transient conditions (i.e. main steam line break). This behavior occurs because radial lengths are not preserved ($D_R = \sqrt{K_v} D_{scaled}$) and distances between channels vary also depending on thermohydraulic feedback.

4.4.3 Horizontal legs

As it is explained in Section 4.2.3, flow regime transitions in horizontal volumes (cold and hot legs) become essential during PWR SBLOCA scenario, and a specific scaling criterion, (4.12), must be considered for reproducing equivalent behaviors and cooldowns in scaled transients. This criterion is based on the dependencies with Froude number and stratified liquid level that Taitel and Dukler [44] [72] established for horizontal transitions. RELAP5mod3 flow regime maps are also based on classical maps performed by Taitel and Dukler, hence analogue transitions and mixture interactions should be expected in RELAP5 scaled calculations after applying the (4.12) relationship.

On the other hand, some relevant special models are not preserved when (4.12) is applied. If both (4.12) and (4.11) are accomplished, velocities between scaled cells vary as follows

$$v_R = K_v^{1/5} v_{scaled} \quad (4.87)$$

Hence, special correlations like Ransom Trapp choking flow model, CCFL model, Abrupt area change model and User-specified form losses model are not preserved given that they depend on fluid velocities (see Sections 4.3.1.4.1, 4.3.1.4.4, 4.3.1.4.6 and 4.3.1.4.7). Some of them, specially choked flow and CCFL model, can have significant impact on cooldown behavior for SBLOCA scenario with high vapour fluxes along the hot legs, thus distortions should be expected for the comparison of counterpart transients.

4.4.4 Environment heat losses

RELAPmod3 does not show a scaling distortion when power to volume scaling criterion is applied to the 1D heat conduction model (Section 4.3.2). Hence, it should be expected that for modelled passive heat structures, environment heat losses will change following (4.83) and (4.84). In that sense, as the scaling factor of heat structures are smaller than K_v factor of fluid volumes, heat losses must increase when NPP nodalizations are scaled-down.

It is also worth mentioning that wall heat transfer coefficients can vary in the scaling process as a result of changing the hydraulic diameter and the length (for natural convection in horizontal legs). Nevertheless, scaling distortions in the heat transfer coefficients are significantly smaller than scaling distortions that results from differences in surface-to-volume ratio.

4.4.5 Non condensable and boron transport equations

For the non condensable transport continuity equation, (4.26), RELAP5 will present scaling distortions. First and second parenthesis of (4.26) depend on, respectively, the volume and the cross sectional area of the cell. Therefore, for horizontal volumes, the scaling factors are different and equation (4.26) is not preserved.

With respect to boron transport equations, the geometric parameters cannot be isolated in the upwind difference scheme (4.23), thus the equation cannot be properly scaled. For the Godunov model (4.24), scaling distortions are only expected for horizontal volumes given that the $\frac{A}{V}$ factor is not preserved.

4.5 PVST

PVST (Power to Volume Scaling Tool) is a software developed by the Group of Thermal-Hydraulic Studies at the UPC for generating scaled input decks following the Power to Volume Scaling criterion. Its main purpose is to provide an easy way for obtaining and comparing counterpart nodalizations at different scales. It makes possible to analyze the distortions that must appear between the RELAP5mod3 simulations as a result of the scaling criterion.

The tool, programmed in C language for a DOS environment, is based on the Master Thesis of Patricia Pla and M. Dolores Gutierrez [78], that developed a preliminary version for processing RELAP5mod3.2 input decks. The software has been improved including the processing of the new RELAP5mod3.3 cards, thus enabling the use of different versions of RELAP5. New features have been also added in order to facilitate the analysis of the different distortions reported on Section 4.4. These are:

- To scale the input decks keeping the surface-to-volume ratio mentioned in Section 4.4.4 for the passive heat structures. It allows generating scaled input decks that preserve the impact of the environment heat losses.
- To scale the input decks considering the Froude Number in selected components. It allows generating scaled input decks that preserve flow regime transitions in horizontal legs.

The running of the program is as follows: PVST asks to the analyst for the name of the input deck to be scaled, and for the K_v factor to be applied (see Figure 4.11). Then, general components, as pipes, branches, single volumes, single junctions, multiple junctions and heat structures, and also specific components, as accumulators, separators, turbines, CANDU channels, jetmixers and eccmixers, will be scaled as a default in the "SCALED.TXT" output deck, increasing by a K_v factor the areas, the volumes, and the mass flow cards, and by a $\sqrt{K_v}$ the diameter cards. In addition, several questions are automatically formulated in order to scale properly specific cards that require additional information. In that sense, PVST asks for the presence or not of pumps, particular time dependent volumes and junctions, control variables and tables that must be scaled (not all are required), and heat structures with parallel channels. Finally, PVST ask to the user if the scaled input deck must preserve the impact of the environment heat losses and the Froude number in particular horizontal volumes and heat structures (see Figure 4.12). With all this information, the selected input deck is processed in a while loop which generates the "SCALED.TXT" output file, that will be a counterpart input deck of the previous one following the particular PtoV criterion specified by the analyst.

As it was mentioned previously, the aim of this software is not to give an answer of the PtoV scaling distortions when a K_v factor is applied to a RELAP5mod3 input deck, rather the PVST package is a tool to ease the task of the analyst to generate a set of scaled input decks that will be use to evaluate the effect of the scale in the simulation results. In other words, by using the generated input decks at different scales, the analyst may be able to establish which of the scaling distortions reported in Section 4.4 modify the global response of a particular NPP scenario.

```

D:\Tesis\6_PVST\Software\PVST.exe
INTRODUCE SCALING FACTOR: 23.5

COMPONENT NAMES IN THE ORIGINAL INPUT CANNOT HAVE BLANKS!!
NAME OF THE INPUT DECK TO SCALE:input.i
NAME OF THE SCALED INPUT DECK WILL BE SCALED.TXT.
IS THE FIRST TIME YOU SCALE THIS INPUT DECK
(NOT MEANS YOU WANT TO CHANGE PREVIOUS DATA)?
1 = YES, 0 = NOT :1

¿ARE THERE PUMPS IN THE INPUT DECK
1 = YES, 0 = NOT :1

HOW MANY? 2
INTRODUCE COMPONENT NUMBER OF EACH PUMP (CCC)
PUMP 1: 260
PUMP 2: 360
¿DO YOU WANT TO SCALE ANY TABLE?
1 = YES, 0 = NOT :1

HOW MANY (MAX. 20)? 1

INTRODUCE THE COMPONENT NUMBER OF EACH TABLE (CCC)
TABLE 1: 401

DO YOU WANT TO SCALE ANY TMDPOOL OR TMDPJUN IN WHICH INDEPENDENT
VARIABLE OF THE CCC0201 TO CCC0299 CARDS REQUIRES TO BE SCALED
with variables as power, mass flows,...)?
1 = YES, 0 = NOT :1

HOW MANY?: 1

INTRODUCE THE COMPONENT NUMBER (CCC):
COMPONENT 1: 580

ARE THE CONTROL VARIABLES OF THE INPUT DECK IN EXPANDED MODE?
1 = 3 DIGITS, 0 = 4 DIGITS:0

ARE THERE CONTROL VARIABLES WHICH ONLY THE INITIAL VALUES ARE
AFFECTED BY THE SCALING FACTOR?
1 = YES, 0 = NOT :1

HOW MANY? 1

INTRODUCE CONTROL VARIABLE NUMBER (avoid leading 0 and
a maximum of 4 digits: ex. 070=NO 70=YES
CONTROL VARIABLE 1: 10

ARE THERE CONTROL VARIABLES WHICH INITIAL VALUES AND FORMULA
COEFFICIENTS ARE AFFECTED BY THE SCALING FACTOR?
1 = YES, 0 = NOT :0

DO YOU WANT TO SCALE HEAT LOSSES AND PASSIVE HEAT STRUCTURES
PRESERVING THE SAME RATIO WITH THE POWER AND THE VOLUME -PU SeqU-
OR FOLLOWING THE TYPICAL POWER-TO-VOLUME SCALING CRITERIUM -PU-?
1 = PU SeqU, 0 = PU :0

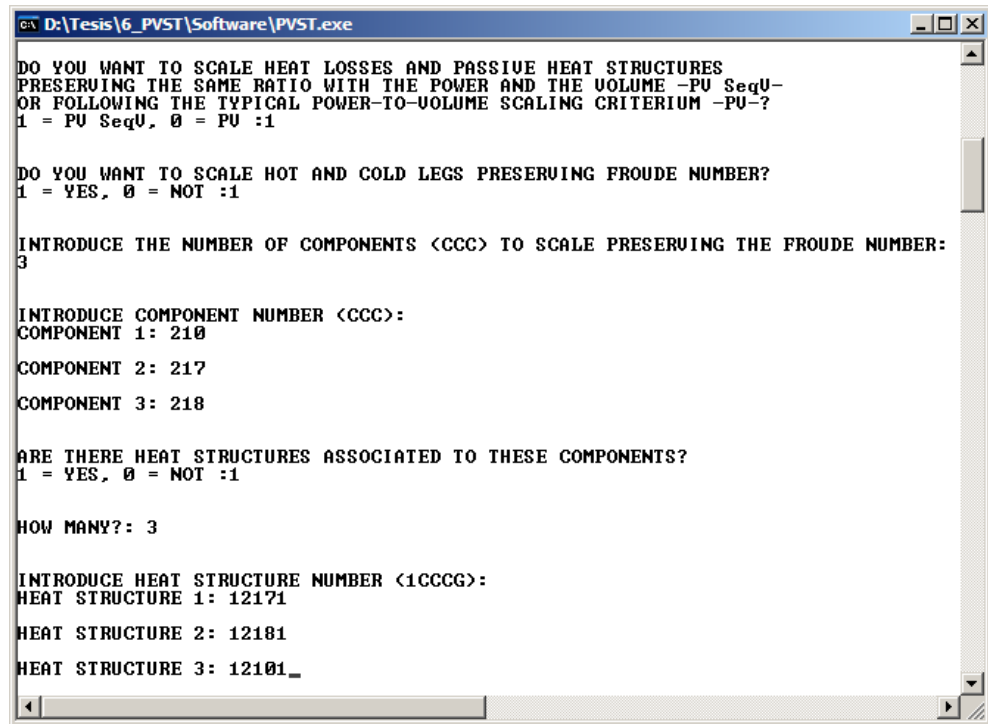
¿ARE THERE HEAT STRUCTURES ASSOCIATED TO COMPONENTS WITH PARALLEL CHANNELS?
1 = YES, 0 = NOT :1

HOW MANY? 1

INTRODUCE HEAT STRUCTURE NUMBER (WITH THE LEADING 1
AND THE GEOMETRY NUMBER -ICCG ex. 11241-):
STRUCTURE 1: 11220

```

Figure 4.11: PVST general questions



```

D:\Tesis\6_PVST\Software\PVST.exe
DO YOU WANT TO SCALE HEAT LOSSES AND PASSIVE HEAT STRUCTURES
PRESERVING THE SAME RATIO WITH THE POWER AND THE VOLUME -PU SeqU-
OR FOLLOWING THE TYPICAL POWER-TO-VOLUME SCALING CRITERIUM -PU-?
1 = PU SeqU, 0 = PU :1

DO YOU WANT TO SCALE HOT AND COLD LEGS PRESERVING FROUDE NUMBER?
1 = YES, 0 = NOT :1

INTRODUCE THE NUMBER OF COMPONENTS <CCC> TO SCALE PRESERVING THE FROUDE NUMBER:
3

INTRODUCE COMPONENT NUMBER <CCC>:
COMPONENT 1: 210
COMPONENT 2: 217
COMPONENT 3: 218

ARE THERE HEAT STRUCTURES ASSOCIATED TO THESE COMPONENTS?
1 = YES, 0 = NOT :1

HOW MANY?: 3

INTRODUCE HEAT STRUCTURE NUMBER <1CCCG>:
HEAT STRUCTURE 1: 12171
HEAT STRUCTURE 2: 12181
HEAT STRUCTURE 3: 12101_

```

Figure 4.12: PVST particular scaling questions

4.6 Assessment of PVST software

In order to show the capabilities and potentials of the PVST package, several scaled-up calculations have been performed over the original input deck of the OECD/NEA ROSA Test 3-1, a SBLOCA ATWS. A detailed description of this experiment as well as the main results obtained for the post-test simulation can be found in Chapter 2.1.4.1. In the following sections, the results of the post-test will be compared with its equivalent obtained with the scaled-up nodalizations. For details about the experiment and its simulation results, it is recommended to review the suggested chapter.

Additionally, results of the Counterpart Test analysis (see Section 6.2) have been also included in order to show the potentials of generating scaled-up input decks using the option of preserving the Froude number. Those volumetric and power parameters of the post-test calculations that are compared in the following figures have been multiplied by the K_v factor in order to ease the comparison with the scaled-up calculations.

4.6.1 PtoV scaled-up nodalizations

A PtoV scaled-up nodalization (Scaled-up A) of the LSTF post-test 3-1 input deck was generated using PVST. This input deck was scaled to a NPP size following the general criterion described by the relationship (4.6) (Asco 2 NPP size using a K_v factor of 40 as it is suggested in [38]). Results of the main events (see table 4.3) showed a quite good agreement with the Post-test simulation until the entrance of the accumulators. Looking more in detail the different thermal-hydraulic parameters of the transient, some discrepancies can be observed. The two most relevant discrepancies are:

- Secondary pressures: it can be seen that the secondary pressure is higher in the scaled-up model (Figure 4.13): at the beginning of the transient, during natural circulation phase, secondary pressure increases faster in the scaled-up A nodalization and safety valves are opened (Figure 4.14); at the end of the transient, after the activation of the LSTF core protection system (that means, at very low power conditions, see Figure 4.15), secondary pressure of the Scaled-up A nodalization stabilizes at higher magnitudes.
- Core dryout: checking the values of the Table 4.3 and the collapsed level of the core Figure 4.16, it can be noticed that the losses across the break are lower for the scaled-up A nodalization (Figure 4.17), delaying the core dryout and the depressurization of the primary system.

| Event | Experimental[s] | Post-test 3-1[s] | Scaled-up A[s] |
|---|-----------------|------------------|----------------|
| Break | 0 | 0 | 0 |
| SCRAM signal: Turbine trip and closure MSIV PZR heater off End of MFW and begin of AFW | 20 | 20 | 20 |
| Start of coastdown of primary coolant pumps | 23 | 23 | 23 |
| Primary coolant pumps stop | 272 | 272 | 272 |
| End of continuous opening of SG RVs, End of two-phase natural circulation, Break flow from one liquid to 2-phase flow | About 300 | 300-400 | 300-400 |
| Core liquid level starts to decrease (core uncover) | About 1100 | 1150 | 1190 |
| Core power decrease by LSTF core protection system | 1630 | 1725 | 1813 |
| Max. fuel rod surface temperature = 930 K | 1825 | 1891 | 1930 |
| Primary pressure lower than SG secondary pressure | About 1900 | About 1890 | About 1930 |
| Initiation of accumulator injection system ($P < 4.5$ MPa) | About 2100 | 2180 | 2170 |
| AFW stopped (SG level < 10.3 m) | About 2700 | 2749 | 2539 |
| Loop seal clearing only in loop without PZR | About 2200 | 2898 | 3140 |
| End of the transient | 5547 | 5547 | 5547 |

Table 4.3: Main events of OECD/NEA ROSA Test 3-1

Finally, it is also worth mentioning that Scaled-up A nodalization shows discrepancies in coolant temperatures of the secondary side. During the period of very low core power (after the initiation of the LSTF core-protection-system), liquid temperature in the riser is at saturation (see Figure 4.18). This phenomenon affects directly the collapsed liquid level of the riser, and therefore, the AFW closure condition (reported in the boundary conditions of Reference [79] -see also Table 4.3). As shown in the Figure 4.18, temperatures of the Scaled-up A nodalization do not reach the saturation distorting the collapsed liquid level 4.23 and hence, delaying the closure of the AFW and the depressurization of the secondary side.

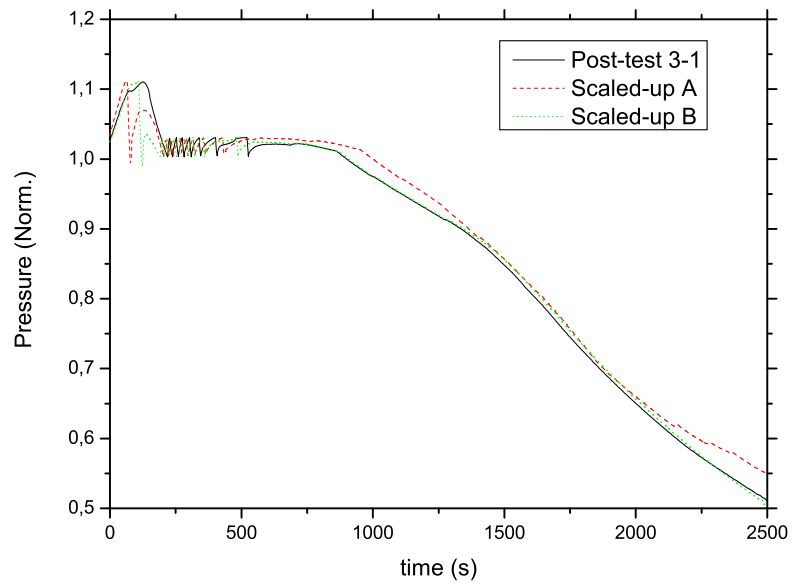


Figure 4.13: Secondary pressure

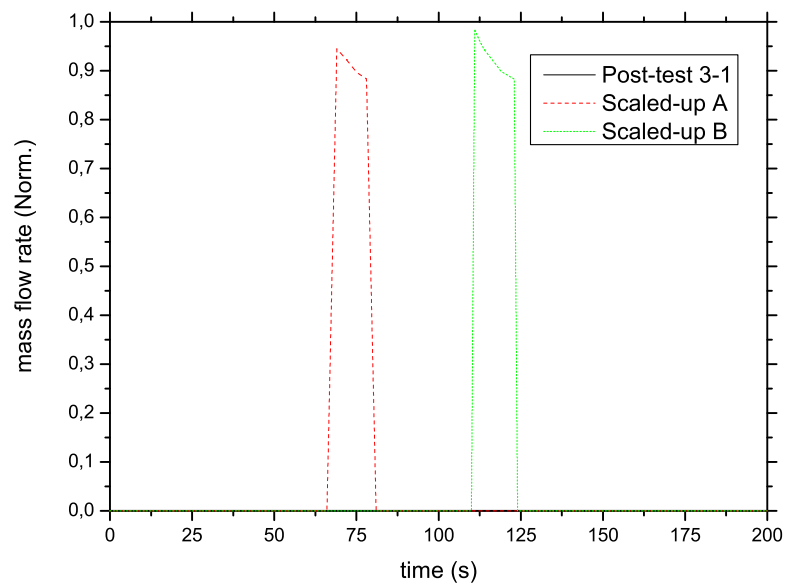


Figure 4.14: Safety valve mass flow rate

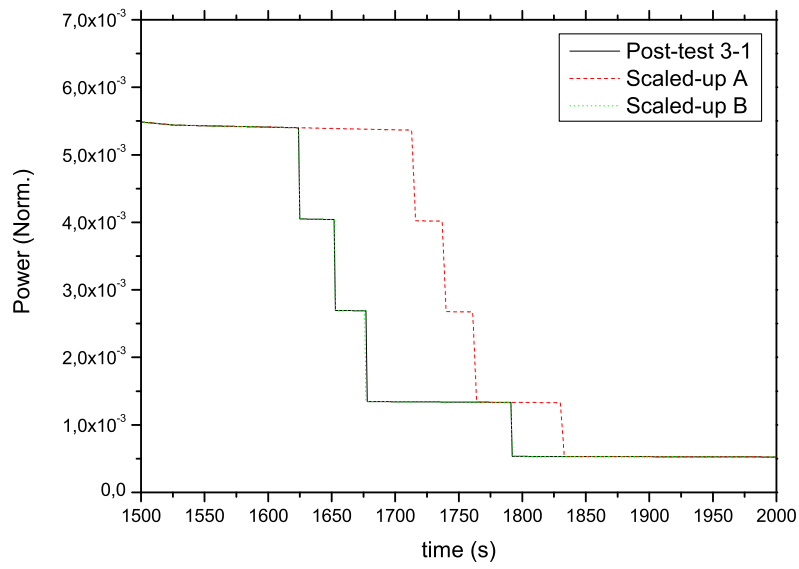


Figure 4.15: Core power

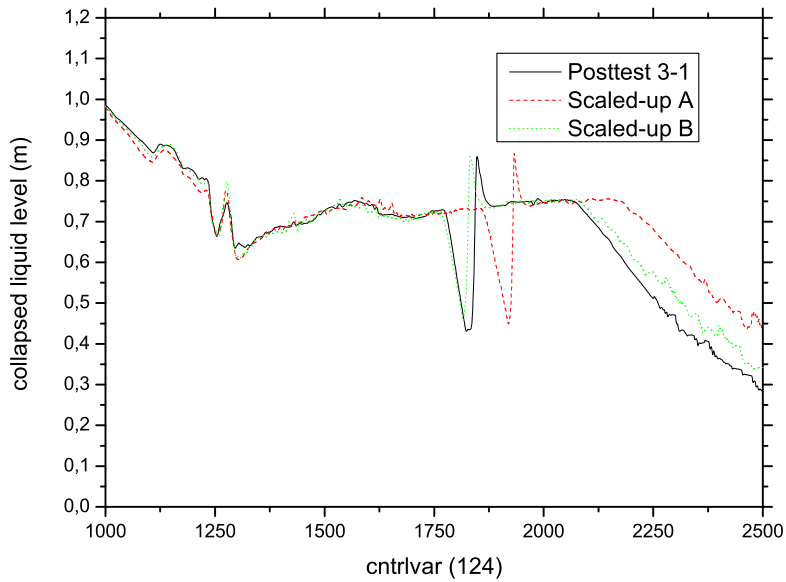


Figure 4.16: Core level

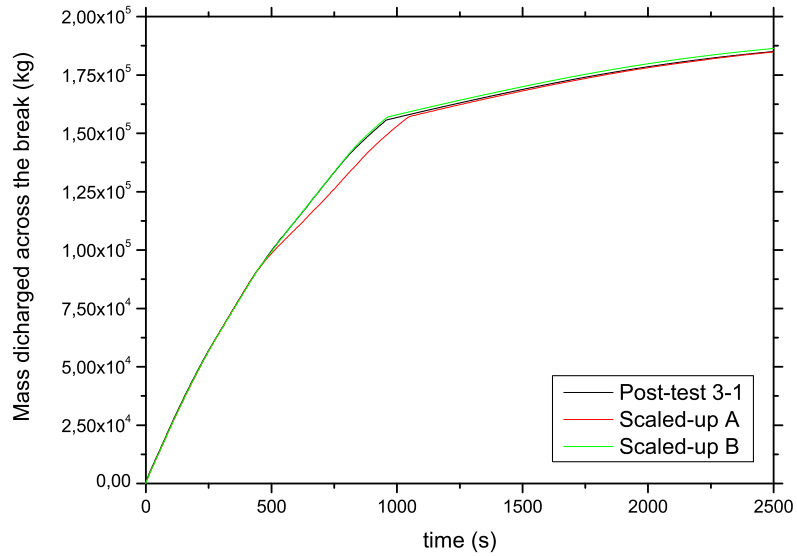


Figure 4.17: Total mass discharged across the break

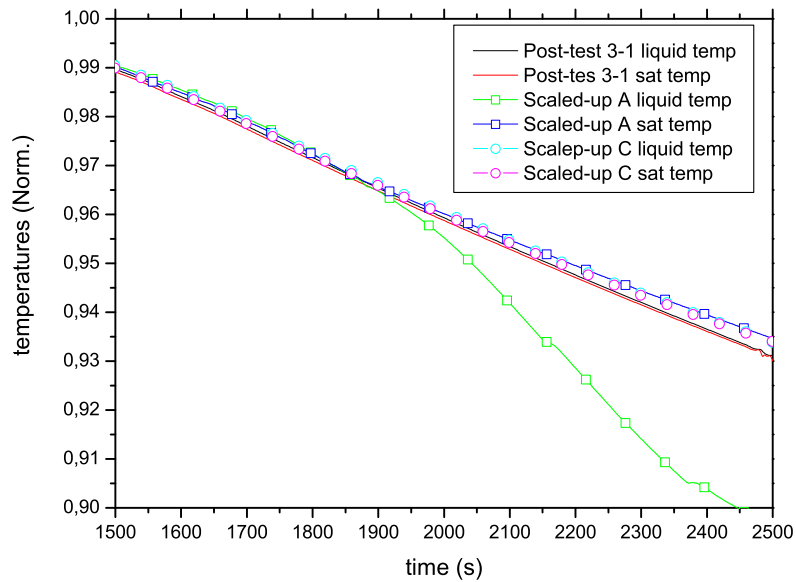


Figure 4.18: Liquid temperatures in the riser of the SG

4.6.2 Assessment of the environment heat losses effect

A new scaled-up input deck (Scaled-up B nodalization) was generated with PVST in order to analyze the effect of the environment heat losses. For this nodalization, the option of scaling-up the passive

heat structures preserving the ratio between the heat exchange surface and the volume of coolant was activated (see Section 4.4.4). Figure 4.19 demonstrates that after activating this option, environment heat losses were preserved. In addition, Figures 4.20 and 4.21 demonstrate that preverting the impact of the environment heat losses, primary-to-secondary heat transfer is reduced and secondary pressure trend is corrected (see Figure 4.13) obtaining a very similar behavior in both the post-test and the scaled-up B nodalization. Moreover, since the system pressures are now more representative of the test conditions, break mass losses become similar (Figure 4.17) and core dryout delay disappears (Figure 4.16).

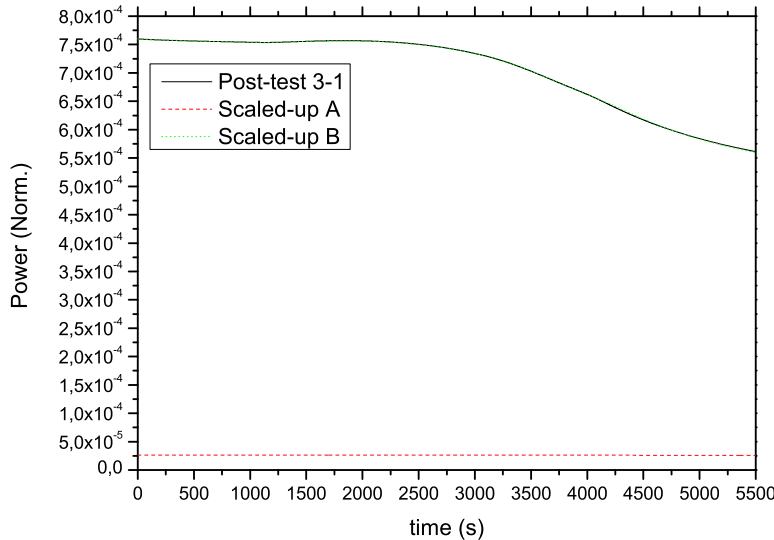


Figure 4.19: Environment heat losses

4.6.3 Assessment of the hydraulic diameters effect

In order to analyze the discrepancy reported in the coolant temperatures of the SGs, an additional Scaled-up C nodalization was generated using PVST. For that case, the hydraulic diameter of the SG DC was modified in order to obtain an idealized scaled-up input deck. Hence, Scaled-up B nodalization was changed just preserving the hydraulic diameter of the post-test nodalization. It was considered that this particular hydraulic diameter may have a relevant impact due to the following reasons:

- After the activation of the LSTF core protection system, the secondary system can be considered to be isolated because the primary to secondary heat transfer drops drastically (see Figure 4.15). Under these conditions effects of dragging, mixing, and interphase exchanges between the subcooled water of the AFW and the saturated vapour of the downcomer become dominant in the balance equations. All these effects are highly dependent on the hydraulic diameter of the SG DC.
- Interphase interactions and drag correlations modelled by RELAP5mod3 closure equations are not preserved in scaled calculations when hydraulic diameter is modified.

The comparison between the Post-test calculation, the Scaled-up B nodalization, and the scaled-up C nodalization demonstrates that preserving the hydraulic diameter internal energies of the water in the DC are corrected (Figure 4.22), obtaining counterpart temperatures (Figure 4.18) and correcting the collapsed liquid levels in the boiler (Figure 4.23).

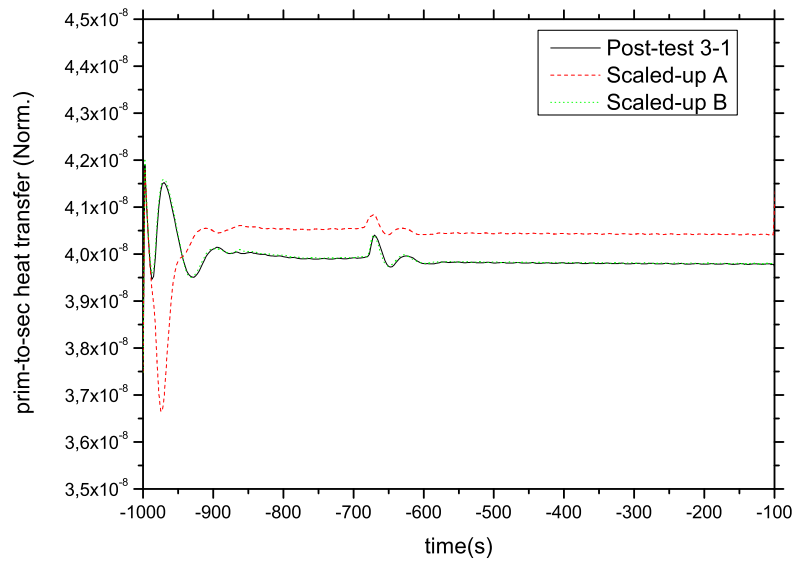


Figure 4.20: Primary-to-secondary heat transfer during conditioning phase

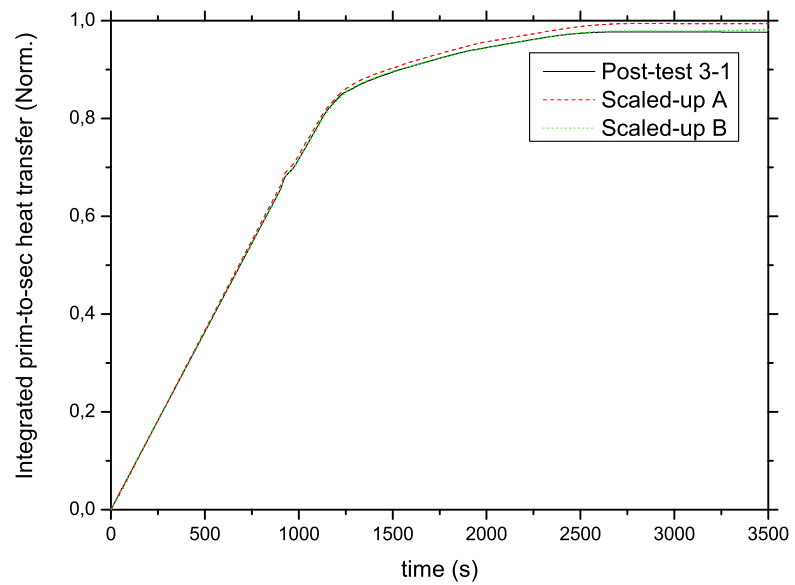


Figure 4.21: Energy transferred from primary to secondary during the transient

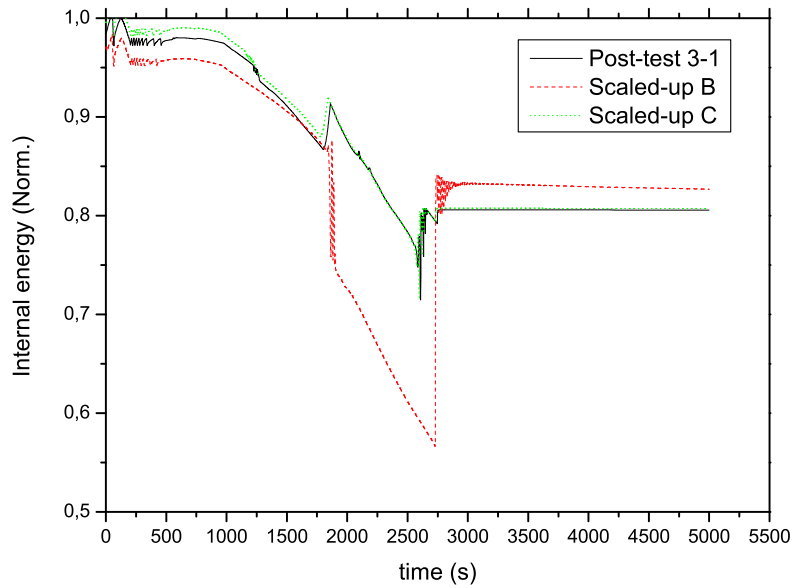


Figure 4.22: Internal energy of the liquid in the SG DC

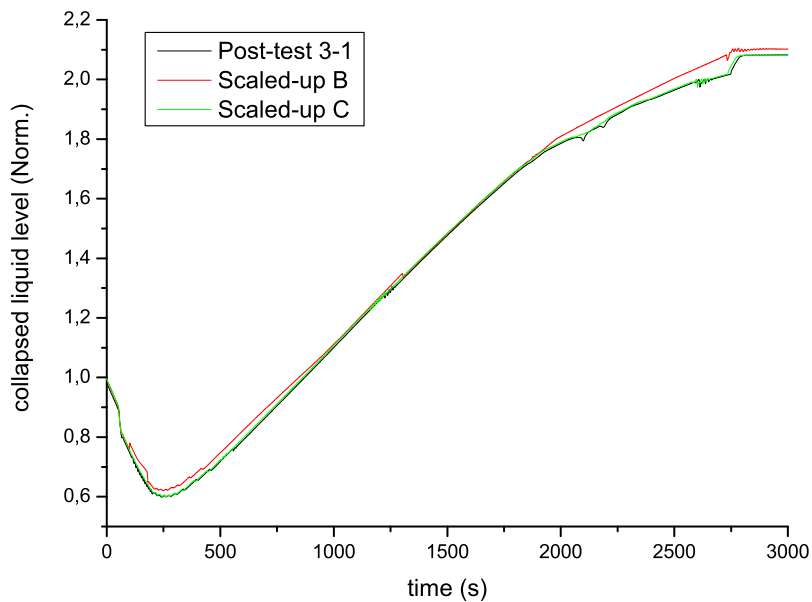


Figure 4.23: Collapsed liquid level in the riser of the SG

4.6.4 Assessment of the Froude number effect

Several scaled-up calculations were carried out related to Post-test 3-1 in order to evaluate the impact of the Froude number without success. After correcting the effect of the environment heat losses,

break mass flow rates became very similar during the two phase natural circulation and reflux and condenser phases (Figure 4.13). Therefore no relevant distortions were detected in the flow regime transitions before core dryout.

The effects of the Froude number conservation can be observed in the scaled-up calculations of the LSTF-PKL counterpart test which is analyzed in Section 6.3.1.

5. Scaling-up Methodology

As it is described in Section 1.4, computational analyses of full scale nuclear power plants have a wide and consolidated application on Nuclear Engineering. During the last 20 years, the Technical University of Catalonia (UPC) has completed several works in this field [28] [29] [31] [30] [32], which deal with the development and usage of NPP nodalizations in the support to plant operation and control. This experience has shown the usefulness and possibilities of this approach. One of the major outcomes is that the continuous development and improvement of NPP nodalizations is not only a requirement but also a difficult task due to the large amount of information contained in a full NPP nodalization. In that sense, methodologies designed to qualify NPP nodalizations take a key role and can be used to both provide an insight in the quality of the produced analyses and, in addition, help the developer in the detection of possible deficiencies in the nodalization. In the framework of the nodalization qualification process and quality guarantee procedures, further development has been performed in the present thesis resulting in a scaling-up methodology.

”UPC scaling-up methodology” follows the guidelines of Kv scaled analysis (see Chapter 3) and UMAE methodology (Section 1.3.6). Besides the connections with the mentioned references, an important development has been performed in order to identify and justify the discrepancies that appear between counterpart simulations at different scales and designs. The present approach is a systematic procedure for qualifying NPP nodalizations taking advantage of the experience acquired through the post-test analysis of ITF experiments. It is devoted to the modeling qualification, which implies that the methodology can only be applied to those phenomena that have been well reproduced in ITF post-test analyses, and that scaling analyses are only performed through code simulations (and do not involve experimental data). There are two main factors that affect the scaling-up of ITF post-test simulations:

- The scaling-down criterion used for the design of the ITF.
- The differences of configuration between the ITF and the NPP.

In order to analyze both, the UPC Scaling-up Methodology uses two approaches, ”Scaled-up nodalizations” and ”Hybrid nodalizations”. It is crucial that they are not confused with the approaches previously presented. Sections 5.4.1 and 5.5 provide some details on how each nodalization is prepared. The so called ”Scaled-up Nodalizations” analyze the effect of the ITF scaling criterion in a scaled-up calculation. On the other hand, the ”Hybrid nodalizations” are defined as modified scaled-up ITF nodalizations in which some components have been adjusted to resemble the configuration of the NPP components. The aim is to evaluate the influence of each feature of the configuration on the ITF simulation results irrespective of the scale.

The ”UPC scaling-up methodology” is shown in Figure 5.1. The procedure is divided into several steps:

- A. To identify a specific scenario for qualifying NPP nodalizations with ITF tests that reproduces its related phenomena. A validation matrix must be defined in order to relate the ITF tests with the particular phenomena to be qualified in the selected scenario (”NPP scenario validation matrix”).
- B. To validate ITF nodalizations and ITF tests selected in the NPP validation matrix (”ITF test & models Validation”).

-
- C. To perform a preliminary plant scaled calculation with the NPP nodalization ("NPP scaled calculation").
 - D. To analyze and establish the Scaling and Design effects in the simulation results by using generated scaled-up and hybrid nodalizations ("Scaling effect analysis and Design effect analysis"). In this step, it is essential to carry out the analyses in series and not in parallel in order to avoid compensating errors.
 - E. To perform an expert judgment by comparing the results of step C combined with conclusions of step D ("Expert judgment"). If results are not consistent, the analyst should improve the NPP nodalization with those modeling remarks obtained from the ITF post-test analysis ("Nodalization improvement"). In the case that the NPP nodalization and the plant scaled calculation results are consistent with the post-test calculation and with the scaling and design effect analysis, the NPP nodalization can then be considered to be qualified ("NPP qualification").

Each of the steps of the "UPC Scaling-up Methodology" is explained in more detail in the following subsections. The results that are shown are described in more detail in Chapter 6, in which the procedure is applied to analyzing the scaling discrepancies that appeared between the post-test simulations of PKL-LSTF counterpart tests performed within the PKL-2 and the ROSA-2 OECD/NEA projects. The discrepancies found are due to differences between the CET and the PCT.

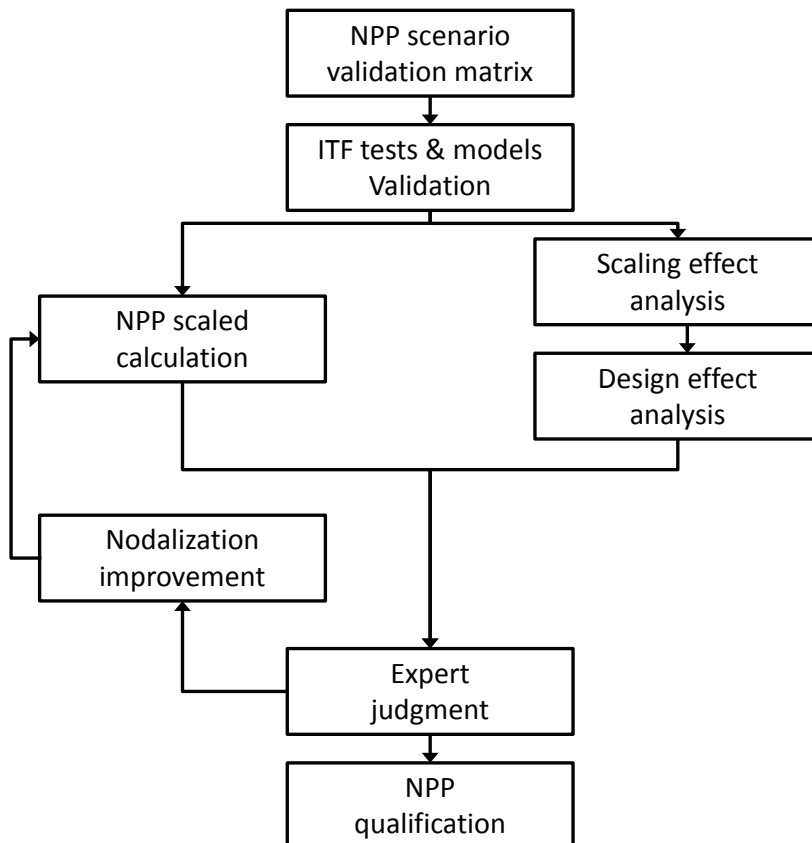


Figure 5.1: UPC Scaling-up methodology

5.1 NPP scenario validation matrix

The initial step of the UPC Scaling-up Methodology requires the analyst to decide the type of scenario for which he wants to validate the NPP nodalization. Once the scenario has been selected, three main features have to be analyzed:

- The relevant thermal-hydraulic phenomena occurring in the selected scenario.
- The design of the ITFs employed in the analysis.
- The choice of ITF experiments.

The aim is that the analyst finds ITFs with similar design to his NPP nodalization in which selected tests include the TH phenomena related to the specific scenario. In that sense, The ITF system description reports, ITF test reports, and most of all, CSNI Code Validation Matrices [16] are therefore of exceptional value.

Once the TH phenomena have been decided upon and the most convenient ITFs have been chosen, an "NPP scenario validation matrix" must be defined in order to ensure which phenomena can be tested by system codes. In Table 5.1 there is an example of a validation matrix for the PWR SBLOCAs and IBLOCAs. In this matrix, the phenomena suggested by the CSNI Matrices [16], the LSTF-PKL Counterpart Test Reports and LSTF Test 2 report, are related to 5 tests performed in 3 different ITFs (LOBI, LSTF and PKL).

When ITF tests are chosen, it is important to pay attention to counterpart tests (tests with identical boundary conditions performed at facilities at different scales) because they allow to check, for different scales and designs, if the codes and the ITFs nodalizations can reproduce the same phenomena. This will not ensure that these phenomena can be extrapolated to the NPP scale (as already mentioned, this point is not within the scope of this methodology), but it will be very effective for translating ITF modeling experience to NPP nodalization qualification because the analyst can evaluate whether the same modeling criteria have been used for different scales and designs. In the example of table 5.1, four of the ITF tests are counterpart experiments and establish a link both between PWR Siemens/KWU (LOBI,PKL) and Westinghouse (LSTF) designs, together with three different scales (1:48 for LSTF, 1:145: for PKL, and 1:700 for LOBI).

5.2 Validation of ITFs tests and nodalizations

In the second step, the analyst should perform post-test analyses of the ITF experiments chosen in the "NPP scenario validation matrix". The aim of this step is to ensure the quality of the results and to draw conclusions on code modeling. The work of the analyst should therefore be focused on two features:

1. Qualifying the ITF nodalizations for several tests beyond those selected in the validation matrix.
2. Assuring the robustness of the nodalization to minimize user effect and compensating errors.

About these points, some papers have been presented during the last few years ([80] and [81]) in order to ensure the quality of modeling through post-test analyses. Both are based on two main ideas: the improvement of ITF nodalizations with the continuous simulation of post-tests and regular checking of nodalization changes by re-executing all the previous tests with the latest version of the ITF nodalization. The idea is to ensure that both a unique and sufficiently detailed nodalization can reproduce the whole post-test library while keeping (or improving) the degree of agreement with experimental results.

| Test phenomena | Counterpart Tests | | Counterpart Tests | | ROSA 2 Test 1 |
|--|-------------------|------------------|-------------------|------------------|------------------|
| | PKL III G7.1 | ROSA 2 Test 3 | LOBI BL-34 | LSTF SB-CL-21 | |
| 1 phase natural circulation | | | X | O | |
| 2 phase natural circulation | X | X | X | O | |
| Reflux and condensation | X | X | X | O | |
| Asymmetric loop behavior | X | | | O | |
| Break flow | X | X | X | O | X |
| Phase separation without mixture level formation | X | X | O | O | X |
| Mixture level and entrainment on SG secondary side | X | X | X | O | |
| Core mixture level | X | X | X | O | X |
| Stratification in horizontal pipes | X | X | X | O | X |
| Phase separation T-junction and effect on break flow | X | X | | O | X |
| ECC-mixing and condensation | X | X | X | O | X |
| Loop seal clearing | | | X | X | X |
| Pool-formation in UP/CCFL | | | | O | X |
| Core-wide void and flow distribution | X | X | | O | X |
| Heat transfer in covered core | X | X | X | O | X |
| Heat transfer in pre-uncovered core | X | X | X | O | X |
| Heat transfer on SG primary side | X | X | X | O | X |
| Heat transfer on SG secondary side | X | X | O | O | X |
| Pressurizer thermalhydraulics | | | | X | |
| Surgeline hydraulics | | | | X | |
| 1 phase 2 phase pumps behavior | | | | O | |
| Structural heat and heat losses | X | X | X | O | X |
| Non-condensable gas effect | | | | | |
| Boron mixing transport | | | | | |
| CETvsPCT relationship | X | X | | | |
| Nomenclature | | | | | |
| X = totally reproduced | | | | | |
| O = partially reproduced | | | | | |

Table 5.1: NPP SBLOCA/IBLOCA validation matrix

Once the ITF nodalization has been qualified and the required tests of the validation matrix have been simulated, phenomena that have been validated for at least two facilities at different scales and designs can be used for qualifying NPP nodalizations. The modeling guidelines derived in both cases need to be consistent. To achieve this, expert judgment will be essential. If counterpart tests have been validated for the same phenomena with the same modeling conclusions, a plant scaled calculation and scaling and design effect analyses will be performed for the counterpart test in which the design of the ITF is closest to the NPP nodalization.

In Reference [82] both LSTF and PKL counterpart tests were validated for phenomena related with the correlation between CET and PCT. Better agreement was achieved by improving the core nodalization using a pseudo-3D modeling. The results showed a closer agreement in both cases (Figures 5.2 and 5.3).

Both nodalizations were previously qualified with the ROSA Post Test 3-1 (Reference [45], see Section 2.1.4.1) and Post-Test 3-2 (Reference [46], see Section 2.1.4.2) for LSTF, and PKL III Test E1.1, E2.2 (ref. [40]) and others (ref. [53] and ref. [54]) for PKL (see Section 2.2.4).

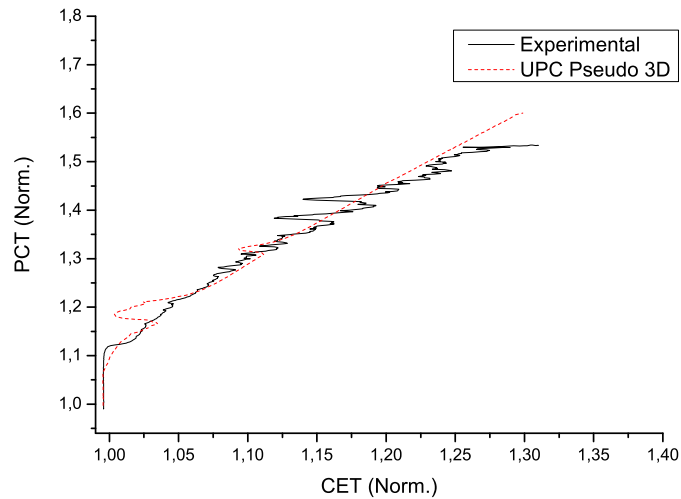


Figure 5.2: PKL CET vs PCT curve

5.3 NPP scaled calculation

As it is explained in Chapter 3, a NPP scaled calculation (also so-called Kv scaled) is a system code simulation in which defined ITF test conditions are scaled-up to an NPP nodalization in order to reproduce the same scenario. It consists on adjusting the transient conditions of an NPP nodalization to the test conditions of an ITF experiment. This approach allows the behavior of the NPP and ITF nodalizations to be compared under the same conditions in order to check the capabilities of the NPP nodalization and the improvement of nodalization when needed.

As regards the "UPC scaling-up methodology", a plant scaled calculation is a unique calculation with two aims:

- To check the applicability of the ITF test in the NPP nodalization for phenomena that has been validated in post-test analyses.
- Being a reference for justifying as an expert judgment those discrepancies that appear in comparison with the results of the post-test analysis. Therefore, scaled-up and hybrid nodalizations explained in Sections 5.4.1 and 5.5 will be essential.

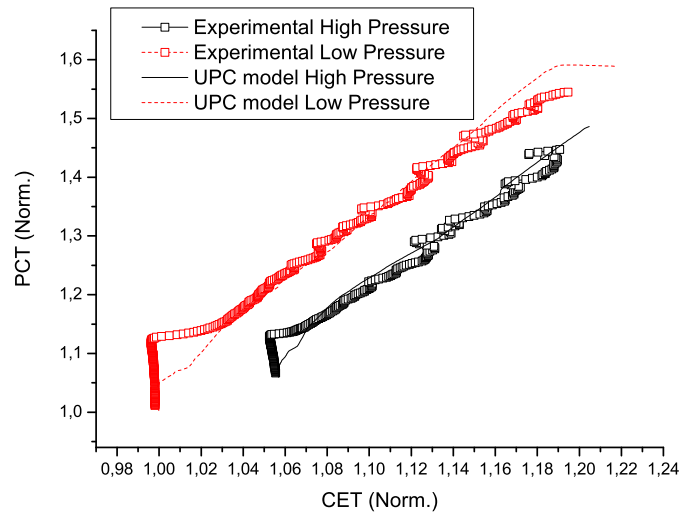


Figure 5.3: PKL CET vs PCT curve

In the example of Figure 5.4 (further information about this Kv scaled calculation can be found in Section 3.2), it is shown that water is retained in U-tubes during the same period of time for both post-test simulation and plant scaled calculation. In that sense, the calculation is showing the applicability of the transient (phenomena are qualitatively reproduced) which fulfills the first aim. Otherwise, results show an amount of water that is larger in the NPP case. In order to qualify the NPP nodalization, this discrepancy should be explained by carrying out scaling and design effect analyses by taking plant scaled calculation as a reference for an expert judgment. It is at this point that the second aim is required and this is what distinguishes the "UPC scaling-up methodology" from a simple plant scaled calculation.

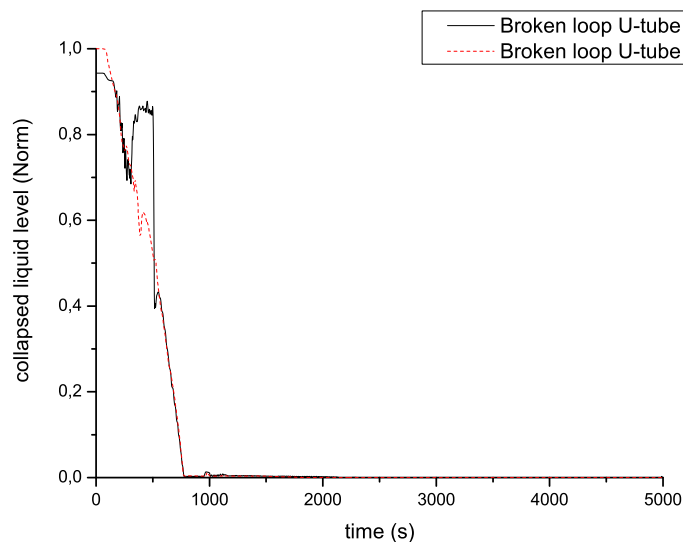


Figure 5.4: U-tube collapsed liquid level

Plant scaled calculation is unique and cannot be tuned during scaling and design effect analyses. Only if the expert judgment considers that the NPP must be improved, should a second calculation be carried out in order to qualify the NPP nodalization improvements.

5.4 Scaling effect analyses

This step shows how the scaling criterion affects the simulation of phenomena validated in the ITF post-test analyses. Scaled-up nodalizations are developed at this level by comparing ITF post-test simulation with ITF scaled nodalizations that have the same size as the NPP nodalization.

5.4.1 Scaled-up nodalizations

Scaled-up nodalizations are developed by following certain scaling criterion. The UPC has developed a "Power-to-Volume Scaling Tool (PVST)" which enables RELAP5mod3 input decks to be scaled by following the Power-to-Volume scaling criterion. This software scales hydrodynamic components, heat structures, control system variables, general tables and unit trips using an input scaling factor (Kv). Volumes, sections, mass flows and powers are modified by means of the Kv factor. Hydraulic diameters and longitudinal surfaces of the heat structures are changed by using its square root. In the case of hydrodynamic components with parallel channels (such as U-tubes, guide tubes or fuel rods), the software has the option of keeping geometry values raising their number with the Kv factor.

In order to analyze the origin of power-to-volume scaling distortions, two options have been included in the software:

- A. Scaling environment and passive heat structures preserving their heat impact whatever the scale.
- B. Scaling input nodalizations preserving the Froude number in horizontal components.

To analyze the scaling effect, several scaled-up nodalizations must be generated using the calculated NPP scaling factor (further information about how to calculate it can be found in Chapter 3). The first nodalization has to be a regular scaled-up nodalization, in which the power-to-volume scaling criterion is applied without any modification of the possible scaling distortion sources. Comparison with the ITF post-test calculation will show the effect of the scaling criterion on the analyzed phenomenon. Whenever any distortion is detected, the analyst must perform another scaled-up nodalization without the scaling distortion source. Comparison with the ITF post-test calculation and the regular ITF scaled-up nodalization allows the effect of this specific scaling distortion source to be observed.

This step must be repeated for all the scaling distortions detected until the user achieves an idealized scaled-up nodalization in which the analyzed phenomenon is simulated in the same way as in the ITF post-test analysis.

In Reference [82] (results available in Section 6.3.1), three scaled-up nodalizations were produced and compared with the PKL counterpart post-test simulation:

- Sc-up nodalization A: a regular scaled-up nodalization.
- Sc-up nodalization B: a regular scaled-up nodalization preserving environment heat losses.
- Sc-up nodalization C: a regular scaled-up nodalization preserving environment heat losses and Froude number.

Comparison between the post-test Sc-up nodalization A and Sc-up nodalization B showed that the increasing system pressures during the reflux and condensation phase were due to a decrease in environment heat losses (see Figure 5.5). Comparison between the post-test, Sc-up nodalization B and Sc-up nodalization C revealed that the break mass flow discrepancies appeared as a result of a different Froude number (see Figure 5.6). The main discrepancies in core dry out and peak cladding

temperature were removed once these two changes were applied (see Figure 5.7). It was considered that no further scaling distortion sources needed to be analyzed.

The final result of the analysis carried out in this section is an ITF scaled-up nodalization in which scaling effects were minimized by following the established rationale. Such nodalization will be used in the next step.

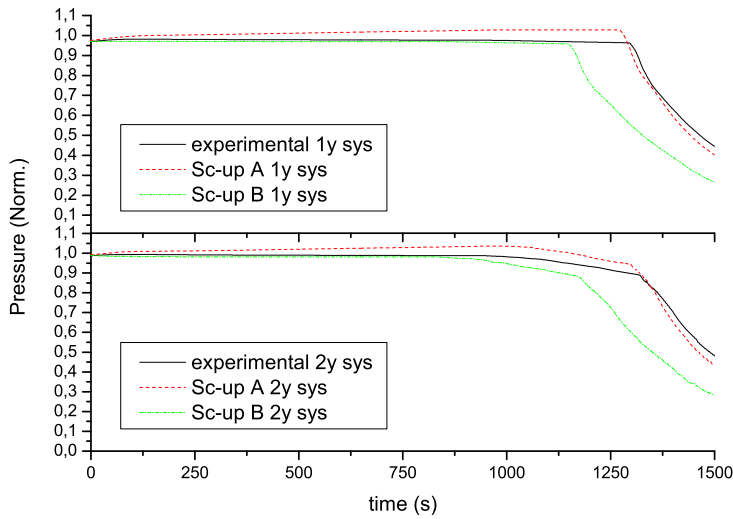


Figure 5.5: System pressures

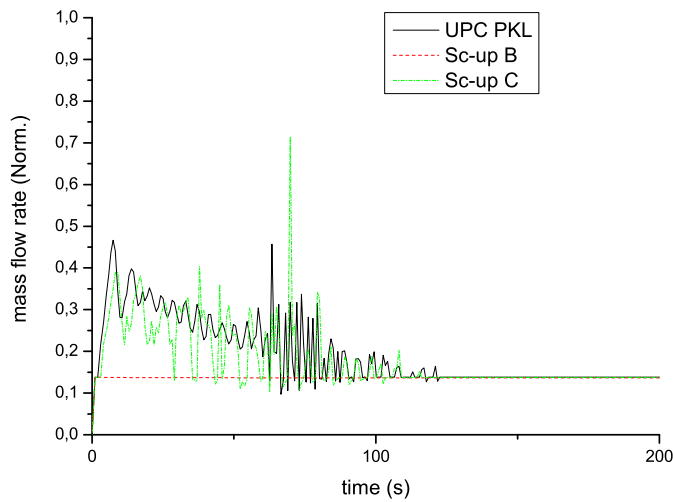


Figure 5.6: Break mass flow rate

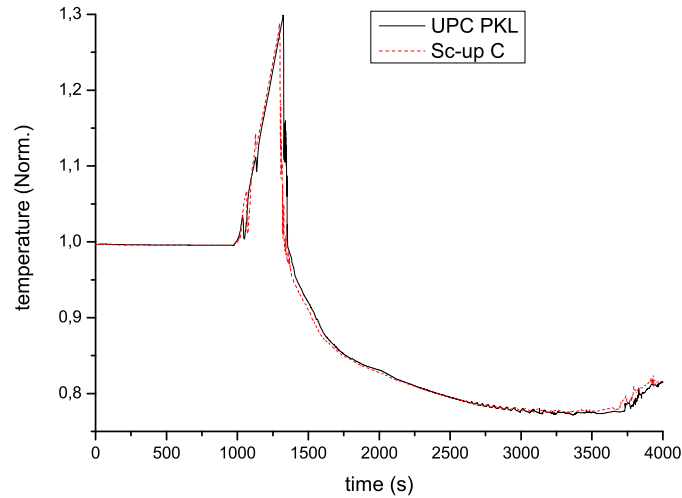


Figure 5.7: Core exit temperature

5.5 Design effect analyses

In this step, the analyst must be able to justify the discrepancies that appear in a Plant scaled calculation by means of the differences in design between the ITF and the NPP. In that sense, hybrid nodalizations are compared with the Plant scaled calculation and the idealized scaled-up nodalization obtained from the Scaling effect analyses. Some components of the NPP nodalization are copied and added to the ITF scaled-up nodalization obtained in the previous step. This allows the impact of each tested component on the simulation to be differentiated.

The work of the analyst in the design effect analyses has to be focused on two main features:

- A. To identify which components and differences in the configuration might affect the phenomena to be validated.
- B. To develop a group of hybrid nodalizations in series for detecting sources of design distortion. Each component has to be added individually to the previous hybrid nodalization in order to distinguish which components may cause a distortion of the results and which do not. Although some discrepancies could be justified by two or more combined sources of design distortion, it will not be necessary to evaluate them separately as all of them are part of the NPP nodalization. Sequential analyses reveal both the effect of each component and that of them all together.

In Reference [82] (results available in Section 6.3.2), a delay in the core dryout (see Figure 5.8) was detected between PKL and LSTF test simulations. Several design differences were considered that could influence the total inventory and mass distribution:

- PZR (differences in scaling ratio mass of water- and surge line height)
- UTs (differences in exchanging surface that could affect reflux and condensation)
- LSTF downcomer-to-hot leg bypass (which has an effect on water stratification in the hot leg that could modify discharge across the break)
- Vessel passive heat structures (could alter vapor generation)

- Vessel geometries excluding the core (PKL and LSTF vessels have different water distribution around the core as a result of a different reference plant - KWU and Westinghouse respectively-)

Once all possible design distortion sources were listed, hybrid nodalizations were prepared for the idealized scaled-up nodalization in which scaling effects were minimized (nodalization C in Figure 5.7):

- PKL Hybrid base nodalization: Sc-up nodalization C with LSTF heat losses and LSTF Froude number
- PKL Hybrid A nodalization: PKL Hybrid base nodalization with LSTF PZR
- PKL Hybrid B nodalization: PKL Hybrid A nodalization with LSTF U-tubes
- PKL Hybrid C nodalization: PKL Hybrid B nodalization with LSTF downcomer bypass
- PKL Hybrid D nodalization: PKL Hybrid C nodalization with LSTF vessel passive heat structures
- PKL Hybrid E nodalization: PKL Hybrid D nodalization with LSTF hydrodynamic components, LSTF vessel walls heat structures and LSTF material properties

Results of Figure 5.9 showed that PZR design, U-tube design, vessel bypasses and passive heat structures were not responsible for the delay in core dryout. In fact, design differences between the KWU vessel and Westinghouse vessel were the reason for the delay (Figure 5.10).

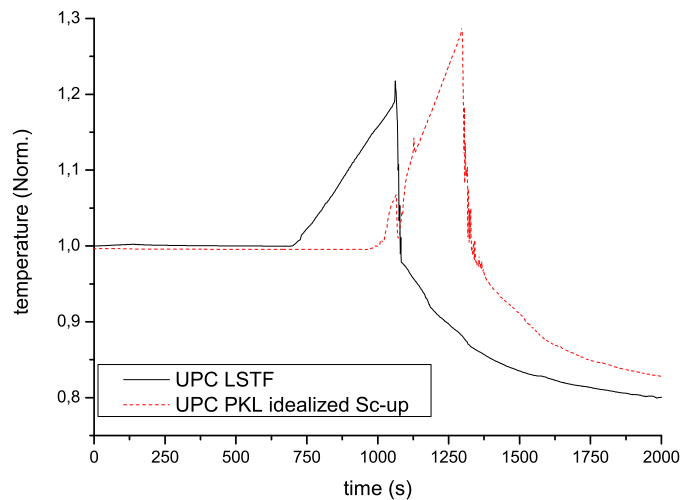


Figure 5.8: Core exit temperature

5.6 Expert judgment

Expert judgment is the final step of the "UPC Scaling-up Methodology". Once the design effect analysis and ITF post-test analyses modeling have been carried out, the analyst should make a decision on whether the NPP can be considered as qualified for the studied phenomenology or whether the NPP nodalization requires improvement. Expert judgment relies on:

- The conclusions from the design effect analysis.
- The NPP Nodalization Handbook.

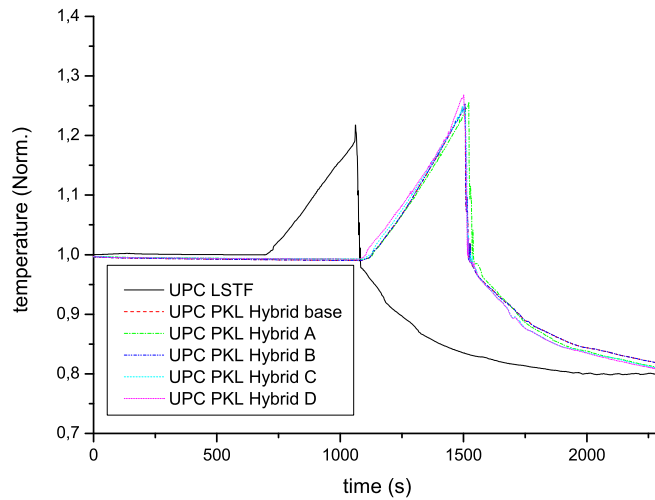


Figure 5.9: Core exit temperature

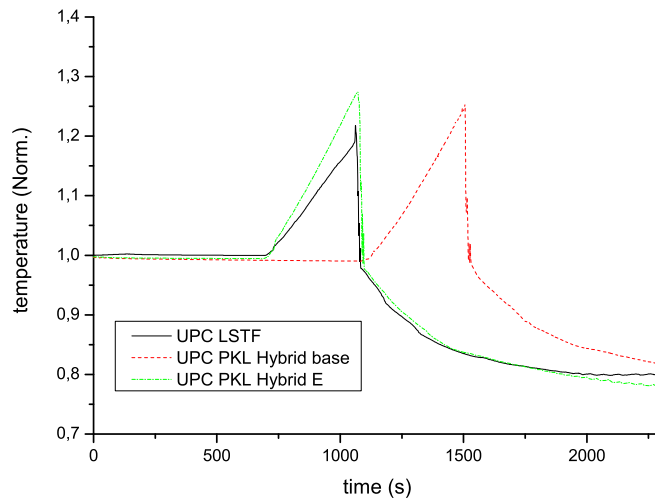


Figure 5.10: Core exit temperature

- Knowledge from ITF modeling.

Once the design effect analysis has been concluded, the user has valuable information about the NPP components that can explain observed discrepancies. When such components are identified, their specification must be thoroughly checked and the analyst must ensure that these components have been consistently modeled. In that sense, the "UPC Scaling-up methodology" is used in the qualification process and continuous improvement of the nodalization.

If the specifications of an NPP component are well transcribed, the analyst, bearing in mind his ITF modeling know-how, has to judge the significance of the modeling details of the component for the tested phenomena in the specific scenario. If after expert judgment, it is considered that a nodalization

improvement is required, a second plant scaled calculation will be necessary, comparing its results with the idealized scaled-up nodalization and one new hybrid nodalization with the new component. Otherwise, it is considered that NPP nodalization is qualified for these phenomena. When all the NPP validation matrix phenomena are validated, the NPP nodalization will be qualified for plant applications and support to plant operation in the specific scenario.

It could occur that after the Design Effect Analysis step, no distortion sources are found that could justify the tested phenomenon discrepancies. In that case, the expert judgment should conclude that the ITF test validation must be reevaluated and the code capabilities be reviewed. In that sense, it would be another evidence of the robustness of the methodology for validating and guaranteeing quality modeling. In any case, in order to avoid these conclusions and to facilitate the work of the analyst, counterpart tests with different scales and designs should be selected to the furthest extend in the NPP scenario validation matrix. These tests should be then validated for the same phenomena with consistent modeling procedures (see Section 5.2).

6. Assessment of the UPC Scaling-up methodology

In Chapter 5 (and also Reference [83]) was presented the "UPC Scaling-up methodology", a systematic approach for qualifying NPP nodalizations using the knowledge acquired from the ITF tests. In the present section the methodology has been tested and checked taking advantage of the Counterpart Test that was performed in 2011 in PKL and LSTF in the framework of the ROSA-2 and PKL-2 OECD/NEA projects.

One of the limitations of the scaling methodologies is the impossibility of demonstrating their theoretical capabilities because of the lack of counterpart experimental data at NPP level. In that sense ROSA-2 PKL-2 Counterpart Test was of great value because it allows comparing an identical transient between two facilities with relevant differences in design and scale. Hence, it was decided by the present author that before to attempt an application of the "UPC Scaling-up methodology" to a NPP nodalization, it was essential to demonstrate that "UPC scaling methodology" could catch distortion sources between counterpart post-test simulations that were validated over experimental data. In consequence, in the following subsections is described the application of the "UPC Scaling-up methodology" to the PKL (the smaller facility) Counterpart Test, and the comparison of the gained results with the LSTF Counterpart Test. This approach would be analogous to the application of the methodology to an ITF post-test and the comparison with a Kv-scaled calculation of it, but with the plus that in this case experimental data assures the quality of the "Kv-scaled" (LSTF counterpart test) calculation.

6.1 PKL-2 ROSA-2 Counterpart Test

In 2011 a counterpart Test was performed in LSTF and PKL Test Facilities as a part of the OECD/NEA ROSA-2 and PKL-2 projects (test 3 [84] and test G7.1 [85] respectively). The objective of both tests was devoted to analyze two aspects:

- Core Exit Temperature (CET) measurement effectiveness in Accident Management (AM) of NPP's.
- Scaling effects between PKL and LSTF Test Facilities.

The selected scenario was an upward oriented 1.5 % hot leg SBLOCA. System failures as no high pressure safety injection and no automatic secondary-side safety cooldown were imposed. The particular test conditions are described in the following subsection. Major features of both PKL and LSTF facilities are detailed in Table 6.1. Further information about them can be found in Chapter 2.

6.1.1 ROSA-2 Test 3 Test conditions

This test was divided in three phases, a high pressure phase, reproducing the NPP scenario at full pressure; a low pressure phase, reproducing the same scenario at counterpart conditions with PKL;

| | LSTF | PKL |
|-------------------------------|----------------------------|----------------------|
| Reference plant | Westinghouse | KWU (Siemens design) |
| Height | Full | Full |
| Volumetric Scaling | 1/48 | 1/145 |
| No. of Loops | 2 | 4 |
| Pressure vessel DC | Cylindrical | Double-pipe |
| U-tubes / SG | 141 | 30 |
| Pressure | Full | Up to 4.5 MPa |
| Core Power | 14% (10 MW) | 10% (2.5 MW) |
| No. of Electrical rods | 1008 | 314 |
| Axial Profile | Chopped cosine | Flat |
| Radial Profile | 3-region | 3-region |
| ECCS | Full | Full |
| Hot leg diameter (m) | 0.207 | 0.128 |
| Special Measurement | Video probe, O2 gas sensor | Boron sensor |
| No. of Instruments | About 1760 | About 1070 |

Table 6.1: PKL and LSTF major features

and finally, an intermediate phase, with the purpose of conditioning the LSTF conditions at the end of the high pressure phase to the PKL counterpart test conditions. Table 6.2 shows the list of imposed conditions for each phase.

Several parameters were adjusted from the PKL test conditions with the aim of having analogous behaviors during the low pressure phase of the transient. A scaling factor $K_v=2.55$ was applied for calculating the opening area of the SG's relief valves, the water volumes of the accumulators, and the injection rates of the low pressure injection (LPI) system. Pressures in the primary and secondary systems were adjusted 1:1 to the PKL test conditions during the conditioning phase, and the mass inventory was reinstated in order to have a similar hot leg liquid level as expected to occur in the PKL test. Reflux and condenser conditions were established in both facilities at the beginning of the counterpart phase. Accumulators' set point was reduced to 2.6 MPa for including their actuation in both facilities.

6.1.2 PKL-2 G7.1 Test conditions

The PKL initial conditions were adjusted at its maximum pressures in order to reproduce as realistic as it can PWR SBLOCA reflux and condensation, core dry-out and Accident Management phases. The test conditions were set identical as those of LSTF low pressure phase conditions (see Table 6.2).

In relation to scaling, the mass inventory in the secondary side was adjusted using K_v factor in order to have the same ratio between liquid and energy storage in the SG's. The Core power was slightly increased above the K_v factor to compensate the differences present between both facilities in the external heat losses.

6.1.3 Experimental results

The Results of the counterpart phases showed a close agreement for reproducing the main phenomena expected for the transient. Both facilities reproduced similarly the three parts of the transient (reflux and condensation, vapor superheating and Accident Management - see Figures 6.1 and 6.2 -) obtaining a wide spectrum of experimental data for analyzing the relationship between CET and PCT and the effectiveness of the CET signal for AM actuations.

| Event | Condition | High pressure phase | Conditioning phase | Low pressure phase | |
|--|--|---------------------|--------------------|--------------------|--|
| Break valve opened | $t = 0 \text{ s}$ | | | | |
| Low pressure scram signal | $P_{\text{prim}} < 12.96 \text{ MPa}$ | | | | |
| Secondary system isolation | scram signal | | | | |
| Initiation of primary coolant pump coastdown | scram signal | | | | |
| Initiation of core power decay curve simulation | scram signal | | | | |
| Initiation of HPI coolant injection into Pressure vessel upper plenum | TPCT $> 750 \text{ K}$ | | | | |
| Break valve closed | $P_{\text{prim}} < 5 \text{ MPa}$ | | | | |
| Power constant | $P_{\text{prim}} < 5 \text{ MPa}$ | | | | |
| Termination of HPI coolant injection into Pressure vessel upper plenum | $H_{HL} \simeq 0.5 \hat{A} \cdot H_{HL}$ | | | | |
| SG's relief valve depressurization | $H_{HL} \simeq 0.5 \hat{A} \cdot H_{HL}$ | | | | |
| Secondary system isolation | $P_{\text{prim}} < 3.9 \text{ MPa}$ | | | | |
| Break valve re-opened | $P_{\text{prim}} > 4.5 \text{ MPa}$ | | | | |
| SG depressurization as AM action | TCET $> 623 \text{ K}$ | | | | |
| Initiation of AFW in both loops | AM action signal | | | | |
| Initiation of ACC system in both loops | $P_{\text{prim}} < 2.6 \text{ MPa}$ | | | | |
| Termination of ACC system in both loops | $P_{\text{prim}} < 1.2 \text{ MPa}$ | | | | |
| Initiation of LPI system in both loops | $P_{\text{prim}} < 1 \text{ MPa}$ | | | | |

Table 6.2: Test conditions of Test 3

Some differences were detected between the results of both facilities:

- Core dryout: there is a delay of 280 s in the core dryout (see Fig. 6.3) which modifies the timing of next phases of the transients.
- CETvsPCT curve: the relationship between the CET and the PCT measurements shows different slope when the CET starts to increase (see Fig. 6.4). Because of it, there is a discrepancy of 55 K in the PCT of both facilities when the condition of the AM action is achieved ($T_{CET} > 623$ K).
- Effectiveness of the SG depressurization takes place at a different rate in each facility. Figure 6.5 compares PCTs of both tests for the interval in which SG depressurization and accumulators' injection take place. Results show that for PKL facility rewetting cannot be assured without the entrance of the passive ECCS system.

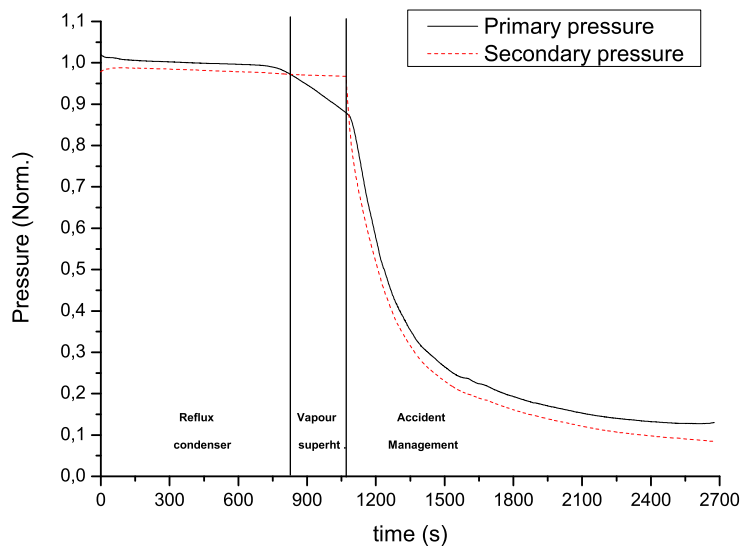


Figure 6.1: LSTF system pressures

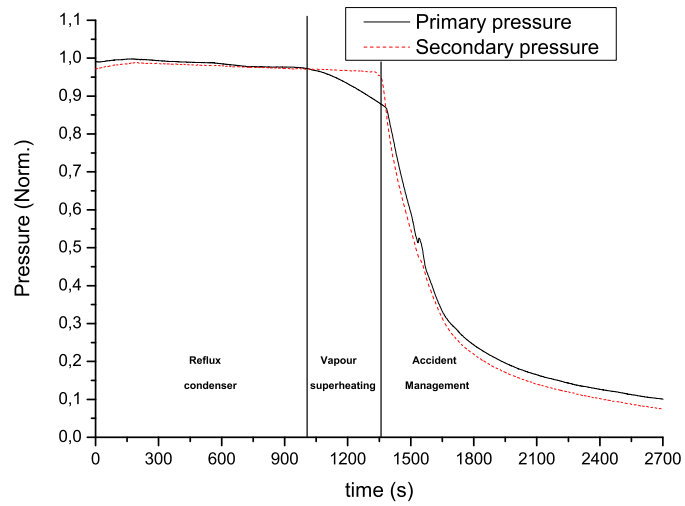


Figure 6.2: PKL system pressure

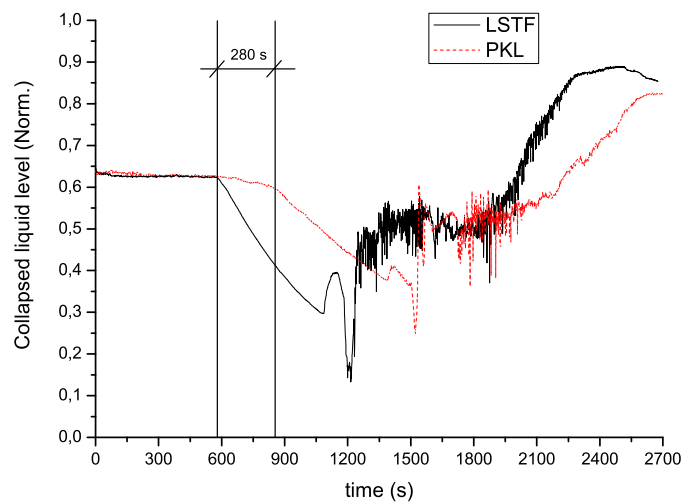


Figure 6.3: core collapsed liquid level

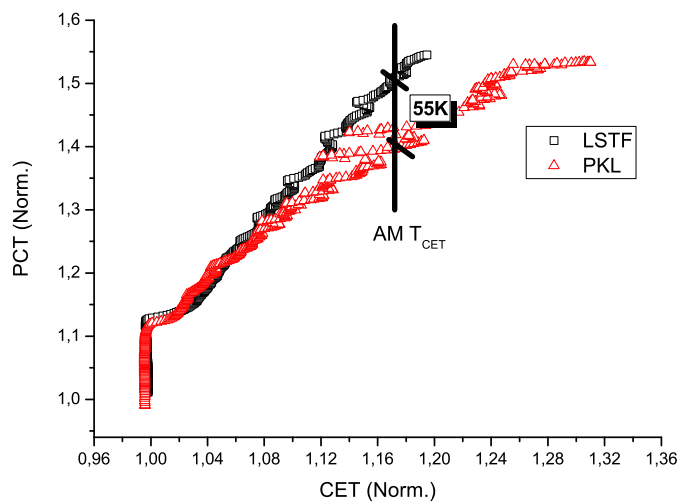


Figure 6.4: CET vs PCT curve

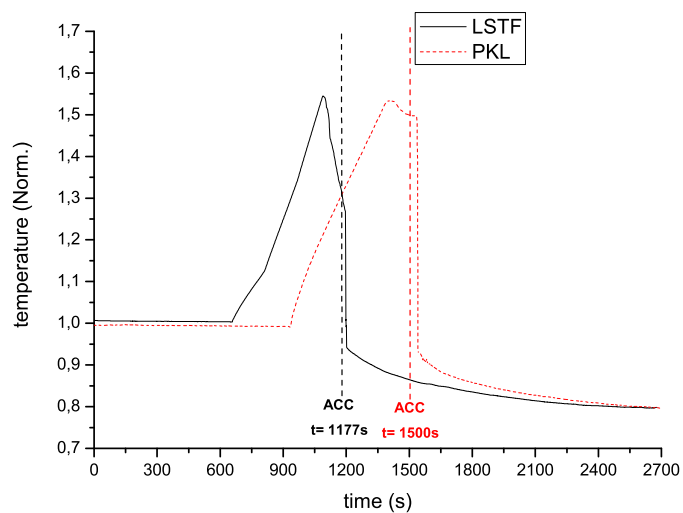


Figure 6.5: Peak cladding temperature

6.2 Results

6.2.1 PKL G7.1 Post-test analysis

Two calculations were performed by making use of the qualified UPC PKL RELAP5mod3.3 nodalization (further information can be found in Section 2.2.3):

- UPC PKL 1D nodalization
- UPC PKL Pseudo-3D nodalization

The differences between both nodalizations were exclusively related to the core and upper plenum modeling. UPC PKL 1D nodalization simulated them with one channel (in addition to the core bypass), having fuel and all passive heat structures (core barrel and unheated rods) linked to the same volumes. The fuel was modeled with three HS's, with the same power ratio and divided in 7 axial levels.

UPC PKL Pseudo-3D nodalization had the core and upper plenum (until the CET thermocouple level) divided in three radial channels (see Fig. 6.6), with one fuel HS for each channel. The HSs for the passive internal metal structures were split for each channel proportionally to the flow path of each one, and the core barrel was linked to the outer zone. The radial flow paths between cells were modeled and transversal momentum equations were activated following the recommendations of Reference [86]. The total number of Core axial meshes was increased to 14 and the upper plenum cell heights were adjusted so that the center of the node coincided with the elevation of the thermocouples in the test facility.

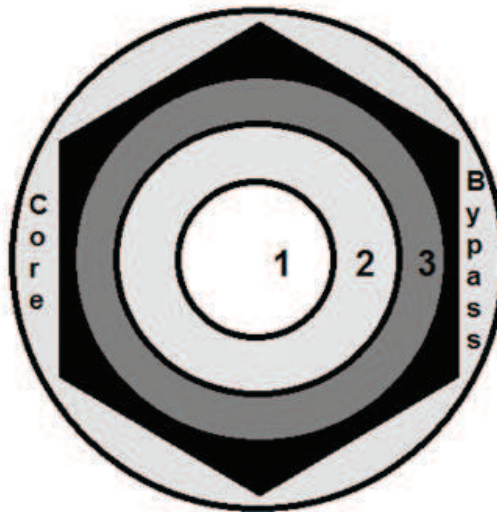


Figure 6.6: UPC PKL Pseudo 3D nodalization core channels

The obtained results showed a quite close agreement for both nodalizations reproducing the initial conditions (see Table 6.3) as well as the general behavior of the transient (Figures 6.7 and 6.8 show a close agreement of both nodalizations for reproducing depressurization rate during three reported phases of the transient - reflux and condensation, vapor superheating and SG depressurization-). The Pseudo 3D nodalization provided closer results for the main events because it reduced the delay in the core uncover (see Table 6.4). This was seen to be a consequence because of a higher vapor generation in the 1D nodalization during the phases of reflux and condensation and vapor superheating. It implied that, for similar break mass losses liquid mass inventory decreased faster and core uncover started before. In Figure 10, the differences between vapor generation and break mass flows are compared (the differences are calculated by subtracting the values of the Pseudo 3D nodalization

to the 1D nodalization).

| | Experimental data | UPC 1D nodalization | UPC Pseudo 3D nodalization |
|-------------------------------------|-------------------|---------------------|----------------------------|
| Core power (Norm.) | 1 | 0,996 | 0,996 |
| Pressurizer pressure (Norm.) | 1 | 1 | 1 |
| Pressurizer liquid level (Norm.) | 1 | 0,7 | 0,7 |
| Secondary-side pressure (Norm.) | 1 | 1 | 0,998 |
| Secondary-side liquid level (Norm.) | 1 | 0,998 | 1 |
| Main feedwater temperature (Norm.) | 1 | 1 | 1 |
| Accumulators pressure (Norm.) | 1 | 1 | 1 |
| Accumulators temperature (Norm.) | 1 | 1 | 1 |
| LPI pressure (setpoint) (Norm.) | 1 | 1 | 1 |
| LPI temperature (Norm.) | 1 | 1 | 1 |

Table 6.3: Initial condition of PKL Test G7.1

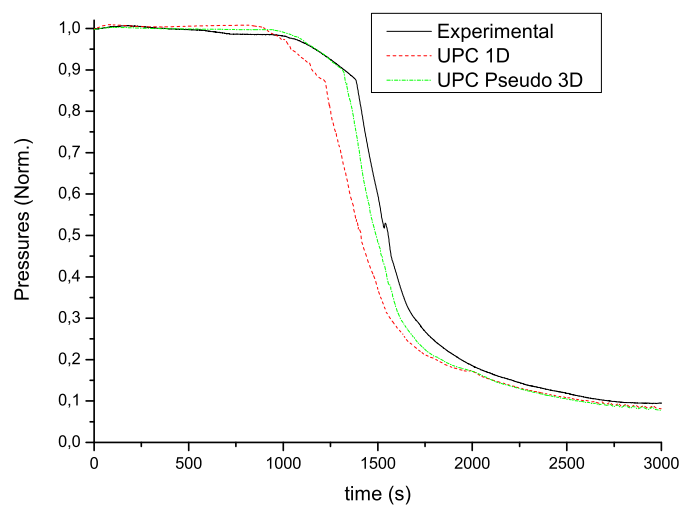


Figure 6.7: PKL G7.1 primary pressure

Finally, the UPC PKL Pseudo 3D nodalization was qualified for reproducing the relationship between the CET and the PCT. This nodalization solved instabilities in the simulation of the overheated CET (Fig. 6.10), obtaining close results in the CETvsPCT curve (Fig. 6.11). The Pseudo 3D nodalization reproduced the same slope of the experimental data as well as the initial increase of the PCT.

On the other hand, the Pseudo 3D nodalization was not qualified for reproducing closely the core quenching after SG depressurization action. Despite core refilling was simulated, in the calculation quench front achieved the top level of the active core before accumulators' injection, showing a discrepancy with experimental results. In Fig. 6.10, each CET curve is associated with a vertical line that indicates the time in which the accumulators' injection starts. The comparison shows that for both simulations, the temperatures dropped before accumulators' injection, unlike experimental data, in which it did not occur.

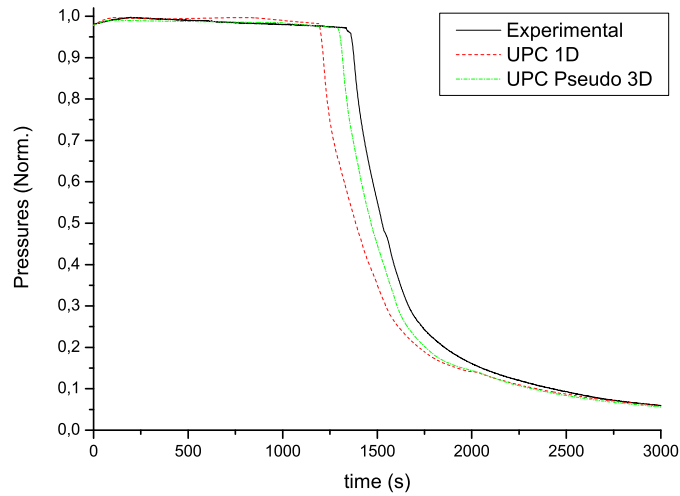


Figure 6.8: PKL G7.1 secondary pressure

| | Experimental (s) | UPC 1D nodalization (s) | UPC Pseudo-3D nodalization (s) |
|--|---------------------|-------------------------------|--------------------------------------|
| Start of the transient | 0 | 0 | 0 |
| Begin of core uncover | 940 | 800 | 940 |
| Primary pressure below secondary pressure | 1020 | 920 | 1010 |
| Secondary side depressurization | 1360 | 1190 | 1295 |
| Start of accum. Injection | 1500 | 1304 | 1450 |
| ACC injection finished | 1860 | 1712 | 1752 |
| LPSI started | 2060 | 1966 | 1993 |
| End of the test | 5685 | 5685 | 5685 |

Table 6.4: Main events of PKL G7.1 Test

6.2.2 LSTF Test 3 Post-test analysis

A base case calculation was performed using the UPC LSTF RELAP5mod3.3 nodalization that had been qualified previously for the ROSA Test 3.1 and ROSA Test 3.2 transients (References [45] and [46]). The major features of the vessel nodalization were: core and fuel modeled with one channel and one heat structure respectively; fuel axial core power calculated as an average of the Low, Medium and High experimental core power profiles; 9 fuel mesh points; characterization of passive heat structures simulating control rods, core barrel, upper core support plate, instrumentation and external heat losses.

Results showed a quite good agreement for reproducing initial steady state conditions and main events of three phases of the transient (see Tables 6.5 and 6.6). There was a slight overestimation of the break mass losses when stratification appeared in the hot leg so the break was in two-phase discharging mode (see Fig. 6.12 from 750 s to 1500 s). As a result of this, core uncover occurred slightly earlier for both phases of the transient (see Table 6.6), and consequently, the SG depressurization signal related with the CET was activated in advance as well (see table 6.6 and Fig. 6.13). In any case, the main parameters were consistently reproduced (see Figures 6.13, 6.14 and 6.15).

Focusing on the relation between the CET and the PCT, results showed a disagreement in the

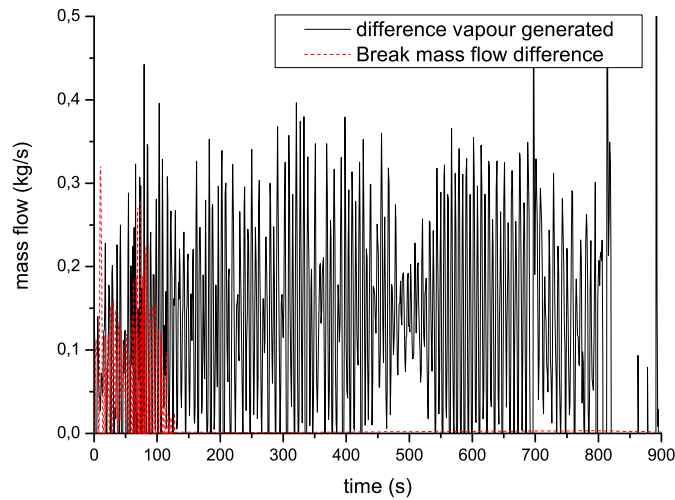


Figure 6.9: PKL G7.1 Mass flow comparison

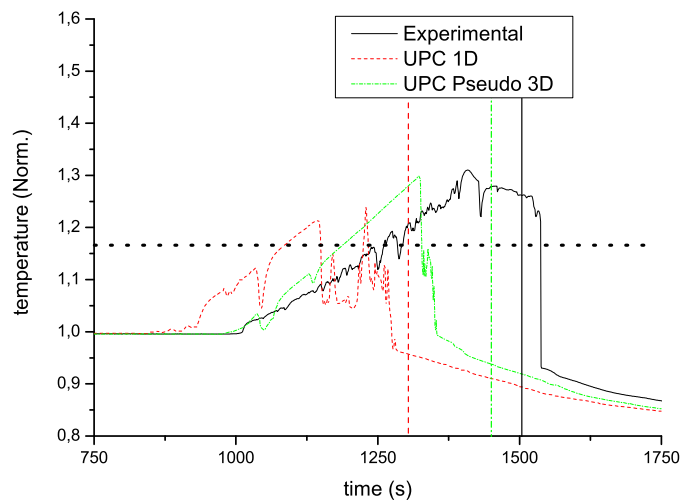


Figure 6.10: PKL G7.1 core exit temperature

slope of the plots (see Figures 6.16 and 6.17). These results suggested that UPC LSTF nodalization should be improved following a similar approach as the one (Pseudo 3D modeling) applied in the PKL analysis.

In that sense, a UPC LSTF Pseudo 3D nodalization was implemented splitting the core in 13 channels with 18 axial levels (see Figure 6.18). The low, medium and high core power axial profiles were simulated, arranging them in each channel as in the experimental radial power distribution. Cartesian crossflows were used for organizing them radially and transversal momentum equations were activated in order to take into account the possible radial ΔP 's. Passive HS's were split according to the geometries. Finally, the upper plenum was modified simulating it with two channels, one hot

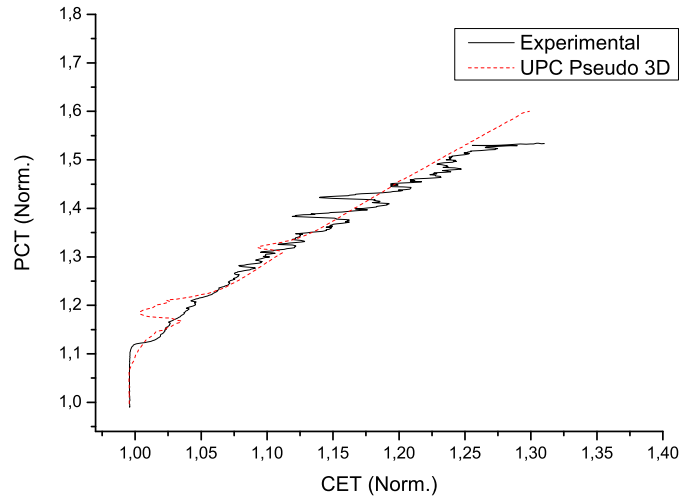


Figure 6.11: PKL G7.1 PCTvsCET

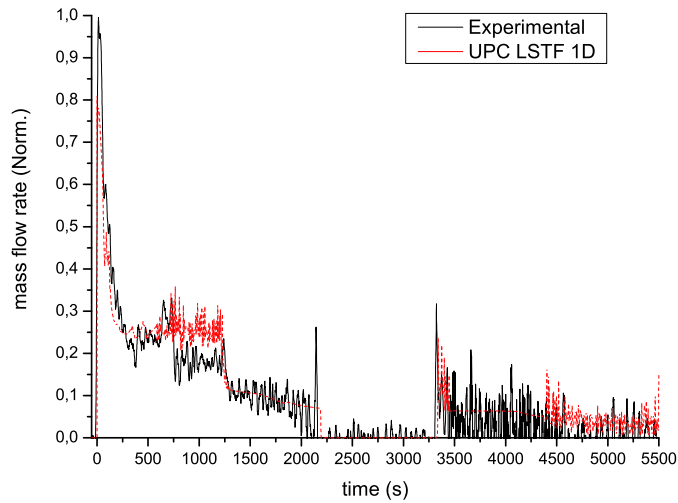


Figure 6.12: Test 3 break mass flow rate

channel, connected to the outlet of the hottest core channel, and another one simulating the rest of the plenum. Transversal momentum equations were activated too in order to consider ΔP 's in the vessel that could affect flow path to the hottest channel during the upper plenum HPI injection. On the other hand HPI mass flow was modified in the conditioning phase in order to match primary mass inventory at the beginning of the low pressure phase. This correction was justified for the analysis of the following counterpart phases in which the achievement of specified initial conditions are necessary.

Results of the UPC LSTF Pseudo 3D nodalization showed a close agreement in the simulation of the CETvsPCT relationship (see Figures 6.16 and 6.17). For both high and low pressure transient phases, Pseudo 3D nodalization reproduces the same slope and correlation with a margin of 50 and

| | Experimental data (loops w / wo PZR) | UPC LSTF nodalization (loops w / wo PZR) |
|---|---|---|
| Core power (Norm.) | 1 | 1 |
| Hot leg temperature (Norm.) | 1 | 1.001 |
| Cold leg temperature (Norm.) | 1 | 1.003 |
| Mass flow rate (x loop) (Norm.) | 1 | 1.002 / 0.998 |
| Downcomer-to-hot-leg bypass (Norm.) | 1 | 1 |
| Pressurizer pressure (Norm.) | 1 | 1 |
| Pressurizer liquid level (Norm.) | 1 | 1.014 |
| Secondary-side pressure (Norm.) | 1 / 1 | 1.004 / 0.997 |
| Secondary-side liquid level (Norm.) | 1 | 0.995 |
| Main feedwater temperature (Norm.) | 1 | 1 |
| Main feedwater flow rate (Norm.) | 1 | 1.007 / 1.004 |
| Accumulators pressure (Norm.) | 1 | 1 |
| Accumulators temperature (Norm.) | 1 | 1 |
| LPI pressure (initiation of system) (Norm.) | 1 | 1.24 |
| LPI temperature (Norm.) | 1 | 1 |
| Steam flow rate (Norm.) | 1 | 1.007 / 1 |

Table 6.5: Initial conditions of LSTF Test 3

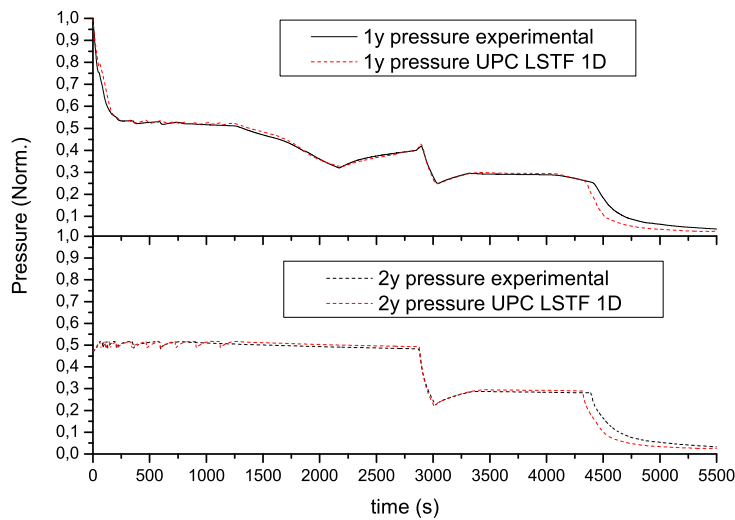


Figure 6.13: Test 3 system pressures

70 K respectively over AM signal established for this particular scenario ($TCET > 623$ K). Regarding to core uncover, the adjustment of initial mass inventory at the beginning of the counterpart phase solves the delay (see low pressure transient phase of Table 6.6), obtaining a closer agreement in the simulation of reflux condenser, vapor superheating and AM phases (see Fig. 6.19).

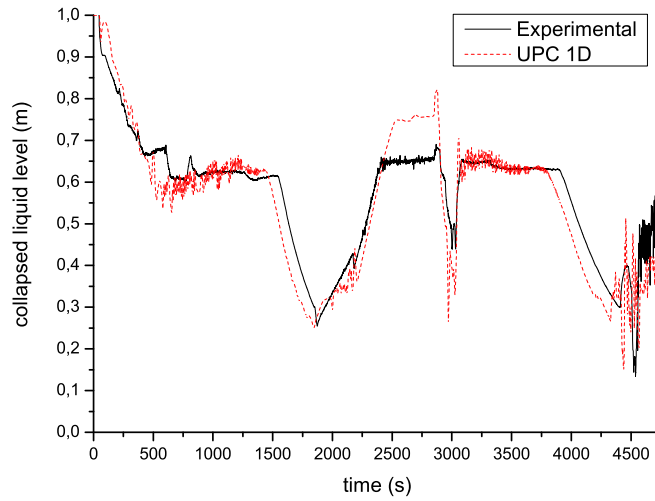


Figure 6.14: Test 3 core collapsed liquid level

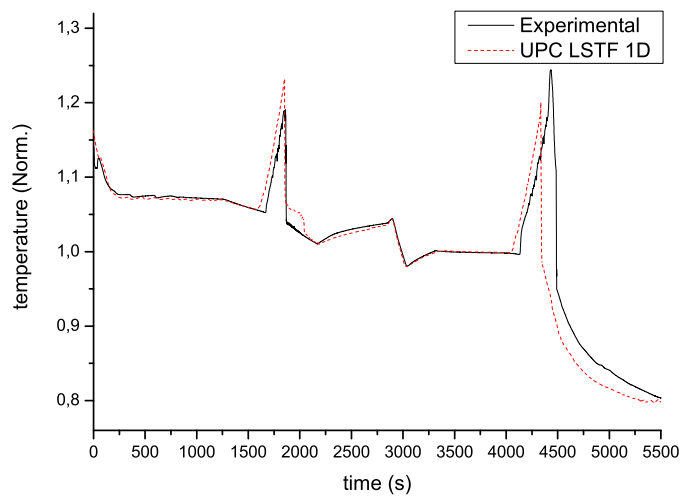


Figure 6.15: Test 3 core exit temperature

| Event | Experimental data [s] | UPC LSTF 1D nodalization [s] | UPC LSTF Pseudo 3D nodalization [s] |
|---|--------------------------|---------------------------------|--|
| High pressure transient phase | - | - | - |
| Break | 0 | 0 | 0 |
| SCRAM signal: · Turbine trip and closure MSIV · PZR heater off · Termination main feedwater | 25 | 33 | 33 |
| Initiation of coastdown of RCPs | 31 | 39 | 39 |
| Termination of continuous opening of SG RVs, termination of 2-phase natural circulation, break flow from 1-phase liquid to 2-phase flow | 600 | 1238 | 1185 |
| Core liquid level starts to decrease (core uncover) | 1545 | 1460 | 1475 |
| End high pressure transient phase (PCT >750 K) | 1840 | 1852 | 1778 |
| Conditioning phase | - | - | - |
| HPI system activated | 1850 | 1862 | 1788 |
| Break valve closed | 2163 | 2169 | 2161 |
| HPI system closed | 2852 | 2852 | 2852 |
| SG depressurization | 2880 | 2892 | 2880 |
| Termination of SG depressurization | 3024 | 3008 | 3012 |
| End of Conditioning phase (break valve re-opening) | 3323 | 3323 | 3323 |
| Low pressure transient phase | - | - | - |
| Break valve re-opening | 3323 | 3323 | 3323 |
| Primary pressure lower than SG secondary pressure | 4108 | 4085 | 4105 |
| SG depressurization (CET >623 K) | 4392 | 4297 | 4388 |
| Initiation of accumulator system (primary pressure = 2.6 MPa) | 4505 | 4419 | 4488 |
| Initiation of LPI system (primary pressure = 1.0 Mpa) | 5005 | 4660 | 4741 |
| End of the transient | 5500 | 5500 | 5500 |

Table 6.6: Test 3 main events

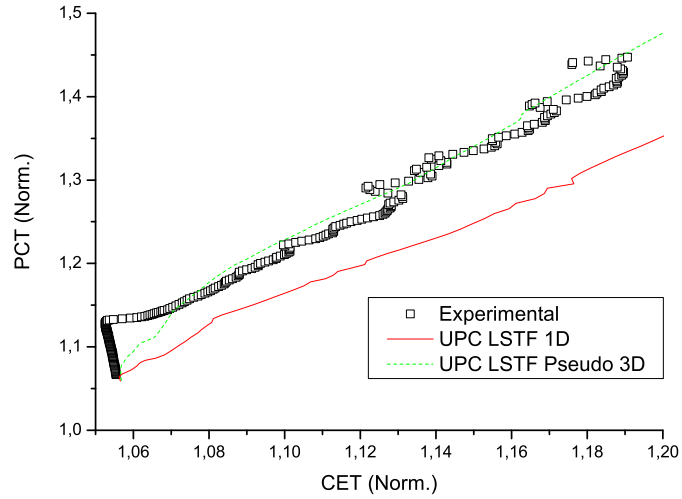


Figure 6.16: PCTvsCET curve during High pressure transient phase

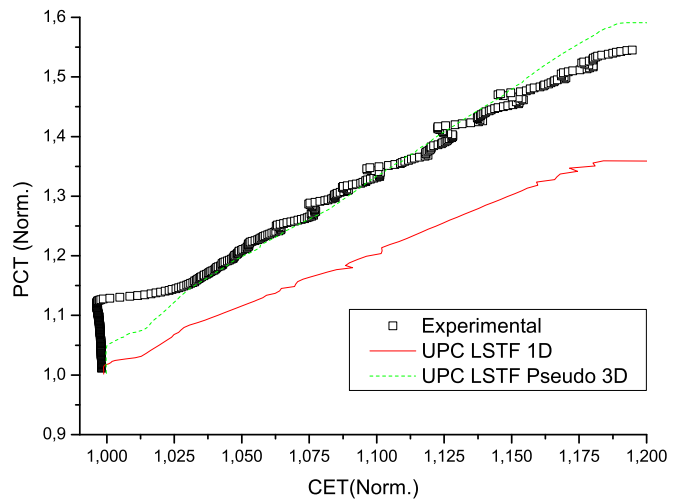


Figure 6.17: PCTvsCET curve during Low pressure transient phase

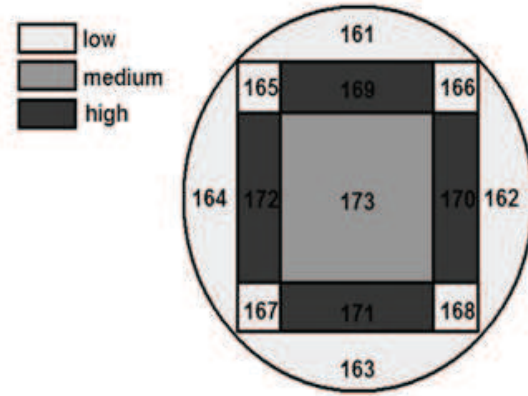


Figure 6.18: UPC LSTF Pseudo 3D nodalization: core channels

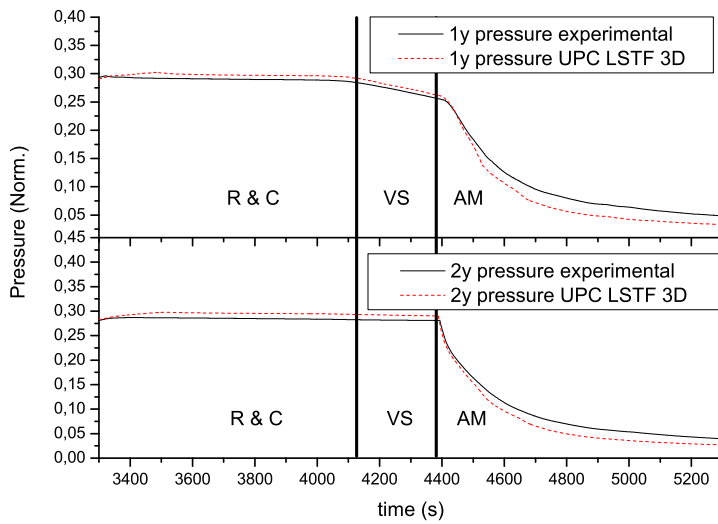


Figure 6.19: Test 3 system pressures

6.3 "Scaling effect analysis" and "Design effect analysis" evaluation

Scaling and Design effect analyses are two merged steps of the UPC Scaled-up methodology (see Figure 5.1) in which the analyst can evaluate how the scale and the design modify the results of an ITF simulation. Both steps must only be applied for those phenomena that have been validated for at least two facilities with different scale and design. The effectiveness of these techniques has been checked taking advantage of the post-test calculations described above. In that sense, PKL-LSTF Counterpart test becomes useful in that it relates two facilities with different scale and design (see table 6.1).

Once the post-test analyses are described, the experimental differences reported in Section 6.1.3 must be checked in order to guarantee the validation of the related phenomena in the simulation. It can be concluded that:

- CET vs PCT correlation discrepancies: UPC LSTF and PKL nodalizations were qualified for simulating CET vs PCT correlation in that they reproduce the phenomenon with close results (see Figures 6.11, 6.16 and 6.17).
- Core dry out delay: once initial mass inventory was readjusted in the LSTF Pseudo 3D nodalization for the low pressure transient phase, the results of both simulations showed a quite good agreement in the reproduction of the core uncovering (see tables 6.4 and 6.6), reproducing qualitatively well the timing of the three phases of the transient in each case. The same criteria were applied in both nodalizations for the modeling of the core (which affects to vapor generation) and the break (which affects to primary mass inventory), therefore both simulations were qualified showing a qualitative consistency respect to experimental data in at least two different facilities.
- SG depressurization effectiveness: Results of the PKL simulation showed the inefficacy of UPC PKL nodalization for reproducing the effect of the SG depressurization in the CET (see Figure 6.10). For this case, PKL nodalization is not qualified and no further analysis can be done.

6.3.1 Scaling effect analysis

The aim of the scaling effect analysis step is to generate an idealized ITF scaled-up nodalization in which the effects of the scaling are minimized. ITF post-test calculation must be scaled to the size of the analyzed Facility/NPP nodalization following the scaling criteria applied in the design of the experimental facility. The reported distortions of the scaling criteria must be studied in order to evaluate how they modify the results and in order to generate an idealized input deck without their effects. Only in the case where the scaling effects have been removed, the design effects can be analyzed.

In the case of the PKL and the LSTF experimental facilities, the power to volume scaling method was followed for their design. For this criterion, scaling distortions are mainly related with changes in hydraulic diameter, which affects to the external heat losses, energy storage in passive structures, friction effects and flow regime transitions (for more detailed information see the related paper [8]). For analyzing scaling effects of the Counterpart Test, PVST software (general description in paper [8]) has been applied to the validated UPC PKL Pseudo 3D nodalization.

As a first step, a nodalization (named Sc-up nodalization A) has been generated using the PKL-LSTF Kv factor suggested by the PKL and LSTF operator agents. This nodalization follows the Power to Volume (PtoV) scaling criterion, so that a PKL nodalization has been obtained with the same size in power and in volume as of those of LSTF. The comparison between Sc-up nodalization A and the UPC PKL Pseudo 3D nodalization shows discrepancies in the system pressures during reflux condenser and vapor superheating phases (see Figure 6.20) despite having similar mass discharged through the break (see Figure 6.21 - the slight discrepancy is because primary pressures are not

equal-). The secondary pressure is higher for Sc-up nodalization A, pushing up the coupled primary pressure during reflux condenser phase.

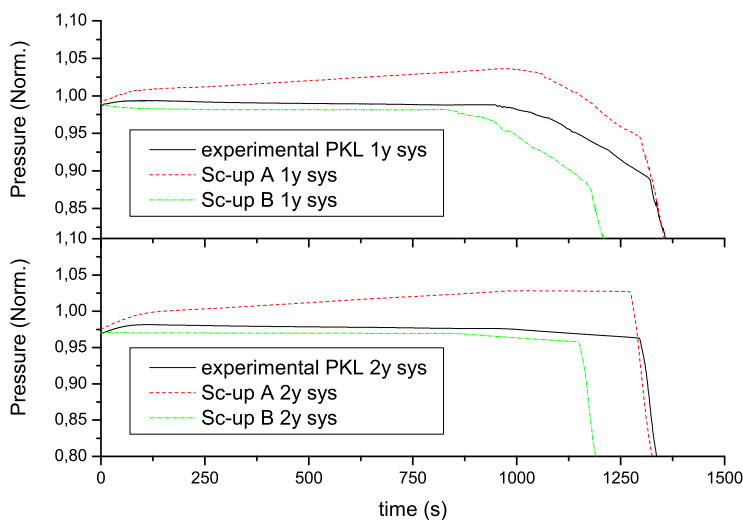


Figure 6.20: System pressures

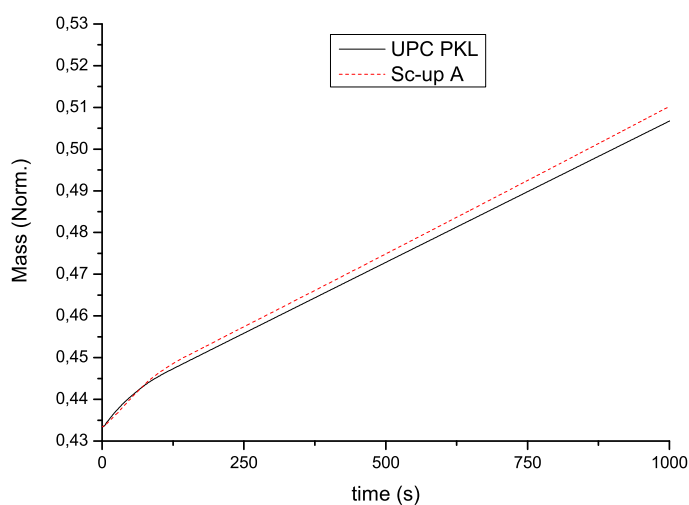


Figure 6.21: Mass discharged through the break

In order to analyze this distortion, a new nodalization, Sc-up nodalization B, is generated. This is a PKL PtoV scaled-up nodalization (as Sc-up nodalization A) in which the heat impact of external heat structures has been preserved. The comparison between the two post-test calculations of Sc-up nodalization A and Sc-up nodalization B confirms that a distortion should be expected in the system pressures as a result of the reduction in the external heat losses (see Fig. 6.20). Because the external heat losses are reduced when PtoV scale is increased, part of this energy is stored in the isolated secondary system, increasing pressures during reflux condenser phase.

Once the external heat losses distortion is corrected, a discrepancy appears in the timing of the SG

depressurization signal (see Fig. 6.20). Taking into account that the aim of the scaling effect analysis is to generate an idealized PKL scaled-up nodalization in which scaling effects are minimized, another scaled-up nodalization must be generated following the previous nodalizations. Therefore, a third nodalization Sc-up nodalization C is produced based on Sc-up nodalization B but with the additional preservation of the L/\sqrt{D} quotient in the hot legs. Keeping this ratio in the horizontal legs, the Froude number and the flow regime transitions should be preserved. The comparison between the PKL post-test calculation and the results obtained by Sc-up nodalizations B and C shows that the hot leg liquid levels in the broken loop are preserved for Sc-up nodalization C during the conditioning phase of the PKL transient (see in Fig. 6.22 from -4000 s to -3500 s and from -2750s to -2500 s intervals), thus providing similar break mass flow rates as in the post-test calculation (see Fig. 6.23). This allows keeping the same primary mass inventory ratio at the beginning of the transient, obtaining similar liquid levels in the hot leg of the broken loop (see Fig. 6.24) and similar break mass flow rates (see Fig. 6.25). This good performance of the mass discharging removes the delay in the core uncovering obtaining a close agreement in the timing of the SG depressurization (see Fig. 6.26).

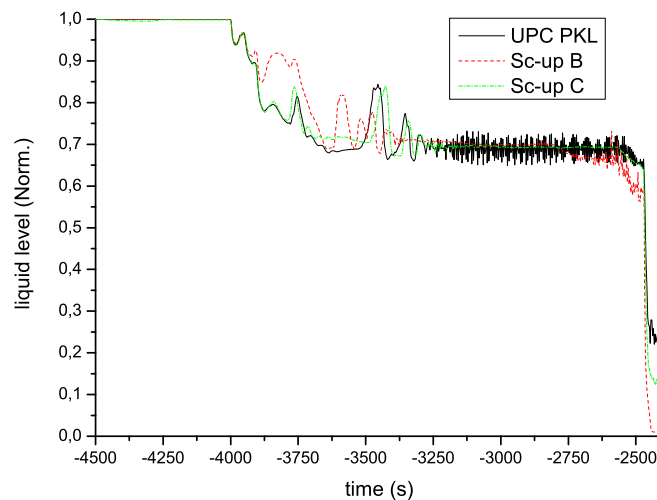


Figure 6.22: HL liquid level

After removing the Froude Number distortion, the main parameters of the transient are compared between UPC PKL Pseudo 3D nodalization calculation and the Sc-up nodalization C calculation in order to assure that an idealized scaled-up nodalization has been obtained. Results of the system pressures (Fig. 6.26), CET temperatures (Fig. 6.27) and PCT temperatures (Fig. 6.28) display a close agreement between the post-test and Sc-up nodalization C. Since the discrepancies to be analyzed between PKL and LSTF simulations are the core uncovering delay and the CETvsPCT correlation, no further scaling effect analysis will be necessary. Friction effects or hydraulic diameters in components where mixing or interface drag occurs (i.e. SG and vessel downcomers) could be studied until a perfect idealized scaled-up nodalization is obtained, but as for this transient, they will not add any relevant scaling effect in the reported LSTF-PKL discrepancies, it would suppose an unnecessary extra work for the analyst. It is in that point where the expert judgment is essential.

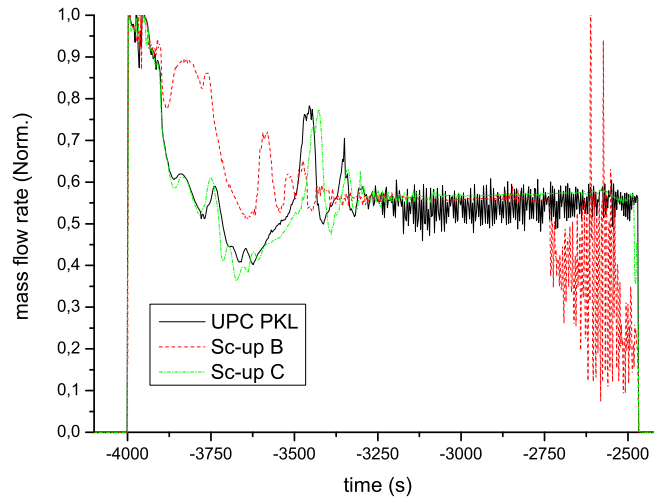


Figure 6.23: Break mass flow rate

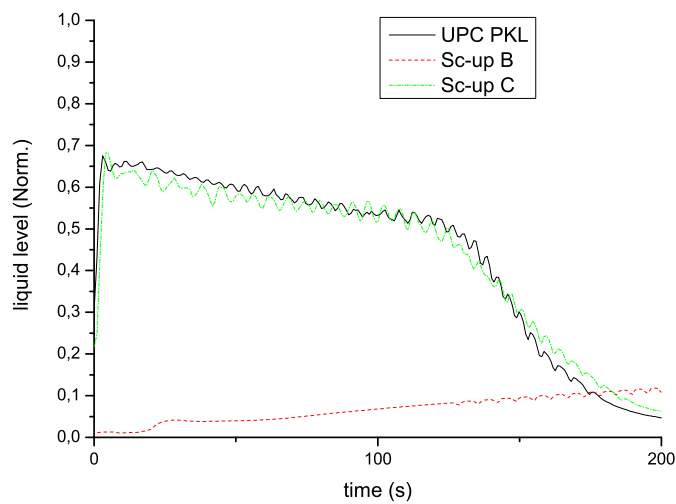


Figure 6.24: HL liquid level

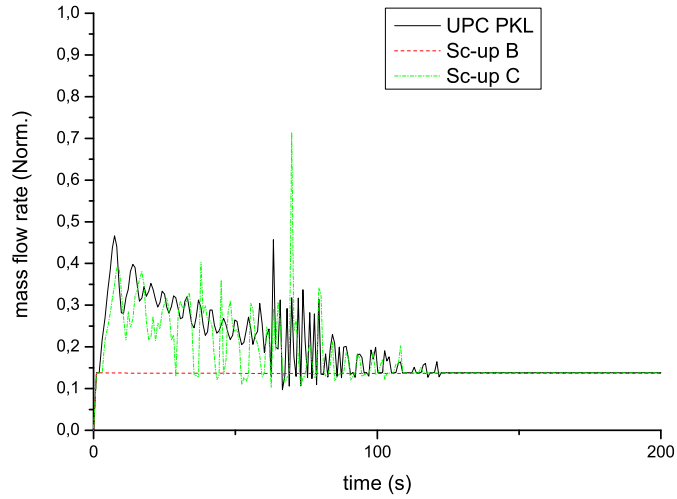


Figure 6.25: Break mass flow rate

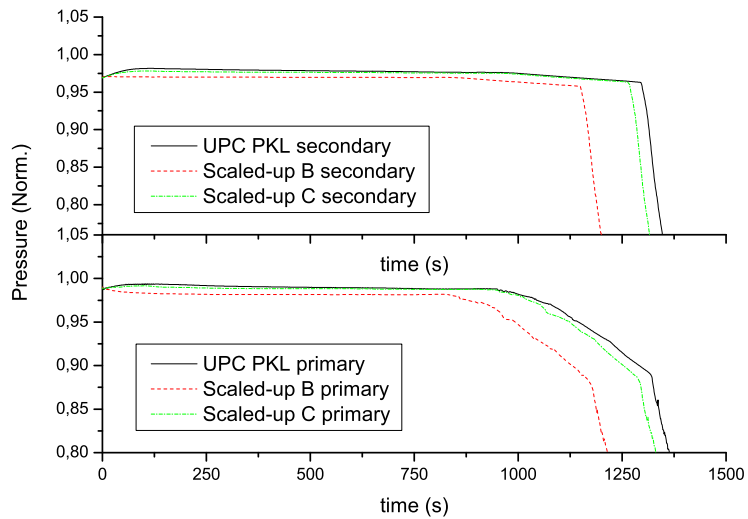


Figure 6.26: System pressures

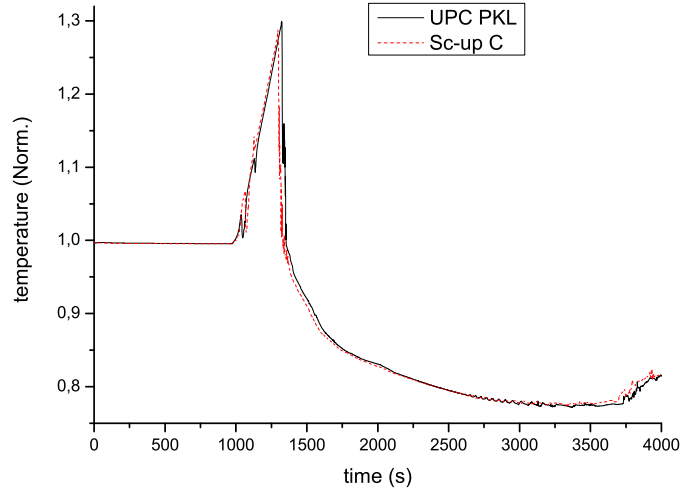


Figure 6.27: Core exit temperature

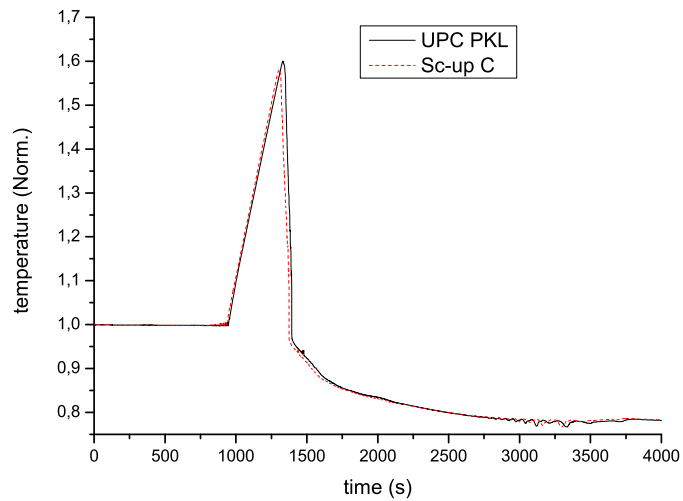


Figure 6.28: Peak cladding temperature

6.3.2 Design effect analysis

Once an idealized PKL scaled-up nodalization has been generated, discrepancies between both counterpart simulations can be analyzed. For this purpose hybrid nodalizations will be compared with qualified LSTF post-test simulation and the idealized PKL scaled-up nodalization. Hybrid nodalizations will include LSTF components in the PKL nodalization in order to check how they modify the results.

6.3.2.1 Core dryout delay

The comparison between UPC LSTF Pseudo 3D nodalization and **PKL idealized scaled-up nodalization** (Sc-up nodalization C of the previous step) shows a disagreement in the core dry out timing despite having a similar amount of water in the primary system (see Figs. 6.29 and 6.30). For analyzing this discrepancy a **PKL hybrid base nodalization** has been generated in order to adapt those scaling effects reported in the previous steps to the intrinsic design characteristics of the LSTF facility. In other words, the idealized PKL scaled-up nodalization is modified by adding the LSTF external heat losses, merging 4 loops into 2 loops, and adjusting the hot leg geometries in order to preserve the LSTF L/\sqrt{D} factor, and finally by removing the compensating heaters during the transient as in the LSTF conditions. The comparison between the 3 nodalizations shows that the external heat losses and the different hot leg geometries do not justify the delay between both nodalizations (see Fig. 6.31)

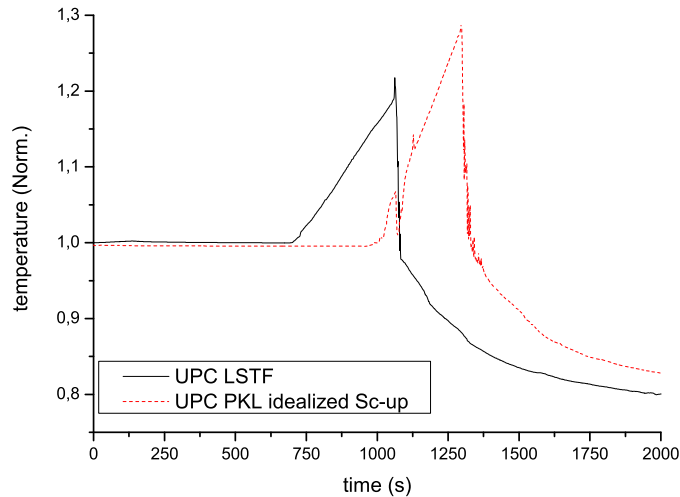


Figure 6.29: Core exit temperatures

For analyzing the discrepancy, components with different configuration that could affect to the mass inventory and distribution have been studied. Those are:

- Pressurizer and surge line: PKL surge line is not connected at the bottom of the pressurizer, giving stagnant water on that during the transient which could affect to the dryout timing.
- U-tube's surface: LSTF and PKL have different ratio between liquid volume and heat exchanging surface (LSTF U-tube surface = 1,01 PKL U-tube surface), that could affect the reflux and condensation and the total amount of water in the primary side.
- LSTF DC-to-HL bypass: LSTF have an external bypass not simulated in PKL which could imply different water distribution between hot legs and cold legs. It could modify break mass losses advancing or delaying core dry out. Core passive heat structures: LSTF and PKL have

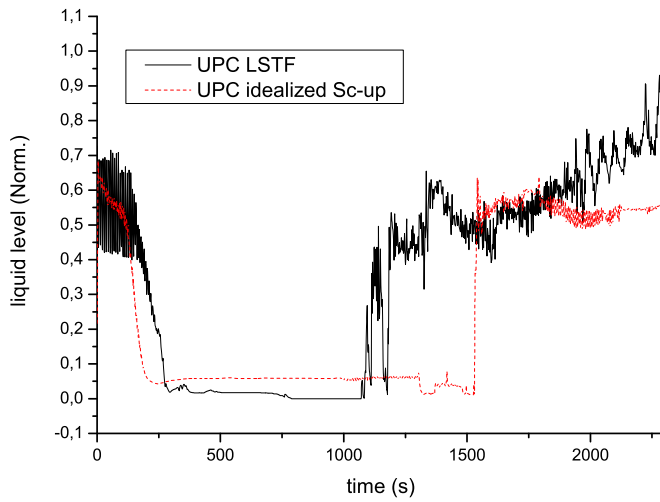


Figure 6.30: HL liquid level

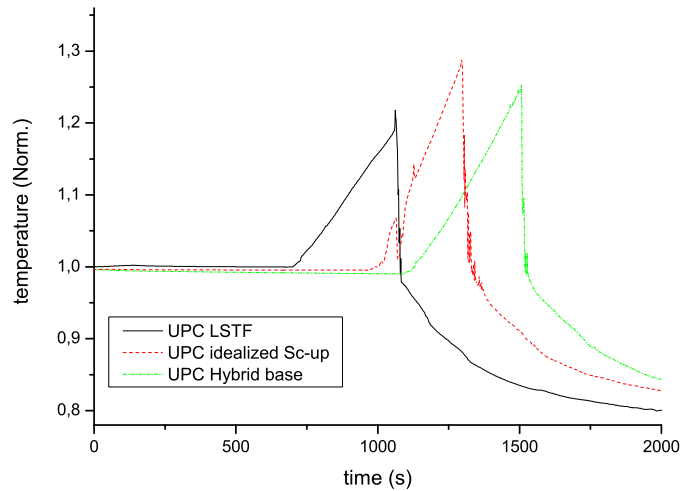


Figure 6.31: Core exit temperature

different volume of core passive structures, which could affect to the vapor generation and core liquid levels.

Four hybrid nodalizations are performed in series adding one to one these LSTF components to the PKL hybrid base nodalization. The aim is to analyze one by one and globally how they modify the timing of the core dryout. The nodalizations are:

- PKL Hybrid A nodalization: PKL Hybrid base nodalization + LSTF PZR
- PKL Hybrid B nodalization: PKL Hybrid A nodalization + LSTF U-tubes surface
- PKL Hybrid C nodalization: PKL Hybrid B nodalization + LSTF HL-to-DC bypass

- PKL Hybrid D nodalization: PKL Hybrid C nodalization + LSTF vessel passive HS

The results of hot leg liquid levels and CET (Figs. 6.32 and 6.33) show that there are no changes in the core dryout timing despite adding LSTF components to the PKL hybrid base nodalization. It demonstrates these design differences do not have an effect on the reported discrepancy.

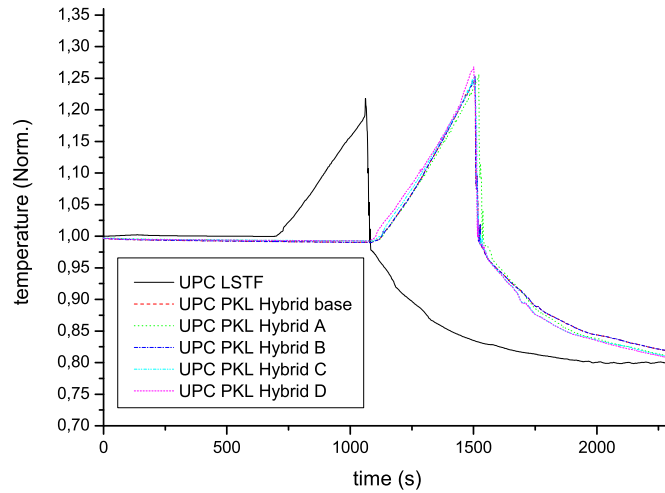


Figure 6.32: Core exit temperature

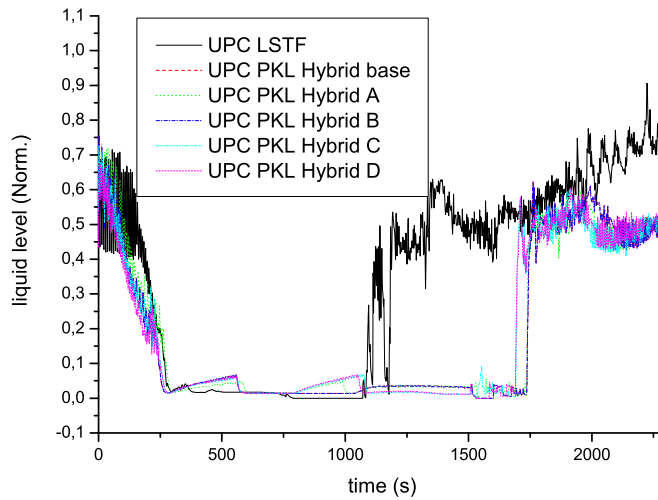


Figure 6.33: HL liquid level

Finally, the vessel characteristics have been compared between both nodalizations, showing relevant differences in the configuration of the downcomer, the simulation of the core bypass flow path, and specially, the amount of water between the bottom of the hot leg and the top of the core, (these features are described in table 6.7). Hence, a **Hybrid E nodalization** is generated adding to the "PKL Hybrid D nodalization" hydrodynamic components, HS's, and material properties of

the LSTF vessel nodalization. The PKL fuel rods HS's are not modified. The results obtained with this new nodalization show that for an identical amount of water in the hot legs at the beginning of the transient (for having the same PKL experimental initial conditions despite the changes in the nodalizations), the core dry out occurs at the same time as of the LSTF post-test calculation just changing the water distribution of the PKL vessel with that of the LSTF vessel (see Figs. 6.33 and 6.33). It demonstrates that delay between core dryout of both simulations is due to the different design of the vessel (KWU for PKL and Westinghouse for LSTF) and not for any scaling effect.

| | LSTF | PKL |
|-------------------------------------|-----------------------------|------------|
| Downcomer | Annulus | 2 pipes |
| Core bypass | No | Yes |
| Mass inventory below hot leg | $\simeq 0.75 \cdot M_{PKL}$ | M_{PKL} |

Table 6.7: LSTF and PKL vessel differences

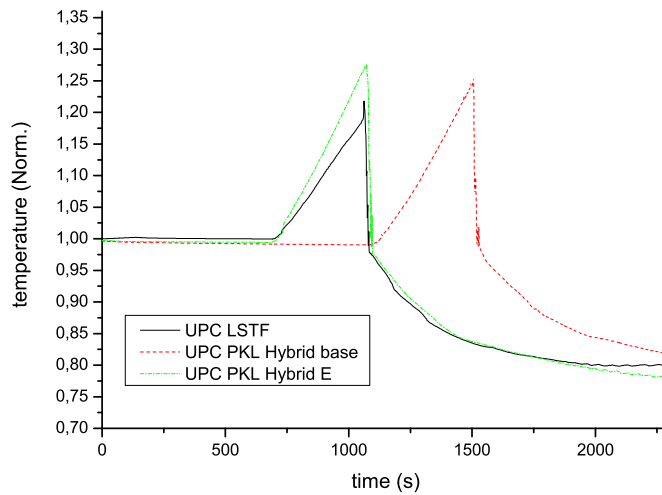


Figure 6.34: Core exit temperature

6.3.2.2 CETvsPCT correlation

Major LSTF-PKL core design differences are - table 6.8:-

| | LSTF | PKL |
|---------------------------|-------------|-----------------------|
| Axial profile | Cosine | Flat |
| Radial profile | 3 | 1 |
| Fuel diameter (mm) | 4,75 | 5,375 |
| Fuel height (m) | 3,66 | 3,9 |
| Fuel surface (m2) | 55,054 | 52,73 ($\cdot K_V$) |
| Number rods | 1008 | 801 ($\cdot K_V$) |

Table 6.8: Core design differences

Two new PKL hybrid nodalizations are set up from the previous PKL Hybrid E nodalization in order to justify the discrepancy. Main characteristics are:

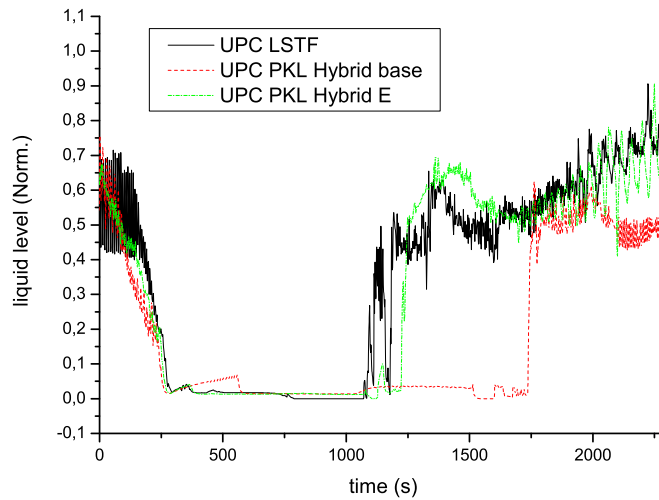


Figure 6.35: HL liquid level

- Previous PKL Hybrid E nodalization:
 - LSTF vessel HS's and hydrodynamic components
 - PKL fuel rods HS's
 - PKL fuel rods materials
 - PKL fuel rods profile (uniform)
- PKL Hybrid F nodalization:
 - PKL Hybrid E nodalization
 - + LSTF fuel rods HS's
 - + LSTF fuel rods materials
- PKL Hybrid G core nodalization:
 - PKL Hybrid F nodalization
 - + LSTF fuel rods profile (cosine)

The comparison of the three hybrid nodalizations with both LSTF and PKL post-test calculations (Fig. 6.36) demonstrate that the discrepancies in the slope of CETvsPCT curves are mainly due to the different power distributions of PKL (uniform) and LSTF (cosine). As modifications between hybrid models has been implemented in a serial process, just when PKL core power profile is modified (PKL hybrid nodalization G) the slope of the curve become similar to the LSTF post-test CETvsPCT slope. On the other hand, previous changes (models E and F) do not show significant modifications in the CETvs PCT correlation.

Finally, CET of the last nodalization (PKL Hybrid G nodalization) is compared with the nodalization that justifies the delay in the core dryout (PKL Hybrid E nodalization). Results show that new modifications do not add distortion (Fig. 6.37), justifying the consistency of the procedure.

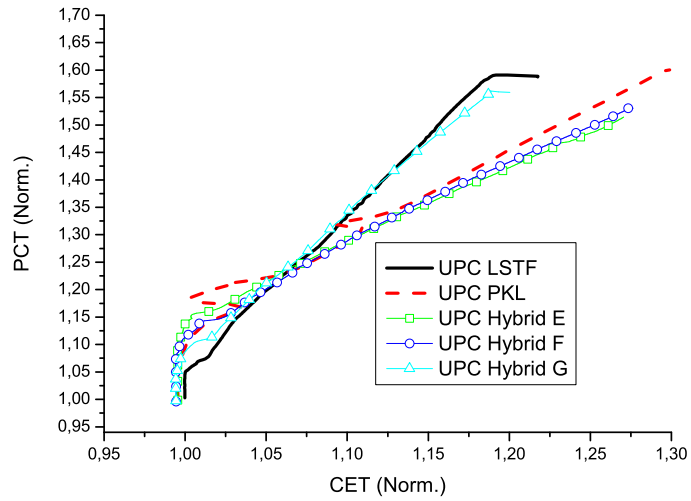


Figure 6.36: PCTvsCET curve

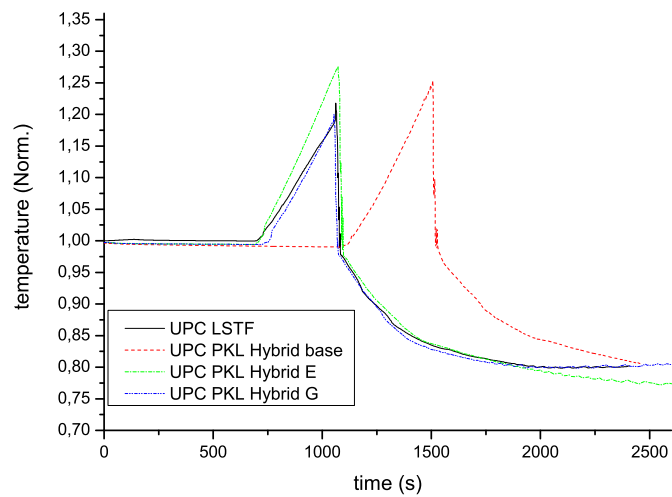


Figure 6.37: Core exit temperature

7. Conclusions

Best estimate codes and computational analyses have a widely used and sound application on Nuclear Engineering. Throughout the last thirty years, thousands of simulations have been carried out giving a sense of their relevance in safety analysis as well as in the support to plant operational and control. Thus, guarantees of code accuracy as well as user expertise and nodalization qualification become essential.

In the present Ph.D. thesis, a scaling-up methodology has been presented in order to fulfil gaps in current nodalization qualification methodologies. The "UPC Scaling-up methodology" is based on the extrapolation of ITF post-test simulations. This step is necessary in the validation and the verification of NPP nodalizations because it allows the capabilities of reproducing relevant TH phenomena reported and simulated by BE codes in ITFs to be checked, as there is a lack of experimental data at NPP level. Using extrapolation, commercial input decks can be tested and improved with modeling experience acquired through ITF simulations, and the range of accident scenario analyses can be increased thus both assuring and strengthening the robustness of the final input decks.

Extrapolation of ITF data and simulations is not new. K_v scaled calculations (see Chapter 3) have been an excellent approach in the past for generating counterpart transients in NPP nodalizations. In combination with qualification methodologies (e. g. "on transient" level qualification using Bonuccelli's methodology -see Section 1.4-) K_v scaled calculations allow qualifying in a qualitative level the capabilities of the NPP input decks to reproduce the same TH phenomena without adding new effects. These methodologies are based on the similarity of the results and on the expert judgement of the analyst. However, they do not include any specific sensitivity approach on which they can be supported.

The present work thus introduces a new feature. The "UPC Scaling-up methodology" also takes advantage of K_v scaled calculations, but justifying their discrepancies with a simple and systematic approach. It is based on three main assumptions: judicious selection of the experimental transients, full confidence in the quality of the ITF simulations, and simplicity in justifying discrepancies that appear between ITF and K_v scaled analyses.

For the first two assumptions, there is a full background and extensive bibliography about how to select experiments and how to qualify ITF calculations. In this sense, the "UPC scaling-up methodology" is a simple compendium of similar approaches to those proposed in CSAU [21], UMAE [14] and CSNI validation matrices [16]. Additionally, for ITF nodalization qualification, it might be interesting for future works to include the FFTBM used by UNIPI for qualifying not only qualitatively but also quantitatively the TH phenomena that will be tested later in NPP nodalizations.

As regards the third assumption, the proposed methodology introduces two new scaling techniques in order to find out how the counterpart transients change from ITF to NPP nodalization:

- "*Scaled-up nodalizations*", which allow effects of the ITF scaling down criterion to be checked (see Section 5.4.1);
- "*Hybrid nodalizations*", which help the user to establish how design and hardware configuration differences modify results (see Section 5.5).

The exercise of explaining discrepancies between ITF and K_v scaled calculations using these intermediate simulations within the framework of an expert judgment, leads to improve nodalizations

and to assure their capabilities with wider reliability and capacity than in the past with previous methodologies which were only based on the knowledge experience, and expertise of the analyst.

As regards "*Scaled-up calculations*", they have been presented as ITF nodalizations in which the size and the geometries of the nodes are increased to be comparable to the NPP nodalization that must be qualified. For performing "*Scaled-up calculations*" it is essential to have an accurate understanding of the scaling-down criterion employed in the design of the ITF as well as the equations and correlations of the code that will be used. This deep understanding allows identification of the distortions that the code introduces with respect to scaling, and to develop specific software for generating easily scaled-up nodalizations. In the present work, an exhaustive analysis of the RELAP5mod3 system and closure equations (Section 4.3) has been completed and PVST software has been developed (Section 4.5) for the Power to volume scaling criterion.

With regard to code scaling distortions, several findings have been reported (Section 4.4). Discrepancies are expected in fluid heat exchange with passive HSs as well as in flow regime transitions for the horizontal volumes (if L/\sqrt{D} is not preserved) when a K_v factor is applied to an ITF nodalization and its particular BIC conditions. Furthermore, if L/\sqrt{D} is preserved, distortions will appear in the results of the Ransom & Trapp choked flow model as well as in the CCFL correlation and in the form losses and local ΔP s. If crossflows and transversal momentum equations are activated in multi-channel regions, distortions can also be expected under significant asymmetrical transient conditions. Furthermore, for vertical volumes, differences can be expected under mixture conditions as a result of the changes in the hydraulic diameters. Finally, results for the non-condensable transport continuity equation and the Godunov scheme will also vary with the application of the PtoV scaling criterion and the preservation of the L/\sqrt{D} factor respectively.

It is worth mentioning that scaling distortions do not mean significant effects in a "*Scaled-up calculation*". Hence, PVST software has been developed for generating easily scaled-up nodalization following the K_v factor of PtoV methodology. In the development of the software several features have been included in order to assess the effects of the hydraulic diameters, the environment heat losses, and the Froude number in both the overall and local behaviour of an ITF transient. Several calculations have been done on the qualified OECD/NEA ROSA Test 3-1 (Section 2.1.4.1) and OECD/NEA ROSA-2 Counterpart Test 3 (Section 6.2.2). Results (Section 4.6) have shown specific conditions in which they modify the overall behaviour of the test as well as the capabilities of the software for detecting distortions associated with the ITF scaling-down criterion. The remaining possible scaling distortions (changes in Ransom & Trapp correlation results, CCFL model, form losses, and boron transport equations,...) have not been assessed because no significant differences have been noticed between the ITF calculations and the "*scaled-up calculations*" once the other scaling distortions have been removed. Nevertheless they could be tested easily with the same software for other transients in which they are relevant. This should be done by modifying the local scaling criterion of the Froude number because the distortions are a consequence of whether preservation of the L/\sqrt{D} ratio is applied or not.

"*Hybrid nodalizations*" are "Idealized scaled-up" nodalizations in which some components are removed and changed by their equivalents in the NPP nodalization. These nodalizations allow the analyst to determine the effect of the design on the simulation of the ITF transient. This kind of analysis requires deep knowledge of the NPP and the ITF nodalizations, as well as the TH phenomena of the transient. As can be seen at this point, application of the "UPC Scaling-up methodology" is not trivial. Two of the weaknesses that can be pointed out are that it does not reduce dependency on expert judgement, and that it increases the number of calculations and nodalizations required. In this sense, the present work does not aim to universalize nodalization qualification or to reduce engineering costs. In fact, it should be considered just a tool for supporting, justifying and demonstrating the discrepancies reported by the analyst, and the improvements that will be applied to the NPP nodalization. It is a step forward in quality assurance, not a simplification of previous approaches.

7.1 Assessment of "UPC Scaling-up methodology"

In order to demonstrate the capabilities and potential of the "UPC Scaling-up methodology", an assessment was carried out by making use of the OECD/NEA ROSA-2 and PKL-2 Counterpart Test. One of the limitations of scaling methodologies is the impossibility to qualify their predictions because of the lack of counterpart experimental data at a NPP level. Thus, the ROSA-2 PKL-2 Counterpart Test is of great value because it allows comparison of an identical transient between two facilities with relevant differences in design and scale. Hence, it was decided that before to attempt an application of the "UPC Scaling-up methodology" to a NPP nodalization, it was essential to demonstrate that the present approach could find sources of distortion between counterpart post-test simulations that had been previously validated with experimental data. In consequence, the assessment was carried out as an application of the "UPC Scaling-up methodology" to the PKL (the smaller facility) Counterpart Test, and the results of the PKL scaled-up and hybrid calculations were compared with the LSTF Counterpart Test simulation. This approach is analogous to the application of the methodology to an ITF post-test and comparison with a K_v scaled calculation of it, but with the advantage that in this case experimental data ensures the quality of the " K_v scaled" (LSTF Counterpart Test) calculation.

Post-test calculations were completed for both PKL and LSTF experiments (Sections 6.2.1 and 6.2.2) making use of two ITF nodalizations extensively qualified in the past. This degree of qualification was necessary to ensure confidence in the calculations and to minimize the user effects and compensating errors (step two of the methodology - Section 5.2-). The results of both calculations show a great confidence in reproducing the overall behaviour of the transient as well as the relationship between CET and PCTs during the core dryout. In both cases, it was necessary to improve the core nodalization using Pseudo 3D modelling and finer axial meshes. For future extrapolations to NPP nodalizations, it can be seen that Pseudo 3D modelling is necessary for a proper assessment of CET accident management actions during core dryout. Finally, confidence between simulations and experimental data also allows reproduction of reported experimental discrepancies between PKL and LSTF experiments. In particular, differences were reproduced for the instant of core dryout as well as in the slope of the CET vs. PCT correlation. These reported discrepancies allowed assessment of the methodology as well as the effectiveness of the scaled-up and hybrid nodalizations for identifying distortion sources.

As regards the PKL "*Scaled-up nodalizations*" conclusions, results (Section 6.3.1) demonstrated the impact of environment heat losses and the geometry of the broken loop hot leg in the behaviour of the ITF transient. When the scale of PKL was increased, higher pressure in the secondary system during the reflux & condenser phase was reported as a result of lower environment heat losses. On the other hand, assessment of the hot leg geometries show that break mass flow discrepancies appeared as a result of different Froude numbers. All these discrepancies disappeared once environment heat losses and L/\sqrt{D} were preserved. Hence, the capabilities of the "*Scaled-up calculations*" for separately identifying scaling distortion sources and their impact on the results have been demonstrated.

Finally, once scaling effects had been identified, PKL "*Hybrid nodalizations*" were generated in order to justify the discrepancies between both counterpart simulations. It was essential to previously generate an idealized scaled-up PKL nodalization in which the scaling effects were deleted. Only if scaling effects are dismissed, can the impact of design be judged. With the application of the hybrid nodalizations, reported discrepancies were justified (see Section 6.3.2). In particular, the delay in the core dryout was due to the differences in design between PKL and LSTF reactor pressure vessels. On the other hand, it was also shown that the differences in the slope of the CET vs. PCT correlations were intrinsically related to the axial distribution of the core power. Therefore, the application of "*Hybrid nodalizations*" to the Counterpart test showed that discrepancies between qualified counterpart simulations can be justified with system codes. Extrapolating it to the qualification process, "*Hybrid nodalizations*" are capable of locating components that generate differences between K_v scaled and ITF calculations. It will depend on the expert judgement of the analyst if that components are properly modelled or if they need to be improved. The response will be found in the documentation of the NPPs description reports and in the modelling experience acquired through the ITF post-test analysis.

7.2 Recommendations for future work

As regards the qualification process, immediate work should be a complete application of the "UPC Scaling-up methodology" at NPP level. Along these lines, the previous work completed for the OECD/NEA ROSA-2 and PKL-2 Counterpart Test should be used. The scaling-up of these experiments has great value because they demonstrate code accuracy for simulating the correlation between CET and PCT at different scales and designs. Furthermore, preliminary studies for Asco NPP nodalization (see Section 3.1 [57]) have shown close agreement between the LSTF Counterpart Test and its equivalent Asco NPP K_v scaled calculation. Few scaling concerns have been reported (e. g. significant differences between the K_v factor associated with the loops and the equivalent of the RPV) and they should be explained in detail using the present methodology. In addition, assessment of the CET accident management signal for a realistic scenario has shown the need for an exhaustive evaluation of the CET set-point criterion. This conclusion acquires greater relevance if we take into account the fact that the only way of assessing the effectiveness of an AM action within the complex simulation of an accident scenario is by using system codes. Therefore, application of qualification methodologies becomes essential.

A second line of research should be to define a strategy to fully integrate the "UPC Scaling-up Methodology" in the scaling issue, and to provide a definite answer to the scaling controversy about extrapolation of code accuracy to NPP level. About this point, no conclusions can be extracted from the present work whereas it is referred to the nodalization qualification and not to the code accuracy. Hence, no stance can be provided in spite of the argument suggested in the "Roadmap to scaling" [7] seems reasonable: thousands of experiments and actual NPP events and accidents have been simulated in a suitable way for different scales and designs, showing the independence of the code accuracy in regards to the scale. About this concern, the present author considers that final solution for assessing the scale independence of the code accuracy has been pointed out in the basic sub-items that Professor D'Auria denoted in the VII step of his "Roadmap to scaling" (Section 1.3.5):

1. "Identification of relevant non-dimensional parameters (...)
2. Setting up a procedure where each code model or constitutive equation which includes one variable part of non-dimensional parameters is identified (...)
3. Setting up of a procedure for proving the scaling invariance from the application of code models in relation to each selected non-dimensional parameter (...)
4. Setting up of basic input decks and calculation by the entire code of scaling invariance where applicable (...)
5. Introduce range of acceptability for the scaling errors derived from the previous steps, consistent with the overall requested precision for the code (...)"

Therefore, future efforts should be aimed at establishing a closed approach for exploring these items successfully. Demonstrating with simple and irrevocable sample input decks that code does not introduce scaling distortion in non-dimensional parameters, and minimizing the arbitrariness of the nodalization qualification process with the techniques presented in the "UPC scaling-up methodology", the capabilities of best estimate codes for licensing with the plus of the uncertainty methods would be irrefutable.

Bibliography

- [1] USNRC, "Acceptance Criteria for Emergency Core Cooling Systems for Light Water Cooled Nuclear Power Reactors," Tech. Rep. Appendix K to 10 CFR 50, U.S. Federal Register, as amended at 53 FR 36004, 1988.
- [2] USNRC, "Quantifying Reactor Safety Margins: Application of CSAU to a LBLOCA," Tech. Rep. NUREG/CR-5249, 1989.
- [3] M. Perez and et al., "Uncertainty and sensitivity analysis of a LBLOCA in a PWR nuclear power plant: results of the phase V of the BEMUSE programme," no. Nuclear Engineering and Design, vol 241 num. 10 p. 4206-4222, 2011.
- [4] F. D'Auria and W. Giannotti, "Development of Code with capability of Internal Assessment of Uncertainty," no. Nuclear Technology, fol. 131, num. 1, 2008.
- [5] H. Glaeser, "GRS Method for uncertainty and sensitivity evaluation of code results and applications," no. Science and Tehcnology of Nuclear Installations, article ID 798901, 2008.
- [6] M. Ishii and et al., "The three level scaling approach with application to the Purdue University Multi-Dimensional Integral Test Assembly (PUMA)," no. Nuclear Engineering and Design 186, 177-211, 1998.
- [7] F. D'Auria and G. Galassi, "Scaling in Nuclear Reactor System Thermal Hydraulics," no. Nuclear Engineering and Design, 240, pp. 3266-3293, 2010.
- [8] N. Zuber, "A Hierarchical, Two-Tiered Scaling Analysis, Appendix D," Tech. Rep. NUREG/CR-5809, EGG-2659, 1991.
- [9] N. Zuber and et al., "An integrated structure and scaling methodology for severe accident technical issue resolution: development of methodology," no. Nuclear Engineering and Design 186, 1-21, 1998.
- [10] J. Reyes and J. Hochreiter, "Scaling analysis for the OSU AP600 test facility (APEX)," no. Nuclear Engineering and Design 186, 53-109, 1998.
- [11] N. Zuber, W. Wulff, U. Rohatgi, and I. Catton, "Application of fractional scaling analysis (FSA) to loss of coolant accidents (LOCA), Part 1: Methodology development.," No. Proceedings of the International Top. Meet. On Nuclear Reactor Thermal Hydraulics (NURETH-11), 2005.
- [12] W. Wulff, N. Zuber, U. Rohatgi, and I. Catton, "Application of Fractional Scaling Analysis (FSA) to Loss of Coolant Accidents (LOCA) - Part 2: System Level Scaling for System Depressurization.," No. Proceedings of the International Top. Meet. On Nuclear Reactor Thermal Hydraulics (NURETH-11), 2005.
- [13] I. Catton, W. Wulff, N. Zuber, and U. Rohatgi, "Application of fractional scaling analysis (FSA) to loss of coolant accidents (LOCA). Part 3. Component level scaling for peak clad temperature.," No. Proceedings of the International Top. Meet. On Nuclear Reactor Thermal Hydraulics (NURETH-11), 2005.
- [14] F. D'Auria, N. Debrechin, and G. Galassi, "Outline of the Uncertainty Methodology based on Accuracy Extrapolation (UMAE)," no. Nuclear Technology, vol. 106., 1995.

-
- [15] A. Navahandi, S. Castellana, and E. Moradkhaniav, "Scaling laws for modeling nuclear reactor systems," no. Nuclear Science and Engineering, 72, 1979.
- [16] OECD/NEA, "CSNI Code Validation Matrix of Thermo-Hydraulic Codes for LWR LOCA and Transients," Tech. Rep. CSNI, 132-rev.1, Paris, France, 1996.
- [17] P. Pla, L. Ammirabile, and A. Annunziato, "The Stresa database: A token for the future," no. Nuclear Engineering and Design, vol. 62, 8-16, 2013.
- [18] F. D'Auria, G. Galassi, and M. Ingegneri, "Evaluation of the data base from high power and low power small break LOCA counterpart tests performed in LOBI, SPES, BETHSY, and LSTF facilities," 1994.
- [19] USNRC, "Acceptance criteria for emergency core cooling systems (ECCS) in light water nuclear reactors (10CFR 50.46)," Tech. Rep. Appendix K to 10 CFR 50, U.S. Federal Register, vol. 43, no. 235 (43 FR 57157), 1978.
- [20] M. O. L. Ghan, "Uncertainty Analysis of Minimum Vessel Liquid Inventory During a Small-Break LOCA in a B & W Plant - An Application of the CSAU Methodology Using the RELAP5/MOD3 Computer Code," no. NUREG/CR-5818, 1992.
- [21] B. Boyack, I. Catton, R. Duffey, P. Griffith, K. Katsma, G. S. Lellouche, S. Levy, U. Rohatgi, G. Wilson, W. Wulff, and N. Zuber, "Quantifying Reactor Safety Margin: Parts 1 to 6," no. J. Nuclear Engineering and Design., 119, 1-117, 1990.
- [22] OECD/NEA, "Separate Effects Test Matrix for Thermal-Hydraulic Code Validation: Phenomena Characterization and Selection of Facilities and Tests," Tech. Rep. OCDE/GD(94)82, Paris, France, 1993.
- [23] R. Bovalini, F. D'Auria, and G. Galassi, "Scaling of complex phenomena in system thermal-hydraulics," no. Nuclear Science and Engineering 115, 89-111, 1993.
- [24] F. D'Auria and M. Ingegnerii, "Use and qualification of the UMAE uncertainty Methodology having as basis the Cathare2 code," no. Nuklearna Tehnologija 13 (2),3-16., 1998.
- [25] S. Belsito, F. D'Auria, and G. M. Galassi, "Application of a Statistical model to the evaluation of Counterpart Test data base," no. Kemtechnik, Vol 59 Nr 3, 1994.
- [26] IAEA, "Accident Analysis for nuclear power plants," Tech. Rep. Safety Reports Series 23, 2002.
- [27] IAEA, "Development and review of plant specific emergency operating procedures," Tech. Rep. Safety Reports Series 48, 2006.
- [28] F. Reventos, "Thermal-Hydraulic Analysis Tasks for ANAV NPPs in Support of Plant Operation and Control," no. Science and technology of nuclear installations, 1-13, 2008.
- [29] F. Reventos, "Analysis of an actual reactor trip operating event due to a high variation of neutron flux occurring in the Vandellos-II nuclear power plantl," no. Nuclear engineering and design, vol. 240, num. 10, p. 2999-3008, 2010.
- [30] C. Llopis and et al., "Analysis of low load transients for the Vandellos-II NPP. Application to operation and control support," no. Nuclear engineering and design, vol. 237, num. 18, p. 2014-2023, 2007.
- [31] F. Reventos and et al., "Advanced qualification process of ANAV NPP integral dynamic models for supporting plant operation and control," no. Nuclear engineering and design, vol. 237, num. 1, p. 54-63, 2007.
- [32] A. Cuadra, J. Gago, and F. Reventos, "Analysis of a main steam line break in asco nuclear power plant," no. Nuclear technology, vol. 146, num. 1, p. 41-48, 2004.
- [33] E. DeAlfonso and F. Reventos, "Convenio UPC-ANAV 2008-2011, TOMO III: Manual de Usuario," Tech. Rep. UPC, ANAV Internal report, 2011.

- [34] M. Bonuccelli, F. D'Auria, M. Debrechin, and G. Galassi, "A methodology for the qualification of thermal-hydraulic codes nodalizations," No. Proceedings of the International Top. Meet. on Nuclear Reactor Thermal Hydraulics (NURETH-6), 1993.
- [35] S. Shahedi, J. Jafari, M. Boroushaki, and F. D'Auria, "Development of a qualified nodalization for small-break LOCA transient analysis in PSB-VVER integral test facility by RELAP5 system code," no. Nuclear Engineering and Design, 2010.
- [36] G. Aprile, F. D'Auria, F. Frogheri, and G. Galassi, "Application of a qualified WWER-1000 plant nodalization for Relap5/mod3.2 computer code," No. Proceedings of the International Conference on Nuclear Option in Countries with Small and Medium Electricity Grid, Opatjia (Hr), 1996.
- [37] L. Garcia-Delgado, M. T. Lopez-Carbonell, and I. I. Gomez-Bernal, "Fuel and Core Design Experiences in Cofrentes 1 NPP," No. ISBN 0-89448-663-2, ICAPP02, 2002.
- [38] V. Martinez-Quiroga, F. Reventos, C. Pretel, and I. Sol, "Code Validation and Scaling of the ROSA/LSTF Test 3-1 experiment," No. International Topical Meeting on Safety of Nuclear Installations TopSafe 2008, 2008.
- [39] P. Pla, F. Reventos, C. Pretel, W. Gianotti, F. D'Auria, and A. Annunziato, "Code Validation and Scaling of the LOBI BL-30 experiment," No. Proceedings of ICCAP 2007, Paper 7492, 2007.
- [40] J. Freixa and et al., "SBLOCA with boron dilution in pressurized water reactors. Impact on operation and safety," no. Nuclear engineering and design vol. 293, num. 4, p. 749-760, 2009.
- [41] J. Freixa and A. Manera, "Verification of a TRACE EPR model on the basis of a scaling calculation of an SBLOCA ROSA test," no. Nuclear engineering and design 241 (3), pp. 888-896, 2011.
- [42] S. Petelin, B. Mavko, B. Koncar, and Y. Hassan, "Scaling of the small-scale thermal-hydraulic transient to the real nuclear power plant," no. Nuclear Technology Volume 158 Number 1 Pages 56-68, 2007.
- [43] The ROSA-V Group, "ROSA-V Large Scale Test Facility (LSTF) System Description for the Third and the Fourth Simulated Fuel Assemblies," Tech. Rep. JAERI-Tech 2003-037, JAERI.
- [44] Y. Taitel and A. E. Dukler, "Model of Predicting Flow Regime Transitions in Horizontal and Near Horizontal Gas-Liquid Flow," no. AIChE Journal. 22. pp. 47-55, 1976.
- [45] V. Martinez, F. Reventos, and C. Pretel, "Post-Test Calculation of the ROSA/LSTF Test 3-1 Using RELAP5/Mod3.3," Tech. Rep. NUREG/IA-0409, 2012.
- [46] V. Martinez, F. Reventos, and C. Pretel, "Post-Test Calculation of the ROSA/LSTF Test 3-2 Using RELAP5/Mod3.3," Tech. Rep. NUREG/IA-0410, 2012.
- [47] JAEA, "OECD/NEA. Quick look Report of ROSA/LSTF Test 3-1(High Power Natural Circulation Experiment SB-CL-38 in JAEA)," Tech. Rep. OECD/NEA ROSA Project, JAERI.
- [48] JAEA, "A Report on Pre-test Analyses to Define Experimental Conditions of ROSA/LSTF Test 3-2 on High Power Natural Circulation," Tech. Rep. OECD/NEA ROSA Projec, JAERI.
- [49] JAEA, "OECD/NEA. Quick look Report of ROSA/LSTF Test 3-2(High Power Natural Circulation Experiment TR-LF-13 in JAEA)," Tech. Rep. OECD/NEA ROSA Project, JAERI.
- [50] H. Kremin, H. limprecht, R. Gijneysu, and K. Umminger, "Description of the PKL III Test Facility," tech. rep., Framatome ANP report, july 2001.
- [51] K. Umminger and W. Kastner, "Thermal hydraulics of PWRs with respect to boron dilution phenomena. Experimental results from the test facilities PKL and UPTF," *Nuclear Engineering and Design*, vol. 204, pp. 191-203, 2001.

- [52] T. Mull, S. Bernhard, and K. Umminger, "Final Report of the PKL Experimental Program within the OECD/SETH Project," Tech. Rep. FANP-NGTT1/04/en/04, Framatome ANP, 2004.
- [53] J. Freixa, *SB-LOCA with Boron Dilution in Pressurized Water Reactors. Impact to the Operation and Safety*. PhD thesis, Universitat Politècnica de Catalunya, 2007.
- [54] J. Freixa and et al., "Boron transport model with physical diffusion for RELAP5," no. Nuclear technology, vol. 160, n.ºm. 2, p. 205-215, 2007.
- [55] A. DelNevo and et al., "Analytical exercise on OECD/NEA/CSNI PKL-2 Project Test G3.1: Main Steam Line Break Transient in PKL-III Facility," Tech. Rep. OECD/NEA PKL-2 project, TH/PKL-2/02(10), 2011.
- [56] S. Lucas, "Millora i adaptació del model simplificat d'Ascó per l'ús de càlculs escalats. Aplicació a l'anàlisi de distorsions en escenaris LOBL," Master's thesis, Universitat Politècnica de Catalunya, 2014. in catalan.
- [57] J. Freixa, V. Martínez-Quiroga, and F. Reventos, "Core Exit Temperature Response during an SBLOCA Event in the Ascó NPP," Tech. Rep. Spanish Regulatory Council Internal Report, 2014.
- [58] S. Petelin, B. Mavko, and O. Gortnar, "Scaling for the Analysis of ISP-27 Accident Scenario Realized on Krsko NPP," no. Anual Meeting of the Nuclear Society of Slovenia, 1994.
- [59] S. Petelin and I. Gunel, "Ideal Scaling of BETHSY 9.1.B Test Results to NPP," no. Nuclear Society of Slovenia. 2nd Regional Meeting: Nuclear Energy in Central Europe, 1995.
- [60] S. Petelin and I. Ravnikar, "Scaling-up of BETHSY 9.1b Experiment to Real NPP Size Transient," no. Anual Meeting of the Nuclear Society of Slovenia, 1997.
- [61] A. Petruzzi, *Development and application of Methodologies for Sensitivity Analysis and Uncertainty Evaluation of the Results of the Best Estimate System Codes Applied in Nuclear Technology*. PhD thesis, University of Pisa, 2008.
- [62] M. Kristof, T. Kliment, A. Petruzzi, and J. Lipka, "RELAP5 simulation of surge line break accident using combined and best estimate plus uncertainty approaches," no. Nuclear Engineering and Design 239 2500-2513, 2009.
- [63] F. D'Auria, N. Debrecin, G. Galassi, and S. Galeazzi, "Application of Relap5/Mod3 to the evaluation of loss of feedwater in test facilities and in nuclear plants ," no. Nuclear Engineering and Design Volume 141, Issue 3, 1 July 1993, Pages 409-428, 1993.
- [64] R. Bovalini, F. D'Auria, A. D. Varti, P. Maugeri, and M. Mazzini, "Analysis of counterpart tests performed in boiling water reactor experimental simulators ," no. Nuclear Technology; v. 97(1) p. 113-130; ISSN 0029-5450, 1992.
- [65] F. D'Auria, , and et. al.i, "Scaling and counterpart tests," no. Proceedings of the CSNI Specialist Meeting on Transient Two-Phase Flow - Current Issues in System Thermal Hydraulics, 1992.
- [66] J. Song and K. Bae, "Evaluation of analytically scaled models of a pressurized water reactor using the RELAP5/MOD3 computer code," no. Nuclear Engineering and Design, 1999.
- [67] H. Park and et. al., "An assessment of a LBLOCA similarity for a reduced-height integral effect test loop design for PWRs," no. Annals of Nuclear Energy 34 (2007) 931-937, 2007.
- [68] F. D'Auria, M. Cherubini, G. Galassi, and N. Muellner, "Analysis of Measured and Calculated Counterpart Test Data in PWR and VVER-1000 Simulators," no. Nuclear Technology and Radiation Protection, 2005.
- [69] F. D'Auria, M. Lanfredini, and N. Muellner, "Scaling Analysis in BEPU licensing of LWR," no. Nuclear Engineering and Technology, Vol. 44, No. 6, 2012.

- [70] A. Petruzzi and F. D'Auria, "Thermal-Hydraulic System Codes in Nuclear Reactor Safety and Qualification Procedures," no. Science and technology of nuclear installations, Volume 2008, Article ID 460795, 16 pages, 2008.
- [71] N. Zuber, "Problems in Modeling of Small Break LOCA," Tech. Rep. NUREG-0724, 1980.
- [72] Y. Taitel, D. Bornea, and A. E. Dukler, "Modeling Flow Pattern Transitions for Steady Upward Gas-Liquid Flow in Vertical Tubes," no. AIChE Journal. pp. 345-354, 1980.
- [73] M. Ishii and T. C. Chawla, "Local Drag Laws in Dispersed Two-Phase Flow," Tech. Rep. NUREG/CR-1230, ANL-79-105, 1979.
- [74] M. Ishii and K. Mishima, "Study of Two-Fluid Model and Interfacial Area.," Tech. Rep. NUREG/CR-1873, ANL-80-111, 1980.
- [75] M. Ishii and G. D. Jarlais, "Inverted Annular Flow Modeling," No. Advanced Code Review Group Meeting, 1982.
- [76] The RELAP5 Code Development Team, *Relap5/Mod3.3 Code Manual. Volume I: Models And Correlations*, 2001.
- [77] The RELAP5 Code Development Team, *Relap5/Mod3.3 Code Manual. Volume IV: Models And Correlations*, 2001.
- [78] M.D. Garcia, and P. Pla, "Diseño de una herramienta de ayuda para la preparacó en de modelos termohidráulicos a escala en centrales nucleares. Aplicación a dos experimentos.," Master's thesis, Universitat Politècnica de Catalunya, 1997. in spanish.
- [79] OECD/NEA, "Quick-look Report of ROSA/LSTF Test 3-1 (High Power Natural Circulation Experiment SB-CL-38 in JAEA)," Tech. Rep. OECD/NEA ROSA project, 2007.
- [80] F. Reventos and et. al., "Consistent Posttest Calculations for LOCA Scenarios in LOBI Integral Facility," no. Science and technology of nuclear installations, vol. 2012, p. 1-16., 2012.
- [81] J. Freixa and A. Manera, "Remarks on Consistent Development of Plant Nodalizations: An Example of Application to the ROSA Integral Test Facility," no. Science and Technology of Nuclear Installations, Vol. 2012, Article ID 158617, 2012.
- [82] V. Martinez-Quiroga, F. Reventos, and J. Freixa, "Applying UPC Scaling-Up Methodology to the LSTF-PKL Counterpart Test," no. Science and Technology of Nuclear Installations, vol. 2014, Article ID 292916, 18 pages, 2014. doi:10.1155/2014/292916, 2014.
- [83] V. Martinez-Quiroga and F. Reventos, "The Use of System Codes in Scaling Studies: Relevant Techniques for Qualifying NPP Nodalizations for Particular Scenarios," no. Science and Technology of Nuclear Installations, vol. 2014, Article ID 138745, 13 pages, 2014. doi:10.1155/2014/138745, 2014.
- [84] JAEA, "OECD/NEA. Quick-look Data Report of ROSA-2/LSTF Test 3 (Counterpart Test to PKL SB-HL-18 in JAEA)," Tech. Rep. OECD/NEA ROSA-2 Project, JAEA.
- [85] Schoen B., and et. al., "PKL III G7.1: SB-LOCA with total failure of HPSI system (Counterpart Testing with ROSA/LSTF - Quick Look Report-," Tech. Rep. Internal report, AREVA.
- [86] The RELAP5 Code Development Team, *Relap5/Mod3.3 Code Manual. Volume II: Code Structure, System Models, And Solution Methods*, 2001.
- [87] E. Buckingham, "On physically similar systems; illustrations of the use of dimensional equations," no. Physical Review 4 (4): 345-376. doi:10.1103/PhysRev.4.345, 1914.
- [88] F. D'Auria, G. Galassi, P. Vigni, and A. Calastri, "Scaling of natural circulation in PWR systems ," no. Nuclear Engineering and Design 2, 187-206, 1991.
- [89] S. N. Aksan and et. al., "User Effects on Thermallyhydraulic Transient System Codes Calculations," no. Proceedings of the CSNI Specialist Meeting on Transient Two-Phase Flow - Current Issues in System Thermal Hydraulics, 1992.

-
- [90] W. Wulff and et. al., "Scaling of Thermohydraulic Systems.," no. Nuclear Engineering and Design, 163, 359 1996, 1996.
- [91] F. D'Auria and G. M. Galassi, "Code Validation and Uncertainties in System Thermohydraulics," no. Progress in Nuclear Energy. Vol. 33, No. 1/2, pp. 175-216, 1998.
- [92] S. Banerjee and et. al., "Scaling in the safety of next generation reactors," no. Nuclear Engineering and Design 186 (1998) 111-133, 1998.
- [93] A. Garcia and et. al., "Study supporting the uncertainty evaluation in WWER-1000," no. Nuclear Energy in Central Europe. NSS, 1998.
- [94] P. F. Peterson and et al., "Scaling for integral simulation of mixing in large, stratified volumes," no. Nuclear Engineering and Design 186 (1998) 213-224, 1998.
- [95] V. H. Ransom, W. Wang, and M. Ishii, "Use of an ideal scaled model for scaling evaluation," no. Nuclear Engineering and Design 186 (1998) 1353148, 1998.
- [96] K. Takeuchi and M. Young, "Assessment of flooding in a best estimate thermal hydraulic code (W6 COBRA:TRAC)," no. Nuclear Engineering and Design 186 (1998) 225-255, 1998.
- [97] K. Takeuchi and et. al., "Scaling effects predicted by W6 COBRA:TRAC for UPI plant best estimate LOCA," no. Nuclear Engineering and Design 186 (1998) 257-278, 1998.
- [98] L. TayJian and et. al., "Power-operated relief valve stuck-open accident and recovery scenarios in the Institute of Nuclear Energy Research integral system test facility," no. Nuclear Engineering and Design 186 (1998) 149-176, 1998.
- [99] G. Wilson and B. Boyack, "The role of the PIRT process in experiments, code development and code applications associated with reactor safety analysis," no. Nuclear Engineering and Design 186 (1998) 23-37, 1998.
- [100] B. Young and et. al., "Application of code scaling applicability and uncertainty methodology to the large break loss of coolant," no. Nuclear Engineering and Design 186 (1998) 39-52, 1998.
- [101] J. Zhang and et. al., "Application of the W6 COBRA:TRAC best-estimate methodology to the AP600 large-break LOCA analysis," no. Nuclear Engineering and Design 186 (1998) 279-301, 1998.
- [102] N. Zuber, "The effects of complexity, of simplicity and of scaling in thermal-hydraulics," no. Nuclear Engineering and Design 204 (2001) 1-27, 2000.
- [103] The RELAP5 Code Development Team, *Relap5/Mod3.3 Code Manual. Volume III: Development Assessment Problems*, 2001.
- [104] The RELAP5 Code Development Team, *Relap5/Mod3.3 Code Manual. Volume V: Code Structure, System Models, And Solution Methods*, 2001.
- [105] The RELAP5 Code Development Team, *Relap5/Mod3.3 Code Manual. Volume VI: Validation of Numerical Techniques in RELAP5/MOD3.0*, 2001.
- [106] The RELAP5 Code Development Team, *Relap5/Mod3.3 Code Manual. Volume VII: Summaries and Reviews of Independent Code Assessment Reports*, 2001.
- [107] The RELAP5 Code Development Team, *Relap5/Mod3.3 Code Manual. Volume VIII: Programmers Manual*, 2001.
- [108] P. P. Goudrev and et. al., "PSB-VVER simulation of Kozloduy NPP "loss of feed water transient" ," no. Nuclear Engineering and Design 235 (2005) 925-936, 2005.
- [109] A. Khedr and et. al., "The effect of code user and boundary conditions on RELAP calculations of MTR research reactor," no. Nuclear Technology and Radiation Protection, 2005.
- [110] A. Khedr and F. D'Auria, "Nodalization effects on RELAP5 results related to MTR research reactor transient scenarios," no. Nuclear Technology and Radiation Protection, 2005.

- [111] JAEA, “Quick-look Data Report of ROSA/LSTF Test 6-1 (1.9Upper-head Small Break LOCA Experiment SB-PV-09 in JAEA),” Tech. Rep. OECD/NEA ROSA Project, JAERI.
- [112] C. Llopis, *Modelos avanzados de sistemas de control y proteccion de una central nuclear de agua a presion: contribucion a la seguridad y a la disponibilidad*. PhD thesis, Universitat Politecnica de Catalunya, 2006. in spanish.
- [113] V. Martinez-Quiroga, F. Reventos, and et. al., “Cálculo post-test del experimento ROSA/LSTF 3.1 con Relap5/mod3.3,” in *Jornadas técnicas del proyecto CAMP Espana*, (Consejo de Seguridad Nuclear, Madrid), 2007.
- [114] F. Reventos and et al., “Analysis of the Feed and Bleed procedure for the Asco NPP First approach study for operation support,” no. Nuclear Engineering and Design 237 (2007) 2006-2013, 2007.
- [115] F. D’Auria, “The role of experimental database in the validation of thermalhydraulic system codes,” Tech. Rep. Internal report. Universita di Pisa.
- [116] M. Cherubini and et. al., “Use of the Natural Circulation FlowMap for Natural Circulation Systems Evaluation,” no. Science and Technology of Nuclear Installations Volume 2008, Article ID 479673, 7 pages doi:10.1155/2008/479673, 2008.
- [117] C. Frepoli and A. Petruzzi, “Scaling, Uncertainty, and 3D Coupled Code Calculations in Nuclear Technology,” no. Science and Technology of Nuclear Installations Volume 2008, Article ID 673587, 3 pages doi:10.1155/2008/673587, 2008.
- [118] JAEA, “Final Data Report of OECD/NEA ROSA Project Test 1-2 (1 % hot-leg break LOCA experiment with HPI: SB-HL-17 in JAEA),” Tech. Rep. OECD/NEA ROSA Project, JAERI.
- [119] A. Petruzzi and F. D’Auria, “Approaches, Relevant Topics, and Internal Method for Uncertainty Evaluation in Predictions of Thermal-Hydraulic System Codes,” no. Science and Technology of Nuclear Installations Volume 2008, Article ID 325071, 17 pages doi:10.1155/2008/325071, 2008.
- [120] K. Wolfert, “Scaling of Thermal-Hydraulic Phenomena and System Code Assessment,” No. International Topical Meeting on Safety of Nuclear Installations TopSafe 2008, 2008.
- [121] V. Martinez-Quiroga, F. Reventos, and et. al., “Explotación y aplicació,”
- [122] F. D’auria, “Thermal-Hydraulics: from Fundamentals to Applications in Nuclear Systems,” in *Speech at Academy of Science in Buenos Aires*, (Academy of Science, Buenos Aires, Argentina), 2010.
- [123] F. D’auria, “Comments on ‘Critical review of conservation equations for two-phase flow in the U.S. NRC TRACE code’ by W. Wulff,” no. Nuclear Engineering and Design 241 (2011) 4277-4279. Letter to the editor, 2011.
- [124] F. D’Auria and O. Mazzantini, “The Best Estimate Plus Uncertainty Challenge in the Current Licensing Process of Present Reactors ,” no. Science and Technology of Nuclear Installations Volume 2011, Article ID 958218, 9 pages doi:10.1155/2011/958218, 2011.
- [125] JAEA, “Final Data Report of OECD/NEA ROSA-2 Project Test 1 (Hot-leg Intermediate break LOCA IB-HL-01 in JAEA),” Tech. Rep. OECD/NEA ROSA-2/LSTF Project, JAEA.
- [126] JAEA, “Final Data Report of OECD/NEA ROSA-2 Project Test 2 (Cold-leg Intermediate break LOCA IB-CL-03 in JAEA),” Tech. Rep. OECD/NEA ROSA-2/LSTF Project, JAEA.
- [127] JAEA, “Final Data Report of OECD/NEA ROSA-2 Project Test 7 (Cold-leg Intermediate break LOCA IB-CL-05 in JAEA),” Tech. Rep. OECD/NEA ROSA-2/LSTF Project, JAEA.
- [128] V. Martinez-Quiroga, F. Reventos, and et. al., “Escalación pura: Efecto de los criterios de escalación de plantas ITF en la validación de modelos de planta,” in *VII Jornadas Técnicas de CAMP Espana*, (Unesa, Madrid), 2011.

- [129] V. Martinez-Quiroga, F. Reventos, and et. al., “Counterpart Test PKL/LSTF: Cálculos pre-test,” in *VII Jornadas Técnicas de CAMP Espana*, (Unesa, Madrid), 2011.
- [130] V. Martinez-Quiroga and F. Reventos, “LSTF-PKL Counterpart Test:Scaling considerations and plan application,” in *OECD Conference Center, France*, (PKL-2 ROSA-2 Analytical Workshop), 2012.
- [131] V. Martinez-Quiroga and F. Reventos, “UPC LSTF Test 3 Post-Test Analyses: Assessment on CET-PCT using RELAP5mod3.3,” in *OECD Conference Center, France*, (PKL-2 ROSA-2 Analytical Workshop), 2012.
- [132] V. Martinez-Quiroga and F. Reventos, “UPC LSTF Test G7.1 Post-Test Analyses: Impact of Pseudo 3D vessel modelling using RELAP5mod3.3,” in *OECD Conference Center, France*, (PKL-2 ROSA-2 Analytical Workshop), 2012.